Interactions between splicing and transcription factors



Gilbert Daniel Ansa

Christ Church

University of Oxford

Supervisor: Professor Shona Murphy

A thesis submitted for the degree of *Doctor of Philosophy* at the University of Oxford, Hilary Term 2024

Table of contents

Acknowledgements……6

Declaration……7

Abstract……8

List of abbreviations……10

Chapter 1. Introduction

1.1 Gene expression in eukaryotes……13

1.2 Transcription in eukaryotes……15

1.3 Transcription initiation……18

1.4 Transcription elongation……21

1.5 The pol II CTD……23

1.6 Transcription termination and RNA 3' end formation……29

1.7 Pre-mRNA splicing……31

1.8 Pre-mRNA splicing and disease……39

1.9 Emerging links between splicing and transcription……41

1.10 Non-canonical roles of splicing factors……43

1.11 Aims of the present work……44

Chapter 2. Materials and Methods

2.1 Cell culture and drug treatments……46

2.2 Total RNA purification and reverse transcription PCR……47

2.3 Chromatin immunoprecipitation (ChIP)……49

2.4 Chromatin and nucleoplasm purification (NET-seq)……53

2.5 Cytoplasm purification……53

2.6 Whole cell protein extraction……54

2.7 Co-immunoprecipitation……54

2.8 Cell fraction co-immunoprecipitation……56

2.9 5-Ethynyl uridine (5-EU) labelling……57

2.10 Immunofluorescence……57

2.11 Western blot analysis……59

Chapter 3. Transcription and RNA processing crosstalk mediated by SF3B1 and CDK9

3.1 Background……62

3.2 Short SF3B1 inhibition causes rapid defects in pre-mRNA splicing and inhibits nascent transcription in human cells……65

3.3 Oct4 inducible compound 2 has no direct effect on *de novo* transcription……69

3.4 Short SF3B1 inhibition induces minimal cytotoxicity and does not promote a stress response……72

3.5 Inhibition of SF3B1 function impairs early transcription elongation……75

3.6 SF3B1 inhibition causes a global loss of SF3B1 and CDK9 from chromatin……77

3.7 SF3B1 and CDK9 weakly interact……79

3.8 Tat-SF1 is a candidate auxiliary factor for the interaction between SF3B1 and CDK9……81

3.9 Discussion……83

Chapter 4. The effect of SF3B1 and CDK9 inhibition on their subcellular localisation and that of interactors

4.1 Background……86

4.2 SF3B1 inhibition changes the nuclear localisation of SF3B1 and CDK9……88

4.3 SF3B1 inhibition does not affect the protein stability of SF3B1 and CDK9……92

4.4 SF3B1 inhibition causes the nuclear export of CDK9……96

4.5 Blocking CDK9 nuclear export does not reverse the effect of SF3B1 inhibition on transcription……99

4.6 Chromatin is a binding platform mediating SF3B1 and CDK9 protein interactions……103

4.7 Tat-SF1 interacts with SF3B1 and CDK9 only on chromatin……106

4.8 SF3B1 inhibition influences the subcellular localisation of Tat-SF1 and SNW1……109

4.9 Other interactors of SF3B1 and CDK9……113

4.10 The effect of SF3B1 inhibition on CDK9 recruiters……117

4.11 Discussion……119

Chapter 5. The effect of other splicing inhibitors on transcription

5.1 Background……125

5.2 Herboxidiene rapidly inhibits pre-mRNA splicing and does not promote a stress response in human cells……128

5.3 Potency of splicing inhibitors on splicing differ in human cells……131

5.4 Splicing inhibitors that target SF3B1 also affect transcription……133

5.5 Splicing inhibition may not be the primary effect of the splicing inhibitor Isoginkgetin……137

5.6 Discussion……141

Chapter 6. Transcriptional kinases and phosphatases regulate SF3B1 phosphorylation

6.1 Background……144

6.2 SF3B1 is predominantly phosphorylated when associated with chromatin……148

6.3 SF3B1 is a substrate of CDK9……150

6.4 SF3B1 is a substrate of other transcriptional kinases……154

6.5 Effects of other cyclin-dependent kinases on SF3B1……158

6.6 PP1/PP2A inhibition affects SF3B1 phosphorylation……160

6.7 PP1/PP2A may not regulate the splicing function of SF3B1……164

6.8 Discussion……167

Chapter 7. Closing remarks……172

Chapter 8. Future Directions……176

Reference list……177

Supplementary material……214

Acknowledgements

In August 2018, after graduating from my undergraduate studies, I got the incredible opportunity to work as a research assistant under the supervision of Prof Shona Murphy at the Sir William Dunn School of Pathology. I enjoyed my time so much as a research assistant that I abandoned my ambitions of medicine to pursue a DPhil instead. I would like to thank Prof Murphy for the advice, guidance, and endless support she has shown me through the years. Her scientific knowledge, expertise, and inquisition in the field is second to none, and has been instrumental in shaping my growth as a scientist.

I would like to thank Dr Michael Tellier for day-to-day supervision, advice, guidance, and continued support throughout the project. I have learnt so much while working with Michael. His vast scientific knowledge and attention to detail has been instrumental in the development of my critical thinking skills for planning experiments, analysing data, and drawing meaningful conclusions. It has been a pleasure to work with Michael and I wish him all the best on his journey as a principal investigator.

I am very grateful to all the people who made my time as a DPhil student so pleasant. A special thank you to my lovely colleagues who became friends, Michael Tellier, Isabella Maudlin, Cecilia Studniarek, Mathias Fagbemi, Aleksandra Pluta, Callum Henfry, Helena Harpham, and Stephanie Barker, and previous lab members Joana Guiro and Firdaus Isa.

Last but not least, I would like to thank the Doctoral Training Partnership as well as the UKRI-BBSRC for providing the opportunity to carry out a DPhil.

Declaration

I declare that the work described in this thesis is my own and all experiments were performed by myself. The experiments were carried out in the Sir William Dunn School of Pathology, University of Oxford. This thesis has not been submitted for any other degree or professional qualifications.

Gilbert Daniel Ansa

April 2024

Abstract

Transcription of human protein-coding genes by RNA polymerase II (pol II) is intimately coupled to RNA processing. Early in the transcription cycle, negative transcription elongation factors (NTEFs) pause pol II at an early-elongation checkpoint, facilitating both the addition of a cap structure to protect the newly forming RNA and RNA processing events. Recruitment of cyclin-dependent kinase (CDK) 9 causes phosphorylation of NTEFs, allowing pol II pause release and transition into productive elongation. The inhibition of an RNA processing factor, SF3B1, a component of the U2 small nuclear ribonucleoprotein (U2 snRNP) implicated in pre-mRNA splicing, by Pladienolide B (PlaB), also causes pol II to pause at the early-elongation checkpoint by reducing CDK9 recruitment. However, the underlying mechanism remains unclear. To gain mechanistic insight into the role of SF3B1 in transcription, I inhibited SF3B1 and CDK9 and determined the effects on pol II and CDK9 occupancy on protein-coding genes and the subcellular localisation of SF3B1, CDK9, and other splicing and transcription factors. I also determined the effects of general splicing inhibition on transcription and investigated the effects of inhibition of transcriptional protein kinases and protein phosphatases on SF3B1 phosphorylation.

I have confirmed that SF3B1 function influences the recruitment and stabilisation of CDK9 to chromatin. In addition, I provide evidence that Tat-SF1 is an auxiliary factor in a complex with SF3B1 and P-TEFb. The loss of SF3B1 function impairs the chromatin association of AFF4, SRSF2, and SNW1, all known CDK9 recruiters, resulting in less CDK9 recruited to paused pol II and enhanced nuclear export of CDK9. I confirm that transcriptional kinases including CDK9, CDK12, and CDK13,

and the protein phosphatase PP1, target SF3B1 and that subcellular localisation and activity of SF3B1 is regulated by phosphorylation. The role of SF3B1 in coupling splicing to transcription is distinct from general splicing inhibition as inhibiting splicing at different stages does not have the same effect on transcription as SF3B1 inhibition. Collectively, these data shed new light on the links between splicing and transcription.

List of abbreviations

%	Percent
°C	Degrees Celcius
3'SS	3' splice site
5'SS	5' splice site
5-EU	5-Ethynyl uridine
as	Analogue-sensitive
ATP	Adenosine triphosphate
Bort	Bortezomib
BP	Branch point
BRE	TFIIB Recognition element
CA	Calyculin A
CDK	Cyclin-dependent kinase
ChIP	Chromatin Immunoprecipitation
CPT	Camptothecin
CTD	Carboxyl terminal domain
ddH_2O	Double distilled H_2O
DMEM	Dulbecco's Modified Eagle's Medium
DMSO	Dimethyl sulfoxide
DNA	Deoxyribonucleic acid
DNase	Deoxyribonuclease
dNTP	Deoxynucleotide
DRB	5,6-Dichlorobenzimidazole 1-β-D-ribofuranoside
DSIF	DRB sensitivity inducing factor
DTT	Dithiothreitol
EDTA	Ethylenediamine tetraacetic acid
h	Hours
HB	Herboxidiene
HEK	Human embryonic kidney
IgA	Immunoglobulin A
IgG	Immunoglobulin G

IP	Immunoprecipitation
Iso	Isoginkgetin
kDa	Kilodalton
LMB	Leptomycin B
M	Molar
Mad	Madrasin
ml	Millilitres
mM	Millimolar
mNET-seq	Mammalian native elongating transcript sequencing
mRNA	mature/messenger RNA
NA	1-NA-PP1
NELF	Negative elongation factor
ng	Nanograms
NM	1-NM-PP1
NTC	PRPF19/nineteen complex
NTEF	Negative transcription elongation factor
NTR	Nineteen-related
O4I2	Oct4 inducible compound 2
PAS	Polyadenylation site
PCR	Polymerase chain reaction
PIC	Pre-initiation complex
PlaB	Pladienolide B
pmol	Picomole
pol	RNA polymerase
pre-mRNA	Precursor mRNA
pSer	Phosphorylated Serine
P-TEFb	Positive transcription elongation factor b
pThr	Phosphorylated Threonine
pTyr	Phosphorylated Tyrosine
qPCR	Quantiative polymerase chain reaction
RNA	Ribonucleic acid

RNase	Ribonuclease
rpm	Revolutions per minute
rRNA	Ribosomal RNA
RT	Reverse transcription
RT-PCR	Reverse transcrption PCR
RT-qPCR	Reverse trancription quantitivative PCR
SEC	Super elongation complex
Ser	Serine
SDS	Sodium dodecyl sulfate
SF3A	U2-associated splicing factor 3 A
SF3B	U2-associated splicing factor 3 B
snoRNA	Small nucleolar RNAs
snRNA	Small nuclear RNA
snRNP	Small nuclear ribonucleoprotein
SR	Serine and argining-rich
TAFs	TBP-associated factors
TBP	TATA-binding protein
Thr	Threonine
tRNA	Transfer RNA
TSS	Transcription start site
TT	Tautomycetin
TTS	Transcirption termination site
Tyr	Tyrosine
U2AF	U2 small nuclear RNA auxiliary factor
v/v	Volume to volume
w/v	Weight to volume
x g	Relative centrifugal force
Δ	Delta
µg	Micrograms
µl	Microliters
µM	Micromolar

Chapter 1. Introduction

1.1 Gene expression in eukaryotes

The Central Dogma of molecular biology describes how the flow of information stored in DNA is used to make functional protein products. DNA encodes sequences of amino acids, which are the building blocks of proteins, but it does not direct protein synthesis. The first fundamental step required to make a protein is transcription, where the information stored in DNA is transcribed into a carrier molecule called RNA. The RNA molecule then serves as a template for protein synthesis in a process called translation. The process of transcription of protein-coding genes happens in the nucleus of a cell with the primary RNA made referred to as a precursor messenger RNA (pre-mRNA) which must then be processed in multiple ways to generate a mature RNA (mRNA) that is exported to the cytoplasm for translation into a protein.

RNA processing is intimately coupled to transcription in eukaryotes. The first RNA processing event is capping, which is the addition of a 7-methyl guanosine to the first nucleotide of the 5' end of a pre-mRNA transcript to protect it from premature degradation. The cap structure also mediates the recruitment of protein factors for further RNA processing events, nuclear export, and translation (Cai et al., 2023; Malbec et al., 2019).

Most protein-coding genes in eukaryotes comprise a combination of non-coding sequences called introns, flanked by coding sequences called exons. Contiguous introns and exons are transcribed together to form the pre-mRNA. Pre-mRNAs in eukaryotes are usually monocistronic. The removal of intronic elements and the

ligation of exons together is called *cis*-splicing or more commonly referred to as pre-mRNA splicing.

The vast majority of eukaryotic protein-coding mRNAs, with the exception of replication dependent histone mRNAs have a long characteristic polyadenylate tail at their 3' ends. The polyadenylate tail is formed by the primary transcript undergoing endonucleolytic cleavage triggered by the specific binding of a multiprotein complex to regulatory *cis*-acting sequence elements on the pre-mRNA. A series of protective adenosine nucleotides not encoded by the DNA are then added to the exposed 3' end of the pre-mRNA in a process called polyadenylation. The 3' polyadenylate tail prevents premature degradation and together with the 5' cap structure are required for nuclear export and efficient translation of the mRNA (Gallie, 1991; Haimov et al., 2015; Passmore and Coller, 2023).

Most pre-mRNAs become mRNAs following 5' capping, pre-mRNA splicing, and 3' end processing. However, several eukaryotic pre-mRNAs are subject to further RNA processing events such as the discrete deamination of a cytosine to a uracil to make it an mRNA molecule (Pecori et al., 2022).

The mRNA molecules must be exported from the nucleus to the cytoplasm, to be translated into a protein by the ribosome. The eventual fate of an mRNA is degradation. Turnover of mRNA is initiated by the shortening of the polyadenylate tail (deadenylation) by exoribonucleases or by mRNA decapping, followed by degradation in the 3'-5' direction by the RNA exosome or 5'-3' direction by the exonuclease Xrn1 (Passmore and Coller, 2023; Charenton and Graille et al., 2018).

1.2 Transcription in eukaryotes

The central dogma describes one class of RNA but in eukaryotes, multiple other classes of RNA molecules exist. DNA is transcribed into RNA by three distinct DNA-dependent RNA polymerases (pol) that specialise in the transcription of different classes of genes. Pol I is located in the nucleolus and transcribes a single transcript, the 47S precursor ribosomal RNA (pre-rRNA), that is processed into 28S, 18S, and 5.8S ribosomal RNA (rRNA), which are structural RNAs that collectively comprise the majority of RNA molecules in a cell. Pol II is located in the nucleus and transcribes a diverse range of transcripts including all protein-coding nuclear pre-mRNA and many non-coding RNAs such as microRNAs, small nuclear RNAs (snRNAs) (except for the U6 snRNA), and small nucleolar RNAs (snoRNAs). Pol III is also located in the nucleus and transcribes a variety of precursor structural RNAs that are processed into transfer RNAs (tRNAs), 5S rRNA, the U6 snRNA, and other non-coding small RNA molecules.

All three polymerases consist of multiple subunits that assemble into complex molecular machines with common features with regard to the composition of their catalytic cores and functional steps of the transcription process. However, each is unique with respect to some of their functional structural elements, subunits, and accessory factors.

Pol II is a large complex with a total mass of over 500 kDa, comprising of 12 distinct subunits (Rpb1-Rpb12) that are highly conserved from yeast to humans. Pol II stands at the centre of a complex machinery, whose composition changes in the course of gene transcription. There are three main stages of pol II transcription: initiation, elongation, and termination (Figure 1.1). During initiation, general

transcription factors assemble with pol II for promoter recognition and melting (Shandilya and Roberts, 2012). Shortly after initiation, the conformation of pol II changes to facilitate stable transcription elongation into the body of the gene. The end of a gene is defined by the emergence of sequence elements including the polyadenylation site (PAS), cleavage site, and downstream element (DSE) signals on RNA, which prompts 3' end cleavage and or processing, and the eventual termination of transcription. Following cleavage, pol II can continue to traverse the DNA template and synthesise miscellaneous RNA transcripts. However, as these RNA transcripts are not protected by 5' cap structures, they are degraded by the 5'-3' exonuclease Xrn2 which eventually triggers the release of pol II from the DNA template (West et al., 2004; Fong et al., 2015).

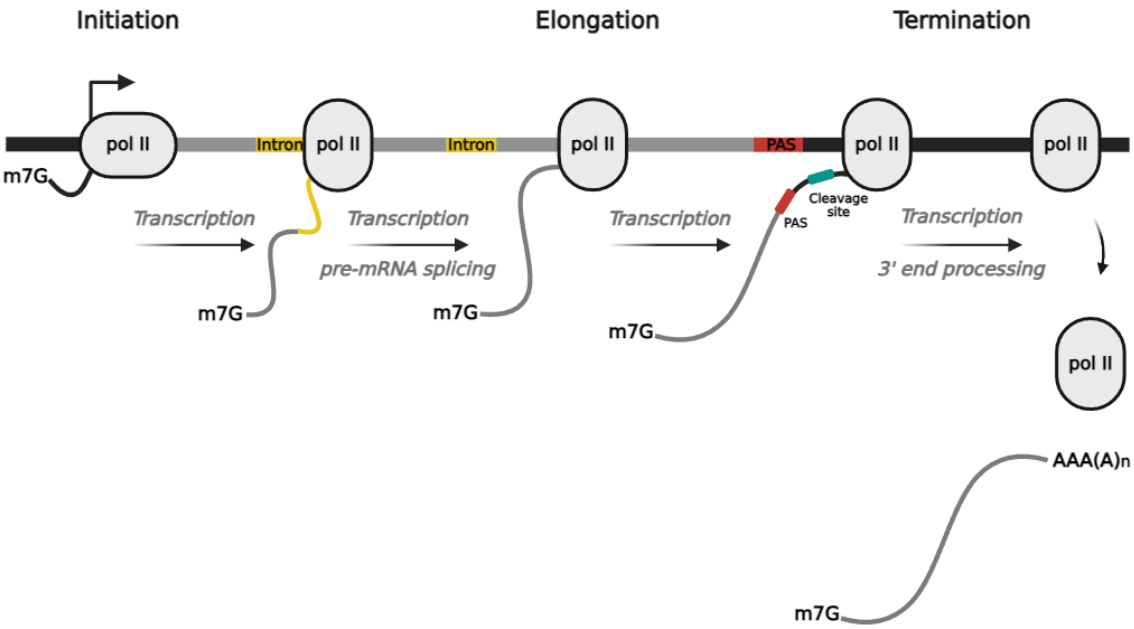


Figure 1.1. Transcription of protein-coding genes by pol II.

The production of an mRNA relies on the efficient progression of pol II through the three main stages of transcription. RNA processing events are intimately coupled to transcription. Following initiation, pol II undergoes confirmational changes to facilitate elongation. It also experiences a pause which allows the 5' end of the emerging pre-mRNA to be capped with a 7-Methylguanosine (m7G) and can regulate gene expression (Kachaev et al., 2020; Core and Adelman, 2019). During elongation, pol II transcribes both exons (grey regions on DNA) and introns (yellow regions on DNA) with introns removed by pre-mRNA splicing. At the end of the gene, transcription of the PAS (red region on the DNA) initiates the 3' processing of the pre-mRNA and the eventual release of pol II from the DNA template. On the DNA, the cornered arrow indicates the transcription start site, and the black regions indicate the promoter and 3' non-coding region. On the RNA transcript, the red and green boxes indicate the PAS and cleavage site, respectively, and the AAA(A)n sequence indicates the polyadenylate tail.

1.3 Transcription initiation

Canonical transcription starts with the assembly of pol II with the general transcription factors TFIIA, TFIIB, TFIID, TFIIE, TFIIF, and TFIIH at the promoter region of a gene to form the pre-initiation complex (PIC). Each gene contains specific DNA sequence elements at its promoter called the core promoter elements that can be located upstream or downstream of the target gene transcription start site (Juven-Gershon et al., 2008; Luse, 2014; Malik and Roeder, 2023). Of the different classes of core promoter elements, the presence or absence of a TATAA recognition sequence is used broadly to classify genes as TATA-containing or TATA-less promoters (Mathis and Chambon, 1981). The majority of eukaryotic promoters from yeast to humans have TATA-less promoters and rely on sequence elements downstream of promoters which are bound by other proteins that help to align pol II at the promoter (Core et al., 2008; Core et al., 2014; Danino et al., 2015; Yella and Bansal, 2017; Anish et al., 2009; Donczew and Hahn, 2017). At TATA-containing promoters, the TATAA recognition sequence is referred to as the TATA-box and it is recognised by the TATA binding protein (TBP), when complexed to TFIID and several TBP-associated factors (TAFs). The site-specific binding of TBP causes the DNA to bend at the TATA sequence at an angle of 80-100° (Starr et al., 1995). TFIIA can stabilise the interaction with TBP at the core promoter and facilitate the ordered assembly of other general transcription factors. A sequence immediately flanking the TATA box is often the TFIIB recognition element (BRE), a sequence motif recognised by TFIIB. TFIIB recruitment is an important step in the formation of a stable ternary complex with TBP-bound DNA (Deng and Roberts, 2007). Following TFIIB recruitment, TFIIF with pol II bound directs pol II to the core promoter, further

stabilising the forming PIC. The recruitment of the mediator complex along with TFIIE and TFIIH forms the PIC.

TFIIH is composed of ten subunits and has two essential activities that control the ATP-dependent transition from a closed to an open PIC, a requirement for productive transcription initiation (Lainé and Egly, 2006). The first essential activity is from the TFIIH subunits, XPB and XPD, both have DNA-dependent ATPase and DNA helicase activities which unwinds a few bases of promoter DNA and allows entry of the template strand DNA into the active site of pol II to form a transcription bubble (Fishburn et al. 2016; Schilbach et al. 2017; Dienemann et al. 2019; Grünberg and Hahn, 2013). Abortive transcription is a phenomenon of pol II attempting to escape the PIC but enters into cycles of synthesis and release of short RNA segments. Confirmational rearrangements of the PIC free the tight association of pol II from the general transcription factors. The second essential activity of TFIIH is by its cyclin-dependent kinase (CDK) 7 subunit which phosphorylates serine (Ser) 5 and 7 residues of the carboxyl-terminal domain (CTD) of the largest subunit of pol II (Rpb1) to facilitate promoter escape and entry into transcription elongation (Akhtar et al., 2009). The CTD is composed of multiple heptad repeats of the consensus amino acid sequence 1-Tyr-Ser-Pro-Thr-Ser-Pro-Ser-7 that undergo reversible modification of the residues to generate a code that changes during the transcription cycle and is read by CTD-binding factors, discussed in more detail in section 1.5.

TFIIH remains associated with pol II but the other general transcription factors at the promoter are recycled for another round of transcription. Order-of-addition experiments combined with *in vivo* analysis led to the determination of the stepwise

PIC assembly (Conaway and Conaway, 1993; Roeder, 1996; Grünberg and Hahn, 2013) (Figure 1.2).

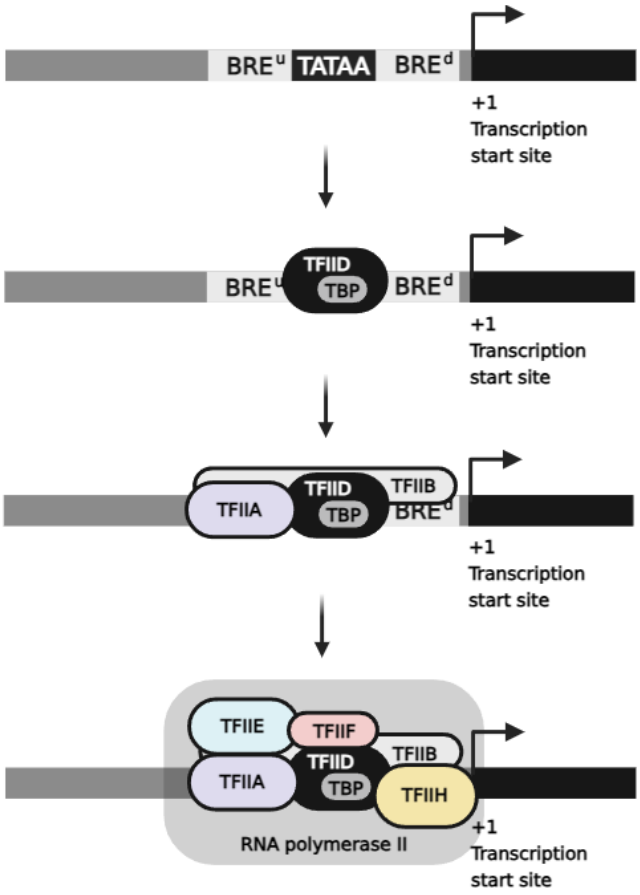


Figure 1.2. Transcription initiation assembly pathway of pol II.

The assembly of the pre-initiation complex (PIC) requires the stepwise recruitment of the general transcription factors TFIIA, B, D, E, F, and H, and pol II. TFIID is among the first general transcription factors to bind the core promoter on TATA-containing genes at the TATA-box *via* its TBP subunit. Next, TFIIA and TFIIB are recruited, the latter binding to the TFIIB recognition element upstream (BRE^u) and downstream (BRE^d) sites. Sequential recruitment of TFIIF/pol II, TFIIE, TFIIH and the multiprotein mediator complex (not shown) lead to the assembly of the PIC for transcription initiation.

1.4 Transcription elongation

The progression of pol II during transcription elongation is orchestrated by the timely recruitment of a number of different transcription elongation factors that regulate the behaviour of pol II to prevent stalling or dissociation before the end of the gene. However, shortly after promoter escape within the first 120 nucleotides, pol II pauses in a phenomenon known as promoter-proximal pausing (Gilmour and Lis 1986; Rougvie and Lis 1988; Adelman and Lis, 2012; Core and Adelman, 2019; Abuhashem et al., 2022) (Figure 1.3). Pol II pausing is an important early elongation checkpoint in metazoan gene expression that allows time for nascent transcripts to be 5' capped and some genes to be prepared for pre-mRNA splicing. The emergence of nascent RNA from pol II serves as a recognition site for negative transcription elongation factors (NTEFs), DRB sensitivity-inducing factor (DSIF) comprising Spt4 and Spt5, and negative elongation factor (NELF) to associate selectively with the pol II elongation complex and cause pol II to pause in a stable manner (Missra and Gilmour 2010; Gressel et al., 2017; Vos et al., 2018.; Aoi et al., 2020). The release of paused pol II into productive transcription elongation is triggered by the transactivating factor, positive transcription elongation factor b (P-TEFb), concomitant with the dephosphorylation of Ser5 of the pol II CTD (Adelman and Lis, 2012). Under steady state conditions, P-TEFb comprising CDK9 and Cyclin T1 is sequestered in an inhibitory complex by interactions with 7SK snRNA through hexamethylene bisacetamide-induced protein 1 (HEXIM1). Nuclear reservoirs of P-TEFb in 7SK small nuclear ribonucleoprotein particles (snRNPs) are tethered to promoter and enhancer regions of many genes allowing the local release of P-TEFb and induction of transcription elongation (McNamara et al., 2016; Ji et al., 2013; Liu et al., 2013; Flynn et al., 2016). Upon release from 7SK snRNP, P-TEFb

phosphorylates both NTEFs causing the ejection of NELF from the elongation complex and the transition of DSIF from a negative to a positive elongation factor to mediate pause release and the transition of pol II into productive trancription elongation (Core and Adelman, 2019). P-TEFb also phosphorylates Ser2 residues of the pol II CTD, which allows the recruitment of transcription and RNA processing factors (Peterlin and Price, 2006; Adelman and Lis, 2012). The efficiency of pause release is a prime determinant of gene expression levels (Core and Adelman, 2019), raising great interest in the mechanisms that drive this process.

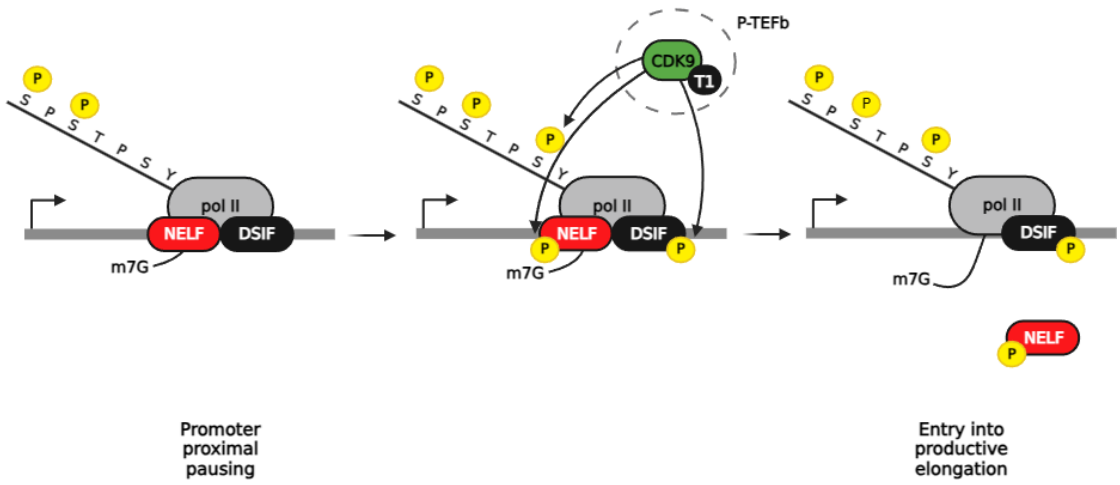


Figure 1.3. Promoter-proximal pausing of pol II.

Pol II pausing occurs shortly after the transcription start site (black arrow) and requires NELF and DSIF, which function cooperatively. Recruitment of P-TEFb causes phosphorylation of NELF, DSIF, and Ser2 of the pol II CTD. This results in the ejection of NELF from the elongation complex and the transition of DSIF from a negative to a positive elongation factor, allowing productive elongation to proceed.

1.5 The pol II CTD

The CTD of pol II is a unique regulatory region not found in pol I and pol III, that protrudes from the catalytic core. The CTD is highly repetitive, unstructured, and is highly conserved between species (Chapman et al., 2008). The *Saccharomyces cerevisiae* CTD comprises 26 mostly consensus repeats (Harlen and Churchman, 2017). In multicellular eukaryotes, a varying number of additional CTD repeats has been acquired through evolution depending on the organism and mammalian pol II has 52 repeats in the CTD (Chapman et al., 2008). The first 21 heptad repeats are largely consensus, whereas the remaining 31 heptad repeats have diverged from the consensus repeat sequence mainly at position 7, which can be asparagine, threonine, or lysine instead of serine (Eick and Geyer, 2013; Egloff et al., 2012; Simonti et al., 2015). The presence of the non-consensus repeats has been suggested to have evolved to perform additional functions in higher eukaryotes, although a CTD with all consensus repeats supports viability in human cells (Hintermair et al., 2012). Although the CTD is not complex in structure, it plays a major role in the regulation of gene expression.

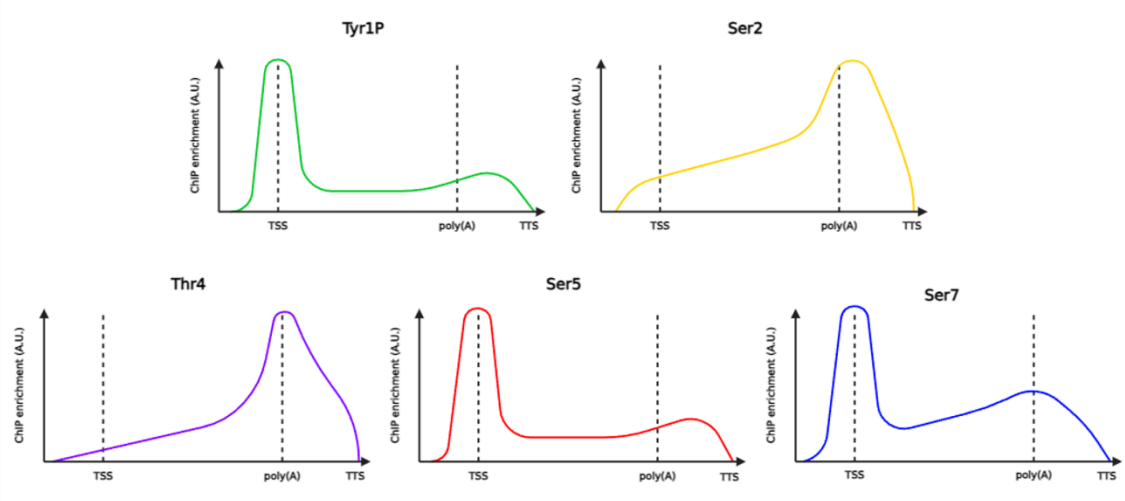
The CTD acts as a landing platform to mediate pol II protein-protein interactions with major transcriptional effector molecules, including the enzymes mediating or removing post-translational modifications (PTMs) of the CTD during specific steps of the transcription cycle, and the proteins that read these modifications *via* specific recognition domains for PTMs (Jeronimo et al., 2016). The timing and activities of each of these CTD interactors are essential for regulating the process of transcription and transcription-associated RNA processing events (Tellier et al., 2020a; Guiro and Murphy, 2017; Zaborowska et al., 2016).

The best characterised form of CTD modification is phosphorylation. The concerted action of multiple CTD kinases and phosphatases dynamically control the phosphorylation state of the residues, predominantly at Ser2 and Ser5 but also at Tyr1, Thr4, and Ser7 within the consensus heptad repeats, generating a code that is read by RNA processing factors and chromatin modifying enzymes at the correct point in the transcription cycle. The importance of these effectors for the expression of human and viral genes has made them attractive therapeutic targets for the treatment of neoplastic conditions and viral infections (Cassandri et al., 2020; Morales and Giordano, 2016; Tavakolian et al., 2020; Yamamoto et al., 2014). A better understanding of the precise functions of these effectors is therefore important both scientifically and clinically.

Specific antibodies to detect precise CTD modifications form the basis for ChIP and mammalian native elongating transcript sequencing (mNET-seq) analyses which find that the average phosphorylation profile of the CTD across protein-coding genes has a pattern that is generally conserved from yeast to humans (Hintermair et al., 2012; Descostes et al., 2014; Nojima et al., 2015) (Figure 1.4A). ChIP analysis indicate that levels of phosphorylated Ser5 (pSer5) of the CTD is enriched near promoters and transcription start sites (Hintermair et al., 2012; Descostes et al., 2014). Ser5 is phosphorylated by CDK7 early in gene transcription where it is thought to stimulate capping activity by creating a binding platform for interaction with the 5' capping enzyme during promoter-proximal pol II pausing (Adelman and Lis, 2012; Akhtar et al., 2009). In the gene body, Ser5 is dephosphorylated by the concerted phosphatase activities of Scp1, RPAP2, and Ssu72 (Yeo et al., 2003; Ni et al., 2014; Mosley et al., 2009; Wani et al., 2014). In contrast, the Ser2 phosporylation profile is low at promoters and increases towards the 3' end of the gene until the

polyadenylation site. Ser2 is phosphorylated by CDK9 (Laitem et al., 2015) during early transcription elongation and later by CDK12 (Cheng et al., 2012; Blazek et al., 2011; Bartkowiak et al., 2010) where it is important for pol II pause release, recruitment of pre-mRNA splicing factors, and splicing catalysis. After the polyadenylation site, Ser2 is dephosphorylated by the TFIIF-associating CTD phosphatase 1 (Fcp1) (Cho et al., 2001; Ghosh et al., 2008) (Figure 1.4B).

A



B

Residue of CTD	Species	Kinase(s)	Phosphatase(s)
Tyrosine 1	Mammals	c-Abl	Unknown
	S. cerevisiae	Slt2	Glc7
Serine 2	Mammals	CDK9, CDK12, CDK13, BRD4, and DYRK1A	Fcp1 and Cdc14
	S. cerevisiae	Bur1 and Ctk1	Fcp1 and Cdc14
Threonine 4	Mammals	Plk1, Plk3, and CDK9	Fcp1
	S. cerevisiae	Unknown	Fcp1
Serine 5	Mammals	CDK7, CDK8, CDK9, CDK12, CDK13, and DYRK1A	Scp1, RPAP2, and Ssu72
	S. cerevisiae	Kin28 and Srb10	Ssu72 and RTR1
Serine 7	Mammals	CDK7 and CDK9	Sssu72
	S. cerevisiae	Kin28 and Bur1	Sssu72

Figure 1.4. Pol II CTD phosphorylation

(A) Schematic of ChIP profile patterns of phosphorylation of the CTD in mammals across the trancription start site (TSS), polyadenylate site (poly(A)), and transcription termination site (TTS). **(B)** Table of known kinases and phosphatases acting on the CTD in mammals and yeast. Figure adapted from Zaborowska et al., 2016.

The functional importance of Ser7, Thr4, and Tyr1 phosphorylation in gene expression is less well understood (Yurko and Manley, 2018). Like Ser5 phosphorylation, Ser7 phosphorylation follows a similar pattern being enriched early in gene transcription near gene promoters by the kinase activity of CDK7 (Akhtar et al., 2009), then is dephosphorylated in the gene body by the phosphatase Ssu72 (Zhang et al., 2012). The biological significance of Ser7 phosphorylation seems to be species-specific. For example, a human Rpb1 derivative with all Ser7 residues mutated to Ala (S7A) was specifically defective in expression of the spliceosomal U1 and U2 snRNAs through impaired 3' cleavage (Egloff et al., 2007). On the other hand, chicken DT40 cells using Rpb1 derivatives found that only the last 26, but not the first 26, heptad repeats of the CTD with S7A mutations were inviable and showed a dramatic and specific decrease in snRNA 3' end formation (Hsin et al., 2014). A parsimonious explanation is that most of the position 7 residues in the last 26 heptad repeats of the CTD are not serine, suggesting that the non-serine mutations to alanine are what disrupt snRNA 3' end processing. In *S. cerevisiae*, snRNA 3' ends are not formed by Integrator like in mammals as it does not exist in yeast, but instead by the Nrd1-Nab3-Sen1 complex, equally not found in vertebrates, which primarily recognises pSer5 and not pSer7 of the CTD (Vasiljeva et al., 2008). Although Ser7 is phosphorylated by Kin28 (CDK7 in mammals) and later by Bur1 (CDK9 in mammals), and dephosphorylated by Ssu72, no clear function has been assigned to Ser7 in *S. cerevisiae*. The role of Ser7 phosphorylation in *S. pombe* is associated with mRNA capping as it enables efficient binding of 5′ cap methyltransferase Pcm1 to the CTD (St Amour et al., 2012).

The roles of Thr4 phosphorylation, much like Ser7 phosphorylation, are different between organisms. In mammals, the Thr4 phosphorylation profile is low near gene

promoters but increases in the 3' region of genes (Hintermair et al., 2012). The kinase activities of CDK9 (Hsin et al., 2011; Hsin et al., 2014) and the Polo-like kinases, Plk3 and Plk1 (Zimmerman and Erikson, 2007; Hintermair et al., 2012; Hintermair et al., 2016), have been shown to phosphorylate Thr4. Fcp1 dephosphorylates Thr4 (Hsin et al., 2014). In mammals, Thr4 phosphorylation is essential for viability and influences transcription elongation genome-wide by affecting promoter-proximal pausing of pol II (Hintermair et al., 2016). mNET-seq analysis which precisely maps the positions of elongating pol II (Nojima et al., 2015), indicates that Thr4 phosphorylation correlates with transcription termination in regions of protein-coding genes (Schlackow et al., 2017). Further, in chicken DT40 cells it is necessary for efficient 3' end processing of non-polyadenylated replication-dependent histone transcripts (Hsin et al., 2011). This function of Thr4 phosphorylation is not applicable in yeast as all histone mRNA 3' ends are polyadenylated. In *S. cerevisiae*, while no study has suggested Thr4 phosphorylation to be necessary for global transcription, it has been linked to chromatin remodelling in certain growth conditions, transcription termination, and post-transcriptional splicing (Rosonina et al., 2014; Harlen et al., 2016).

Biological functions of Tyr1 phosphorylation, much like Ser7 and Thr4, seem to significantly differ between metazoans and yeast. In mammals, the Tyr1 phosphorylation profile resembles that of Ser5 phosphorylation, being highest near gene promoters and rapidly declining through the gene body. The kinases and phosphatases responsible for the reversible phosphorylation of Tyr1 differ between vertebrates and yeast. In mammals, Tyr1 is phosphorylated by the kinase c-Abl only after DNA damage, and in *S. cerevisiae* is by the orthologue of the MAP kinase I, Slt2 (Baskaran et al., 1993; Baskaran et al., 1999; Yurko et al., 2017). The principal

phosphatase for Tyr1 in yeast appears to be Glc7 (Schreieck et al., 2014), whereas the identity of the Tyr1 phosphatase in mammals has yet to be discovered. In vertebrates, Tyr1 phosphorylation plays an important role in maintaining the stability of the CTD, in addition to the regulation of anti-sense transcription and the stability of those transcripts (Descostes et al., 2014; Hsin et al., 2014). In yeast, Tyr1 phosphorylation is important for the recruitment of factors to mediate transcription termination (Mayer et al., 2012).

1.6 Transcription termination and pre-mRNA 3' end formation

Productive transcription elongation of pol II continues through the gene body until encountering downstream sequence elements to signal the 3' end processing of the pre-mRNA. The 3' end of a pre-mRNA transcript is defined by three highly conserved sequence motifs, the PAS, the DSE, and a cleavage site. Pre-mRNA cleavage factors are directed to the cleavage site by proteins recognising the PAS and DSE sequences. Following endonucleolytic cleavage, multiple adenosine nucleotides are added to the 3' end of the pre-mRNA by the polyadenylate polymerase (PAP). The newly synthesised polyadenylate tail is covered by the polyadenylate-binding nuclear protein 1 (PABPN1) which stabilises and facilitates nuclear export of the mRNA (Apponi et al., 2010; Wolin and Maquat, 2019).

While 3' end processing of the pre-mRNA is happening, pol II continues to transcribe beyond the PAS, and the 5' end of downstream pol II-associated transcripts produced following PAS cleavage are targeted for 5'-3' degradation by the nuclear exonuclease, Xrn2, as they do not have protective 5' cap structures. Pol II transcription termination employs two non-mutually exclusive pathways that are

fairly conserved across eukaryotes (Eaton and West, 2020) (Figure 1.6). The allosteric model posits that transcription of a PAS causes the dissociation of factors and or a conformational change in pol II that promotes its termination. Antitermination factors such as SCAF4 and SCAF8 interact with pol II and suppress termination until the desired PAS has been transcribed (Gregersen et al., 2019). The torpedo model describes the 5'-3' exonuclease Xrn2 binding to the 5' end of the pol II-associated transcript produced after PAS cleavage and degrading it until it reaches the polymerase and causes the disengagement of pol II from the DNA template. A number of other mechanisms contribute to pol II elongation capacity beyond the PAS. The sitting duck-torpedo model of termination describes an allosteric switch mediated by PAS-dependent Spt5 dephosphorylation to slow down pol II elongation and allow the Xrn2 torpedo to catch up with pol II and disengage it from DNA (Cortazar et al., 2019). Many cues transmitted to pol II influence its choice of termination pathway (Mischo and Proudfoot, 2013).

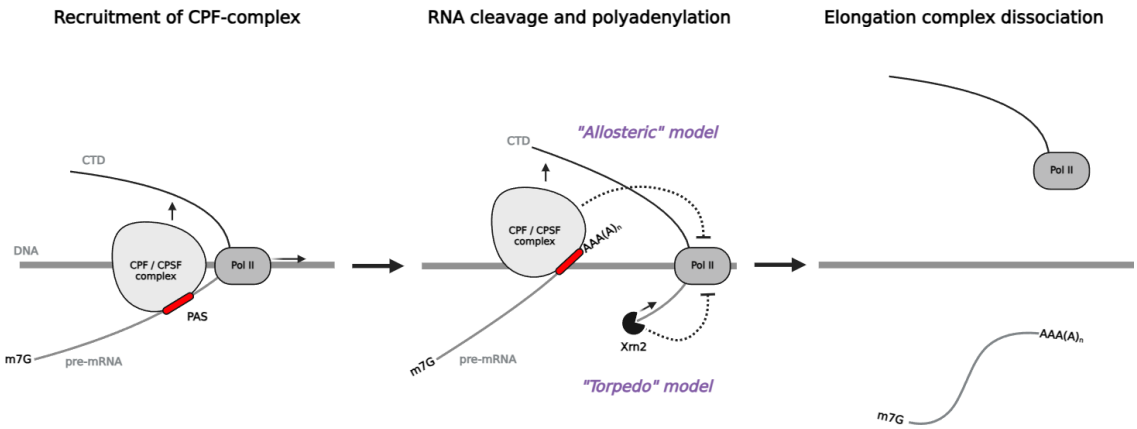


Figure 1.6. Transcription termination pathways of pol II.

The two main models, the allosteric model and torpedo model, describe how pol II is released from the DNA template. According to the allosteric model, the pol II elongation complex encounters termination signals in the region of the PAS, committing it to termination because of a conformational change, possibly due to the loss of pol II elongation factors. The torpedo model describes transcription termination being promoted on Xrn2 reaching the polymerase, which depends on previous cleavage of the nascent RNA by the multiprotein cleavage and polyadenylation factor (CPF/CPSF) complex. Figure adapted from Porrua et al., 2016.

1.7 Pre-mRNA splicing

One of the most unanticipated findings in molecular biology was the discovery that eukaryotic genes are discontinuous, meaning the organisation of genes comprise protein-coding exon sequences disrupted by intervening non-coding intron segments. In higher eukaryotes, the removal of introns from pre-mRNAs is not only essential for one gene producing one protein product, but for the production of multiple proteins from a single gene in a process called alternative pre-mRNA splicing. Pre-mRNA splicing can occur to a great extent that scales with organismal complexity. For example, the mouse and human genomes both contain approximately 20,000 protein-coding genes, yet the number of isoforms or expressed proteins differ considerably due to alternative pre-mRNA splicing

occurring in over 95% of human genes compared with approximately 63% of mouse genes, giving approximately 200,000 expressed proteins in humans relative to the approximately 95,000 expressed proteins in mice (Pan et al., 2008; Merkin et al., 2012; Barbosa-Morais et al., 2012). Alternative splicing significantly expands the form and function of eukaryotic proteomes and can serve many regulatory functions from cell identity and sex determination to phenotypic plasticity (Wright et al., 2022). There are multiple classes of alternative splicing events, including: cassette exons (exon skipping), retained introns, mutually exclusive exons, alternative promoters or PAS usage, alternative 5' or 3' splice site usage within exons, and reverse splicing reactions (back splicing) that generate circular RNA molecules (Wang et al., 2015; Marasco and Kornblihtt, 2023; Liu and Chen, 2022).

The aetiology of numerous diseases fundamentally can be attributed to errors in pre-mRNA splicing (Padgett, 2012). More than half of the over 31,000 known disease-causing mutations are predicted to affect splicing (Soemedi et al., 2017). Inefficient pre-mRNA splicing can lead to the production of defective proteins that cause disease or are incompatible with life, illustrating that the correct regulation of splicing is important for the proper functioning of individual cells to whole organisms (Wang and Cooper, 2007). For example, splicing contributes to liver homeostasis in a number of physiological contexts, including circadian rhythms (McGlincy et al., 2012), liver development, damage and regeneration (Baralle and Giudice, 2017; Bhate et al., 2015; Bangru et al., 2018), and in response to internal body temperature fluctuations (Preußner et al., 2017).

The fundamental mechanism of pre-mRNA splicing is conserved across eukaryotes (Collins and Penny, 2005), with humans and *S. cerevisiae* sharing a common set of

about 85 core spliceosomal proteins (Fabrizio et al., 2009). The architecture of an intron is defined by three important sites, the 5' splice site (5'SS), branch point (BP) adenosine, and 3' splice site (3'SS), all of which are defined by short conserved sequences that when mutated reduce splicing efficiency or completely abolish splicing (Langford et al., 1984; Chanfreau and Jacquier, 1993; Chanfreau et al., 1994). In humans, the 5'SS is defined by a consensus dinucleotide GU sequence, and the 3'SS typically by a consensus YAG trinucleotide, in which Y is a pyrimidine. Upstream of the 3'SS is a uridine and cytosine rich polypyrimidine tract 10 to 15 nucleotides in length (Sheth et al., 2006), preceded by the BP sequence with a consensus motif YUR<u>A</u>Y, where Y are pyrimidines, R is a purine, and the underlined A is the BP adenosine (Keller et al., 1985; Gao et al., 2008). Biochemically, splicing entails two S_N2-type transesterification steps (Figure 1.7A). In the first transesterification reaction (termed branching), the 2' hydroxyl group of the BP adenosine carries out a nucleophilic attack on the phosphate group of the guanosine of the 5'SS, separating the RNA. The exposed 5' end of the intron then forms a 2'-5' phosphodiester linkage with the BP adenosine, generating an intermediate loop structure known as a lariat. In the second transesterification reaction (termed exon ligation), the exposed 3' hydroxyl group of the 5' exon attacks the phosphodiester linkage of the last nucleotide of the 3'SS, resulting in the ligation of the 5' and 3' exons and the release of the intron lariat.

The two pre-mRNA splicing reactions are catalysed by the spliceosome, a large and highly dynamic RNA and protein (ribonucleoprotein) complex consisting of five snRNPs, as well as other auxiliary and ancilliary proteins involved in fine tuning. In the major spliceosome, responsible for the recognition and splicing of more than 99.5% of introns in humans, the five snRNPs are U1, U2, U4, U5, and U6 (Wilkinson

et al., 2020; Akinyi and Frilander, 2021). Each snRNP consists of a snRNA, seven Sm proteins that form a ring (or seven Lsm proteins in the case of U6), and a variable number of snRNP-specific proteins (Will and Lührmann, 2011). The five snRNPs and approximately 100 proteins assemble *de novo* in a stepwise manner on the pre-mRNA substrate to form the spliceosome (Kastner et al., 2019). The generation of the spliceosome active site requires extensive structural and compositional rearrangements (Will and Lührmann, 2011), mainly driven by eight evolutionary conserved DExD/H-box ATPases or RNA helicases that trigger RNA-RNA and RNA-protein rearrangements (Cordin and Beggs 2013).

Initially, the U1 snRNP base pairs with the pre-mRNA between the 5' end of the U1 snRNA and the 5'SS, with interactions stabilised by U1-associated proteins such as serine and arginine-rich (SR) proteins (Cho et al., 2011) and the cap-binding complex (Pabis et al., 2013). At the 3' end, splicing factor 1 (SF1) with help from additional protein interactors including the heterodimer of U2 small nuclear RNA auxiliary factor 2 (U2AF2, also known as U2AF65) which binds the polypyrimidine tract and U2 small nuclear RNA auxiliary factor 1 (U2AF1, also known as U2AF35) which binds the 3'SS at the intron-exon junction, is able to identify and interact with the pre-mRNA non-specifically to stabilise its binding to the BP sequence (Berglund et al., 1998). Together, these proteins form the early (E) complex in mammalian systems (Michaud and Reed, 1993), or commitment complex in yeast, as it commits the pre-mRNA to splicing catalysis. Interactions between the ATP-dependent RNA helicase UAP56 with U2AF2 cause the displacement of SF1 from the BP sequence and the recruitment of the U2 snRNP to stably bind the BP sequence, forming the pre-spliceosome or A complex (Fleckner et al., 1997; Zhang and Green, 2001). Base-pairing of the U2 snRNA to the BP sequence causes the BP adenosine to bulge out

into a pocket formed by the U2-associated splicing factor 3 B (SF3B) complex, mainly SF3B subunits 1 (SF3B1) and 7 (SF3B7) (Tholen et al., 2022), exposing the 2' hydroxyl group of the BP adenosine to nucleophilic attack the 5'SS during the first catalytic step of splicing. The U2 snRNA to BP interaction is stabilised by the U2-associated heteromeric protein complexes SF3A and SF3B, where the largest subunit of the SF3B complex, SF3B1 interacts with U2AF2 and with upstream and downstream nucleotides of the BP sequence (Gozani et al., 1998).

Next, the pre-assembled U4/U6·U5 tri-snRNP joins the A complex, generating the pre-catalytically activated spliceosome or B complex in which stable tri-snRNP integration requires the actions of the ATP-dependent RNA helicases BRR2 to initially unwind the U4/U6 snRNA duplex (Cordin and Beggs, 2013; Häcker et al, 2008), and the ATP-dependent RNA helicase PRP28 to disrupt U1 snRNP interaction with the 5'SS (Boesler et al., 2016). In this way, the U1 and U4 snRNPs are destabilised and leave the spliceosome, allowing the U6 snRNA after extensive restructuring to base pair with the 5'SS of the intron and the U2 snRNA to form the catalytic centre of the spliceosome. The activities of the ATP-dependent RNA helicases also mediate the recruitment of about 20 protein components mainly constituting three classes: the PRPF19/nineteen complex (NTC), the nineteen-related (NTR), and splicing factors, to form the activated spliceosome or B^{act} complex (Wahl et al., 2009). The SKI interacting protein, SNW1, is an integral component of the spliceosome that is recruited as part of the NTC complex and interacts with the U5 snRNP (Neubauer et al, 1998; Makarova et al, 2004).

Despite a well-formed active site, the B^{act} complex cannot catalyse the first step of splicing due to spatial separation of the BP sequence from the 5'SS. The spliceosome

is catalytically activated in an ATP-dependent manner by the RNA helicase PRP2, which releases components the U2 snRNP SF3A and SF3B to uncover the BP adenosine, generating the B* complex competent in catalysing the first step of splicing - branching reaction generating the cleaved 5' exon and intron lariat-3' exon intermediate. The resulting catalytic first step spliceosome generates the C complex and through ATP-dependent structural remodelling by the RNA helicase PRP16 releases factors required for the first step of splicing and allows binding of second step factors to generate the C* complex which performs the second catalytic step - exon ligation of the 5' exon with the 3' exon, yielding the post-spliceosome or P complex (Horowitz, 2012). The release of the mRNA, which generates the intron lariat spliceosome is catalysed by the ATP-dependent RNA helicase PRP22. The intron lariat spliceosome if dismantled by the ATP-dependent helicase PRP43, and the U2, U5, U6 snRNPs are released and recycled for future rounds of splicing.

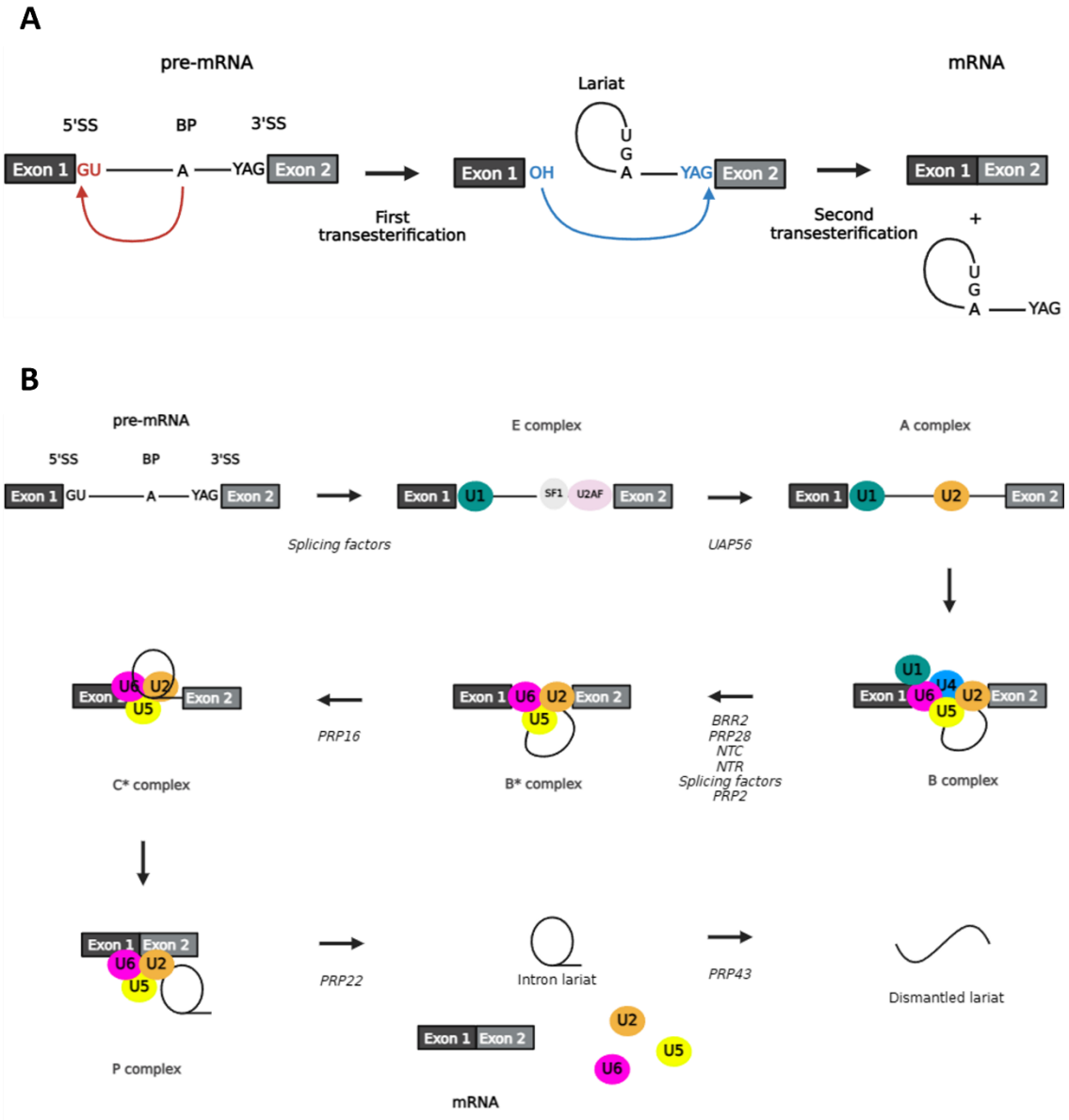


Figure 1.7. Pre-mRNA splicing process

(A) Splicing involves two transesterification reactions. First, the 2' hydroxyl group (OH) of the branch point (BP) adenosine performs a nucleophilic attack on the first nucleotide of the intron at the 5' splice site (SS) to create a phosphodiester bond, forming the lariat intermediate. Second, the 3'OH of the released 5' exon then performs a nucleophilic attack at the last nucleotide of the intron at the 3'SS creating a phosphodiester bond that ligates the 5' and 3' exons forming a mature RNA transcript (mRNA) and releases the intron lariat. **(B)** The stepwise assembly of the spliceosome from its snRNP and splicing factor components. First, binding of the U1 snRNP to the 5'SS and splicing factor 1 (SF1), and the U2AF2/U2AF1 to the 3' end of the intron results in the formation of the E complex. The release of SF1 and subsequent recruitment of the U2 snRNP, to the BP forms the A complex. The U4/U6·U5 tri-snRNP joins the A complex to form the B complex. Removal of the U1 and U4 snRNP and entensive structural rearrangements lead to the activation of the spliceosome or B* complex that

catalyses the first splicing step. Further structural remodelling of the spliceosome leads to the C* complex that catalyses the second splicing step to generate a mature spliced RNA transcript that's released from the post-spliceosome (P) complex. The activities of numerous ATP-dependent DExH/D-box RNA ATPases/helicases are vital to the progression of splicing catalysis as they induce dynamic RNA-protein rearrangements during spliceosome assembly and splicing. Figure adapted from Shi, 2017.

Although the 5'SS, 3'SS and BP sequence are required for pre-mRNA splicing, these sequence elements alone are often insufficient for exon/intron recognition. Additional regulatory sequence elements termed exonic or intronic splicing enhancers (ESEs or ISEs) are found in the majority of exons and introns of pre-mRNAs. Splicing factors, such as SR proteins including the serine and arginine rich splicing factor 2 (SRSF2) generally bind to ESEs or ISEs and facilitate spliceosome assembly through interactions with the U1 snRNP and U2AF (Phelan et al., 2012; Daubner et al., 2012; Takeiwa et al., 2020).

Compared to the major spliceosome, pre-mRNA splicing by the minor spliceosome is rare, accounting for the recognition and splicing of approximately 0.5% of introns in humans. The minor spliceosome targets a rare group of introns with highly conserved sequences at the 5' and 3' ends of the intron (El Marabti et al., 2021). Minor introns coexist in the same genes with major introns and while the two intron types are spliced by their respective spliceosomes, the two splicing machineries can cooperate, interacting with one another to drive pre-mRNA processing in genes containing minor introns (Akinyi and Frilander, 2021). Although there are some differences, spliceosome assembly and overall splicing chemistry is similar between the two spliceosome machineries (Singh and Cooper, 2012; Turunen et al., 2013; Matera et al., 2014; Wilkinson et al., 2020). One difference is that the 5'SS and BP

sequence are initially recognised by the U11/U12 di-snRNP complex in the minor spliceosome opposed to the separate recognition by the U1 and U2 snRNPs respectively, in major spliceosomes. Another difference is that the polypyrimidine tract and 3'SS are recognised by the ZRSR2 protein in minor spliceosomes, whereas in major spliceosomes they are recognised by the heterodimer of U2AF2/U2AF1. Following this initial recognition, the formation of the pre-catalytically activated spliceosome or B complex requires the joining of the preassembled U4atac/U6atac·U5 tri-snRNP in minor spliceosomes, opposed to the U4/U6·U5 tri-snRNP in major spliceosomes to facilitate intron excision.

1.8 Pre-mRNA splicing and disease

Pre-mRNA splicing is controlled by a complex regulatory system that consists of numerous sequence elements and *trans*-acting splicing factors; therefore, it is not surprising that this complexity makes the splicing machinery susceptible to sequence polymorphisms and deleterious mutations, many of which are implicated in the aetiologies of numerous human diseases, including cancer (Scotti and Swanson, 2016; Singh and Cooper, 2012; Padgett, 2012). There are over 15,000 tumour-associated splice variants in a wide variety of cancers (Padgett, 2012). One frequently mutated cancer-splicing factor is SF3B1.

The SF3B complex constitutes seven components, SF3B1-7 with distinct domains. SF3B1 is the largest subunit of the SF3B complex and functions by serving as a core component of the U2 snRNP, which is critical for BP recognition and for the early stages of spliceosome assembly (Will and Luhrmann, 2011). Structurally, the N-terminus of SF3B1 has a stretch of U2AF ligand motifs which specifically interacts

with proteins such as U2AF2 and Tat-SF1 (Thickman et al., 2006; Kielkopf et al., 2004). Two-thirds of the C-terminus consists of 22 non-identical HEAT (Huntingtin, elongation factor 3, subunit An of protein phosphatase 2A, and phosphatidylinositol 3-kinase (PI3K) target of rapamycin 1) repeats, which form a superhelix, providing major scaffolding for the U2 snRNP to support interactions with other SF3B subunits including SF3B6, where together they form a composite RNA-binding platform for BP recognition (Cretu et al., 2016; Bertram et al., 2017).

In human diseases, almost all mutations in the *SF3B1* gene are in the HEAT repeats. The HEAT domain is a hotspot for mutation being implicated as common drivers of hematologic malignancies. Somatic SF3B1 mutations are found in approximately 30% of patients with myelodysplastic syndrome (MDS), 20% of patients with myelodysplastic/myeloproliferative neoplasm (MDS/MPN) (Cazzola et al., 2013), and in 15% of patients with chronic lymphocytic leukaemia (CLL) (Scott and Rebel, 2013). More recently, high incidence of SF3B1 mutations have been identified in some solid tumours, such as various pigmented tumours including uveal melanoma (Ellis et al., 2012), leptomeningeal melanoma (Küsters-Vandevelde et al., 2016), blue nevus-like cutaneous melanoma (Kong et al., 2014), and neuroblastomas that arise following chromothripsis (Molenaar et al., 2012), oestrogen receptor-positive breast cancers (Banerji et al., 2012), pancreatic ductal adenocarcinoma (Biankin et al., 2012), prostate cancer (Armenia et al., 2018), prolactinomas (Li et al., 2020), acute myeloid leukaemia (Yu et al., 2020) and many others (Rose et al., 2018; Je et al., 2013).

1.9 Emerging links between splicing and transcription

Classically, splicing was understood to happen at the post-transcriptional level. However, over the years numerous studies have revealed that most splicing events occur co-transcriptionally, meaning splicing happens as pol II is still transcribing the gene, before transcription termination (Cramer et al., 1997; Beyer and Osheim, 1988; Kornblihtt et al., 2004; Bentley, 2014; Carrocci and Neugebauer, 2019). Advancements in methods for imaging and the development of sensitive biochemical assays, and genome-wide profiling of nascent transcriptome and pol II occupancy in diverse species has helped to uncover the extent of co-transcriptional splicing and the roles splicing factors play in connecting splicing and transcription.

In yeast, the extent of splicing-dependent pol II pausing was first shown by purifying chromatin-associated nascent RNA and using high-density tiling microarrays to analyse the amount of splicing that occurred before transcription was complete (Carillo Oesterreich et al., 2010). This revealed that over 80% of pre-mRNAs are spliced before transcription termination, suggesting pol II pauses in terminal exons to allow enough time for co-transcriptional splicing to occur. The inhibition of splicing either by introducing a temperature-sensitive mutant allele of the RNA helicase Prp5, or by introducing mutations in the BP sequence or the U2 snRNA increases pol II occupancy on introns in a Cus2p-dependent manner, suggesting the activation of a transcription elongation checkpoint to allow spliceosome assembly (Chathoth et al., 2014). Genome-wide analyses using NET-seq has revealed that pol II pauses/slows down near splice sites in both mammalian cells and yeast, indicating the conserved influence of splicing on transcription from lower to higher eukaryotes (Harlen et al., 2016; Mayer et al., 2015; Nojima et al., 2015).

In higher eukaryotes, studies have implicated the splicing process in transcription elongation. The first splicing factor identified to have roles in transcription was SRSF2, that when depleted causes pol II accumulation in the body of some genes (Lin et al., 2008). More recently, SRSF2 has been found to be involved in the regulation of pol II pausing by helping to dissociate P-TEFb from the inhibitory 7SK complex to facilitate pol II pause release and transcription progression (Ji et al., 2013; Tripathi et al., 2012). The presence of the splicing factor, U2AF2 was found to significantly and specifically reduce the dwell time of pol II near promoter regions indicating splicing factors may stimulate transcription progression (Ujvári and Luse, 2004). The U2 snRNP helps recruit the transcription elongation factor Tat-SF1, which in turn recruits P-TEFb to facilitate transcription elongation (Fong and Zhou, 2001). The release of paused pol II can be aided by transcription elongation factors such as TFIIS (Churchman and Weissman, 2011). Interactions between the U2 snRNP and Tat-SF1 may be through SF3 complexes, as the yeast Tat-SF1 orthologue Cus2 interacts with SF3A66 and SF3B1 (Loerch et al., 2019; Talkish et al., 2019; Yan et al., 1998). Specifically, the function of SF3B1 has been shown to regulate global nascent RNA synthesis, pol II pause release, and P-TEFb recruitment to promoter-proximally paused pol II (Caizzi et al., 2021). The ability of both SF3B1 and P-TEFb to engage with one another indicates that there is a two-way relationship between splicing and transcription. The evidence for splicing influencing transcription is increasing, but the molecular mechanisms underlying this remain unclear.

1.10 Non-canonical roles of splicing factors

The SF3B complex, notably SF3B1, is emerging as an important splicing factor involved in roles beyond splicing. Nuclear pre-mRNA splicing is not a solitary process but is coupled to other gene expression steps, including transcription, 5' capping, 3' end processing, and mRNA nuclear export.

U2-snRNP-dependent roles of SF3B implicate the complex in 3' end processing of pre-mRNA. The U2 snRNP *via* SF3B3 physically interacts with the cleavage and polyadenylation specificity factor (CPSF) 160 to positively couple and regulate splicing to pre-mRNA 3' end formation (Kyburz et al., 2006). Interactions between the U2 snRNP and CPSF is also important for the 3' end processing of pre-mRNAs which contain no introns such as replication-dependent histone pre-mRNAs. The U2 snRNP *via* SF3B1 contacts, both *in vivo* and *in vitro*, a 22 nucleotide RNA element present in the majority of histone pre-mRNAs with no sequence similarity to the BP sequence of pre-mRNA introns, in conjunction with the ATP-dependent RNA helicase Prp43 bound at the same site, to stimulate U7-snRNP-dependent cleavage. Thus, the U2 snRNP plays a non-splicing role in histone mRNA maturation (Friend et al., 2007). Further, SF3B1-enhanced cross-linking and IP (eCLIP) experiments indicate that SF3B1 binds several different sequence motifs that are unique to one another at the sequence level on exons, indicating SF3B1 binds intronless and spliced mRNAs at sites distict from BP sequences of pre-mRNA introns (Wang et al., 2019). SF3B1 also binds the purine-rich ceramide-responsive RNA *cis*-element 1 (CRCE1) located in an exon of Bcl-x pre-mRNA (Massiello et al., 2006).

SF3B is also implicated in mRNA export. After the initiation of transcription and during co-transcriptional splicing of pre-mRNA, two multimeric complexes, the

transcription-export (TREX) complex and the exon junction complex (EJC), are gradually deposited on the processing pre-mRNA molecules, and both engage in subsequent mRNA export (Cheng et al., 2006). Recently, the SF3B complex was found to be involved in the recruitment of the TREX complex onto both spliced and intronless mRNAs, implicating SF3B in RNA export (Wang et al., 2019). Specifically, knockdown of SF3B1 causes nuclear retention for both spliced and intronless mRNA molecules. The disruption of the U2 snRNP using an antisense morpholino did not impair but promoted SF3B and TREX interaction and mRNA export indicating the role played by SF3B here is independent of the U2 snRNP. In addition, other U2 snRNP protein components including the SF3A complex are dispensable for the SF3B and TREX interaction, emphasising that SF3B has non-canonical roles beyond its function in splicing (Sun, 2020).

1.11 Aims of the present work

It has become clear that gene expression relies on extensive and dynamic crosstalk between the transcription and RNA processing machineries. The SF3B complex as part of the U2 snRNP was previously thought to be limited to splicing. However, important non-canonical U2-dependent and U2-independent roles are emerging for the SF3B complex. The functions of the SF3B component, SF3B1, intimately link splicing and transcription. However, the molecular mechanisms underlying some of the links between splicing and transcription remain unclear.

The present work used human cells to study the complex and dynamic molecular mechanisms involved in the transcription of human genes by investigating the molecular mechanisms governing the links between splicing and transcription.

I explored this by answering the following key research questions using a range of molecular analyses:

- What is the molecular mechanism behind transcription and RNA processing crosstalk mediated by SF3B1 and CDK9?
  - A small molecule that selectively inhibits SF3B1 was used to validate the effect of rapid SF3B1 inhibition on splicing and transcription.

- What is the effect of SF3B1 and CDK9 inhibition on their subcellular localisation and that of interactors?
  - Rapid SF3B1 and CDK9 inhibition were used to assess and compare the cellular fates of SF3B1 and P-TEFb following their inhibition.

- What are the effects of other splicing inhibitors on transcription?
  - Rapid SF3B1 and general splicing inhibition were used to assess and compare the potencies of splicing inhibitors on splicing as well as whether they could impair transcription in the same mechanistic way as SF3B1.

- Which transcriptional kinases and protein phosphatases regulate SF3B1 phosphorylation?
  - Rapid pharmacological and selective CDK inhibitions were used to evaluate whether transcriptional kinases and protein phosphatases target select SF3B1 residues to regulate its function.

Chapter 2. Materials and methods

2.1 Cell culture and drug treatments

HeLa and human embryonic kidney (HEK) 293 cells obtained from ATCC (ATCC® CCL-2™ and ATCC® CRL-1573™, respectively), and HEK293 derived CDKas cells were grown and maintained in Dulbecco's modified Eagle's medium (DMEM) supplemented with 10% heat-inactivated fetal bovine serum (FBS; Gibco, Invitrogen), 100 U/ml penicillin, 100 μg/ml streptomycin and 2 mM L-glutamine at 37°C in a humidified atmosphere containing 5% CO2.

All cells were seeded and grown to 80% confluence on 60 mm, 100 mm, or 150 mm plates 24 h before experiments. HeLa and HEK293 cells were treated with either DRB (Sigma Aldrich), PlaB (Cayman Chemical), Herboxidiene (Cayman Chemical), Isoginkgetin (Sigma Aldrich), Madrasin (Cayman Chemical), Camptothecin (Sigma Aldrich), Bortezomib (Cayman Chemical), Leptomycin B (Cell Signaling), O4I2 (Tocris Bioscience), Tautomycetin (Tocris Bioscience), or Calyculin A (Cayman Chemical) for times ranging between 15 minutes to 24 hours. CDKas cells were treated with either 1-NA-PP1 (Cayman Chemical) or 1-NM-PP1 (Cayman Chemical) for 30 minutes. A list of all drugs with treatment conditions used in this study can be found in Table 1. The resuspension vehicle for all drugs except for Leptomycin B was DMSO. The resuspension vehicle for Leptomycin B was ethanol. The resuspension vehicles served as negative controls in experiments.

Table 1. Table of drugs and range of treatment conditions used in this study

Drug	Treatment concentration (μM)	Treatment time (hours)
5,6-Dichlorobenzimidazole 1-β-D-ribofuranoside (DRB) (D1916, Sigma Aldrich)	100	0.5 – 4
Pladienolide B (PlaB) (16538, Cayman Chemical)	0.1 – 1	0.5 – 24
Herboxidiene (HB) (25136, Cayman Chemical)	1	0.5 – 4
Isoginkgetin (Iso) (548-19-6, Sigma Aldrich)	30	0.5 – 6
Madrasin (Mad) (S7537, Cayman Chemical)	90	0.5 -1
Camptothecin (CPT) (7689-03-4, Sigma Aldrich)	25	1
Bortezomib (Bort) (10008822, Cayman Chemical)	1	1
Leptomycin B (LMB) (9676S, Cell Signaling)	0.020	1
Oct4 inducible compound 2 (O4I2) (5664, Tocris Bioscience)	1 – 30	1
Tautomycetin (TT) (2305, Tocris Bioscience)	0.025 - 0.100	0.5 -4
LB-100 (S7537, Selleckchem)	0.0025	1 – 4
Calyculin A (CA) (19246, Cayman Chemical)	0.0005 - 0.0025	0.5 -4
1-NA-PP1 (NA) (10954, Cayman Chemical)	15	0.5
1-NM-PP1 (13330, Cayman Chemical)	7.5	0.5

2.2 Total RNA purification and reverse transcription PCR

RNA were extracted from HeLa or HEK293 cells using a RNeasy mini kit (Qiagen) according to the manufacturer's instructions. Reverse transcription (RT) of RNA were performed by first mixing RNA (500 ng), random hexamers (50 – 250 ng), and 1 μl of dNTPs (10 mM), topped up with RNase-free water to 13 μl. The mix then heated at 65°C for 5 minutes, incubated on ice for 1 minute, pulse centrifuged, then

mixed with reagents from the SuperScript III reverse transcriptase kit (Invitrogen) complemented with 0.5 µl RNaseOUT™ Recombinant Ribonuclease Inhibitor (10777019, Invitrogen), following the manufacturer's instructions. The following temperature parameters were used for cDNA synthesis: 25°C for 5 minutes, 50°C for 60 minutes, then 70°C for 15 minutes. The cDNA was then diluted to a final volume of 50 µl in ddH_2O.

For PCR, Phusion High-Fidelity DNA polymerase (NEB) was used according to the manufacturer's instructions to amplify 10 µg of cDNA fragments. A list of primers used for RT-PCR can be found in Table 2.

For quantitative RT-PCR (RT-qPCR) analysis, 1 µl of cDNA (50 µl cDNA) was diluted in 499 µl of ddH_2O. Each RT-qPCR reaction contained: 1 µl cDNA, 3 µl RNase/DNase-free water (204245, Qiagen), and 5 µl 2x QuantiTect SYBR Green qPCR mix (204245, Qiagen). Each reaction was run in technical triplicates. The qPCR samples were run on a Rotor-Gene Q (Qiagen), using the Rotor-Gene Q Series Software, and cycling parameters: 95°C for 15 minutes, 40 cycles of 94°C for 15 seconds, 57°C for 15 seconds, 72°C for 15 seconds, with the last cycle ending with a 10 minute melt curve from 50°C to 99°C, with a 1°C increment increase every 5 seconds. Relative fold gene expression was measured using the $2^{-\Delta\Delta CT}$ method. ΔCt values were determined by normalising the average Ct (copies/µl) of the target gene to the housekeeping average Ct. Average ΔCt of the control group was then determined. ΔΔCt values were determined by normalising the ΔCt of each target to the average ΔCt of the control group. The normalised expression ratio (relative mRNA levels) of the target was determined using base 2 with ΔΔCt as the negative exponent. Primer efficiencies for each reaction were not determined. Each primer was assumed to have an

amplification efficiency of 100%, signified by base 2 to measure normalised expression ratios.

1. ΔCt = Average Ct (target) – Average Ct (housekeeping)
2. ΔΔCt = ΔCt (target) – Average Ct (control group)
3. Normalised expression ratio = $2^{-\Delta\Delta Ct}$

Welch's tests were performed to determine the P-values for differences observed between non-treated and treated conditions. A list of primers used for RT-qPCR can be found in Table 2.

Table 2. List of primers used in this study for RT-PCR and RT-qPCR

Name	Forward primer	Reverse primer
RT-PCR		
BRD2 E4/5	CAAAATTATAAAACAGCCTATGGACATG	TTTTCCAGCGTTTGTGCCATTAGGA
DNAJB1 E2/3	GGCCTGATGGGTCTTATCTATGG	AATGAGGTCCCCACGTTTCTCGGGTGT
7SK	CTGATCTGGCTGGCTAGGCGGG	GAAGACCGGTCCTCCTCTATCGG
RT-qPCR		
Pre-rRNA	CCTGCTGTTCTCTCGCGCGTCCGAG	AACGCCTGACACGCACGGCACGGAG
Nascent KPNB1	GAGGAGTGTGCACGGATGCTGAA	CCAAGATGGCCGATGTTATGG
7SK	CTGATCTGGCTGGCTAGGCGGG	GAAGACCGGTCCTCCTCTATCGG

2.3 Chromatin immunoprecipitation (ChIP)

HeLa cells were cross-linked using 1% formaldehyde for 10 minutes at room temperature following drug treatment. Crosslinking reaction was stopped by adding glycine (final concentration: 125 mM) to the cells for 5 minutes at room

temperature. Cells were washed twice with cold PBS, scraped, then centrifuged (1500 rpm, 5 minutes, 4°C). After centrifugation, cells were lysed in lysis buffer (10 mM Tris pH 8.0, 0.25% Triton X-100, and 10 mM EDTA) supplemented with protease inhibitor cocktail (cOmplete™, EDTA-free Protease Inhibitor Cocktail, Roche) on ice for 10 minutes, centrifuged (1500 x g, 5 minutes, 4°C), washed with wash buffer (10 mM Tris pH 8.0, 200 mM NaCl, and 1 mM EDTA) supplemented with protease inhibitor cocktail (Roche), then centrifuged again (1500 x g, 5 minutes, 4°C). Pellet was resuspended in sonication buffer (10 mM Tris pH 8.0, 100 mM NaCl, and 1 mM EDTA, and 0.1% SDS) supplemented with protease inhibitor cocktail (Roche), then chromatin DNA sheared at high amplitude for 7 cycles using the Bioruptor Pico sonication device (Diagenode) or 30 cycles 30 seconds on and 30 seconds off using the QSonica Thermocube Q800R. The sheared chromatin was precleared with 10 µl of Dynabead Protein G (Invitrogen) for 30 minutes at 4°C. Approximately 100 µg of pre-cleared chromatin was incubated overnight with 1 µg of negative control anti-IgG (sc-2027, Santa Cruz Biotechnology), 5 µg of anti-RNA pol II (D8L4Y, Cell Signaling), and 3 µg anti-CDK9 (D-7) antibody (sc-13130, Santa Cruz Biotechnology), respectively. Fifteen microlitres of a slurry of Dynabeads Protein G were rotated at 16 rpm overnight at 4°C in 15 µl RIPA buffer containing 4 mg/mL of BSA. Antibody bound chromatin was incubated with blocked beads for 1 hour at 4°C. Following incubation, the supernatant of IgG immunoprecipitants were saved to use as total input of chromatin and was processed with the eluted immunoprecipitates. Immunoprecipitants were washed three times with RIPA buffer, three times with high-salt wash buffer (10 mM Tris pH 8.0, 500 mM NaCl, 1 mM EDTA, 1% Triton X-100, 0.1% sodium deoxycholate, and 0.1% SDS), twice with LiCl wash buffer (10 mM Tris pH 8.0, 250 mM LiCl, 1 mM EDTA, 1% NP-40, and 1% sodium deoxycholate),

and twice with TE (10 mM Tris pH 7.5, and 1 mM EDTA). Immunoprecipitants were eluted twice by suspending beads in 50 µl elution buffer (100 mM NaHCO3 1% SDS, and 10 mM DTT) and incubating with 1400 rpm horizontal agitation for 15 min at 25°C. RNA was then degraded with 10 µg RNase A for 30 minutes at 37°C, then crosslinks reversed with NaCl (final concentration: 200 mM) for 5 to 8 hours at 65°C. Chromatin fragments were precipitated with the addition of 2.5 times volume of ethanol overnight at -20°C. Precipitated chromatin fragments were collected by microcentrifugation (14,000 rpm, 20 minutes, 4°C) then dissolved in 100 µl TE, 25 µL 5x Proteinase K buffer (50 mM Tris pH 7.5, 25 mM EDTA, and 1.25% SDS), and 1.5 µl Proteinase K (Sigma) and incubated for 2 hours at 45°C. The DNA was then purified using the MiniElute PCR Purification Kit (Qiagen) according to the manufacturer's instructions and eluted in 50 µl of EB.

ChIP samples were analysed by quantitative PCR, with each reaction mix containing 1 µl of purified ChIP DNA template, 10 pmol/µl of each primer pair, 3 µl of nuclease-free water, 5 µl of 2x QuantiTect SYBR Green kit (Qiagen) reagent. For each set of qPCR primer reactions, a standard curve was made using known amounts of genomic DNA (serial dilutions of 1:5, 1:25, 1:125, and 1:625 using input DNA sample) and a primer pair for an efficiency that is set to 1 for downstream normalisation. Both control DNA samples and immunoprecipitated samples were run in technical triplicate. The qPCR samples were run on a Rotor-Gene Q (Qiagen), using the Rotor-Gene Q Series Software, and cycling parameters: 95°C for 15 minutes, 40 cycles of 94°C for 15 seconds, 57°C for 15 seconds, 72°C for 15 seconds, with the last cycle ending with a 10 minute melt curve from 50°C to 99°C, with a 1°C increment increase every 5 seconds.

The Ct value for each sample were quantified relative to the standard and subtracted by the IgG control Ct value. The resulting values are the percent input being pulled down. The position of amplicons are shown for each gene in the respective ChIP graph figure. Experiments were repeated three times unless specified. Error bars represent ± SEM (standard error of the mean) of three independent experiments. Dunnet's tests were performed to determine P-values for differences observed between untreated and treatment conditions. Primers used in ChIP-qPCR can be found in Table 3.

Table 3. List of primers used in this study for ChIP-qPCR

Name	Forward primer	Reverse primer
ChIP-qPCR		
KPNB1 TSS	ACAGCCTCCCTTCCTTCTTTC	TTACTTCCTCCCTCCAAATGGG
KPNB1 TSS +3.2	GCCCAGAGAACAAGAAATCG	GGAATGGACAAGCTGTGTTG
KPNB1 pA -4.8	CTGAGGAAACTGAAGAACCAAG	GAAGGCAGTGCTTGCCAGAAT
KPNB1 pA -2.9	GAGGAGTGTGCACGGATGCTGAA	CCAAGATGGCCGATGTTATGG
KPNB1 pA -0.4	TAGTTACCGTCTGCTTGGGAAGATG	CCTCTGACAGCAAGTCCAACATT
KPNB1 pA +1.4	GACTCATCACACCAAGGTCAC	GATAGTGCTGGGAAGGAAATGG
KPNB1 pA +2.6	GTACATCTCAGCTTTGGCATATG	GCCCAGAACATAGCAGGCATTGC
KPNB1 pA +4.1	GTTTCACCGTGTTAGCCAGGATGG	CCACAGCCATGTTCATTTCTGC
SLCO4A1 TSS	CCAGCGGATGAATGAAGCG	ACTCACCGTCCCCGTCTC
LDLR TSS	AATCACCCCACTGCAAACTC	TAGCTGGAAACCCTGGCTTC
Neg	TGGTACAACCACAGCTCAGTG	AAGCTGGACATGGTTGTGTG

2.4 Chromatin and nucleoplasm purification (NET-seq)

HeLa cells were washed once with cold PBS, harvested *via* scraping, then centrifuged (420 x g, 5 minutes, 4°C). Pellets were resuspended in 4 ml of HLB+N (10mM Tris pH 7.5, 10 mM NaCl, 2.5 mM MgCl2 and 0.5% (v/v) Nonidet P-40 (NP-40)) and incubated on ice for 5 minutes. The cell pellets were gently underlaid with 1 ml HLB+NS (10 mM Tris pH 7.5, 10 mM NaCl, 2.5 mM MgCl2, 0.5% (v/v) NP-40 and 10% (w/v) Sucrose) then centrifuged (420 x g, 5 minutes, 4°C). The nuclear pellets were then resuspended in 120 µl NUN1 buffer (20 mM Tris pH 7.9, 75 mM NaCl, 0.5 mM EDTA and 50% (v/v) Glycerol), then transferred to 1.2 ml of NUN2 buffer (20 mM HEPES-KOH pH 7.6, 300 mM NaCl, 0.2 mM EDTA, 7.5 mM MgCl2, 1% (v/v) NP-40 and 1 M Urea) supplemented with protease inhibitor cocktail (Roche) and PhosSTOP (Roche) and incubated on ice for 15 minutes with a frequent vortex step every 3 minutes. Nuclear fractions were centrifuged (16,000 x g, 10 minutes, 4°C) to isolate chromatin from nucleoplasm content. Chromatin pellets were washed with PBS then treated with 1 µl of Benzonase in 100 µl nuclease-free water and incubated at 37°C for 10 minutes with agitation (1,400 rpm) to digest accessible nucleic acids.

2.5 Cytoplasm purification

HeLa cells were washed twice with cold PBS then scraped into 15 ml tubes and centrifuged (1,000 rpm, 5 minutes, 4°C). The pellet was resuspended thoroughly in 1 ml of Lysis buffer B (10 mM Tris-HCl (pH 8-8.4), 140 mM NaCl 1.5 mM MgCl2, and 0.5% NP40) supplemented with protease inhibitor cocktail (Roche) and PhosSTOP (Roche) by slow pipetting and then transferred to a 1.7 ml tube. The lysate was centrifuged (1,000 xg, 3 minutes, 4°C) then 500 µl of the supernatant of the

unpurified cytoplasmic fraction was transferred to a new tube. Purified cytoplasmic fraction was achieved by centrifugation (10,000 xg, 1 minute, 4°C).

2.6 Whole cell protein extraction

HeLa cells were incubated on ice for 5 minutes, then washed twice with cold PBS. Cells were scraped, centrifuged (3,000 x g, 5 minutes, 4°C), then lysed in 100 µl RIPA buffer (10 mM Tris pH 8.0, 150 mM NaCl, 1 mM EDTA, 1% Triton X-100, 0.1% sodium deoxycholate, and 0.1% SDS) supplemented with protease inhibitor cocktail (Roche) and PhosSTOP (Roche) on ice for 30 minutes, with a frequent vortex step every 10 minutes. Cell lysates were centrifuged (14,000 x g, 15 minutes, 4°C) and their supernatants collected.

2.7 Co-immunoprecipitation

For each sample and IgG control: 120 µl of Dynabeads M-280 Sheep anti-mouse IgG (Thermo Fisher) or a 1:1 mix of 20 µl of Dynabeads Protein A (Invitrogen) and 20 µl of Dynabeads Protein G (Invitrogen) beads were pre-blocked overnight at 4°C on a wheel at 16 rpm in 1 ml of PBS supplemented with 0.5% BSA. The next day, the beads were washed three times in IP buffer (25 mM Tris–HCl pH 8.0, 150 mM NaCl, 0.5% NP-40, 10% Glycerol, 2.5 mM MgCl2), before being incubated for two hours at 4°C on a wheel at 16 rpm in 600 µl of IP buffer containing the appropriate conjugate antibody and protease inhibitor cocktail (Roche). For Dynabeads M-280 beads, 5 µg of SF3B1/SAP155 (D221-3, MBL International) was added. For Dynabeads A/G, 5 µg of Cyclin T1 (81464, Cell Signaling, SNW1 (NB100-2367, Novus Biologicals),

SRSF2 (ab204916, abcam), and c-MYC (sc-764, Santa Cruz Biotechnology) was added. During the 2 hours of antibody incubation, a 70–80% confluent 15 cm dish of HeLa cells was washed twice with ice-cold PBS and scrapped with ice-cold PBS supplemented with protease inhibitor cocktail. The cells were pelleted at 500 g for 5 minutes at 4°C. The pellets were re-suspended in 800 µl of Lysis buffer (50 mM Tris–HCl pH 8.0, 150 mM NaCl, 1% NP-40, 10% glycerol, 2.5 mM MgCl2, protease inhibitor cocktail, PhosSTOP (Sigma-Aldrich), 1× PMSF (Sigma-Aldrich), and 25–29 units of Benzonase (Merck Millipore)) and incubated at 4°C on a wheel at 16 rpm for 30 minutes. Benzonase was not added to the Lysis buffer for nuclease-free samples, these samples were rather sonicated using a Bioruptor Pico sonication device (Diagenode) for 5 cycles 30 seconds on and 30 seconds off at 4°C following 30 minutes of lysis. Following lysis, samples were centrifuged for 15 minutes at 13,000 g at 4°C for their supernatant containing proteins, which was then diluted in 800 µl of Dilution buffer (150 mM NaCl, 10% glycerol, 2.5 mM MgCl2, protease inhibitor cocktail, PhosSTOP, and 1× PMSF). The beads conjugated with antibodies were washed three times with IP buffer supplemented with protease inhibitor cocktail before being incubated with 1 mg of proteins at 4°C on a wheel at 16 rpm for 2 hours. The beads were washed three times with IP buffer supplemented with protease inhibitor cocktail and three times with IP buffer without NP-40 supplemented with protease inhibitor cocktail. Proteins were eluted in 40 µl of 1× LDS plus 100 mM DTT for 10 minutes at 70°C. Western blots were performed with NuPAGE Novex 3–8% Tris-Acetate Protein Gels (Life Technologies).

2.8 Cellular fraction co-immunoprecipitation

For each sample and IgG control: 120 µl of Dynabeads M-280 Sheep anti-mouse IgG (Thermo Fisher) or a 1:1 mix of 20 µl of Dynabeads Protein A (Invitrogen) and 20 µl of Dynabeads Protein G (Invitrogen) beads were washed three times with 1 ml of cold NET-2 buffer (50 mM Tris-HCl pH 7.4, 150 mM NaCl and 0.05 % NP-40) by vortex at room temperature. Beads were then resuspended and blocked in 120 µl of cold NET-2 buffer supplemented with 0.5% BSA for 8 hours. Beads were washed three times using 1 ml cold NET-2 buffer after blocking. For each IP, 5 µg of the appropriate antibody or for IP control, 5 µg of mouse IgG antibody were diluted added to 600 µl of NET-2 buffer containing protease inhibitor cocktail (Roche) and added to washed beads, then incubated at 4°C on a wheel at 16 rpm overnight. For Dynabeads M-280 beads, 5 µg of SF3B1/SAP155 (D221-3, MBL International) was added. For Dynabeads A/G, 5 µg of Cyclin T1 (81464, Cell Signaling) was added. The next day, during antibody incubation, chromatin, nucleoplasm, or cytoplasm fractions were purified as described in sections 2.5 and 2.6, respectively. The purified fractions were quantified with Bradford assay, then 1 mg of protein diluted in 800 µl of cold NET-2 buffer supplemented with protease inhibitor cocktail and placed on ice. Once purified fractions were prepared, the beads conjugated with antibodies were washed two times with cold NET-2 buffer by vortex, then the 1 mg purified fractions diluted in cold NET-2 buffer were added and incubated at 4°C on a wheel at 16 rpm for 1 hour. The beads were washed eight times by inverting the tubes with cold NET-2 buffer supplemented with protease inhibitor cocktail and once with cold NET buffer (50 mM Tris-HCl pH 7.4 and 150 mM NaCl) supplemented with protease inhibitor cocktail. Proteins were eluted in 40 µl of 1× LDS plus 100

mM DTT for 10 minutes at 70°C. Western blots were performed with NuPAGE Novex 3–8% Tris-Acetate Protein Gels (Life Technologies).

2.9 5-Ethynyl uridine (5-EU) labelling

HeLa cells were seeded on 13 mm sterile round coverslips overnight at 37°C to get 60-70% confluent cells. To measure *de novo* RNA synthesis, 5-EU labelling's were performed on HeLa cells using the Click-iT™ RNA Alexa Fluor™ 488 Imaging Kit (C10329, Invitrogen) according to the manufacturer's instructions. 5-EU labelled cells on coverslips were sealed to glass slides using nail polish then left overnight, protected from light at room temperature to dry. Once dry, glass slides were stored at 4°C, protected from light until imaging. Cells were detected and imaged by a Zeiss 880 Airyscan microscope. Fluorescent intensity was analysed and quantified with ImageJ (version 1.53q) by first using the DAPI channel ($\lambda_{Ex}/\lambda_{Em}$ (with DNA) = 350/461 nm) image to define the nucleus, then GFP channel ($\lambda_{Ex}/\lambda_{Em}$ = 495/519 nm) to measure the fluorescent intensity within the nucleus. Data were plotted by violin plot with GraphPad Prism 9.5 software with the following settings: min to max values with the median and 25-75 percentile range.

2.10 Immunofluorescence

HeLa cells were seeded on 13 mm sterile round coverslips overnight at 37°C to get 60-70% confluent cells. Following respective drug treatments, cells on coverslips were washed twice with PBS then fixed using 4% paraformaldehyde (Sigma Aldrich) for 15 minutes at room temperature. Coverslips were washed twice with PBS then

permeabilised and blocked in blocking solution (0.1% Triton X-100, 10% FBS, and PBS) for 30 minutes at room temperature. Blocking solution was removed and coverslips were incubated with primary antibodies diluted in blocking solution overnight at 4°C. Following incubation, primary antibody solution was removed, and coverslips washed three times with PBS for 5 minutes each. Coverslips were then incubated with secondary antibody diluted in solution (1% FBS and PBS) for 1 hour at room temperature. Following incubation, secondary antibody solution was removed, and coverslips washed three times with PBS for 5 minutes each. Coverslips were incubated in Hoechst 33342 solution (62249, Thermo Fisher) (diluted 1:1,000 in PBS) protected from light for 10 minutes at room temperature. Hoechst 33342 solution was removed then coverslips were washed twice with PBS and mounted upside down on a drop of FluorSave Reagent (345789, Millipore) on a clean glass slide. Coverslips were sealed to glass slides using nail polish then left overnight, protected from light at room temperature to dry. Once dry, glass slides were stored at 4°C, protected from light until imaging. Cells were detected and imaged by a Zeiss 880 Airyscan microscope. Fluorescent intensity was analysed and quantified with ImageJ (version 1.53q) by first using the DAPI channel ($\lambda_{Ex}/\lambda_{Em}$ (with DNA) = 350/461 nm) image to define the nucleus, then GFP channel ($\lambda_{Ex}/\lambda_{Em}$ = 495/519 nm) to measure the fluorescent intensity within the nucleus. Data were plotted by box-and-whisker or violin plot with GraphPad Prism 9.5 software with the following settings: min to max values with the median and 25-75 percentile range. All primary and secondary antibodies used are listed in Table 4. Antibody validation is provided on the manufacturer's website.

Table 4. Primary and secondary antibodies used for immunofluorescence

Primary Antibody	Concentration	Conditions
Rabbit anti-G3BP1 (17798, Cell Signaling)	1:500	Overnight 4°C
Mouse anti-CDK9 (D-7) (sc-13130, Santa Cruz Biotechnology)	1:500	Overnight 4°C
Rabbit anti-SC35 (SRSF2) (ab204916, abcam)	1:100	Overnight 4°C
Secondary Antibody	**Concentration**	**Conditions**
Goat anti-Mouse IgG (H+L) Secondary Antibody, DyLight™ 488 (35502, Invitrogen)	1:500	1 hour RT
Goat anti-Rabbit IgG (H+L) Highly Cross-Abssorbed Secondary Antibody, Alexa Fluor™ Plus 488 (A-11034, Invitrogen)	1:500	1 hour RT

2.11 Western blot analysis

Western blot analyses were performed using 25 µg of proteins from whole cell protein extractions. For chromatin, nucleoplasm, or cytoplasm purifications, 10 µg of proteins were used. For western blots directly comparing subcellular fractions, cell nuclei equivalents were used based on the volume the fraction was diluted in.

All samples from were boiled in NuPAGE LDS Sample buffer (Thermo Scientific) for 10 minutes at 70°C with 1400 rpm agitation. Electrophoretic separation of all sample proteins on NuPAGE 4-12% Bis-Tris protein gel (Invitrogen) then transferred to nitrocellulose membranes (Thermo Scientific) using a wet-transfer unit (Bio-rad) at 30 V for 16 hours at 4°C in Tris-Glycine transfer buffer (200 mM Tris, 1.5 M glycine) with 20% ethanol. Membranes were blocked in Tris Buffered Saline with 0.05% Tween-20 (TBS-T) containing 5% (w/v) BSA (A3059, Sigma Aldrich) for 1 hour with gentle rocking. Primary antibodies were diluted in blocking

solution and incubated overnight at 4°C. The membranes were washed 4 times for 10 minutes each in TBS-T before incubating with the appropriate secondary antibodies diluted in TBS-T containing 5% (w/v) BSA for 1 hour with gentle rocking at room temperature. The membranes were washed 3 times for 10 minutes each in TBS-T, followed by a final wash in TBS without Tween-20.

An iBright FL1000 (Thermo) was used to visualise the chemiluminescence of proteins of interest. Band intensities were quantified using the Image Studio Lite software version 5.2.5 (LI-COR Bioscience). All primary and secondary antibodies used are listed in Table 5. Antibody validation is provided on the manufacturer's website.

Table 5. Primary and secondary antibodies used for western blot analysis

Primary Antibody	Concentration	Conditions
Rabbit anti-RNA pol II (D8L4Y, Cell Signaling)	1:1,000	Overnight 4°C
Rabbit anti-Phospho-Rpb1 CTD (pSer2) (E1Z3G, Cell Signaling)	1:1,000	Overnight 4°C
Rabbit anti-SF3b155/SAP155 (A300-996A, Bethyl Laboratories)	1:2,000	Overnight 4°C
Rabbit anti-Phospho-SF3B1 Ser129 (PD043, MBL International)	1:1,000	Overnight 4°C
Rabbit anti-Phospho-SF3B1 Thr142 (Tellier et al., 2022, Eurogentec)	1:1,000	Overnight 4°C
Rabbit anti-Phospho-SF3B1 Thr211 (PA5-105427, Invitrogen)	1:1,000	Overnight 4°C
Rabbit anti-Phospho-SF3B1 Thr313 (D8D8V, Cell Signaling)	1:1,000	Overnight 4°C
Rabbit anti-Tat-SF1 (A302-023A, Bethyl Laboratories)	1:2,000	Overnight 4°C
Rabbit anti-CDK9 (ab76320, Abcam)	1:1,000	Overnight 4°C
Rabbit anti-Phospho-CDK9 (pThr186) (2549, Cell Signlaing)	1:1,000	Overnight 4°C
Rabbit anti-Cyclin T1 (ab184703, Abcam)	1:1,000	Overnight 4°C

Rabbit anti-SNW1 (A300-784A, Bethyl Laboratories)	1:1,000	Overnight 4°C
Rabbit anti-c-MYC (sc-764, Santa Cruz Biotechnology	1:1,000	Overnight 4°C
Rabbit anti-SC35 (SRSF2) (ab204916, abcam)	1:1,000	Overnight 4°C
Rabbit anti-BRD4 (A301-985A100, Bethyl Laboratories)	1:1,000	Overnight 4°C
Rabbit anti-MCEF (AFF4) (A302-539A, Bethyl Laboratories)	1:1,000	Overnight 4°C
Rabbit amti-gamma-H2A.X (Ser139) (MA5-33062, Invitrogen)	1:1,000	Overnight 4°C
Mouse anti-U1A (3F9-1F7, Novus Biologicals)	1:1,000	Overnight 4°C
Rabbit anti-Actin (C-11) (sc-1615, Santa Cruz Biotechnology)	1:1,000	Overnight 4°C
Rabbit anti-α-Tubulin (2144S, Cell Signaling)	1:5,000	Overnight 4°C
Rabbit anti-Nucleolin (ab305947), Abcam)	1:10.000	Overnight 4°C
Rabbit anti-Histone H3 (ab1791, Abcam)	1:20,000	Overnight 4°C
Secondary Antibody	**Concentration**	**Conditions**
Goat anti-Mouse IgG HRP conjugate (12-349, Millipore)	1:10,000	1 hour RT
Goat anti-Rabbit IgG HRP conjugate (12-348, Sigma Aldrich)	1:10,000	1 hour RT

Chapter 3. Transcription and RNA processing crosstalk mediated by SF3B1 and CDK9

3.1 Background

Transcription has long been known to affect pre-mRNA splicing but recently it has become apparent that splicing can affect transcription by influencing pol II (Herzel et al., 2017; Tellier et al., 2020a), linking the two processes both physically and functionally (Bentley, 2014; Herzel et al., 2017; Tellier et al., 2020a). Shortly after transcription initiation, pol II becomes promoter-proximally paused, mediated by the repressive actions of NELF and DSIF (discussed in section 1.5). The release of pol II into productive elongation is mediated by the recruitment of the P-TEFb complex comprising Cyclin T1 and the catalytic kinase subunit, CDK9, which phosphorylates NELF and DSIF (Core and Adelman, 2019). The emergence of the RNA from pol II is thought to recruit splicing factors to sites of transcription and there is increasing evidence that these factors in turn influence transcription (Fong and Zhou, 2001). The first splicing factor found to have a direct role in transcription was SRSF2. Depletion of SRSF2 causes pol II to accumulate in the body of some genes (Lin et al., 2008). SRSF2 depletion also causes pol II accumulation at gene promoters and impairs P-TEFb recruitment (Ji et al., 2013).

Splicing inhibitors have recently been developed that inhibit different stages of spliceosome assembly prior to catalysis. These inhibitors are powerful tools to study the effects of the inhibition of a particular stage of splicing on transcription. One class of splicing inhibitors is the pladienolides, a family of natural macrocyclic lactone compounds with potent anti-tumour properties (Kotake et al., 2007). Pladienolide B (PlaB) targets the well-conserved spliceosomal protein, SF3B1,

which is a component of the U2 snRNP (Kotake et al., 2007; Yokoi et al., 2011). PlaB binds to SF3B1 and arrests it in an open conformation (Cretu et al., 2018), preventing the stabilisation of the association of the U2 snRNP with BP sequences in introns (Effenberger et al., 2016). The loss of SF3B1 function caused by PlaB influences pol II by reducing the level of pSer2 of the CTD in human cells (Koga et al., 2015). A recent study where the effect of PlaB on the kinetics of pol II elongation was analysed found that SF3B1 function has a positive effect on pol II transcriptional velocity as it is required for efficient pol II pause release (Caizzi et al., 2021). Cramer and colleagues demonstrated that PlaB affects pol II pause release by causing genome-wide reductions in the occupancy of the P-TEFb subunit, Cyclin T1, and presumably also CDK9, around promoter regions of protein-coding genes in human cells.

An emerging non-canonical function for SF3B1 beyond splicing is therefore to regulate P-TEFb recruitment/stabilisation to promoter-proximally paused pol II. Consistent with this, the transcriptional phenotype of SF3B1 loss overlaps with P-TEFb function. No direct physical interaction between SF3B1 and P-TEFb has been demonstrated (Szklarczyk et al., 2023), suggesting that an auxiliary factor may facilitate their interaction.

A candidate auxiliary factor is the Tat-specific factor 1 (Tat-SF1), a well conserved protein that promotes transcription elongation by binding to proteins that function in transcription, including pol II, P-TEFb and SF3B1 (Parada and Roeder, 1999; Zhou et al., 1998; Fong and Zhou, 2001; Abramczuk et al., 2017; Agafonov et al., 2011; Loerch et al., 2019; Kielkopf et al., 2004). In addition, Tat-SF1 has been implicated in pre-mRNA splicing through protein complexes with SF3B1 that controls intron

retention in ribosomal protein genes (Corsini et al., 2018). Another candidate auxiliary factor is SNW1, a splicing factor that can bind to P-TEFb in the nucleus to regulate pol II-dependent elongation of NF-κB responsive genes or enhance transcription elongation by HIV-1 Tat (Verma et al., 2019; Brès et al., 2005). SNW1 is also a substrate of P-TEFb (Decker et al., 2019). SNW1 as part of the activated spliceosome, B^{act} complex, interacts with SF3B1 (Zhang et al., 2018). In addition, the yeast orthologue of SNW1, Prp45 has been shown to be essential for pre-mRNA splicing through interactions with the ATP-dependent RNA helicase, Prp22 (Albers et al., 2003), and an interactor of SF3B1, the SF3A subcomplex component, Prp11 (Krogan et al., 2006; Bai et al., 2018; Plaschka et al., 2018). Tat-SF1 and SNW1 are therefore both good candidates to examine for involvement in mediating crosstalk between SF3B1 and P-TEFb.

A high-throughput screen from a library of 250,000 chemicals identified compounds which induced the gene expression of OCT4 for the generation of human induced pluripotent stem cells (Cheng et al., 2015). OCT4-inducing compound 2 (O4I2) was found to have SF3B1 as its top interacting molecular target (Gama-Brambila et al., 2021). O4I2 binds and activates SF3B1, resulting in enhanced transcription. Analysis of the effect of this compound on splicing and transcription could therefore provide insight into the role of SF3B1 in transcription.

At the start of my research, the molecular mechanisms underlying the effect of SF3B1 inhibition on P-TEFb recruitment and function were unclear. I therefore analysed the mechanistic effects of both SF3B1 and CDK9 inhibition on transcription by pol II ChIP-qPCR and fractionation, with subsequent *in vivo* interactions determined by co-immunoprecipitation.

3.2 Short SF3B1 inhibition causes rapid defects in pre-mRNA splicing and inhibits nascent transcription in human cells

To determine the effect of short treatment times with PlaB (Figure 3.1A) on pre-mRNA splicing catalysis in human cells, reverse-transcription PCR (RT-PCR) was performed using a concentration of 1 μM PlaB for times ranging between 30 minutes to 4 hours to evaluate total RNA for spliced and unspliced transcripts of the intron-containing genes, *BRD2* and *DNAJB1* (Figure 3.1B, Figure S1B). *BRD2* and *DNAJB1* are among several genes identified as being responsive to sensitive changes in pre-mRNA splicing efficiency for detecting the presence of unspliced intronic sequences in Hela cells (Kotake et al., 2007; Yokoi et al., 2011). In the absence of SF3B1 inhibition, the proportion of introns that were unspliced relative to those that were spliced is low at a ratio of 0.14 for the intron between exons 4 and 5 of *BRD2*, and 0.02 for the intron between exons 2 and 3 of *DNAJB1*. In the presence of SF3B1 inhibition, rapid intron retention ensues within 30 minutes by 279% for the intron between exons 4 and 5 of *BRD2* and by 175% for the intron between exons 2 and 3 of *DNAJB1*, increasing over time.

The effect of the CDK9 inhibitor, DRB, on pre-mRNA splicing catalysis was also assessed by RT-PCR using the same primers (Figure 3.1C). DRB treatment for 1 hour did not cause intron retention. As CDK9 inhibition impairs pol II productive elongation, it is possible that there might not be enough transcripts produced to be able to see any changes, making it difficult to examine pre-mRNA splicing efficiency in these conditions.

To determine whether inhibition of the formation of the spliceosome at an early-stage impairs nascent transcription genome-wide, 5-ethynyl-labelled uridine (5-EU-

labelling) was used to measure *de novo* RNA synthesis following SF3B1 inhibition treatment for 1 hour (Figure 3.1D). Inhibition of SF3B1 on average causes a significant reduction in nascent RNA synthesis to 33% compared to control conditions (Kruskal-Wallis test, $P<0.0001$). In comparison, CDK9 was inhibited for 1 hour and nascent RNA synthesis was reduced to 47% compared to control (Kruskal-Wallis test, $P<0.0001$).

To determine the effects of SF3B1 and CDK9 inhibition on pol II pSer2, a modification mark indicative of active transcription, western blotting was performed on purified whole cell extracts treated for times ranging between 30 minutes to 4 hours (Figure 3.1E). As expected, DRB treatment at a concentration of 100 μM for 4 hours did not significantly affect the total level of pol II but did on average significantly reduce pol II pSer2 by 56% in HeLa cells (Kruskal-Wallis test, $P<0.0001$). PlaB treatment at a concentration of 1 μM for 30 minutes to 4 hours also did not significantly affect the total level of pol II, but consistently resulted in a significant reduction in pol II pSer2 on average by 28% in HeLa cells (Kruskal-Wallis test, $P<0.05$). These PlaB treatment conditions affected pSer2 in both Hela and HEK293 cell lines (Figure S1D).

Taken together, a concentration of 1 μM PlaB for 30 minutes is suitable for inducing rapid pre-mRNA splicing and transcription defects in human cells. This also suggests that PlaB partially inhibits CDK9.

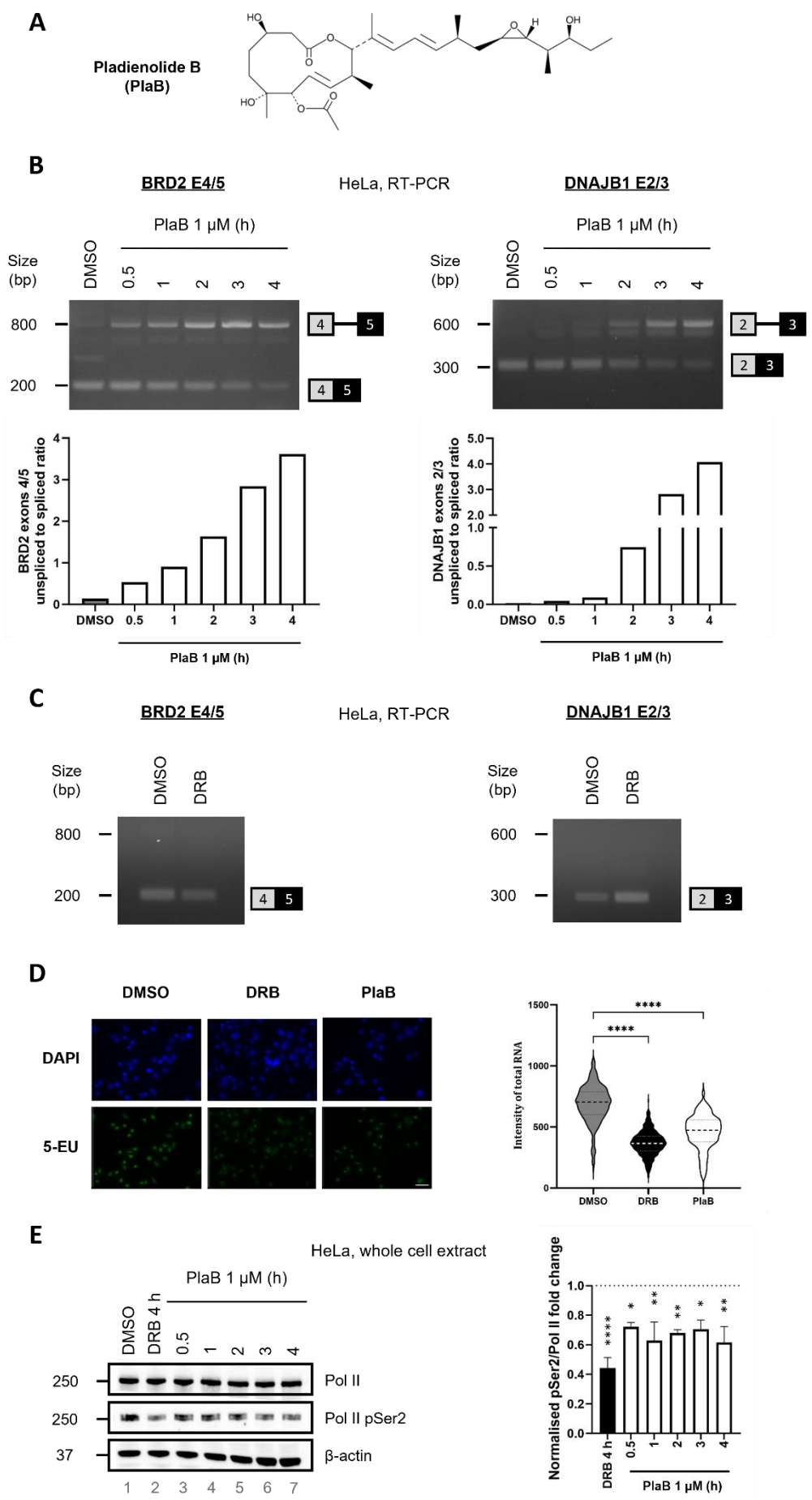

A
Pladienolide B
(PlaB)
B
BRD2 E4/5
HeLa, RT-PCR
DNAJB1 E2/3
PlaB 1 μM (h)
Size
(bp)
DMSO
0.5
1
2
3
4
800
200
600
300
BRD2 exons 4/5
unspliced to spliced ratio
DNAJB1 exons 2/3
unspliced to spliced ratio
C
BRD2 E4/5
HeLa, RT-PCR
DNAJB1 E2/3
DRB
D
DMSO
DRB
PlaB
DAPI
5-EU
Intensity of total RNA
****
E
HeLa, whole cell extract
PlaB 1 μM (h)
DRB 4 h
250
Pol II
Pol II pSer2
37
β-actin
Normalised pSer2/Pol II fold change

Figure 3.1 Short SF3B1 inhibition causes rapid defects in pre-mRNA splicing and inhibits nascent transcription in human cells

(A) Chemical structure of PlaB (Cayman Chemical) **(B, top)** RT-PCR with primers amplifying the intron located between exons 4 and 5 of *BRD2* or the intron located between exons 2 and 3 of *DNAJB1.* HeLa cells were treated with DMSO or 1 μM PlaB for times ranging between 30 minutes to 4 hours. The locations of the spliced and unspliced RNA are shown to the right of each gel image. **(B, bottom)** Quantification of relative band intensity as a ratio of unspliced to spliced RNA for DMSO (grey) and PlaB (white). **(C)** RT-PCR with primers amplifying the intron located between exons 4 and 5 of *BRD2* or the intron located between exons 2 and 3 of *DNAJB1.* HeLa cells were treated with DMSO or 100 μM DRB for 4 hours. The locations of the spliced RNA are shown to the right of each gel image. **(D, left)** Representative images of 5-EU incorporation in HeLa cells treated with DMSO, 100 μM DRB, or 1 μM PlaB for 1 hour. DAPI (blue), 5-EU (green), scale bar: 100 μm. **(D, right)** Quantification of 5-EU incorporation per nucleus for DMSO (grey), DRB (black), and PlaB (white). Violin plot settings are: min to max values with the median and 25-75 percentile range. 400 nuclei were quantified per condition. Statistical test: Kruskal-Wallis test. P-value: **** < 0.0001. **(E, left)** Western blot analysis of whole cell extracts of HeLa cells treated with DMSO, 100 μM DRB for 4 hours, or with 1 μM PlaB for times ranging between 30 minutes to 4 hours. Proteins were resolved by SDS-PAGE and immunoblotted with anti-pol II, anti-pol II pSer2, and anti-β-actin as a loading control. **(E, right)** Quantification of the western blots for DMSO (black horizonal line), DRB (black bar) and PlaB (white bar). Each pol II or pol II pSer2 quantification signal was normalised to the β-actin signal, pol II pSer2 to total pol II ratio determined, then compared to the ratio for the DMSO condition. Bars represent the normalised pol II pSer2 to total pol II fold change relative to DMSO of 3 biological replicates. Error bars = standard error of the mean. Statistical test: ordinary one-way ANOVA test. P-value: * < 0.05, ** < 0.01, **** < 0.0001.

3.3 Oct4 inducible compound 2 has no direct effect on *de novo* transcription

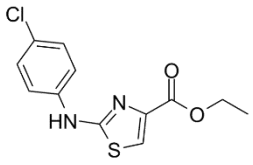
A small molecule initially identified as an Oct4 inducing agent (O4I2) (Cheng et al., 2015) (Figure 3.2A), was shown to bind and activate SF3B1, which results in increased transcription (Gama-Brambila et al., 2021). However, the mechanism leading to increased transcription remains unclear. To determine the primary effects of the O4I2 agent on transcription, titration of O4I2 for 1 hour was performed followed by western blotting on purified whole cell extracts using antibodies against pol II and pol II pSer2 (Figure 3.2B). There was no change in pol II pSer2 relative to total pol II for O4I2 concentrations between 1 μM to 30 μM for 1 hour.

It was possible that pol II under normal conditions, in the absence of any transcription impedance, is saturated with pSer2 marks regardless of any kinetic increases in transcription processivity, making it difficult to detect changes by western blotting of whole cell extracts. To determine whether *de novo* RNA synthesis increases in the presence of O4I2, 5-EU-labelling was performed following O4I2 treatments for times ranging between 1 hour to 4 hours (Figure 3.2C). O4I2 treatments did not significantly change the levels of *de novo* RNA synthesis (Kruskal-Wallis test, $P>0.05$).

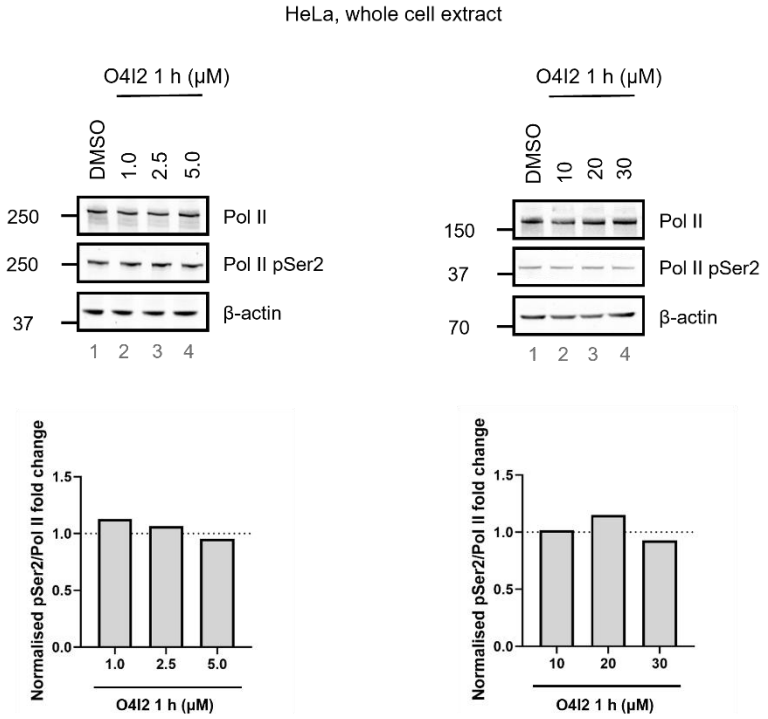
In summary, O4I2 did not show evidence of increased transcription processitivty at the conditions tested.

A

Oct4 inducing agent 2 (O4I2)



B



C

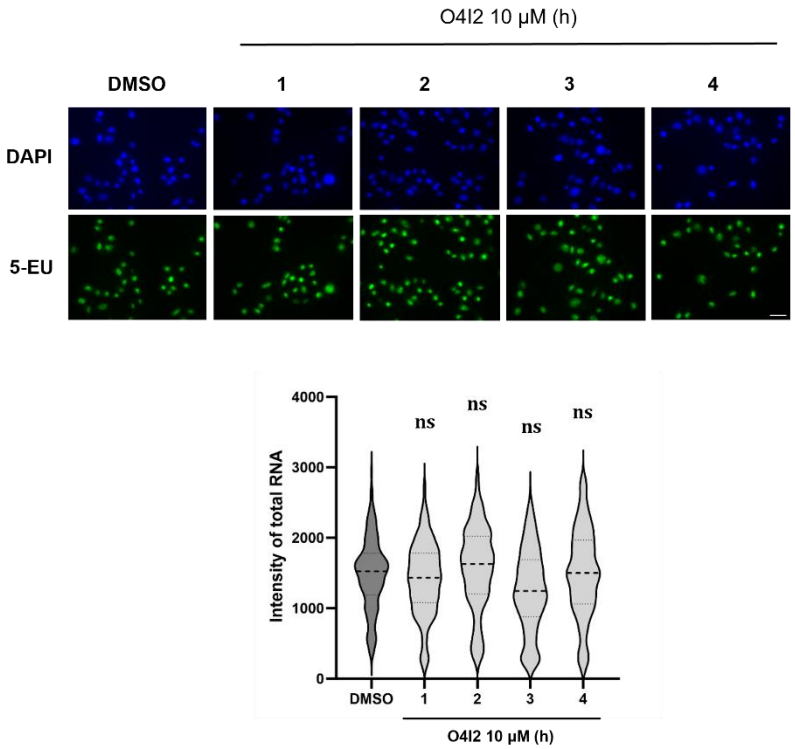


Figure 3.2. Oct4 inducible compound 2 has no direct effect on *de novo* transcription

(A) Chemical structure of O4I2 (Tocris Bioscience). **(B, top)** Western blot analysis of whole cell extracts of HeLa cells treated with DMSO or with O4I2 concentrations ranging from 1 μM to 30 μM for 1 hour. Proteins were resolved by SDS-PAGE and immunoblotted with anti-pol II, anti-pol II pSer2, and anti-β-actin as a loading control. **(B, bottom)** Quantification of the western blots for DMSO (black horizonal line) and O4I2 (light grey bar). Each pol II or pol II pSer2 quantification signal was normalised to the β-actin signal, pol II pSer2 to total pol II ratio determined, then compared to the ratio for the DMSO condition. Bars represent normalised antibody fold-change relative to the DMSO condition for 1 biological replicate. **(C, top)** Representative images of 5-EU incorporation in HeLa cells treated with DMSO or with 10 μM O4I2 for times ranging between 1 hour to 4 hours. DAPI (blue), 5-EU (green), scale bar: 100 μm. **(C, bottom)** Quantification of 5-EU incorporation per nucleus for DMSO (grey), O4I2 (light grey). Violin plot settings are: min to max values with the median and 25-75 percentile range. 7,000 nuclei were quantified per condition. Statistical test: Kruskal-Wallis test. P-value: ns > 0.05.

3.4 Short SF3B1 inhibition induces minimal cytotoxicity and does not promote a stress response

PlaB is a potent SF3B1 inhibitor that is cytotoxic to several tumour cell lines, inhibiting their growth at low IC_{50} values (Mizui et al., 2004; Sakai et al., 2004). SF3B1 interacts with histones in a cell-cycle dependent manner (Murthy et al., 2018), therefore, these cytotoxic effecs can be mediated through cell cycle arrest during the G_1 phase and G_2 to M transition (Effenberger et al., 2014; Mizui et al., 2004; Kaida et al., 2007; Nakajima et al., 1996). To determine the cytotoxic effects of PlaB on HeLa cells, a concentration of 1 μM PlaB was assessed using 5-EU-labelling to measure *de novo* RNA synthesis and cell survival over the course of 24 hours (Figure 3.3A). Short treatment times, for example 1 hour, showed greater cell survival while prolonged exposure resulted in loss of adherence to the surface of cultured plates and cell death by eye observation.

To determine whether cytotoxic stress responses are induced during short inhibition of SF3B1, which could explain transcriptional and splicing changes, at least partially, immunofluorescence was performed using an antibody against the general stress response marker, G3BP1 (Kedersha et al., 2016), following 30 minutes of PlaB treatment (Figure 3.3B). In these conditions, average fluorescent intensity of G3BP1 showed no statistical difference between treatment and non-treatment conditions (Kruskal-Wallis test, $P>0.05$).

Taken together, shorter treatment times of PlaB are necessary for assessing the primary effects of SF3B1 inhibition while limiting the cytotoxic effects of inhibition on HeLa cells.

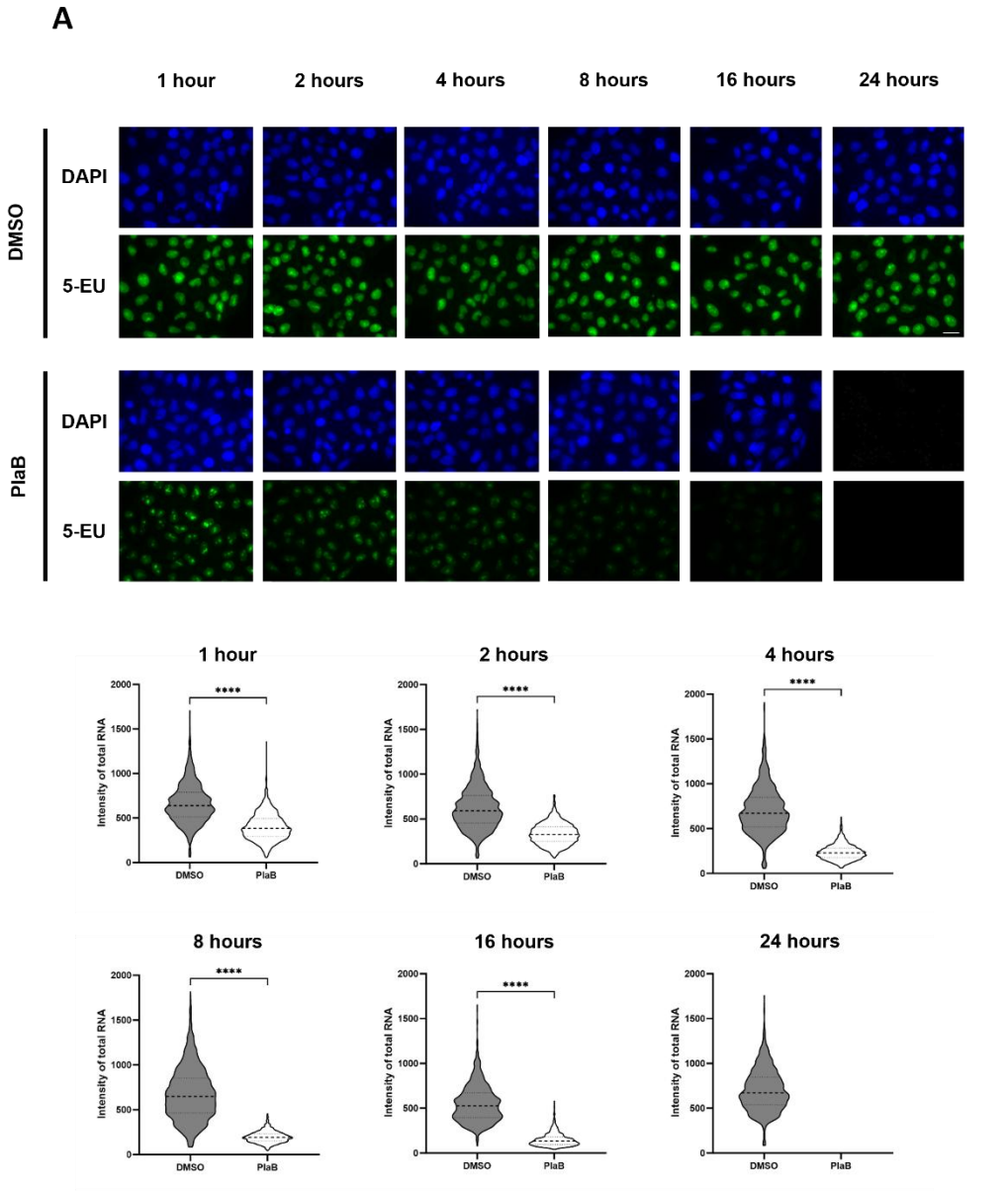

A
1 hour
2 hours
4 hours
8 hours
16 hours
24 hours
DMSO
DAPI
5-EU
PlaB
DAPI
5-EU
1 hour
2 hours
4 hours
8 hours
16 hours
24 hours
Intensity of total RNA
****
DMSO
PlaB
B
- DMSO
+ DMSO
PlaB
DAPI
G3BP1
Merged
Fluorescent Intensity of G3BP1
ns
ns
- DMSO
+ DMSO
PlaB

Figure 3.3. Short SF3B1 inhibition induces minimal cytotoxicity and does not promote a stress response

(A, top) Representative images of 5-EU incorporation in HeLa cells treated with DMSO or 1 μM PlaB for times ranging between 1 hour to 24 hours. DAPI (blue), 5-EU (green), scale bar: 50 μm. **(A, bottom)**. Quantification of 5-EU intensity per nucleus for DMSO (grey) and PlaB (white). Violin plot settings are: min to max values with the median and 25-75 percentile range. 1,500 nuclei were quantified per condition. Statistical test: Mann Whitney test **(B, left)** Representative images of immunofluorescence analysis in HeLa cells without treatment or treated with DMSO or 1 μM PlaB for 30 minutes. DAPI (blue), G3BP1 (green), scale bar: 100 μm. **(B, right)**. Quantification of fluorescent intensity per nucleus for no treatment (light grey), DMSO (grey) and PlaB (white). Violin plot settings are: min to max values with the median and 25-75 percentile range. >10,000 nuclei were quantified per condition. Statistical test: Kruskal-Wallis test. P-value: ns > 0.05.

3.5 Inhibition of SF3B1 function impairs early transcription elongation.

To determine whether short SF3B1 inhibition impairs the transition of pol II into active transcription elongation, ChIP was performed on HeLa cells treated with DRB or PlaB for 30 minutes using antibodies against pol II (RPB1) and CDK9, followed by qPCR around the promoter region of the intron-containing genes, *KPNB1*, *SLCO4A1*, and *LDLR* (Figure 3.4, Figure S2). The control ChIP profile of pol II following rapid inhibition of CDK9 using DRB was as expected showing increased occupancy of pol II near the gene promoter of *KPNB1* by 44% (Figure 3.4B). Similarly, inhibition of SF3B1 using PlaB for 30 minutes significantly increases pol II occupancy near the *KPNB1* gene promoter on average by 48% (Dunnett's test, $P<0.05$) (Figure 3.4C).

ChIP-qPCR using an antibody against CDK9 showed that CDK9 inhibition causes increased occupancy of CDK9 downstream of the gene promoter of *KPNB1*, in regions after the early-elongation checkpoint (Figure 3.4B). In contrast, SF3B1 inhibition for 30 minutes results in a significant decrease in the occupancy of CDK9 near the *KPNB1* gene promoter on average by 76%, and in regions after the early-elongation checkpoint on average by 64% (Dunnett's test, $P<0.05$) (Figure 3.4C). In agreement with previously published data (Caizzi et al., 2021), SF3B1 inhibition generally results in reduced occupancy of CDK9 near gene promoters of the protein-coding genes (Figure S2).

In conclusion, SF3B1 inhibition causes a CDK9-inhibition-like phenotype on pol II but a distict loss of CDK9 from the beginning of genes.

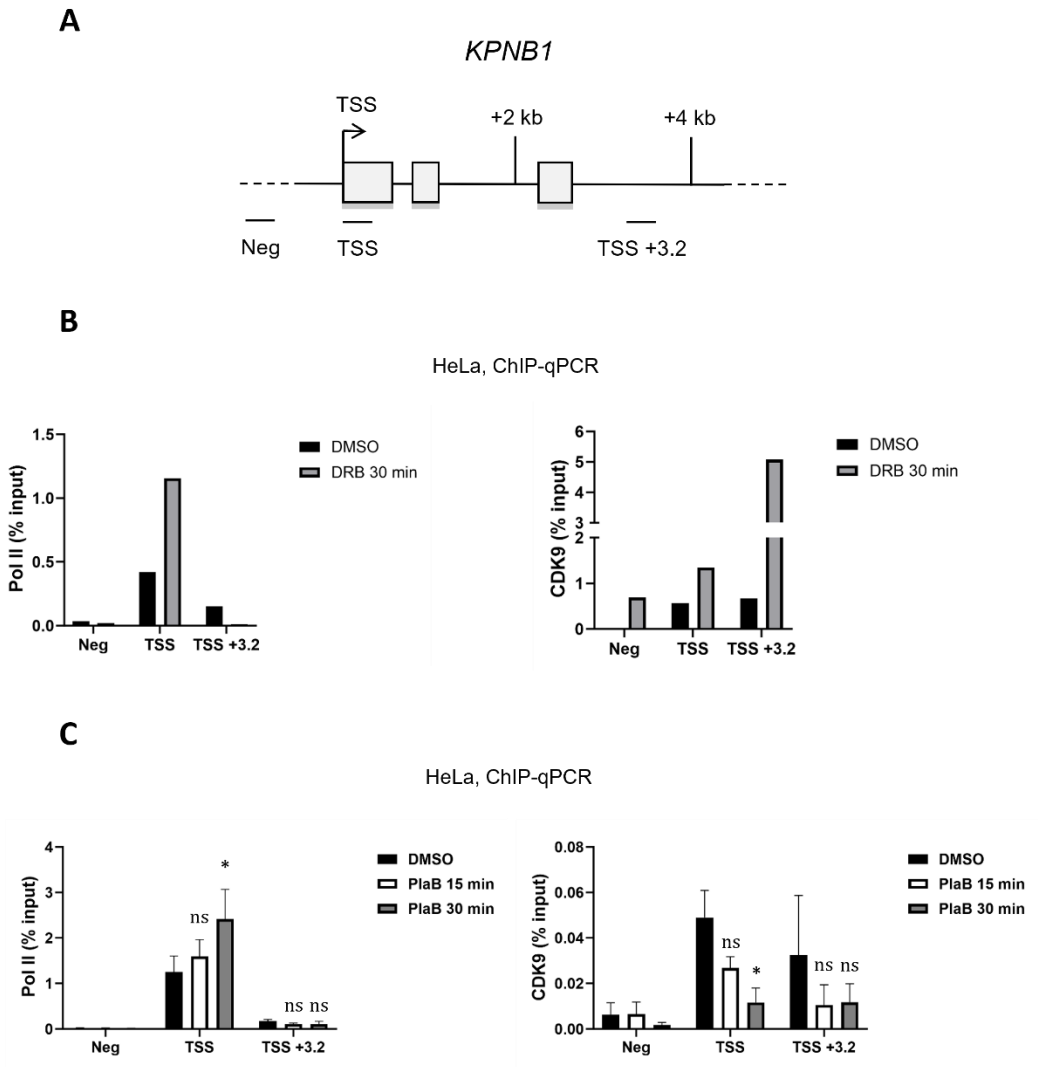


Figure 3.4. Inhibition of SF3B1 function impairs early transcription elongation

(A) Schematic of genic region around the promoter of *KPNB1*. **(B)** ChIP-qPCR of total pol II and CDK9 around the promoter region of the *KPNB1* intron-containing gene in HeLa cells treated with DMSO (black) or 100 μM DRB for 30 minutes (grey) for 1 biological repeat. **(C)** ChIP-qPCR of total pol II and CDK9 around the promoter region of the *KPNB1* intron-containing gene in HeLa cells treated with DMSO (black) or 1 μM PlaB for 15 minutes (white) or 30 minutes (grey). Mean of 3 biological repeats. Error bars = standard error of the mean. Statistical test: Dunnett's multiple comparison test. P-value: ns > 0.05, * < 0.05.

3.6 SF3B1 inhibition causes a global loss of SF3B1 and CDK9 from chromatin

Having observed effects on the pausing of pol II and loss of CDK9 around promoters of protein-coding genes following SF3B1 inhibition, it was next determined whether there is a global loss of CDK9 from chromatin and if SF3B1 chromatin association is altered in these conditions (Figure 3.5, Figure S3). Western blotting analyses was performed with antibodies against SF3B1, CDK9, the active CDK9 phospho-mark Thr186, and Cyclin T1 using chromatin extracts with and without PlaB treatment for times ranging between 30 minutes to 4 hours. These antibodies were also tested against chromatin extracts with and without 4 hours of DRB treatment to assess the apparent differences between SF3B1 inhibition and CDK9 inhibition.

After SF3B1 inhibition, there is a significant loss of chromatin associated SF3B1, on average by 46% within the first 30 minutes of treatment and by 47% on average over 4 hours of treatment (Dunnett's test, $P<0.05$). Further, there is a clear loss of SF3B1 phosphorylation, shown by the loss of the upper band that is present in the control. SF3B1 inhibition results in a partial loss of total CDK9, CDK9 in its active form indicated by the phospho-Thr186 mark, and Cyclin T1 globally from chromatin within the first 30 minutes of treatment. CDK9 inhibition also causes a significant loss of SF3B1 on average by 60% (Dunnett's test, $P<0.01$) from chromatin and a loss of SF3B1 phosphorylation over 4 hours of treatment. However, association of CDK9, its active phospho-Thr186 mark and Cyclin T1 with chromatin increases.

In conclusion, the effects of SF3B1 inhibition are distinct from CDK9 inhibition causing a reduction in SF3B1 and a partial loss of P-TEFb binding to chromatin.

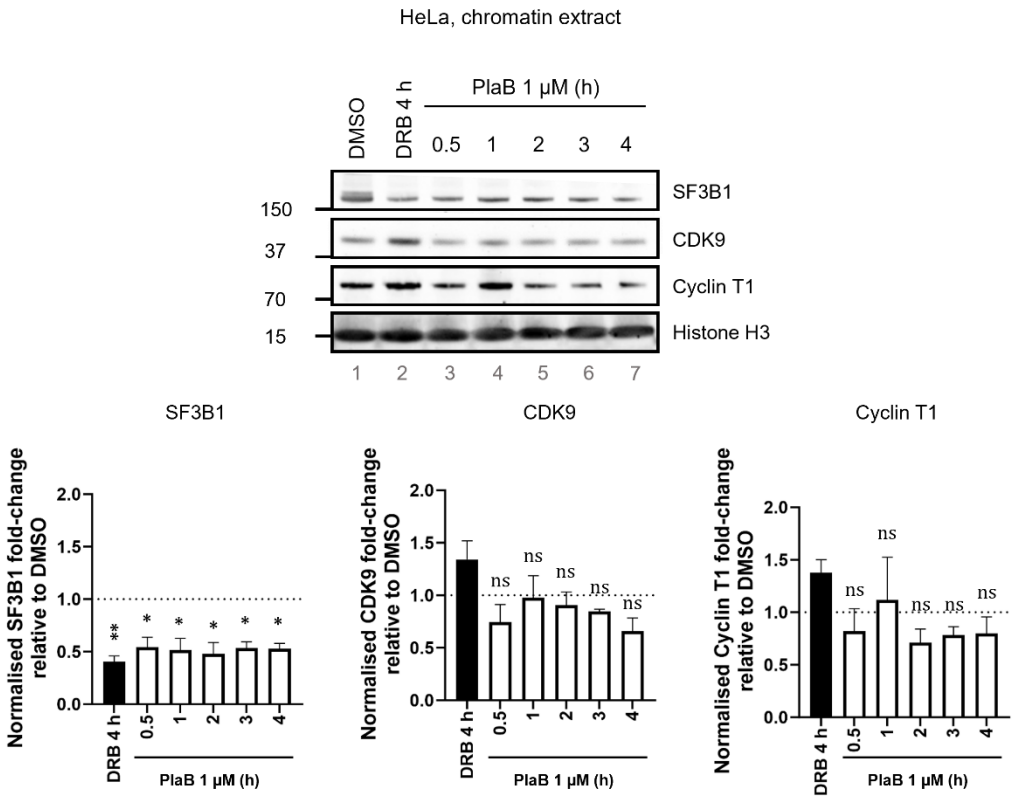


Figure 3.5. SF3B1 inhibition causes a global loss of SF3B1 and CDK9 from chromatin

(Top) Western blot analysis of chromatin extracts of HeLa cells treated with DMSO, 100 µM DRB for 4 hours, or with 1 µM PlaB for times ranging between 30 minutes to 4 hours. Proteins were resolved by SDS-PAGE and immunoblotted with anti-SF3B1, anti-CDK9, anti-Cyclin T1, and anti-Histone H3 as a loading control. **(Bottom)** Quantification of the western blots for DMSO (black horizonal line), DRB (black bar), and PlaB (white bar). Each quantification signal was normalised to the Histone H3 signal, then to the DMSO condition. Bars represent normalised antibody fold-change relative to the DMSO condition for 3 biological replicates. Error bars = standard error of the mean. Statistical test: Dunnett's multiple comparison test. P-value: ns > 0.05, * < 0.05, ** < 0.01.

3.7 SF3B1 and CDK9 weakly interact

Previous protein-protein interaction studies did not find SF3B1 and CDK9 to be direct physical interaction partners (Szklarczyk et al., 2023). To determine whether SF3B1 and CDK9 interact, co-immunoprecipitation experiments were performed where SF3B1 and Cyclin T1 were pulled down using antibodies against endogenous SF3B1 or Cyclin T1, followed by western blotting analyses using antibodies against SF3B1, CDK9, and Cyclin T1 (Figure 3.6). The non-specific binding of proteins directly to beads was very low and no negative control β-actin was detected in either SF3B1 or Cyclin T1 pull downs, meaning the co-immunoprecipitations were specific. SF3B1 co-immunoprecipitation showed SF3B1 interacting with both CDK9 and Cyclin T1. The reverse Cyclin T1 co-immunoprecipitation showed Cyclin T1 weakly interacting with SF3B1 but strongly interacting with CDK9.

In summary, SF3B1 and P-TEFb interact but their subcellular interactions are weak.

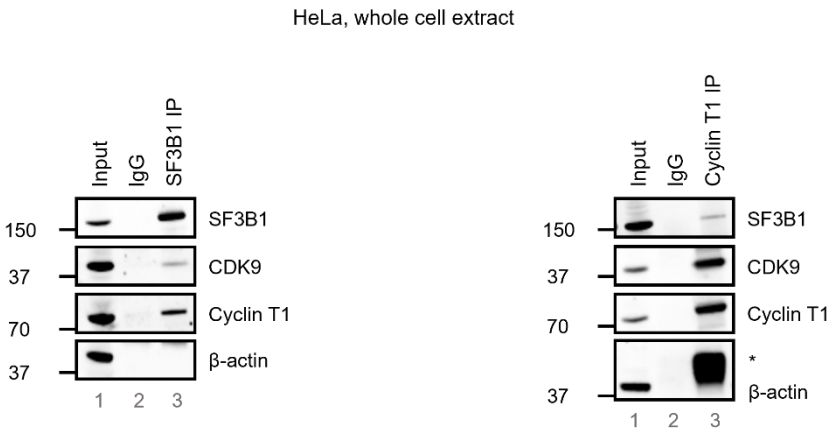


Figure 3.6 SF3B1 and CDK9 weakly interact

Western blot analysis from co-immunoprecipitation experiments on whole cell extracts of HeLa cells. SF3B1 and Cyclin T1 were immunoprecipitated using antibodies against the endogenous proteins. Rabbit IgG were used as negative controls for non-specific binding. Proteins were resolved by SDS-PAGE and immunoblotted with anti-SF3B1, anti-CDK9, anti-Cyclin T1, and anti-β-actin as a control. *: IgG.

3.8 Tat-SF1 is a candidate auxiliary factor for the interaction between SF3B1 and CDK9

In the context of previous protein-protein interaction studies that did not find any direct interactions between SF3B1 with CDK9 or Cyclin T1, it was possible that the weak cellular interactions detected (Figure 3.6) may be indirect and that an auxiliary factor may facilitate their interaction. To determine the auxiliary factor that could link SF3B1 and CDK9, two candidate factors, Tat-SF1 and SNW1 known to interact with SF3B1 (Loerch et al., 2019; Zhang et al., 2018), and both CDK9 and Cyclin T1 (Fong and Zhou, 2001; Verma et al., 2019) were investigated by performing co-immunoprecipitation experiments in which whole cell interaction partners of SF3B1 and Cyclin T1 were pulled down using antibodies against endogenous SF3B1 or Cyclin T1, followed by western blotting analyses using antibodies against SF3B1, Cyclin T1, Tat-SF1 and SNW1 (Figure 3.7). The non-specific binding of proteins directly to beads was very low and no negative control β-actin was detected in either SF3B1 or Cyclin T1 pull downs, meaning the co-immunoprecipitations were specific. SF3B1 co-immunoprecipitation showed SF3B1 interaction with Tat-SF1 but not with SNW1. The reverse Cyclin T1 co-immunoprecipitation showed Cyclin T1 interaction with Tat-SF1 but not with SNW1.

In summary, SF3B1 and P-TEFb both interact with Tat-SF1 whereas SNW1 shows no clear interaction.

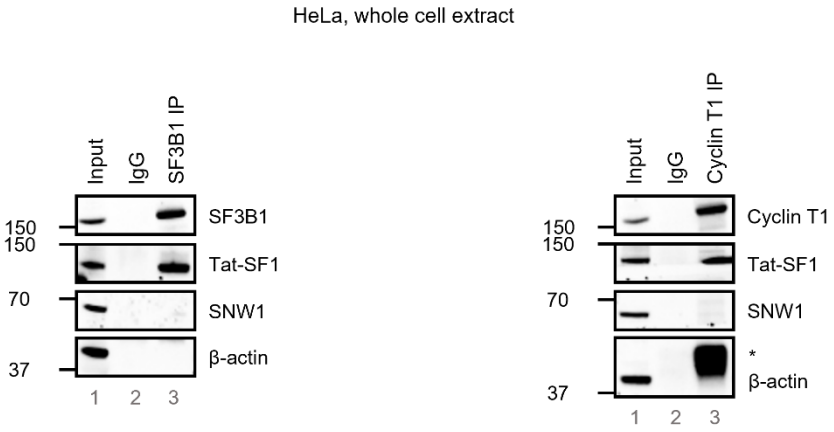


Figure 3.7. Tat-SF1 is a candidate auxiliary factor for the interaction between SF3B1 and CDK9

Western blot analysis from co-immunoprecipitation experiments on whole cell extracts of HeLa cells. SF3B1 and Cyclin T1 were immunoprecipitated using antibodies against the endogenous proteins. Rabbit IgG were used as negative controls for non-specific binding. Proteins were resolved by SDS-PAGE and immunoblotted with anti-SF3B1, anti-Cyclin T1, anti-Tat-SF1, anti-SNW1 and anti-β-actin as a control. *: IgG.

3.9 Discussion

In transcription, CDK9, as part of P-TEFb, helps to co-ordinate productive elongation and mRNA processing, including capping, splicing, and polyadenylation through phosphorylation of NTEFs and Ser2 of the pol II CTD, which mediates the recruitment of RNA processing factors (Zaborowska et al., 2016; Tellier et al., 2020a). However, the precise molecular mechanisms underlying CDK9 recruitment/stabilisation have not yet been fully elucidated. By using the small molecule inhibitor, PlaB, to rapidly inhibit splicing through SF3B1, the experiments described here provide mechanistic insights into the links between the splicing and transcription elongation machinery in human cells. Although previous reports found that splicing inhibition affects pol II occupancy and transcription, the data described here shows that SF3B1 is a specific splicing factor important for the efficient release of paused pol II into active transcription elongation, adding an additional level of control to fine-tune the expression of human protein-coding genes.

Here, evidence is provided for SF3B1 inhibition mirroring the effect of CDK9 inhibition on pol II at promoter-proximal regions of transcribed human genes (Figure 3.4). However, the mechanism underlying SF3B1 transcription regulation is unique to that of direct CDK9 transcription regulation. In line with previous results, fractionation experiments showed that the direct loss of CDK9 function increases the association of CDK9 with chromatin (Faust et al., 2018) (Figure 3.5, Figure S3). ChIP experiments showed increased CDK9 occupancy on chromatin near promoter-proximal regions of protein-coding genes, the site of the early-elongation checkpoint (Figure 3.4). In contrast, ChIP experiments of SF3B1 inhibition show that SF3B1

function is necessary for the recruitment/stabilisation of the pause release factor CDK9 near the promoters of protein-coding genes, complementing recent Cyclin T1 occupancy studies (Caizzi et al., 2021) (Figure 3.4). Further, fractionation experiments revealed that this effect is widespread across the genome and is associated with increased phosphorylation of SF3B1 (Figure 3.5). Transcriptional protein kinases that phosphorylate SF3B1 are explored further in Chapter 6.

Previous protein-protein interaction studies suggest that crosstalk between SF3B1 and CDK9 may involve the transcription co-factors Tat-SF1 or SNW1 (Yang et al., 2023; Fong and Zhou, 2001; Zhang et al., 2018; Verma et al., 2019). Consistent with co-immunoprecipitation data presented here, Tat-SF1 interacts with SF3B1 (Yang et al., 2023), and with P-TEFb (Parada and Roeder, 1999, Fong and Zhou, 2001) (Figure 3.7). SNW1 was previously shown to associate with SF3B1 (Zhang et al., 2018) and with P-TEFb (Verma et al., 2019; Brès et al., 2005). However, co-immunoprecipitation experiments here did not find evidence for cellular interactions (Figure 3.7). Before the co-immunoprecipitation of cellular proteins, whole cell lysates were treated with the nuclease, Benzonase, therefore, it is possible that interactions between SNW1 with SF3B1 and P-TEFb are dependent on chromatin or RNA.

The O4I2 small molecule was shown to bind SF3B1 and enhance transcription (Cheng et al., 2015, Gama-Brambila et al., 2021). However, the molecular details for how transcription is increased remain unclear. The increased RNA synthesis effect of O4I2 was demonstrated in human fibroblasts using a concentration of 10 μM O4I2 over 4 hours. In this study, 5-EU experiments using analogous O4I2 treatment conditions did not show a change on average in transcription efficiency in HeLa cells

(Figure 3.2C). Furthermore, pol II pSer2 marks were not elevated in the presence of O4I2 to suggest greater transcription processivity (Figure 3.2B). The immortalised nature and rapid proliferation characteristics of HeLa cells may possibly be allowing transcription near full capacity for already over-expressed genes. Examining O4I2 in primary cells or less proliferative cell lines could give a clearer indication of any transcriptional effects in human cells. O4I2 could therefore be a good tool to assess whether enhancing transcription through SF3B1 has the reverse mechanistic effects as PlaB which reduces transcription through SF3B1 in a different cell system.

Together, experiments described here suggest SF3B1 is a global regulator of CDK9 recruitment/stabilisation for the transcription of protein-coding genes. The mechanistic detail of SF3B1-dependent regulation of CDK9 on chromatin is distinct from that of direct CDK9 inhibition. Beyond chromatin, examining the effect of SF3B1 and CDK9 inhibition on the subcellular localisation of factors will help clarify the function of SF3B1 in regulating transcription.

Chapter 4. The effect of SF3B1 and CDK9 inhibition on their subcellular localisation and that of interactors

4.1 Background

Beyond chromatin, cyclin T1 is exclusively nuclear and is present in nuclear-speckled structures (Herrmann and Mancini, 2001), whereas CDK9, albeit mainly nuclear, has a propensity to localise in the cytoplasm (Napolitano et al., 2002). CDK9 is actively exported from the nucleus but the presence of Leptomycin B (LMB), a specific nucleocytoplasmic transport inhibitor, impairs this process (Napolitano et al., 2002). The inhibition of SF3B1 reduces the association of catalytically active P-TEFb to chromatin. However, the effect this has on the nuclear availability of P-TEFb is yet to be determined.

The interaction of SF3B1 and CDK9 is likely mediated through an auxiliary factor. Tat-SF1 and SNW1 are good candidates as they have previously been shown to both interact with SF3B1 and CDK9 (Yang et al., 2023; Fong and Zhou, 2001; Zhang et al., 2018; Brès et al., 2009) and the results presented in Chapter 3 confirm that Tat-SF1 interacts well with both proteins (Figure 3.7). Other transcription and splicing factors including c-MYC and SRSF2 have also been shown to interact with P-TEFb and or SF3B1. The transcription factor c-MYC, is a key regulator of cellular processes that recruits CDK9 and Cyclin T1 through binding to control transcription, cellular proliferation, and apoptosis (Brès et al., 2009; Kanazawa et al., 2003). As previously described, the absence of SRSF2 has a similar phenotypic effect on pol II as the loss of SF3B1 function and is exclusively nuclear, playing a key role in nuclear processes (Cazalla et al., 2002). SRSF2 is also found in the interactomes of both SF3B1 and CDK9 (Ji et al., 2013; Deckert et al., 2006). These factors are therefore all good

candidates in mediating the crosstalk between SF3B1 and P-TEFb, although the results presented in Chapter 3 argue against SNW1 as the intermediary.

4.2 SF3B1 inhibition changes the nuclear localisation of SF3B1 and CDK9

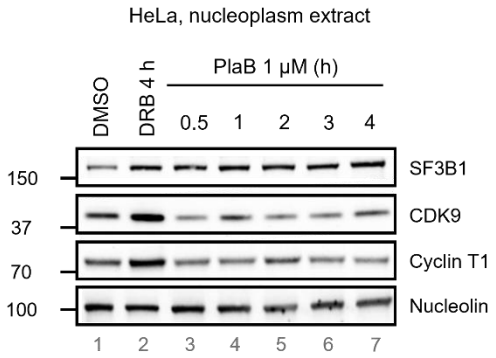
To determine whether SF3B1 and CDK9 released from chromatin share a similar nuclear fate following SF3B1 inhibition, western blotting analyses were performed with antibodies against SF3B1, CDK9 and its active phospho-mark Thr186, and Cyclin T1, using nucleoplasm extracts with and without PlaB treatment for times ranging between 30 minutes to 4 hours (Figure 4.1A, Figure S4A). To better understand how SF3B1 inhibition differs to that of CDK9 inhibition, these antibodies were also tested against nucleoplasm extracts with and without DRB treatment for 4 hours. In conditions of SF3B1 inhibition, SF3B1 levels increased to, on average, 42% whereas CDK9 and its active phospho-Thr186 mark, and Cyclin T1 levels decreased, on average, 36%, 29%, and 21% respectively, within the first 30 minutes of treatment. In contrast, CDK9 inhibition resulted in increased levels, on average, 49% for SF3B1, 66% for CDK9, 146% for the active CDK9 phospho-Thr186 mark, and 57% for Cyclin T1 over 4 hours of treatment.

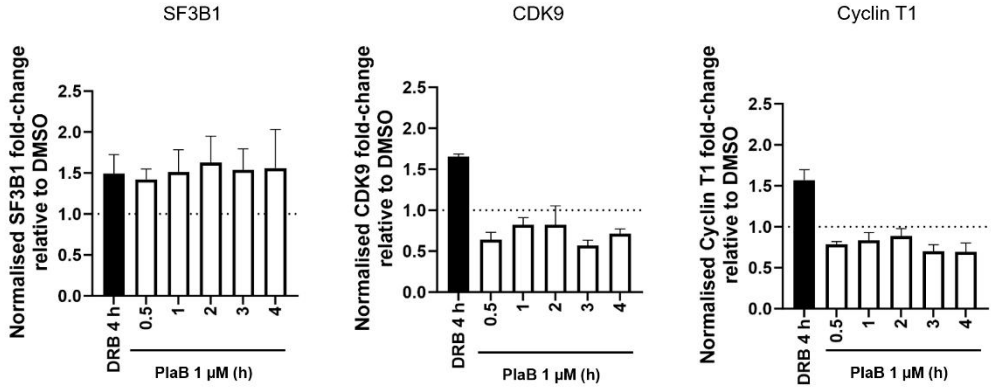
Immunofluorescence using an antibody against CDK9 further showed that the fluorescence intensity of CDK9 in the nucleus significantly reduced by 6% following 30 minutes of PlaB treatment (Mann-Whitney test, $P<0.0001$) (Figure 4.1B).

Western blotting analyses with antibodies against SF3B1 and CDK9 using cell nuclei equivalents to compare protein abundance of subcellular regions with and without 30 minutes of PlaB treatment showed a shift in SF3B1 from chromatin to the nucleoplasm and cytoplasm (Figure 4.1C). The abundance of CDK9 is reduced on chromatin as well as in the nucleoplasm but increased in the cytoplasm following PlaB treatment.

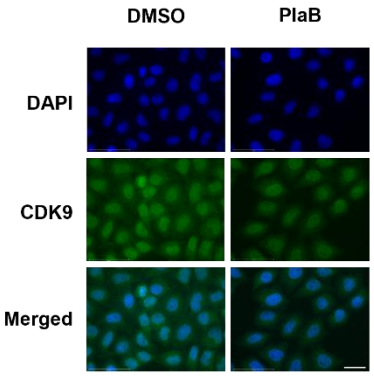
Taken together, the effects of SF3B1 inhibition are distinct from CDK9 inhibition in causing the subcellular localisation of SF3B1 and P-TEFb to change noticeably from one another.

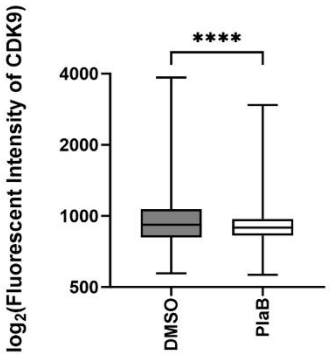
A


HeLa, nucleoplasm extract
DMSO
DRB 4 h
PlaB 1 μM (h)
0.5 1 2 3 4
150
37
70
100
SF3B1
CDK9
Cyclin T1
Nucleolin
1 2 3 4 5 6 7


SF3B1
CDK9
Cyclin T1
Normalised SF3B1 fold-change relative to DMSO
Normalised CDK9 fold-change relative to DMSO
Normalised Cyclin T1 fold-change relative to DMSO
2.5
2.0
1.5
1.0
0.5
0.0
DRB 4 h
0.5
1
2
3
4
PlaB 1 μM (h)

B


DMSO
PlaB
DAPI
CDK9
Merged


****
log2(Fluorescent Intensity of CDK9)
4000
2000
1000
500
DMSO
PlaB

C

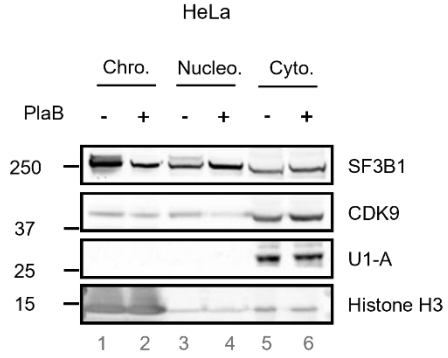

HeLa
Chro.
Nucleo.
Cyto.
PlaB
- + - + - +
250
37
25
15
SF3B1
CDK9
U1-A
Histone H3
1 2 3 4 5 6

Figure 4.1. SF3B1 inhibition changes the nuclear localisation of SF3B1 and CDK9

(A, top) Western blot analysis of nucleoplasm extracts of HeLa cells treated with DMSO, 100 μM DRB for 4 hours, or with 1 μM PlaB for times ranging between 30 minutes to 4 hours. Proteins were resolved by SDS-PAGE and immunoblotted with anti-SF3B1, anti-CDK9, anti-Cyclin T1, and anti-Nucleolin as a loading control. **(A, bottom)** Quantification of the western blots for DMSO (black horizonal line), DRB (black bar), and PlaB (white bar). Each quantification signal was normalised to the nucleolin signal, then to the DMSO condition. Bars represent normalised antibody fold-change relative to the DMSO condition for 3 biological replicates. Error bars = standard error of the mean. Statistical test: Dunnett's multiple comparison test. **(B, left)** Representative images of immunofluorescence analysis in HeLa cells treated with DMSO or 1 μM PlaB for 30 minutes. DAPI (blue), G3BP1 (green), scale bar: 20 μm. **(B, right)**. Quantification of fluorescent intensity per nucleus for DMSO (grey) and PlaB (white). Box plot settings are: min to max values with the median and 25-75 percentile range. >10,000 nuclei were quantified per condition. Statistical test: Kruskal-Wallis test. P-value: **** < 0.0001. **(C)** Western blot analysis of chromatin, nucleoplasm, and cytoplasm extracts of HeLa cells treated with DMSO or with 1 μM PlaB for 30 minutes. Cell nuclei equivalents were used for each blot. Proteins were resolved by SDS-PAGE and immunoblotted with anti-SF3B1, anti-CDK9 and either anti-Histone H3 or anti-U1-A as a control.

4.3 SF3B1 inhibition does not affect the protein stability of SF3B1 and CDK9

The loss of CDK9 from chromatin and general lower abundance in the nucleus after SF3B1 (but not CDK9 inhibition) could be explained in two ways: SF3B1 inhibition either promotes active degradation of CDK9 or the nuclear export of CDK9.

To distinguish between these two possibilities, western blotting analyses was first performed with antibodies against SF3B1, CDK9 and Cyclin T1 using whole cell lysates with and without 30 minutes of PlaB treatment (Figure 4.2A). Cellular levels of SF3B1, CDK9, and Cyclin T1 on average show no significant change in these conditions (Dunnett's test, $P > 0.05$). In addition, DRB treatment on average also showed no significant change in the cellular levels of SF3B1, CDK9, and Cyclin T1 (Dunnett's test, $P > 0.05$).

The possibility of active proteasome degradation of CDK9 after SF3B1 inhibition was further investigated using a proteasome inhibitor system. Camptothecin (CPT) is a compound that induces DNA double-strand breaks by inhibiting the helicase activity of topoisomerase I (TOP1) (Pommier, 2006). Under normal conditions, stalled-TOP1 is targeted for degradation leading to the progressive phosphorylation of Histone H2AX at Ser139 (γH2AX) at the exposed DNA damage site (Debéthune et al., 2002; Interthal et al., 2005; Cristini et al., 2016). Inhibition of stalled-TOP1 degradation using proteasome inhibitors such as MG-132 or Bortezomib, suppress the induction of γH2AX and subsequent DNA damage repair (Cristini et al., 2019).

To determine the conditions necessary for efficient proteasome inhibition, western blotting analyses were performed with antibodies against γH2AX using whole cell lysate with and without 1 hour treatment of CPT, MG-132, or Bortezomib (Figure S5). CPT treatment showed an increase in γH2AX. Dual treatment of CPT followed

by Bortezomib was able to decrease γH2AX to levels comparable to that of lone Bortezomib treatment. Proteasome inhibition using Bortezomib for 1 hour was therefore a suitable amount of time to prevent proteasome degradation.

To determine whether SF3B1 inhibition promotes active degradation of CDK9, western blotting analyses were performed with antibodies against SF3B1, CDK9, Cyclin T1, and total pol II as a negative control using chromatin and nucleoplasm extracts with and without 1 hour Bortezomib and or 30 minutes PlaB treatment (Figure 4.2B). Lone proteasome inhibition when compared to conditions of no treatment show no change to chromatin associated or nucleoplasm SF3B1, CDK9, or Cyclin T1 levels. Proteasome inhibition followed by SF3B1 inhibition, when compared to lone SF3B1 inhibition, show no difference in levels of chromatin associated and nucleoplasm SF3B1, CDK9, or Cyclin T1 levels.

In summary, SF3B1 inhibition does not cause the active degradation of SF3B1 or P-TEFb.

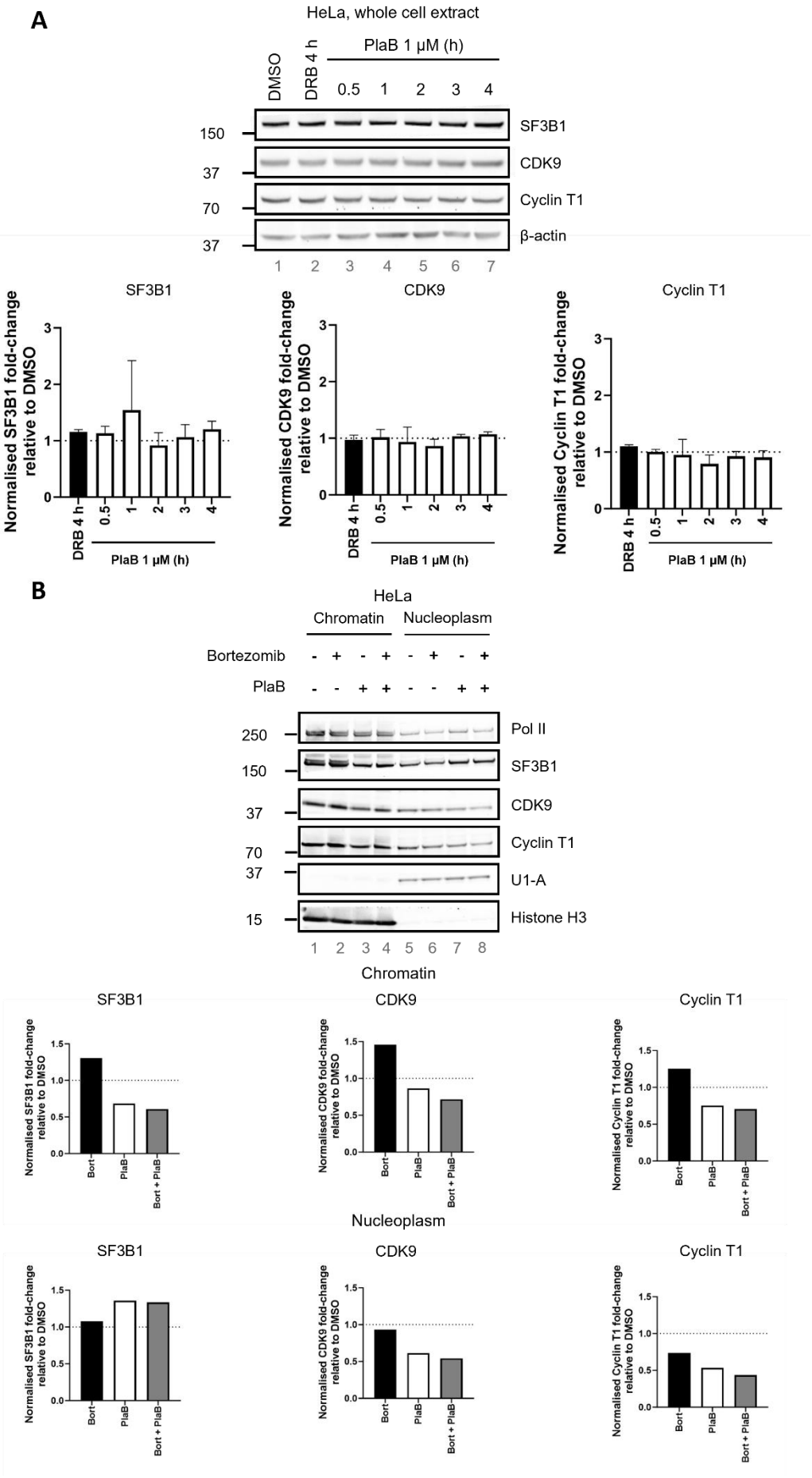

A
HeLa, whole cell extract
DMSO
DRB 4 h
PlaB 1 µM (h)
0.5 1 2 3 4
150
SF3B1
37
CDK9
70
Cyclin T1
37
β-actin
1 2 3 4 5 6 7
SF3B1
CDK9
Cyclin T1
Normalised SF3B1 fold-change relative to DMSO
Normalised CDK9 fold-change relative to DMSO
Normalised Cyclin T1 fold-change relative to DMSO
DRB 4 h
PlaB 1 µM (h)
B
HeLa
Chromatin
Nucleoplasm
Bortezomib - + - + - + - +
PlaB - - + + - - + +
250
Pol II
150
SF3B1
37
CDK9
70
Cyclin T1
37
U1-A
15
Histone H3
1 2 3 4 5 6 7 8
Chromatin
SF3B1
CDK9
Cyclin T1
Normalised SF3B1 fold-change relative to DMSO
Normalised CDK9 fold-change relative to DMSO
Normalised Cyclin T1 fold-change relative to DMSO
Bort
PlaB
Bort + PlaB
Nucleoplasm
SF3B1
CDK9
Cyclin T1

Figure 4.2. SF3B1 inhibition does not affect the protein stability of SF3B1 and CDK9

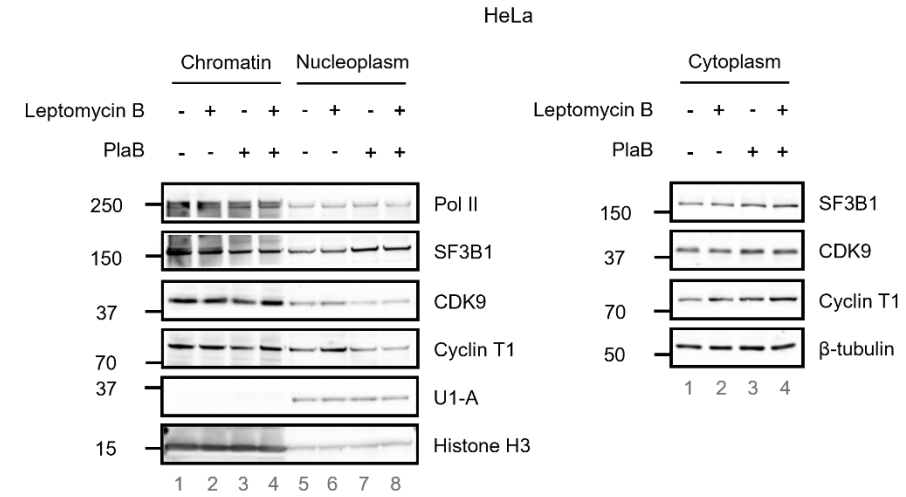
(A, top) Western blot analysis of whole cell extracts of HeLa cells treated with DMSO, 100 μM DRB for 4 hours, or with 1 μM PlaB for times ranging between 30 minutes to 4 hours. Proteins were resolved by SDS-PAGE and immunoblotted with anti-SF3B1, anti-CDK9, anti-Cyclin T1, and anti-β-actin as a loading control. **(A, bottom)** Quantification of the western blots for DMSO (black horizonal line), DRB (black bar), and PlaB (white bar). Each quantification signal was normalised to the β-actin signal, then to the DMSO condition. Bars represent normalised antibody fold-change relative to the DMSO condition for 2 biological replicates. Error bars = standard error of the mean. Statistical test: Dunnett's multiple comparison test. **(B, top)** Western blot analysis of chromatin and nucleoplasm extracts of HeLa cells treated with DMSO, 1 μM Bortezomib for 1 hour and or with 1 μM PlaB for 30 minutes. Cell nuclei equivalents were used for each blot. Proteins were resolved by SDS-PAGE and immunoblotted with anti-pol II, anti-SF3B1, anti-CDK9, anti-Cyclin T1, and either anti-Histone H3 or anti-U1-A as a loading control. **(B, bottom)** Quantification of the western blots for DMSO (black horizonal line), DRB (black bar), and PlaB (white bar). Each quantification signal was normalised to the Histone H3 signal for chromatin samples or the U1-A signal for nucleoplasm samples, then to the DMSO condition. Bars represent normalised antibody fold-change relative to the DMSO condition for 1 biological replicate.

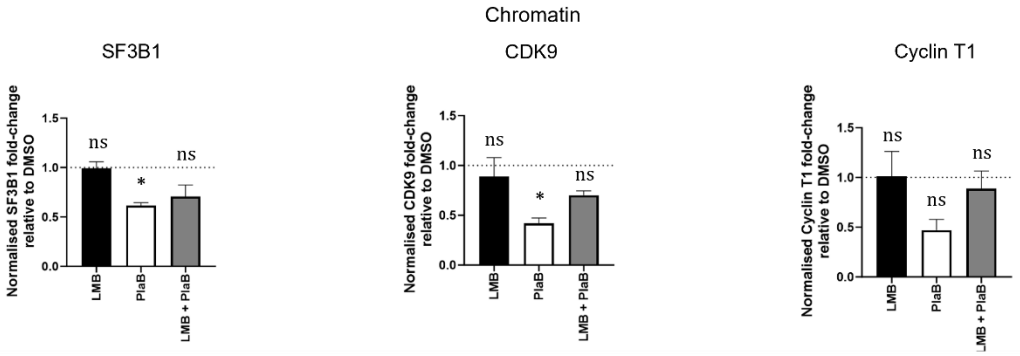
4.4 SF3B1 inhibition causes the nuclear export of CDK9

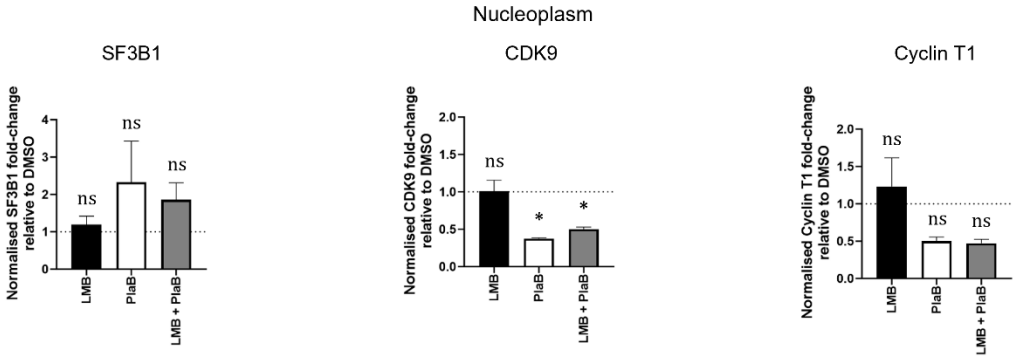
The major export of proteins and RNA from the nucleus to the cytoplasm is facilitated by Chromosome region maintenance 1 (CRM1)/exportin-1 (Fornerod et al., 1997; Fukuda et al., 1997; Ossareh-Nazari et al., 1997; Kudo et al., 1998; Mougel et al., 2020). Selective inhibitors of nuclear export such as LMB target and inhibit the activity of CRM1, impairing nucleocytoplasmic transport.

To assess whether SF3B1 inhibition promotes the nuclear export of CDK9, western blotting analyses were performed with antibodies against SF3B1, CDK9, Cyclin T1, and total pol II as a negative control using chromatin, nucleoplasm, and cytoplasm extracts with and without 1 hour LMB and/or 30 minutes PlaB treatment (Figure 4.3). Inhibition of nuclear export alone, when compared to no treatment conditions show no change on average to chromatin associated, nucleoplasm or cytoplasm SF3B1, CDK9, or Cyclin T1 levels. Nuclear export inhibition followed by SF3B1 inhibition, when compared to lone SF3B1 inhibition, show on average that levels of SF3B1, CDK9 and Cyclin T1 do not change in the nucleoplasm or cytoplasm but become more enriched on chromatin, indicating that PlaB treatment promotes the nuclear export of P-TEFb.

In summary, SF3B1 inhibition promotes a rapid increase in P-TEFb nuclear export. However, 1 hour pre-treatment with LMB is not sufficient to block P-TEFb nuclear export due to the mechanism of action of LMB (discussed in more detail in section 4.11) but does partially restore P-TEFb on chromatin.


HeLa
Chromatin
Nucleoplasm
Cytoplasm
Leptomycin B
PlaB
Pol II
SF3B1
CDK9
Cyclin T1
U1-A
Histone H3
β-tubulin
250
150
37
70
15
50
1 2 3 4 5 6 7 8
1 2 3 4


Chromatin
SF3B1
CDK9
Cyclin T1
Normalised SF3B1 fold-change relative to DMSO
Normalised CDK9 fold-change relative to DMSO
Normalised Cyclin T1 fold-change relative to DMSO
ns
*
LMB
PlaB
LMB + PlaB


Nucleoplasm
SF3B1
CDK9
Cyclin T1
Normalised SF3B1 fold-change relative to DMSO
Normalised CDK9 fold-change relative to DMSO
Normalised Cyclin T1 fold-change relative to DMSO
ns
*
LMB
PlaB
LMB + PlaB

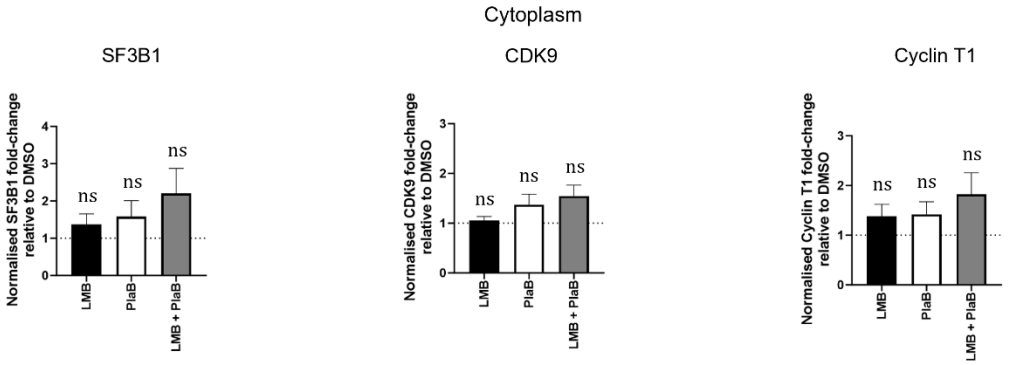

Cytoplasm
SF3B1
CDK9
Cyclin T1
Normalised SF3B1 fold-change relative to DMSO
Normalised CDK9 fold-change relative to DMSO
Normalised Cyclin T1 fold-change relative to DMSO
ns
LMB
PlaB
LMB + PlaB

Figure 4.3. SF3B1 inhibition causes the nuclear export of CDK9

(Top) Western blot analysis of chromatin, nucleoplasm, and cytoplasm extracts of HeLa cells treated with DMSO or ethanol, 20 nM LMB for 1 hour and or with 1 μM PlaB for 30 minutes. Cell nuclei equivalents were used for each blot. Proteins were resolved by SDS-PAGE and immunoblotted with anti-pol II, anti-SF3B1, anti-CDK9, anti-Cyclin T1, and either anti-Histone H3, anti-U1-A, or anti-β-tubulin as a loading control. **(Bottom)** Quantification of the western blots for DMSO (black horizonal line), DRB (black bar), and PlaB (white bar). Each quantification signal was normalised to the Histone H3 signal for chromatin samples, U1-A signal for nucleoplasm samples, or β-tubulin signal for cytoplasm samples, then to the DMSO condition. Bars represent normalised antibody fold-change relative to the DMSO condition for 2 biological replicates. Error bars = standard error of the mean. Statistical test: Ordinary one-way ANOVA. P-value: ns > 0.05, * < 0.05.

4.5 Blocking CDK9 nuclear export does not reverse the effect of SF3B1 inhibition on transcription

To determine whether chromatin enriched CDK9 following nuclear export block could reverse the effects of SF3B1 inhibition on transcription, 5-EU-labelling was performed to measure *de novo* RNA synthesis following 1 hour LMB and or 30 minutes PlaB or DRB treatment (Figure 4.4A). As a positive control, CDK9 inhibition with DRB showed a significant decrease in RNA synthesis on average of 58% (Kruskal-Wallis test, $P<0.0001$). Nuclear export inhibition followed by SF3B1 inhibition showed a significant decrease in RNA synthesis on average by 43% (Kruskal-Wallis test, $P<0.0001$). This was greater than that of lone nuclear export inhibition or lone SF3B1 inhibition which showed significant decreases in RNA synthesis on average by 26% and 16% respectively (Kruskal-Wallis test, $P<0.0001$).

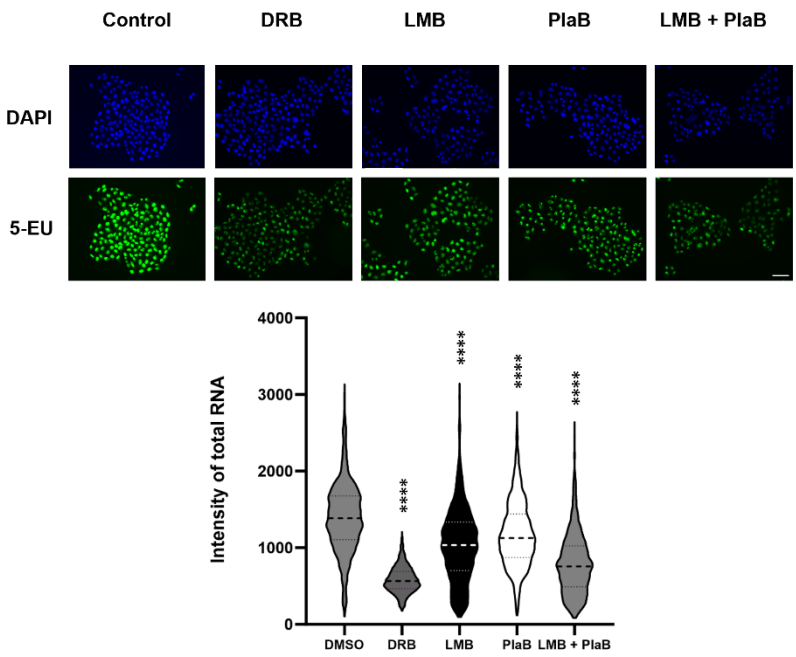
The RNA synthesis readout from 5-EU-labelling is global, therefore is not able to discriminate between the activities of the different human RNA polymerases contributing to the overall transcription signal. To determine which human RNA polymerase is affected after nuclear export inhibition or SF3B1 inhibition, RT-qPCR was performed on total (steady state) RNA using primers for transcripts of the pre-ribosomal gene to detect changes to pol I transcription, and the *KPNB1* nascent protein-coding gene to detect changes to pol II transcription (Figure 4.4B). Transcripts of the pre-ribosomal gene significantly decreased in conditions of lone nuclear export inhibition on average by 29%, whereas lone SF3B1 inhibition showed no change (Welch's test, $P<0.05$). In contrast, nascent transcripts of *KPNB1* do not change in conditions of lone nuclear export inhibition but show a significant

decrease in conditions of lone SF3B1 inhibition and dual nuclear export and SF3B1 inhibition on average by 76% and 58% respectively (Welch's test, $P<0.05$).

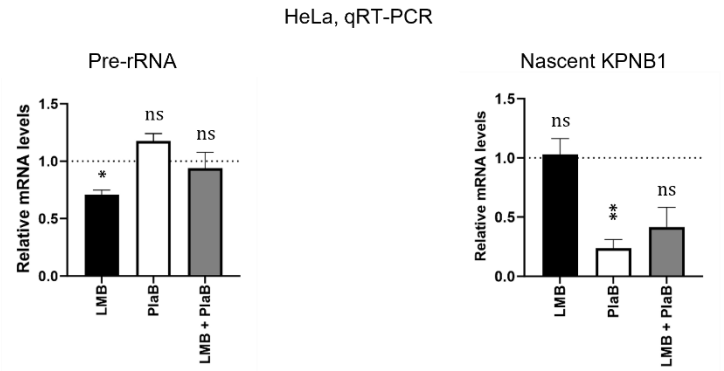
ChIP-qPCR analyses showed that, although not statistically significant, there is an effect on the occupancy of pol II downstream the promoter-proximal pause site for the intron-containing gene *KPNB1*, when comparing lone nuclear export inhibition to conditions of no treatment (Figure 4.4C). In contrast, the occupancy of pol II across the gene body of *KPNB1* decreased in response to conditions of lone SF3B1 inhibition or dual inhibitory nuclear export and SF3B1 inhibition.

Taken together, these results indicate that blocking the nuclear export of P-TEFb using LMB does not reverse the effect of SF3B1 inhibition on transcription.

A


Control
DRB
LMB
PlaB
LMB + PlaB
DAPI
5-EU
Intensity of total RNA
4000
3000
2000
1000
0
****
****
****
****
DMSO
DRB
LMB
PlaB
LMB + PlaB

B


HeLa, qRT-PCR
Pre-rRNA
Nascent KPNB1
Relative mRNA levels
1.5
1.0
0.5
0.0
*
ns
ns
**
ns
LMB
PlaB
LMB + PlaB

C

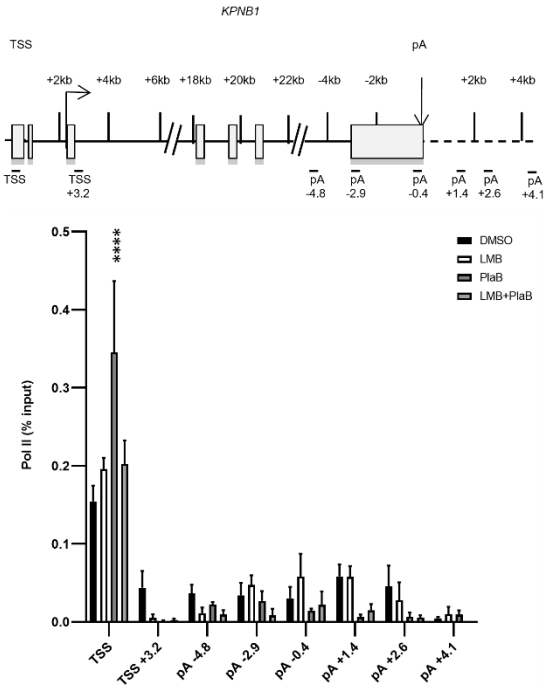

KPNB1
TSS
pA
+2kb
+4kb
+6kb
+18kb
+20kb
+22kb
-4kb
-2kb
+2kb
+4kb
TSS
TSS +3.2
pA -4.8
pA -2.9
pA -0.4
pA +1.4
pA +2.6
pA +4.1
DMSO
LMB
PlaB
LMB+PlaB
Pol II (% input)
0.5
0.4
0.3
0.2
0.1
0.0
****
TSS
TSS +3.2
pA -4.8
pA -2.9
pA -0.4
pA +1.4
pA +2.6
pA +4.1

Figure 4.4. Blocking CDK9 nuclear export does not reverse the effect of SF3B1 inhibition on transcription

(A, top) Representative images of 5-EU incorporation in HeLa cells treated with DMSO, 100 μM DRB, 20 nM LMB, and or 1 μM PlaB for 1 hour. DAPI (blue), 5-EU (green), scale bar: 100 μm. **(A, bottom)** Quantification of 5-EU incorporation per nucleus for DMSO (grey), DRB (dark grey), LMB (black), PlaB (white), and LMB + PlaB (grey). Violin plot settings are: min to max values with the median and 25-75 percentile range. 1620 nuclei were quantified per condition. Statistical test: Kruskal-Wallis test. P-value: **** < 0.0001. **(B)** qRT-PCR with primers amplifying a region from the pol I transcribed pre-ribosomal RNA or nascent *KPNB1* gene. HeLa cells were treated with DMSO, 20 nM LMB or with 1 μM PlaB for 1 hour. cDNA was generated with random hexamers. Values are normalised to the 7SK rRNA and shown as relative to DMSO for 3 biological replicates. Error bars = standard error of the mean. Statistical test: Welch's test. P-value: ns > 0.05, * < 0.05, ** < 0.01. **(C, top)** Schematic of *KPNB1* gene. **(C, bottom)** ChIP-qPCR of total pol II across the *KPNB1* intron-containing gene in HeLa cells treated with DMSO (black), 20 nM LMB (light grey), 1 μM PlaB (white) or LMB + PlaB (grey) for 30 minutes. Mean of 3 biological repeats. Error bars = standard error of the mean. Statistical test: Dunnett's multiple comparison test. P-value: **** < 0.0001.

4.6 Chromatin is a binding platform mediating SF3B1 and CDK9 protein interactions

To begin to understand whether SF3B1 and CDK9 protein interaction is dependent on the physical presence of chromatin or RNA tethering them together, or whether their protein-interactions is mediated through interactions with an auxiliary factor, co-immunoprecipitation experiments were performed by exposing whole cell lysates to either Benzonase, an endonuclease that degrades all accessible nucleic acid material, or sonication, a method to shear nucleic acids into small fragments and retain them. Following benzonase or sonication treatment, whole cell interaction partners of Tat-SF1 and CDK9 were pulled down using antibodies against endogenous Tat-SF1 or CDK9, followed by western blotting analyses using antibodies against Tat-SF1, SF3B1, CDK9 and Cyclin T1 (Figure S7). The interaction of Tat-SF1 with SF3B1, CDK9, and Cyclin T1 does not require chromatin or RNA, as the addition of Benzonase did not affect the Tat-SF1 co-immunoprecipitation. CDK9 co-immunoprecipitation only showed interaction with Cyclin T1 with the interaction being chromatin- and RNA-independent.

To determine the subcellular location of the interactions between SF3B1, CDK9, and Cyclin T1, and how they could change following 30 minutes of PlaB treatment, co-immunoprecipitation experiments were performed in which interaction partners of SF3B1 and Cyclin T1 were pulled down from chromatin, nucleoplasm, or cytoplasm fractions using antibodies against endogenous SF3B1 or Cyclin T1, followed by western blotting analyses using antibodies against SF3B1, CDK9 and Cyclin T1 (Figure 4.5).

In the control condition, SF3B1 interacts with both CDK9 and Cyclin T1 on chromatin but not, or to a low level, in the nucleoplasm and cytoplasm. Inhibition of SF3B1 with PlaB does not affect SF3B1 interaction with CDK9 and Cyclin T1 on chromatin, nor does it change the lack of interaction in the nucleoplasm and cytoplasm. In agreement, Cyclin T1 interacts with both CDK9 and SF3B1 on chromatin, but only interacts with CDK9 in the nucleoplasm and cytoplasm in the DMSO and PlaB conditions.

These results indicate that a complex comprising SF3B1, P-TEFb, and Tat-SF1 only forms on chromatin and is independent of chromatin or RNA for interaction.

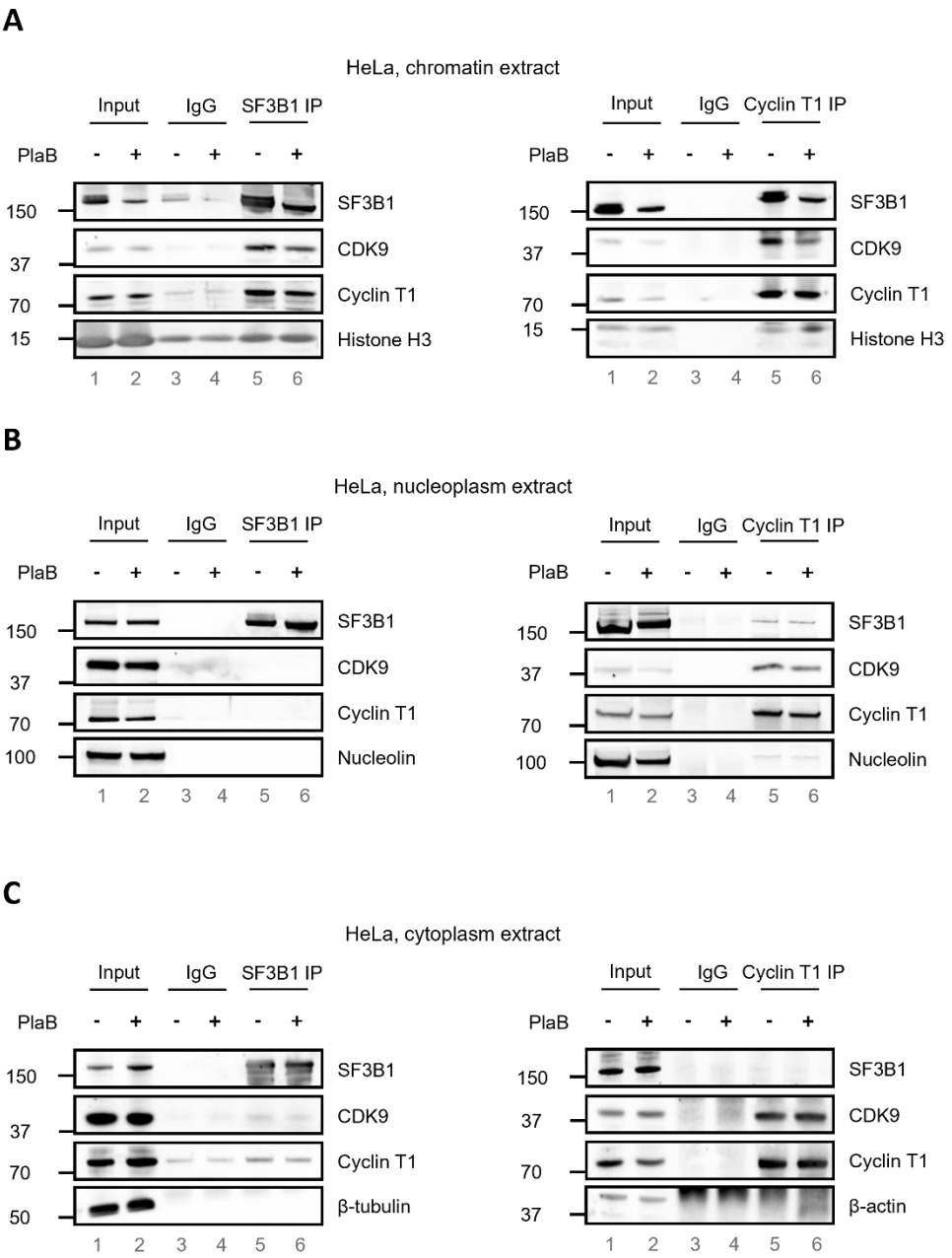


Figure 4.5. Chromatin is a binding platform mediating SF3B1 and CDK9 protein interactions

(A, B, C) Western blot analysis from co-immunoprecipitation experiments of chromatin (A), nucleoplasm (B), or cytoplasm (C) extracts of HeLa cells treated with DMSO or 1 μM PlaB for 30 minutes. SF3B1 and Cyclin T1 were immunoprecipitated using antibodies against the endogenous proteins. Rabbit IgG were used as negative controls for non-specific binding. Proteins were resolved by SDS-PAGE and immunoblotted with anti-SF3B1, anti-CDK9, anti-Cyclin T1, and either anti-Histone H3, anti-Nucleolin, or anti-β-tubulin as a control.

4.7 Tat-SF1 interacts with SF3B1 and CDK9 only on chromatin

To determine the subcellular location of interactions between SF3B1 and Cyclin T1 with Tat-SF1 or SNW1, and how the interactions could change following 30 minutes of PlaB treatment, co-immunoprecipitation experiments were performed in which chromatin, nucleoplasm, or cytoplasm interaction partners of SF3B1 and Cyclin T1 were pulled down using antibodies against endogenous SF3B1 or Cyclin T1, followed by western blotting analyses using antibodies against SF3B1, Cyclin T1, Tat-SF1 and SNW1 (Figure 4.6, Figure S6).

In the control condition, SF3B1 interacts with both Tat-SF1 and SNW1 on chromatin, but only interacts with Tat-SF1 and not SNW1 in the nucleoplasm and cytoplasm. Following PlaB treatment, there is a stronger interaction of SF3B1 with Tat-SF1 but decreased interaction with SNW1 on chromatin. SF3B1 interacts only with Tat-SF1, and not SNW1, in the nucleoplasm and cytoplasm, with stronger interaction in the nucleoplasm following SF3B1 inhibition. The inputs of both SF3B1 and Cyclin T1 co-immunoprecipitations with and without SF3B1 inhibition show decreased SNW1 chromatin association with a slight increase in levels in the nucleoplasm.

In the control conditions, Cyclin T1 interacts with both Tat-SF1 and SNW1 on chromatin but does not interact with Tat-SF1 or SNW1 in the nucleoplasm and cytoplasm (SNW1 only). After PlaB treatment, Cyclin T1 still interacts with Tat-SF1 and to a reduced level with SNW1 on chromatin. After SF3B1 inhibition, Cyclin T1 still does not interact with Tat-SF1 or SNW1 in the nucleoplasm and cytoplasm (SNW1 only).

In summary, both Tat-SF1 and SNW1 bind SF3B1 and P-TEFb on chromatin. Tat-SF1 binding is independent of SF3B1 function whereas SNW1 binding depends on

SF3B1 function. Beyond chromatin, Tat-SF1 only interacts with SF3B1 indicating that P-TEFb disscociates from a complex comprising SF3B1, Tat-SF1, and P-TEFb when not bound to chromatin. On the other hand, SNW1 does not interact with either SF3B1 or P-TEFb beyond chromatin indicating that a complex comprising SF3B1, SNW1, and P-TEFb fully dissociates when not bound to chromatin.

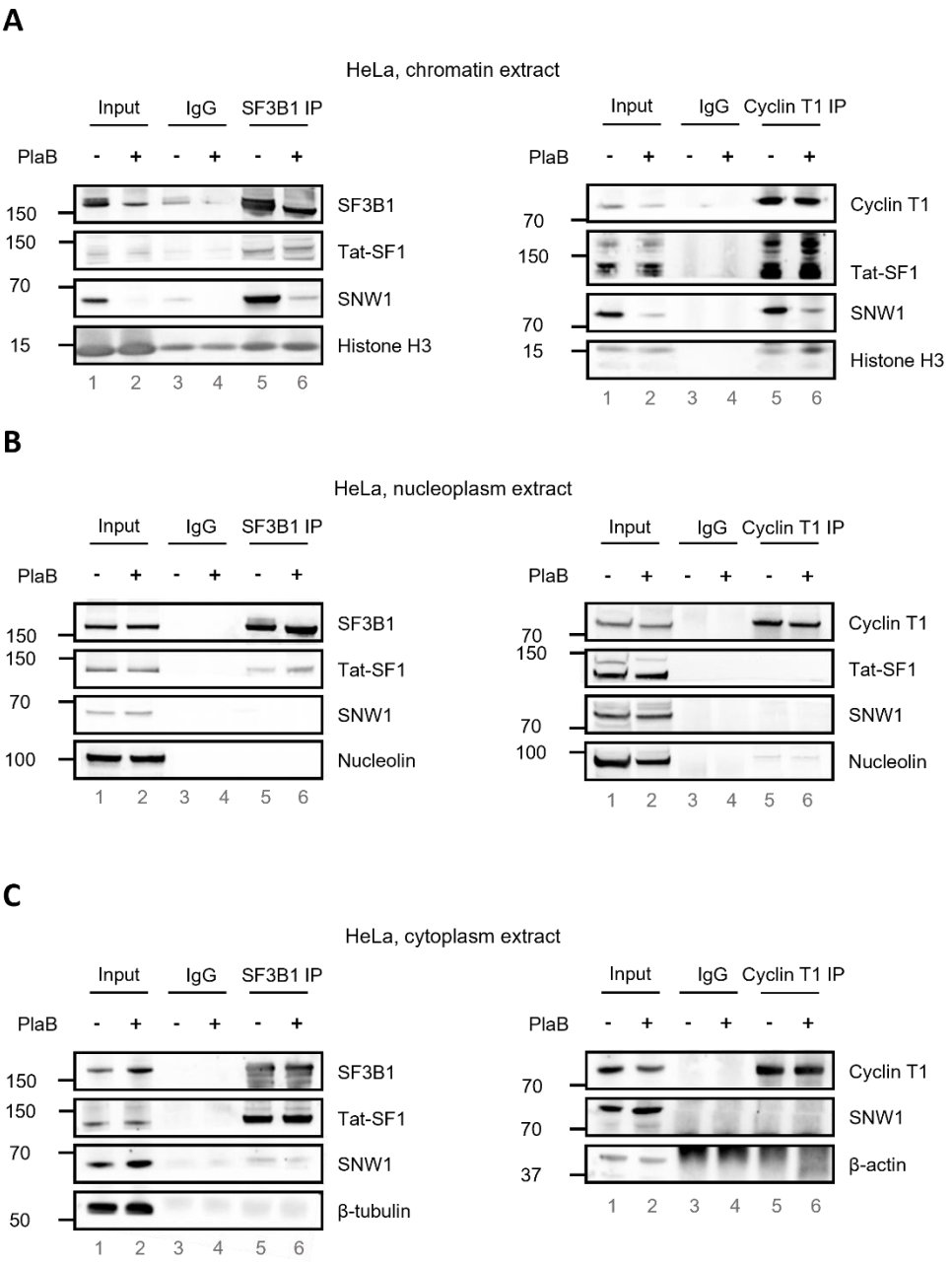


Figure 4.6. Tat-SF1 interacts with SF3B1 and CDK9 only on chromatin

(A, B, C) Western blot analysis from co-immunoprecipitation experiments of chromatin (A), nucleoplasm (B), or cytoplasm (C) extracts of HeLa cells treated with DMSO or 1 μM PlaB for 30 minutes. SF3B1 and Cyclin T1 were immunoprecipitated using antibodies against the endogenous proteins. Rabbit IgG were used as negative controls for non-specific binding. Proteins were resolved by SDS-PAGE and immunoblotted with anti-SF3B1, anti-Cyclin T1, anti-Tat-SF1, anti-SNW1 and either anti-Histone H3, anti-Nucleolin, anti-β-tubulin or anti-β-actin as a control.

4.8 SF3B1 inhibition influences the subcellular localisation of Tat-SF1 and SNW1

To determine whether Tat-SF1 and SNW1 share the same nuclear fate as SF3B1 or CDK9 following SF3B1 inhibition, western blotting analyses was performed with antibodies against Tat-SF1 and SNW1 using chromatin and nucleoplasm extracts with and without PlaB treatment for times ranging between 30 minutes to 4 hours (Figure 4.7A, Figure 4.7B). These antibodies were also tested against chromatin and nucleoplasm extracts with and without DRB treatment for 4 hours to assess the effect of CDK9 inhibition. In conditions of lone SF3B1 or CDK9 inhibition, both Tat-SF1 and SNW1 show a reduction in chromatin association within 30 minutes and an accumulation in the nucleoplasm that increases over time.

To determine whether the cellular stability of Tat-SF1 changes after SF3B1 inhibition, western blotting analyses were performed with an antibody against Tat-SF1 using whole cell lysates with and without 30 minutes PlaB treatment (Figure 4.7C). Cellular protein levels of Tat-SF1 did not change following SF3B1 inhibition.

To determine whether the subcellular localisation of SNW1 is consistent with that of SF3B1 or CDK9 after SF3B1 inhibition, western blot analysis was performed against SNW1 using chromatin, nucleoplasm and cytoplasm extracts with or without 1 hour LMB and or 30 minutes PlaB treatment (Figure 4.7D). Lone nuclear export inhibition, when compared to no treatment conditions show no change to chromatin-associated, nucleoplasmic, or cytoplasmic SNW1. Dual nuclear export inhibition followed by SF3B1 inhibition mirrors the effect of lone SF3B1 inhibition with reduced chromatin association and increased cytoplasmic SNW1 levels.

Taken together, Tat-SF1 and SNW1 follow the same nuclear fate as SF3B1 following SF3B1 inhibition. Interestingly, unlike Tat-SF1, the magnitude of loss of SNW1 from chromatin following SF3B1 inhibition is more profound than that of SF3B1 or P-TEFb loss from chromatin (Figure 3.5). Further, SF3B1 inhibition promotes the export of SNW1 from the nucleus.

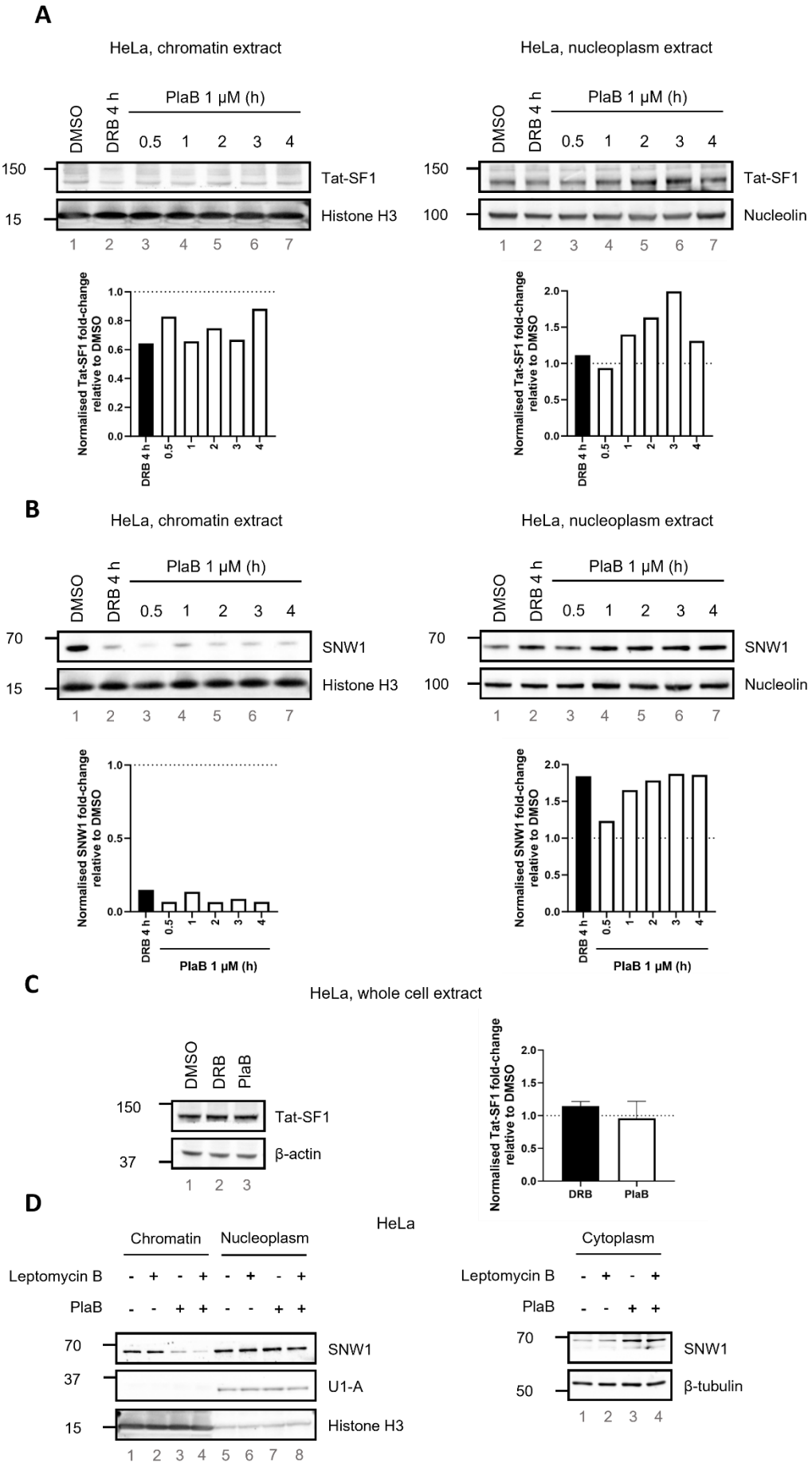

A
HeLa, chromatin extract
HeLa, nucleoplasm extract
DMSO
DRB 4 h
PlaB 1 μM (h)
0.5 1 2 3 4
150
Tat-SF1
15
Histone H3
100
Nucleolin
1 2 3 4 5 6 7
Normalised Tat-SF1 fold-change relative to DMSO
B
HeLa, chromatin extract
HeLa, nucleoplasm extract
70
SNW1
Normalised SNW1 fold-change relative to DMSO
C
HeLa, whole cell extract
DMSO
DRB
PlaB
37
β-actin
Normalised Tat-SF1 fold-change relative to DMSO
D
HeLa
Chromatin
Nucleoplasm
Cytoplasm
Leptomycin B
PlaB
SNW1
37
U1-A
Histone H3
50
β-tubulin
1 2 3 4 5 6 7 8

Figure 4.7. SF3B1 inhibition influences the subcellular localisation of Tat-SF1 and SNW1

(A and B, top) Western blot analysis of chromatin and nucleoplasm extracts of HeLa cells treated with DMSO, 100 μM DRB for 4 hours, or with 1 μM PlaB for times ranging between 30 minutes to 4 hours. Proteins were resolved by SDS-PAGE and immunoblotted with anti-Tat-SF1, anti-SNW1 and either anti-Histone H3 or anti-Nucleolin as a loading control. **(A and B, bottom)** Quantification of the western blots for DMSO (black horizonal line), DRB (black bar), and PlaB (white bar). Each quantification signal was normalised to the Histone H3 or Nucleolin signal, then to the DMSO condition. Bars represent normalised antibody fold-change relative to the DMSO condition for 1 biological replicate. **(C, left)** Western blot analysis of whole cell extracts of HeLa cells treated with DMSO, 100 μM DRB for 4 hours, or with 1 μM PlaB for 30 minutes. Proteins were resolved by SDS-PAGE and immunoblotted with anti-Tat-SF1 and anti-β-actin as a loading control. **(C, right)** Quantification of the western blots for DMSO (black horizonal line), DRB (black bar), and PlaB (white bar). Each quantification signal was normalised to the β-actin signal, then to the DMSO condition. Bars represent normalised antibody fold-change relative to the DMSO condition for 2 biological replicates. Error bars = standard error of the mean. **(D)** Western blot analysis of chromatin, nucleoplasm, and cytoplasm extracts of HeLa cells treated with DMSO, 20 nM LMB for 1 hour and or with 1 μM PlaB for 30 minutes. Cell nuclei equivalents were used for each blot. Proteins were resolved by SDS-PAGE and immunoblotted with anti-SNW1 and either anti-Histone H3, anti-U1-A, or anti-β-tubulin as a loading control.

4.9 Other interactors of SF3B1 and CDK9

The interactomes of both SF3B1 and CDK9 include several other factors that could facilitate their interaction. Splicing factors such as SRSF2 has been shown to interact with both SF3B1 and CDK9 (Deckert et al., 2006, Ji et al., 2013), and transcription factors such as c-MYC have been shown to interact with CDK9 (Deckert et al., 2006).

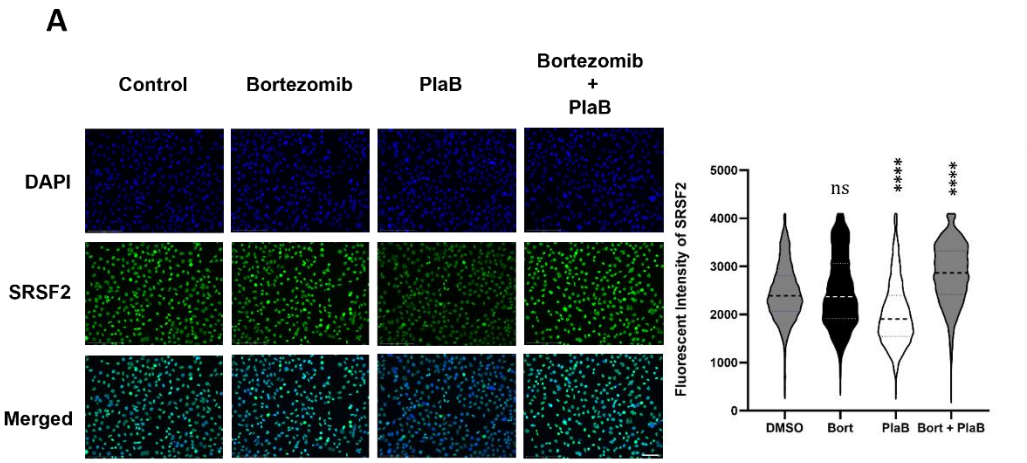
To determine whether SRSF2 could act as an auxiliary factor linking SF3B1 and CDK9, immunofluorescence was performed using an antibody against endogenous SRSF2 to assess the nuclear localisation of SRSF2 after 30 minutes PlaB treatment (Figure S8). SF3B1 inhibition showed on average a significant reduction in nuclear SRSF2 by 69% (Mann-Whitney test, $P<0.0001$).

To determine whether the loss of nuclear SRSF2 following SF3B1 inhibition is a result of targeted proteasome degradation or the nuclear export of SRSF2, immunofluorescence was performed using an antibody against endogenous SRSF2 after 1 hour of Bortezomib and or 30 minutes PlaB treatment (Figure 4.8A). Lone proteasome inhibition, when compared to no treatment conditions, did not significantly affect the average SRSF2 nuclear fluorescent intensity. Dual inhibition of the proteasome and SF3B1, when compared to lone SF3B1 inhibition conditions showed the average nuclear fluorescent intensity of SRSF2 to increase to levels comparable to the control condition, indicating SF3B1 inhibition causes SRSF2 protein degradation.

To determine the protein-protein interactions of SRSF2, c-MYC, and SF3B1 with and without 30 minutes of PlaB treatment, co-immunoprecipitations were performed in which whole cell interaction partners of SRSF2, c-MYC, and SF3B1 were pulled down using antibodies against the endogenous proteins, followed by western blotting

analyses using antibodies against SRSF2, c-MYC, SF3B1, CDK9 and Cyclin T1 (Figure 4.8B). Western blotting analyses after SRSF2 co-immunoprecipitation shows SRSF2 weakly interacts with SF3B1, with little to no interaction with CDK9 or Cyclin T1, before and after SF3B1 inhibition. c-MYC co-immunoprecipitation shows no interaction of c-MYC with SF3B1, CDK9 or Cyclin T1. SF3B1 co-immunoprecipitation shows no interaction of SF3B1 with SRSF2 or c-MYC.

Taken together, SF3B1 inhibition promotes the degradation of SRSF2. However, SRSF2 and c-MYC do not show interactions consistent with that of an intermediary mediating interaction between SF3B1 and CDK9.


A
Control
Bortezomib
PlaB
Bortezomib + PlaB
DAPI
SRSF2
Merged
Fluorescent Intensity of SRSF2
5000
4000
3000
2000
1000
0
ns
****
****
DMSO
Bort
PlaB
Bort + PlaB

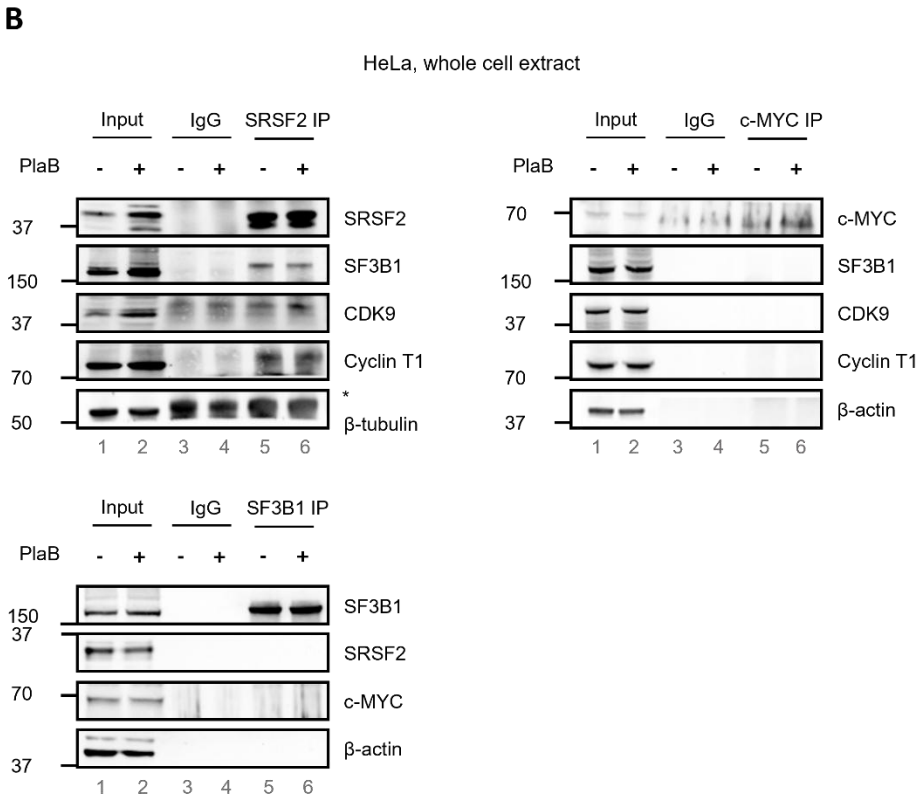

B
HeLa, whole cell extract
Input
IgG
SRSF2 IP
PlaB
- + - + - +
37
150
37
70
50
SRSF2
SF3B1
CDK9
Cyclin T1
*
β-tubulin
1 2 3 4 5 6
Input
IgG
c-MYC IP
PlaB
- + - + - +
70
150
37
70
37
c-MYC
SF3B1
CDK9
Cyclin T1
β-actin
1 2 3 4 5 6
Input
IgG
SF3B1 IP
PlaB
- + - + - +
150
37
70
37
SF3B1
SRSF2
c-MYC
β-actin
1 2 3 4 5 6

Figure 4.8. Other interactors of SF3B1 and CDK9

(A, left) Representative images of immunofluorescence analysis in HeLa cells treated with DMSO, 1 μM Bortezomib for 1 hour and or with 1 μM PlaB for 30 minutes. DAPI (blue), G3BP1 (green), scale bar: 100 μm. **(A, right)**. Quantification of fluorescent intensity per nucleus for DMSO (grey), Bortezomib (black), PlaB (white), and Bortezomib + PlaB (grey). Violin plot settings are: min to max values with the median and 25-75 percentile range. >10,000 nuclei were quantified per condition. Statistical test: Kruskal-Wallis test. P-value: ns > 0.05, **** < 0.0001 **(B)** Western blot analysis from co-immunoprecipitation experiments of whole cell extracts of HeLa cells treated with DMSO or 1 μM PlaB for 30 minutes. SRSF2, c-MYC, and SF3B1 were immunoprecipitated using antibodies against the endogenous proteins. Rabbit IgG were used as negative controls for non-specific binding. Proteins were resolved by SDS-PAGE and immunoblotted with anti-SRSF2, anti-c-MYC, anti-SF3B1, anti-CDK9, anti-Cyclin T1, and either anti-β-tubulin or anti-β-actin as a control.

4.10 The effect of SF3B1 inhibition on CDK9 recruiters

CDK9 is known to be recruited to chromatin by the atypical kinase bromodomain-containing protein (BRD4) (Fujinaga et al., 2004; Kim and Sharp, 2001; Schröder et al., 2012; Zhou et al., 2022), the super elongation complex component, AFF4 (Lin et al., 2010; Zhou et al., 2022), as well as the general transcription factor, c-MYC (Rahl et al., 2010).

To determine whether known CDK9 recruiters are affected by SF3B1 inhibition, western blotting analysis were performed with antibodies against BRD4, AFF4, and c-MYC using chromatin and nucleoplasm extracts with and without 30 minutes of PlaB treatment (Figure 4.9). Inhibition of SF3B1 affects the chromatin association of AFF4 causing it to decrease and accumulate in the nucleoplasm. On the other hand, SF3B1 inhibition had no clear effect on the chromatin association or nucleoplasm level of BRD4 or c-MYC.

In summary, SF3B1 function influences CDK9 recruitment to chromatin through AFF4, but not BRD4 or c-MYC.

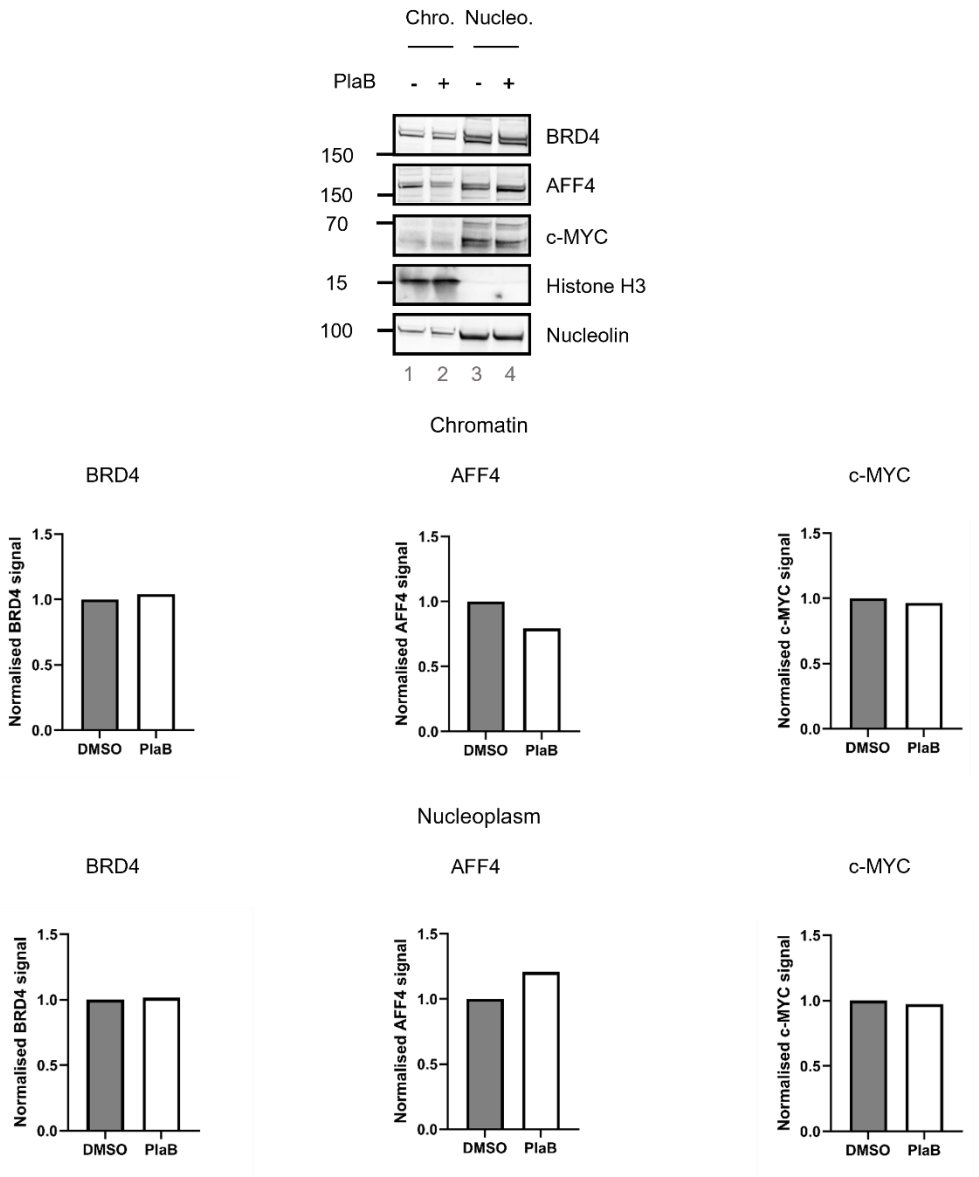


Figure 4.9. The effect of SF3B1 inhibition on CDK9 recruiters

(Top) Western blot analysis of chromatin and nucleoplasm extracts of HeLa cells treated with DMSO or with 1 μM PlaB for 30 minutes. Cell nuclei equivalents were used for each blot. Proteins were resolved by SDS-PAGE and immunoblotted with anti-BRD4, anti-AFF4, anti-c-MYC, and either anti-Histone H3 or anti-Nucleolin as a control. **(Bottom)** Quantification of the western blots for DMSO (grey) and PlaB (white). Each quantification signal was normalised to the Histone H3 signal for chromatin extracts or to Nucleolin for nucleoplasm extracts. Bars represent normalised antibody signal for 1 biological replicate.

4.11 Discussion

While CDK9 is mainly nuclear, there is a significant pool of inhibitory 7SK snRNP-P-TEFb complex that serves as an inactive reservoir of P-TEFb in the cytoplasm (Ramanathan et al., 1999; Faust et al., 2018). Cytoplasmic P-TEFb is released and shuttled into the nucleus during homeostasis but also diverse signalling events for subsequent transcriptional regulation in gene expression (Napolitano et al., 2002 ; Amente et al., 2009; Bartholomeeusen et al., 2012; Biglione et al., 2007; Nguyen et al., 2001; Faust et al., 2018). The transcriptional inhibitor, DRB, stimulates the localisation of P-TEFb from the cytoplasm to the nucleus, enriching on chromatin (Faust et al., 2018). In line with previous results, fractionation experiments showed that the direct loss of CDK9 function increases the nuclear availability and association of potentially active CDK9 to chromatin (Figure 4.1, Figure S3).

CDK9 in the nucleus is also known to be actively exported from the nucleus (Napolitano et al., 2002). In this study, the nuclear distribution of CDK9 in its active form, along with Cyclin T1, was found to localise more in the nucleoplasm than on chromatin (Figure S4B). Here, evidence is also provided for SF3B1 function regulating the nucleocytoplasmic transport of the active form of CDK9 (Figure 4.1, Figure S4A). Interestingly, the loss of SF3B1 function also induces the nuclear export of Cyclin T1. Fractionation experiments further revealed that blocking the nuclear export of P-TEFb using LMB before SF3B1 inhibition does not impair nucleocytoplasmic export, likely due to treatment times being too short (Figure 4.3). A novel mechanism proposed for the mode of action of LMB is that it only affects the nuclear import capabilities of CRM1, therefore, CRM1 continues to shuttle cargo out of the nucleus to the cytoplasm until there is no longer any CRM1 available in the

nucleus (Rahmani and Dean, 2017) (Figure 4.10). Interestingly, ChIP experiments showed LMB treatment alone affects pol II entering productive transcription elongation on KPNB1, suggesting that longer treatment times could result in decreased gene expression and, therefore, may not be useful (Figure 4.4C). The blocking of nuclear export before SF3B1 inhibition also causes an increase of CDK9 on chromatin, suggesting a possible reversal of the effect of SF3B1 inhibition on transcription (Figure 4.3). RT-PCR and ChIP experiments revealed that the restored CDK9 has no effect on pol II occupancy and transcription elongation (Figure 4.4).

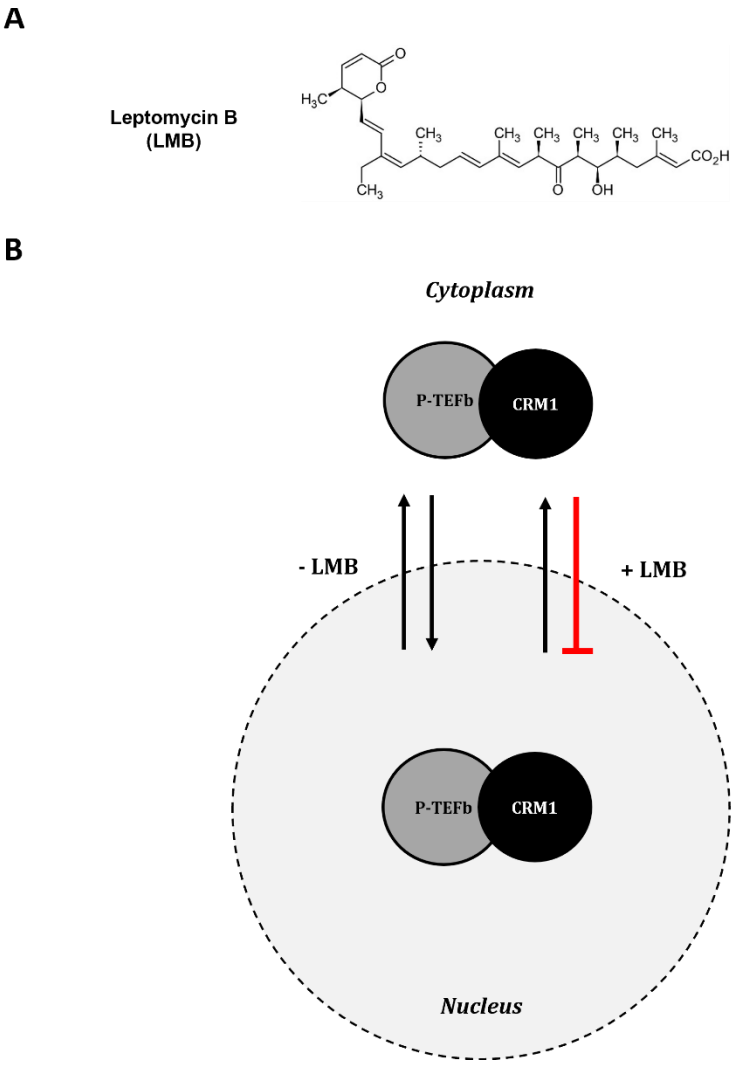


Figure 4.10. Novel mechanism of action for LMB nucleocytoplasmic transport.

(A) Chemical structure of LMB (Cell Signaling). **(B)** Nucleocytoplasmic shuttling of CRM1 cargo in the absence or presence of LMB described by Rahmani and Dean, 2017.

Previous protein-protein interaction studies hint that the transcription co-factor, Tat-SF1 mediates crosstalk between SF3B1 and CDK9. Consistent with data provided here, Tat-SF1 interacts with SF3B1 (Yang et al., 2023) and stimulates transcription elongation *in vitro* (Chen et al., 2009; Fong and Zhou, 2001; Loerch et al., 2019). Tat-SF1 interacts with CDK9 and Cyclin T1 (Parada and Roeder, 1999, Fong and Zhou, 2001) as well as with other components of the U2 snRNP *in vivo*

(Abramczuk et al., 2017) and *in vitro* (Agafonov et al., 2011). The yeast orthologue of Tat-SF1, Cus-2 interacts with SF3B1 (Talkish et al., 2019). Co-immunoprecipitation experiments here revealed that the protein interactions of Tat-SF1 with SF3B1, CDK9 and Cyclin T1 is independent of chromatin or RNA (Figure S7). The mechanism of action of PlaB is to bind SF3B1 and arrests it in an open conformation (Cretu et al., 2018), preventing the stabilisation of the U2 snRNP to BP sites in introns (Effenberger et al., 2016). Recent structural reports show that Tat-SF1 binds to SF3B1 in the open conformation and that displacement of Tat-SF1 must occur to allow stable U2 snRNP to interact with the BP site (Zhang et al., 2020; Tholen et al., 2022). Consistent with co-immunoprecipitation data presented here, the association of Tat-SF1 with SF3B1 is enhanced in the presence of PlaB as it extends the period SF3B1 is held in its open confirmation (Figure 4.6). Proteolysis targeting chimera (PROTAC) or degradation tagging (dTAG) against Tat-SF1 would be important for determining whether it is indeed the auxiliary factor involved in mediating the role of SF3B1 in transcription.

Another potential candidate for linking SF3B1 and CDK9 is SNW1. SNW1 associates with SF3B1 as part of the activated spliceosome, B^{act} complex. SNW1 associates with CDK9 and Cyclin T1 to activate inducible genes (Brès et al., 2009) and drive the nuclear factor κB pathway (Verma et al., 2019). SNW1 is also a substrate of P-TEFb (Decker et al., 2019). Here, co-immunoprecipitations show that SNW1 co-immunoprecipitates with SF3B1 and Cyclin T1 only on chromatin and is dependent on SF3B1 function (Figure 4.6). Inhibition of SF3B1 causes a striking loss of chromatin associated SNW1 that gets exported from the nucleus (Figure 4.7B, Figure 4.7D). Interestingly, loss of SNW1 does not have much of an effect on the interactions between SF3B1, Tat-SF1, and P-TEFb, indicating that SNW1 is likely not

the auxiliary factor linking SF3B1 and CDK9 in this SF3B1-dependent transcription mechanism, but may explain why there is less P-TEFb recruited/stabilised on chromatin after SF3B1 inhibition, as SNW1 a known CDK9 recruiter (Verma et al., 2019), is not there anymore (Figure 4.6).

SRSF2 and c-MYC are also found in the interactome of CDK9 (Ji et al., 2013, Brès et al., 2009). SRSF2 co-immunoprecipitation experiments revealed that SRSF2 has weak interactions with CDK9 or Cyclin T1 indicating an indirect, possibly protein complex-based association of SRSF2 to CDK9 and Cyclin T1 (Figure 4.8B). SRSF2 is also an interactor of SF3B1 (Deckert et al., 2006). SRSF2 co-immunoprecipitation showed SRSF2 binds SF3B1 (Figure 4.8B). However, the reverse SF3B1 co-immunoprecipitation did not show binding of SF3B1 to SRSF2 suggesting that a fraction of SF3B1 interacts with SRSF2, whereas a lot of SRSF2 interacts with SF3B1 in HeLa cells. Co-immunoprecipitation experiments of c-MYC did not co-immunoprecipitate known interactors of c-MYC such as CDK9 or Cyclin T1 possibly due to poor antibody quality (Figure 4.8B).

The recruitment of CDK9 to promoter-proximally paused pol II sites on chromatin is a significant step regulating transcription elongation. The actions of BRD4 together with the Jumonji domain containing protein 6 (JMJD6) (Liu et al., 2013; Jang et al., 2005; Lee et al., 2020), AFF4 as part of the super elongation complex (Lin et al., 2010; Zhou et al., 2022), the transcription factor c-MYC (Rahl et al., 2010), and splicing factors SNW1 (Verma et al., 2019) and SRSF2 (Ji et al., 2013), have all been shown to be important for mediating CDK9 recruitment. In this study, SF3B1 inhibition has been shown to influence CDK9 recruitment. However, the effect of SF3B1 inhibition on known CDK9 recruiters is unknown. Fractionation experiments

revealed that SF3B1 inhibition does not interfere with the recruitment of BRD4 or c-MYC, suggesting SF3B1 is not involved in their respective CDK9 recruitment pathways (Figure 4.9). However, SF3B1 inhibition affects AFF4 by reducing its chromatin association and increasing its abundance in the nucleoplasm. In addition, fractionation and immunofluorescence experiments revealed SF3B1 inhibition induces the nuclear export of SNW1 (Figure 4.7D), and the active degradation of SRSF2 (Figure 4.8A), suggesting that the loss of SNW1 and SRSF2 in the nucleus, or AFF4 and SNW1 from chromatin, could be responsible for the partial reduction in CDK9 recruitment to paused pol II sites, explaining the decrease in elongating pol II after SF3B1 inhibition (Figure 3.4C).

A key finding in the present study is that while SF3B1 complexed to Tat-SF1 can recruit P-TEFb on chromatin, as Tat-SF1 still interacts with Cyclin T1 on chromatin after SF3B1 inhibition, this is surprisingly not the factor explaining the loss of P-TEFb from chromatin following SF3B1 inhibition as previously thought (Fong and Zhou, 2001).

Together, the data presented here further reveals the mechanistic differences between the primary effects of SF3B1 and CDK9 inhibition. SF3B1 function in transcription is important for regulating the subcellular localisation of CDK9 and subsequent gene expression.

Chapter 5. The effect of other splicing inhibitors on transcription

5.1 Background

SF3B1 is canonically known as a splicing factor. Therefore, examining whether splicing inhibition generally correlates with the effects of SF3B1 inhibition would determine whether the effects of SF3B1 inhibition on transcription are unique.

In 1992, Herboxidiene was the first splicing inhibitor discovered and was described at the time as a natural product of *Streptomyces chromofuscus* with phytotoxic activity (Isaac et al., 1992; Miller-Wideman et al., 1992). In 2002, it was re-discovered in a different strain of *Streptomyces* as one of a group of molecules called GEX1 compounds, a set of compounds with potent cytotoxic effects in the low to mid-nanomolar range against human tumour cell lines (Sakai et al., 2002a; Sakai et al., 2002b). In 2004, PlaB, a natural product discovered in *Streptomyces platensis* was found to inhibit the growth of several tumour cell cultures from a panel of 39 cancer cell lines at low nanomolar IC_{50} values (Mizui et al., 2004; Sakai et al., 2004). Structurally, Herboxidiene and PlaB are very different (Bonnal et al., 2012). However, further characterisation of the compounds revealed that they share virtually identical mechanisms of action, both targeting the splicing factor SF3B1 (Bonnal et al., 2012; Kotake et al., 2007), to disrupt pre-mRNA splicing (Hasegawa et al., 2011; Effenberger et al., 2014).

Generally, SF3B1 inhibitors are highly potent and selective compounds. Several studies have demonstrated that the impact of SF3B1 inhibitors on cells closely parallel those of SF3B1 knockdown, which is consistent with the effects of these inhibitors being mediated by SF3B1 (Corrionero et al., 2011; Laetsch et al., 2014;

Papasaikas et al., 2015). In addition, the point mutation R1074H in the gene of SF3B1 was found to confer resistance to the inhibitory action of PlaB on cell proliferation and splicing, indicating that SF3B1 is a direct target of PlaB (Yokoi et al., 2011).

Isoginkgetin is a biflavonoid with anti-tumour properties (Yoon et al., 2006). In 2008, Isoginkgetin was discovered from a library of about 8,000 compounds as a natural product that acts *in vivo* and *in vitro,* at similar micromolar concentrations, as a general inhibitor of both the major and minor spliceosomes (O'Brien et al., 2008). The mechanism of action of Isoginkgetin is that it prevents the stable recruitment of the U4/U6·U5 tri-snRNP, causing the accumulation of the pre-spliceosomal A complex (O'Brien et al., 2008).

In 2014, Madrasin was identified by structure-activity relationships analysis from a library of over 70,000 drug-like small molecules as a compound that both inhibits pre-mRNA splicing *in vitro* and modifies splicing of endogenous pre-mRNA *in vivo* (Pawellek et al., 2014). Similar to Isoginkgetin, Madrasin interferes with the first step chemistry of the splicing reaction by stalling the assembly of the pre-spliceosomal A complex but not through the targeting of SF3B1 (Pawellek et al., 2014). The cellular target(s) of Madrasin are yet to be identified.

These compounds are all small molecule splicing inhibitors that cause spliceosome assembly to stall at the step of A complex formation, the stage where the U2 snRNP joins the BP sequence. With the exception of Madrasin, these splicing inhibitors are natural compounds with distinct structures.

The potencies of these compounds relative to one another on pre-mRNA splicing is unknown. Further, it remains poorly understood whether the inhibition of splicing

generally affects transcription or if SF3B1 is a unique factor mediating crosstalk between the splicing and transcription machineries. To better understand this, the present work describes the evaluation of the potencies of SF3B1-specific inhibitors against general splicing inhibitors on pre-mRNA splicing and on transcription, through the assessment of the subcellular localisation of SF3B1 and P-TEFb.

5.2 Herboxidiene rapidly inhibits pre-mRNA splicing and does not promote a stress response in human cells

To determine whether short treatment times with Herboxidiene (Figure 5.1A) influences pre-mRNA splicing catalysis in human cells, RT-PCR was performed using a concentration of 1 μM Herboxidiene for times ranging between 30 minutes to 4 hours to evaluate total RNA for spliced and unspliced transcripts of the intron-containing genes, *BRD2* and *DNAJB1* (Figure 5.1B). In the absence of Herboxidiene, there are little or no detectable introns retained in these transcripts. The presence of Herboxidiene induces rapid intron-retention within 30 minutes by 498% for the intron between exons 4 and 5 of *BRD2* and by 807% for the intron between exons 2 and 3 of *DNAJB1*, increasing over time.

To determine whether short Herboxidiene treatment induces cytotoxic stress responses, immunofluorescence was performed using an antibody against the general stress response marker, G3BP1 (Kedersha et al., 2016), following 30 minutes of Herboxidiene treatment (Figure 5.1C). The average fluorescent intensity of G3BP1 did not show a significant statistical change between Herboxidiene treatment and non-treatment conditions (Kruskal-Wallis, $P>0.05$).

These results confirm that short inhibition of SF3B1 is sufficient to affect splicing without inducing cytotoxicity in HeLa cells.

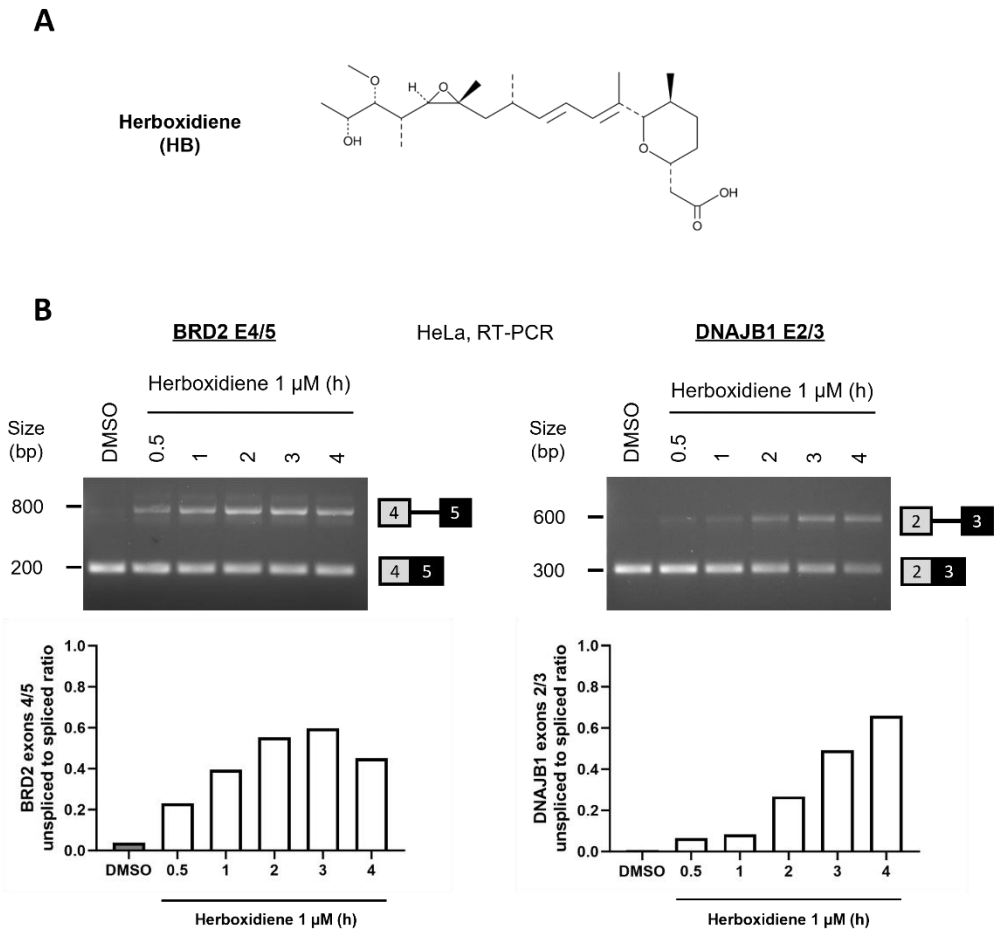

A
Herboxidiene
(HB)
B
BRD2 E4/5
HeLa, RT-PCR
DNAJB1 E2/3
Herboxidiene 1 µM (h)
Size
(bp)
DMSO
0.5
1
2
3
4
800
200
600
300
BRD2 exons 4/5
unspliced to spliced ratio
DNAJB1 exons 2/3
unspliced to spliced ratio
C
- DMSO
+ DMSO
Herboxidiene
DAPI
G3BP1
Merged
Fluorescent Intensity of G3BP1
ns
HB

Figure 5.1. Herboxidiene rapidly inhibits pre-mRNA splicing and does not promote a stress response in human cells

(A) Chemical structure of Herboxidiene. **(B, top)** RT-PCR with primers amplifying the intron located between exons 4 and 5 of *BRD2* or the intron located between exons 2 and 3 of *DNAJB1.* HeLa cells were treated with DMSO or 1 μM Herboxidiene for times ranging between 30 minutes to 4 hours. The locations of the spliced and unspliced RNA are shown to the right of each gel image. **(B, bottom)** Quantification of relative band intensity as a ratio of unspliced to spliced RNA for DMSO (grey) and Herboxidiene (white). **(C, left)** Representative images of immunofluorescence analysis in HeLa cells without treatment or treated with DMSO or 1 μM Herboxidiene for 30 minutes. DAPI (blue), G3BP1 (green), scale bar: 100 μm. **(C, right)**. Quantification of fluorescent intensity per nucleus for no treatment (light grey), DMSO (grey) and Herboxidiene (white). Violin plot settings are: min to max values with the median and 25-75 percentile range. >10,000 nuclei were quantified per condition. Statistical test: Kruskal-Wallis test. P-value: ns > 0.05,

5.3 Potency of splicing inhibitors on splicing differs in human cells

Small molecule splicing modulators interfere with different aspects of the spliceosome and exhibit a spectrum of capacities to inhibit splicing catalysis (Effenberger et al., 2017). Splicing inhibitors of the Herboxidiene family target SF3B1 and stall the assembly of the A complex, whereas other splicing inhibitors such as Isoginkgetin are more general and prevent stable recruitment of the U4/U6·U5 tri-snRNP (O'Brien et al., 2008). The cellular target(s) and mechanism of splicing inhibition for some splicing inhibitors such as Madrasin and Isoginkgetin are yet to be identified.

To compare the potencies of some splicing inhibitors that target different components of the spliceosome, RT-PCR was performed using the SF3B1 inhibitors, PlaB and Herboxidiene, and general splicing inhibitors, Isoginkgetin and Madrasin, for 1 hour to evaluate total RNA for spliced and unspliced transcripts of the intron-containing genes, *BRD2* and *DNAJB1* (Figure 5.2). The absence of inhibitory splicing conditions causes little to no detectable intron retention. The presence of the SF3B1 inhibitors, PlaB and Herboxidiene, induce rapid intron retentions of over 3,000% for *BRD2* and 350% for *DNAJB1* transcripts respectively, compared to Madrasin and Isoginkgetin that cause less intron retentions (approximately 40% for *BRD2* and 20% for *DNAJB1*, respectively).

These results indicate that inhibiting different points of spliceosome assembly does not have the same effect on splicing.

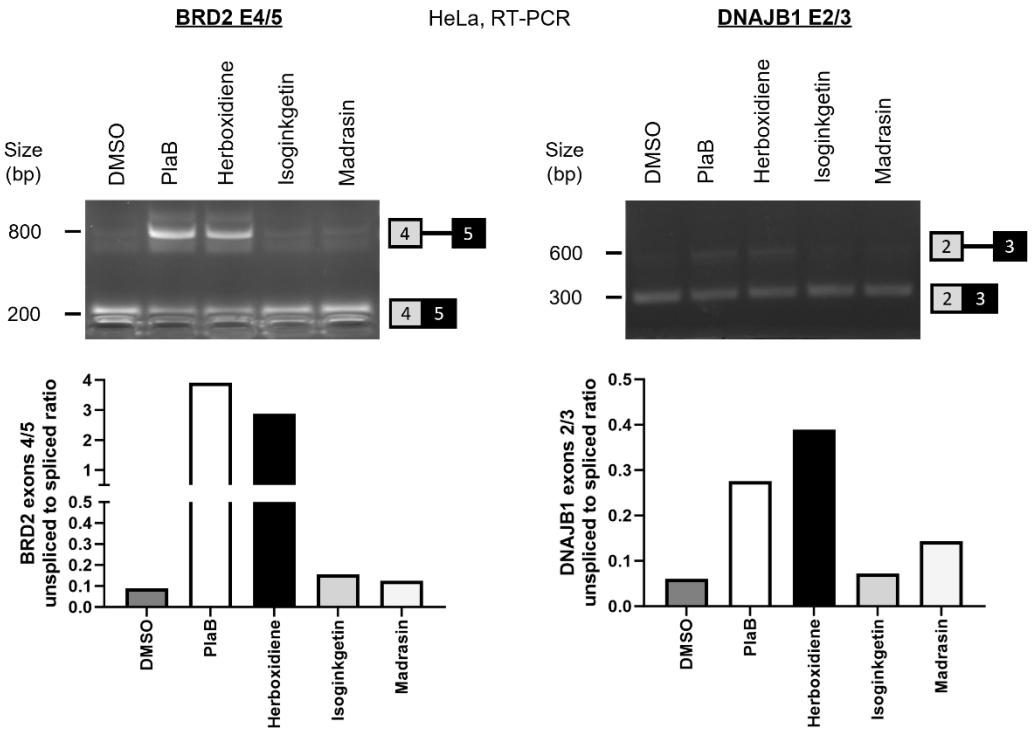


Figure 5.2. Potency of splicing inhibitors on splicing differs in human cells

(A, top) RT-PCR with primers amplifying the intron located between exons 4 and 5 of *BRD2* or the intron located between exons 2 and 3 of *DNAJB1.* HeLa cells were treated with DMSO, 1 μM PlaB, 1 μM Herboxidiene, 30 μM Isoginkgetin, or 90 μM Madrasin for 1 hour. The locations of the spliced and unspliced RNA are shown to the right of each gel image. **(B, bottom)** Quantification of relative band intensity as a ratio of unspliced to spliced RNA for DMSO (grey), PlaB (white), Herboxidiene (black), Isoginkgetin (stone grey), Madrasin (light grey).

5.4 Splicing inhibitors that target SF3B1 also affect transcription

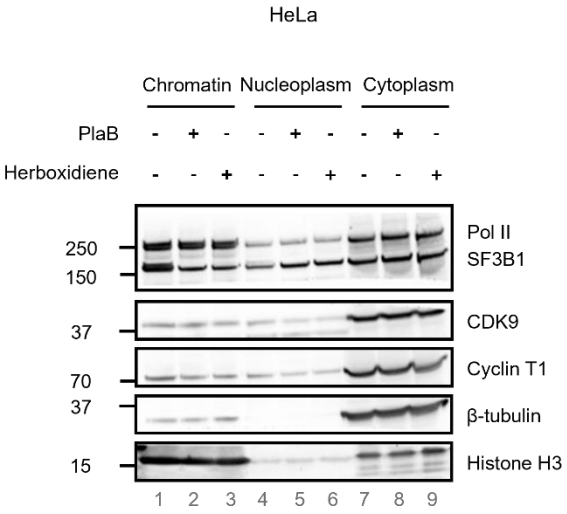
To determine whether the mechanism following SF3B1 inhibition is unique or that inhibition of splicing generally causes the same phenotypic effects on transcription, western blotting analyses was performed with antibodies against SF3B1, CDK9, Cyclin T1, and total pol II as a negative control using chromatin, nucleoplasm, and cytoplasm extracts with and without PlaB, Herboxidiene, Madrasin, or Isoginkgetin treatment for 30 minutes (Figure 5.3A, Figure 5.3B). Inhibiting SF3B1 using PlaB or Herboxidiene caused the same effects by reducing the chromatin association of SF3B1, CDK9, and Cyclin T1, increasing SF3B1 in the nucleoplasm, while also reducing CDK9 and Cyclin T1 in the nucleoplasm. In contrast, non-SF3B1-specific splicing inhibition using Madrasin and Isoginkgetin had different effects. Madrasin treatment causes a reduction in chromatin-bound SF3B1, an increase in chromatin-bound CDK9 and Cyclin T1, and an increase of SF3B1, CDK9, and Cyclin T1 in the nucleoplasm. The effects of Madrasin on SF3B1, CDK9, and Cyclin T1 mirror CDK9 inhibition with DRB (Figure S3, Figure S4A). Isoginkgetin treatment has no effect on SF3B1 bound to chromatin but reduces CDK9 and Cyclin T1 chromatin association, while SF3B1 in the nucleoplasm increases and CDK9 and Cyclin T1 in the nucleoplasm remain unchanged.

To determine the effects the different splicing inhibitors have on transcription, 5-EU-labelling was performed to measure *de novo* RNA synthesis following PlaB, Herboxidiene, Madrasin or Isoginkgetin treatments for 1 hour (Figure 5.3C). SF3B1 inhibition causes a significant reduction in nascent RNA synthesis by 36% and 25% for PlaB and Herboxidiene, respectively (Kruskal-Wallis test, $P<0.0001$). Madrasin treatment also causes a significant reduction in nascent RNA synthesis, although to

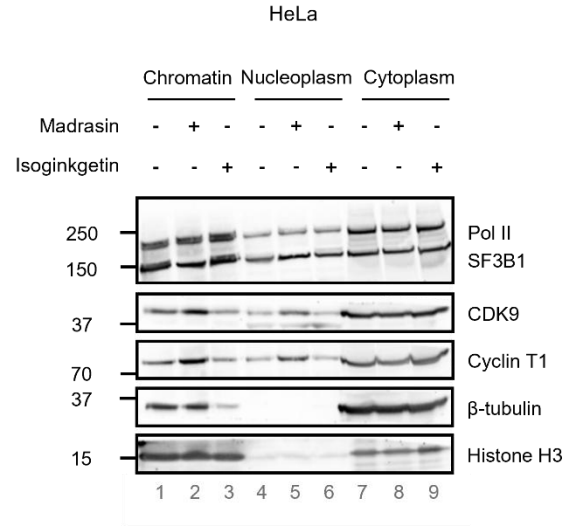
a smaller extent (7%) (Kruskal-Wallis test, $P<0.0001$). Isoginkgetin treatment did not cause a statistically significant change in nascent RNA synthesis (Kruskal-Wallis test, $P>0.05$).

In summary, SF3B1 inhibition differs in the subcellular distribution of SF3B1 and P-TEFb and affects transcription to a greater degree compared to non-SF3B1 specific splicing inhibition.

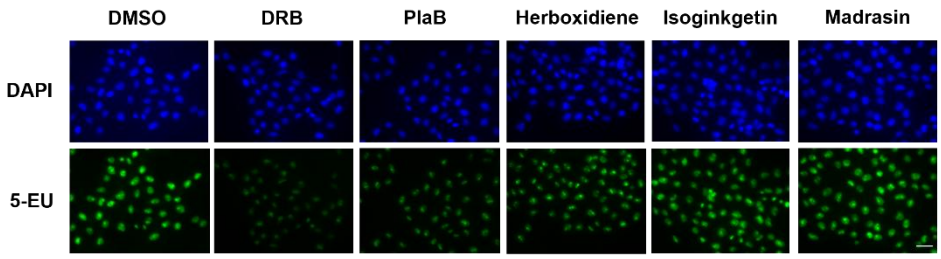
A


HeLa
Chromatin Nucleoplasm Cytoplasm
PlaB - + - - + - - + -
Herboxidiene - - + - - + - - +
250
150
Pol II
SF3B1
37
CDK9
70
Cyclin T1
37
β-tubulin
15
Histone H3
1 2 3 4 5 6 7 8 9

B


HeLa
Chromatin Nucleoplasm Cytoplasm
Madrasin - + - - + - - + -
Isoginkgetin - - + - - + - - +
250
150
Pol II
SF3B1
37
CDK9
70
Cyclin T1
37
β-tubulin
15
Histone H3
1 2 3 4 5 6 7 8 9

C


DMSO
DRB
PlaB
Herboxidiene
Isoginkgetin
Madrasin
DAPI
5-EU

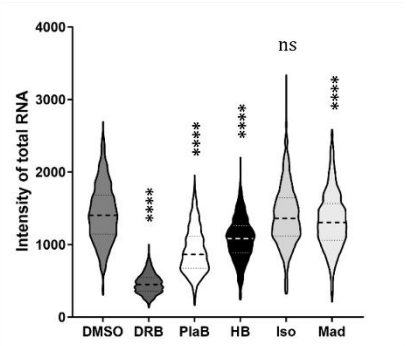

Intensity of total RNA
4000
3000
2000
1000
0
ns
****
****
****
****
DMSO DRB PlaB HB Iso Mad

Figure 5.3. Splicing inhibitors that target SF3B1 also affect transcription

(A and B) Western blot analysis of chromatin, nucleoplasm, and cytoplasm extracts of HeLa cells treated with DMSO, 1 μM PlaB, 1 μM Herboxidiene, 30 μM Isoginkgetin, or 90 μM Madrasin for 1 hour. Cell nuclei equivalents were used for each blot. Proteins were resolved by SDS-PAGE and immunoblotted with anti-pol II, anti-SF3B1, anti-CDK9, anti-Cyclin T1, and either anti-Histone H3 or anti-β-tubulin as a loading control. **(C, top)** Representative images of 5-EU incorporation in HeLa cells treated with DMSO, 100 μM DRB, 1 μM PlaB, 1 μM Herboxidiene, 30 μM Isoginkgetin, or 90 μM Madrasin for 1 hour. DAPI (blue), 5-EU (green), scale bar: 50 μm. **(C, bottom)** Quantification of 5-EU incorporation per nucleus for DMSO (grey), DRB (dark grey), PlaB (white), Herboxidiene (Black), Isoginkgetin (stone grey), and Madrasin (light grey). Violin plot settings are: min to max values with the median and 25-75 percentile range. 1033 nuclei were quantified per condition. Statistical test: Kruskal-Wallis test. P-value: ns > 0.05, **** < 0.0001.

5.5 Splicing inhibition may not be the primary effect of the splicing inhibitor Isoginkgetin

Isoginkgetin is currently understood to prevent the recruitment of the U4/U6·U5 tri-snRNP, resulting in accumulation of the prespliceosomal A complex (O'Brien et al., 2008). These observations were made by assessing overnight Isoginkgetin treatment on HEK293 cells expressing splicing reporters. It was possible that the effect of Isoginkgetin (Figure 5.4A) on splicing and possibly transcription is only seen with long treatment times.

To determine whether longer Isoginkgetin treatment influences splicing catalysis, RT-PCR was performed using Isoginkgetin for times ranging between 1 hour to 3 hours, for transcripts of the intron-containing gene, *BRD2* (Figure 5.4B). Isoginkgetin treatment of 3 hours did not induce intron-retention.

To determine whether longer Isoginkgetin treatment influences transcription through SF3B1, CDK9, or Cyclin T1, western blotting analyses was performed with antibodies against SF3B1, CDK9, and Cyclin T1 using chromatin and nucleoplasm extracts with and without Isoginkgetin treatment for times ranging between 1 hour and 3 hours (Figure 5.4C). Isoginkgetin treatment of 3 hours did not show a change in SF3B1 chromatin association or nucleoplasm level but did show a gradual decrease of CDK9 and Cyclin T1 on chromatin as well as in the nucleoplasm over time.

To determine whether longer Isoginkgetin treatment influences nascent transcription, 5-EU-labelling was performed to measure *de novo* RNA synthesis following Isoginkgetin treatment for times ranging between 1 hour to 6 hours

(Figure 5.4D). Isoginkgetin treatment began to show a significant decrease in transcription from about 5 hours.

In summary, Isoginkgetin has no detectable effects on splicing with short treatment times indicating that the primary effect of Isoginkgetin is not splicing inhibition.

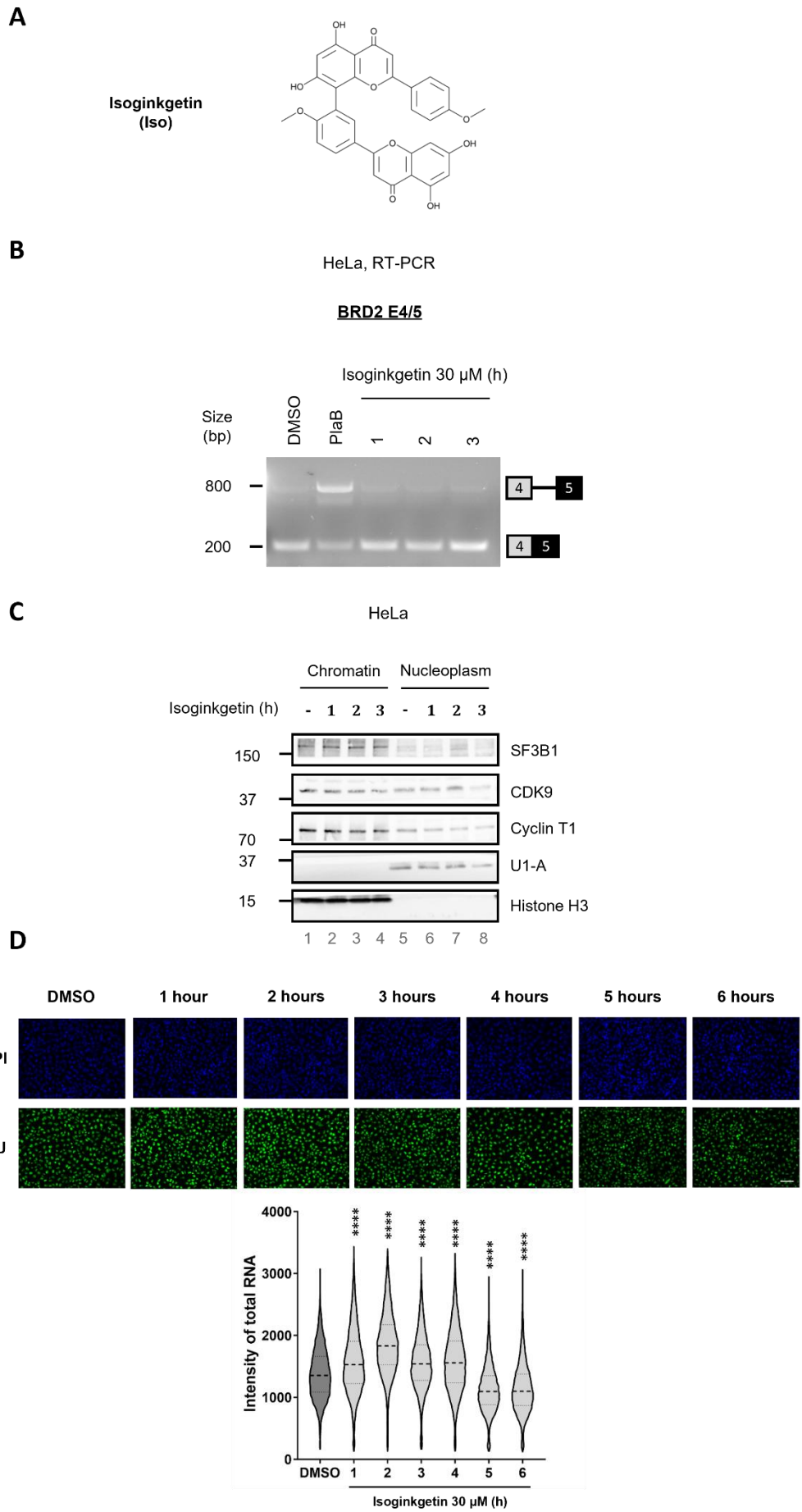

A
Isoginkgetin
(Iso)
B
HeLa, RT-PCR
BRD2 E4/5
Isoginkgetin 30 µM (h)
Size
(bp)
DMSO
PlaB
1
2
3
800
200
4
5
C
HeLa
Chromatin
Nucleoplasm
Isoginkgetin (h)
- 1 2 3 - 1 2 3
150
37
70
37
15
SF3B1
CDK9
Cyclin T1
U1-A
Histone H3
1 2 3 4 5 6 7 8
D
DMSO
1 hour
2 hours
3 hours
4 hours
5 hours
6 hours
DAPI
5-EU
Intensity of total RNA
4000
3000
2000
1000
0
****
DMSO 1 2 3 4 5 6
Isoginkgetin 30 µM (h)

Figure 5.4. Splicing inhibition may not be the primary effect of the splicing inhibitor Isoginkgetin

(A) Chemical structure of Isoginkgetin (Sigma Aldrich). **(B)** RT-PCR with primers amplifying the intron located between exons 4 and 5 of *BRD2.* HeLa cells were treated with DMSO, 1 μM PlaB as a control, or 30 μM Isoginkgetin for times ranging between 1 hour to 3 hours. The locations of the spliced and unspliced RNA are shown to the right of each gel image. **(C)** Western blot analysis of chromatin and nucleoplasm extracts of HeLa cells treated with DMSO or with 30 μM Isoginkgetin for times ranging between 1 hour to 3 hours. Cell nuclei equivalents were used for each blot. Proteins were resolved by SDS-PAGE and immunoblotted with anti-SF3B1, anti-CDK9, anti-Cyclin T1, and either anti-Histone H3 or anti-U1-A as a loading control. **(D, top)** Representative images of 5-EU incorporation in HeLa cells treated with DMSO or with 30 μM Isoginkgetin for times ranging between 1 hour and 6 hours. DAPI (blue), 5-EU (green), scale bar: 100 μm. **(D, bottom)** Quantification of 5-EU incorporation per nucleus for DMSO (grey) or Isoginkgetin (stone grey). Violin plot settings are: min to max values with the median and 25-75 percentile range. 8466 nuclei were quantified per condition. Statistical test: Kruskal-Wallis test. P-value: **** < 0.0001.

5.6 Discussion

Transcription is known to affect co-transcriptional pre-mRNA splicing through two non-mutually exclusive possibilities: by the speed of pol II, and or by interactions between pol II or the transcription elongation machinery with the splicing machinery (Bentley, 2014; Merkhofer et al., 2014; Saldi et al., 2016; Wallace and Beggs, 2017; Tardiff et al., 2006; Tellier et al., 2020a). Transcription and pre-mRNA splicing are more intimately coupled than previously thought and that splicing talks back to transcription to influence the behaviour of pol II (Fiszbein et al., 2019; Caizzi et al., 2021; Nojima et al., 2015; Tellier et al., 2020a). The discovery of natural compounds which inhibit splicing has been central to furthering our understanding. However, mechanistic insight into how different splicing inhibitors influence transcription is yet to be fully elucidated. By evaluating the effects of short treatment time of the small molecule inhibitors, PlaB, Herboxidiene, Madrasin, and Isoginkgetin, the experiments described here reveal the differential effects of splicing inhibitors on CDK9, providing mechanistic insight into how they each affect transcription.

The spliceosome has over 200 components participating in the dynamic assembly pathway (Jurica et al., 2003), targets for an array of different splicing inhibitors conferring a range of splicing inhibitory potencies. Here, the potencies of splicing inhibition of Madrasin (Pawellek et al., 2014), a splicing inhibitor whose cellular target(s) are unknown but do not include SF3B1, and Isoginkgetin (O'Brien et al., 2008), a biflavonoid that prevents the stable recruitment of the U4/U6·U5 tri-snRNP during splicing catalysis, were assessed against the SF3B1 inhibitors, PlaB and Herboxidiene, known to strongly inhibit splicing (Bonnal et al., 2012; Kotake et al.,

2007). Short treatment times revealed Madrasin and Isoginkgetin to be far less potent splicing inhibitors than the SF3B1 inhibitors (Figure 5.2). A recent study found that inactive analogues of PlaB and Herboxidiene interchangeably compete with the active versions of each other, suggesting that they have a shared pharmacophore through the same site of interaction on SF3B1, despite their different structures (Effenberger et al., 2016). Splicing assays assessing short inhibition of SF3B1 with PlaB or Herboxidiene revealed that both SF3B1 inhibitors induce rapid intron retention in transcripts to the same degree, supporting the findings that these compounds have the same interaction with SF3B1 and a common pharmacophore (Figure 5.2).

Here, evidence is provided for SF3B1 inhibition having a unique mechanism to mediate crosstalk between the splicing and transcription machineries. Short treatments to limit the influence of secondary/indirect effects showed that the SF3B1 inhibitors, PlaB and Herboxidiene, have the same effect on the subcellular localisation of SF3B1 and P-TEFb, albeit the effect of PlaB on global transcription is stronger (Figure 5.3). In contrast, Madrasin and Isoginkgetin, splicing inhibitors that are not known to target SF3B1, show distinct effects on the subcellular localisation of SF3B1 and P-TEFb. The effect of Madrasin resembles that of CDK9 inhibition (Figure S3, Figure S4A), whereas the effects of Isoginkgetin over time are more like that of SF3B1 inhibition for P-TEFb but not for SF3B1, lends credence to the idea that the primary effect of Isoginkgetin is not splicing inhibition but perhaps inhibition of transcription.

Both Madrasin and Isoginkgetin were discovered and characterised as general splicing inhibitors (Pawellek et al., 2014; O'Brien et al., 2008), but a compound can

interfere with any number of spliceosome assembly steps prior to catalysis to confer a loss of splicing chemistry. Alternatively, the effect of these two small molecules on splicing is a secondary/indirect effect, meaning transcription is affected before splicing.

Together, experiments described here suggest SF3B1 inhibition is far more potent at inhibiting splicing catalysis than that of SF3B1-independent splicing inhibition. It is emerging that the cellular effects of SF3B1 inhibition does not correlate with the general inhibition of splicing (Angel et al., 2024), suggesting that the role of SF3B1 in transcription may be mechanistically unique. It is possible that although Madrasin is not potent, if it were, it would also affect transcription as data presented here appears to show the more you affect splicing, the more you affect transcription. However, previous reports chemically inhibiting SF3B1 using PlaB or Spliceostatin A, or using an antisense morpholino oligo targeting the U2 snRNA (U2 AMO) show that the different methods of inhibition all disrupt splicing to the same degree, but RNA synthesis is impaired far more profoundly with Spliceostatin A and the U2 antisense morpholino oligo compared to PlaB (Caizzi et al., 2021).

Chapter 6. Transcriptional kinases and phosphatases regulate SF3B1 phosphorylation

6.1 Background

SF3B1 contains a high number of phosphorylation sites and its subcellular localisation and activity are known to be regulated by phosphorylation (Seghezzi et al., 1998; Boudrez et al., 2002; de Graaf et al., 2006; Girard et al., 2012). The phosphorylation of SF3B1 is tightly correlated with the progress of catalysis during splicing (Wang et al., 1998). However, the molecular details and functional significance of this modification within the active spliceosome is largely undefined. SF3B1 has been identified as a substrate of a few cellular protein kinases. The dual-specificity tyrosine-phosphorylation regulated kinase 1A (DYRK1A) phosphorylates SF3B1 mainly at the pThr434 residue (de Graaf et al., 2006). CDK1 complexed with cyclin B phosphorylates SF3B1 *in vitro*, mediating SF3B1 recognition by nuclear inhibitor of protein phosphatase-1 (NIPP1), subsequently directing SF3B1 to protein phosphatase-1 (PP1) (Boudrez et al., 2002; Tanuma et al., 2008). CDK2 complexed with cyclin E phosphorylates the N-terminus of SF3B1 (Seghezzi et al., 1998), to also mediate interactions with NIPP1 (Boudrez et al., 2002). CDK2-cyclin E kinase activity specifically targets SF3B1 at Thr313 (Boudrez et al., 2002; Murthy et al., 2018), a residue temporally associated with active splicing (Wang et al., 1998; Girard et al., 2012).

The development of technologies to assess the *in vivo* role of individual CDKs by highly specific inhibition has been pivotal for characterisation. Analogue-sensitive kinase technology is a chemical-genetic technique using a mutant CDK variant sensitised to inhibition by bulky, non-hydrolysable adenine analogues that do not

inhibit wild-type kinases (CDKas) (Figure 6.1) (Bishop et al., 2000; Alaimo et al., 2001). The identification of high-confidence putative P-TEFb substrates using an analogue-sensitive mutant of CDK9 revealed an enrichment of proteins implicated in transcription and the processing of RNA (Sansó et al. 2016). Among the RNA processing factors phosphorylated by CDK9 was SF3B1 at 6 sites including pThr142 but did not include the active splicing associated pThr313 phospho-site. A more recent study, this time using pharmacological inhibition and SILAC-based phosphoproteomics, also found CDK9 to target SF3B1 at several sites including pThr142 (Tellier et al., 2022).

Several other transcriptional kinases have also been found to phosphorylate SF3B1. A kinome-wide investigation into the direct roles of CDK7 in transcription showed that CDK7 along with Cyclin H and MAT1 form an CDK-activating kinase (CAK) complex that phosphorylates transcriptional CDKs including CDK9, CDK12, and CDK13 (Rimel et al., 2020). Further, Taatjes and colleagues identified an extensive requirement for CAK activity in splicing. SF3B1 was the splicing factor most affected by the loss of CAK activity, with 18 residues including SF3B1 pThr313 identified as a high-confidence CDK7 substrate. A study assessing the kinome-wide selectivity of CDK11 linked its kinase activity to be necessary for splicing chemistry and transcription dynamics (Hluchý et al., 2022). Blazek and colleagues demonstrated CDK11 binds to and phosphorylates SF3B1 at multiple threonine residues including the SF3B1 pThr313 site required for spliceosome activation. The paralogous transcriptional kinases, CDK12 and CDK13, when pharmacologically inhibited simultaneously impair splicing of a subset of promoter-proximal introns characterised by weak 3’ splice sites (Panzeri et al., 2023). Sette and colleagues found retention of the same introns were seen following SF3B1 inhibition using

PlaB. Further, CDK12 and CDK13 were shown to promote SF3B1 interaction with the introns as well as with pol II phosphorylated at Ser2. A study using radiolabelling and SILAC-based phosphoproteomics found that CDK12 and CDK13 kinase activities directly phosphorylate SF3B1 at pThr326 *in vitro* and *in vivo* (Krajewska et al., 2019).

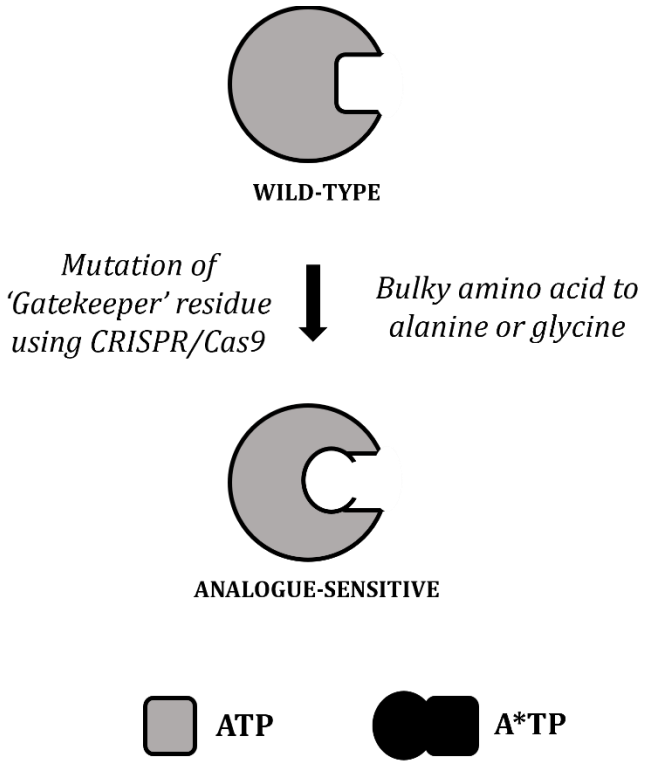


Figure 6.1. Illustration of analogue-sensitive kinase technology

A wild-type protein kinase using CRISPR/Cas9 genome engineering can become analogue-sensitive by increasing the size of its active site to accommodate non-hydrolysable adenine analogues.

In humans, protein phosphatases (PP) are known to have a broad and diverse set of substrates involved in the regulation of many cellular processes (Moorhead et al., 2007; Tomiyama et al., 2019). PP1 and PP2A are one of the most abundant cellular

proteins, prominent phosphatases with defined roles in controlling key fundamental processes including RNA processing and gene transcription through regulating the activity of numerous protein kinases (Rebelo et al., 2015; Cossa et al., 2020; Welsh and Gardini, 2023). For example, multiple CDK9 targets have been found to also be substrates of PP1 and PP2A (Parua et al., 2018; Huang et al., 2020; Parua et al., 2020; Shi, 2009; Tellier et al., 2022). SF3B1 is a substrate of CDK9 and is known to be dephosphorylated in a redundant manner on some residues by PP1 and some PP2A family phosphatases to promote the second step chemistry of splicing (Shi et al., 2006). The SF3B1 pThr142 phospho-residue is a confirmed target of PP1 (Tellier et al., 2022). However, whether other substrate SF3B1 phospho-residues are targeted by PP1 and PP2A, the potency of PP1 and PP2A inhibition on pre-mRNA splicing, and the regulatory roles of protein phosphatase activity on the emerging transcriptional functions of SF3B1 remains unclear.

In the present work, analogue-sensitive cell lines for the specific inhibitions of CDK7, CDK8, CDK9, CDK12, and CDK13, and pharmacological inhibition of PP1 and PP2A, were used to explore transcriptional kinase and protein phosphatase activities regulating the phosphorylation status of SF3B1. The effects on SF3B1 phosphorylation were determined by whole cell extractions, and the requirement of protein phosphatase activity on pre-mRNA splicing determined by RT-PCR.

6.2 SF3B1 is predominantly phosphorylated when associated with chromatin

SF3B1 activity and function is closely associated with its phosphorylation status as phosphorylated SF3B1 is detected with nucleosomes positioned over exons which facilitates the splicing recognition of exons (Kfir et al., 2015), and with functional spliceosomes concomitant with splicing catalysis (Wang et al., 1998).

To better understand the phosphorylation status of SF3B1 in the nucleus, several SF3B1 phospho-marks were assessed for their abundance by performing western blotting analyses with antibodies against total SF3B1 and SF3B1 phospho-marks pSer129, pThr142, pThr211, and pThr313 using chromatin and nucleoplasm extracts without any treatment (Figure 6.2). In line with previous published data (Girard et al., 2012), SF3B1 is mostly phosphorylated when bound to chromatin, having little to no phosphorylation at the phospho-sites tested in the nucleoplasm.

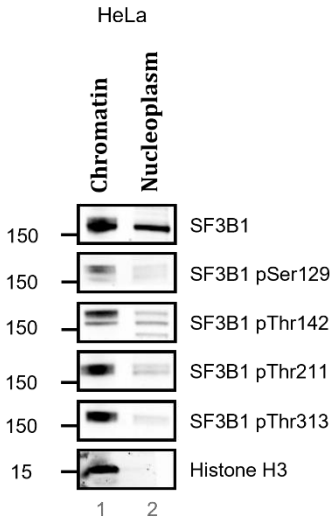


Figure 6.2. SF3B1 is predominantly phosphorylated when associated with chromatin

Western blot analysis of chromatin and nucleoplasm extracts of HeLa cells without any treatment. Cell nuclei equivalents were used for each blot. Proteins were resolved by SDS-PAGE and immunoblotted with anti-SF3B1, anti-SF3B1 pSer129, anti-SF3B1 pThr142, anti-SF3B1 pThr211, anti-SF3B1 pThr313 and anti-Histone H3 as a loading control.

6.3 SF3B1 is a substrate of CDK9

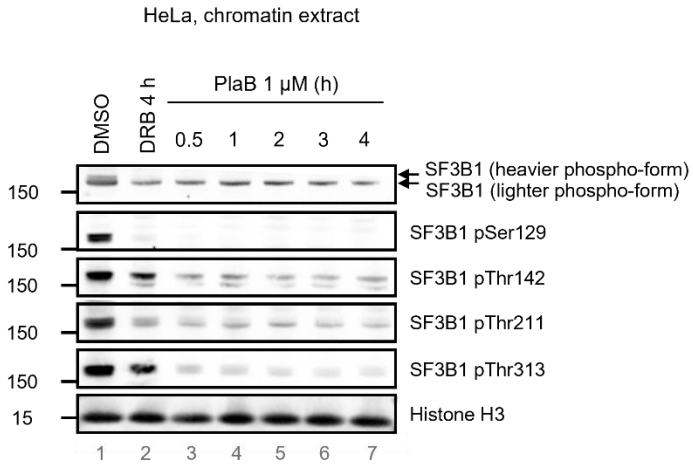
The many phospho-sites of SF3B1 are substrates for multiple transcriptional kinases including CDK9 (Sansó et al., 2016), which has been shown to specifically target SF3B1 pThr142, pThr227, and pThr436 residues, promoting the interaction of SF3B1 with pol II (Tellier et al., 2022). To determine whether other SF3B1 phospho-sites are substrates for CDK9, western blotting analyses were performed with antibodies against total SF3B1 and SF3B1 phospho-marks pSer129, pThr142, pThr211, and pThr313 using chromatin and nucleoplasm extracts with and without PlaB treatment for times ranging between 30 minutes to 4 hours or DRB treatment for 4 hours (Figure 6.3A, Figure 6.3B). On chromatin, SF3B1 inhibition after 30 minutes causes the loss of the slower migrating, heavier phospho-form of SF3B1 and reduces the abundance of the faster migrating, lighter phospho-form. Accordingly, there is a strong reduction in the abundance of all the SF3B1 phospho-marks. In a similar way, CDK9 inhibition has the same effect on total SF3B1 associated with chromatin and shows a reduction in all phospho-marks, particularly at the pSer129 and pThr211 phospho-sites which show reductions equivalent to SF3B1 inhibition with PlaB. In the nucleoplasm, both SF3B1 and CDK9 inhibition conditions cause the accumulation of total SF3B1, whereas with exception of the pThr211 phospho-mark, all other phospho-marks decrease, indicating the role of CDK9 activity on SF3B1 and the strong loss of SF3B1 phosphorylation once dissociated from chromatin, supporting previously published data (Kfir et al., 2015).

To determine the effect selective loss of CDK9 activity has on SF3B1 phosphorylation status, western blotting analyses were performed with antibodies against total SF3B1 and SF3B1 phospho-marks pSer129, pThr142, pThr211, and pThr313 using

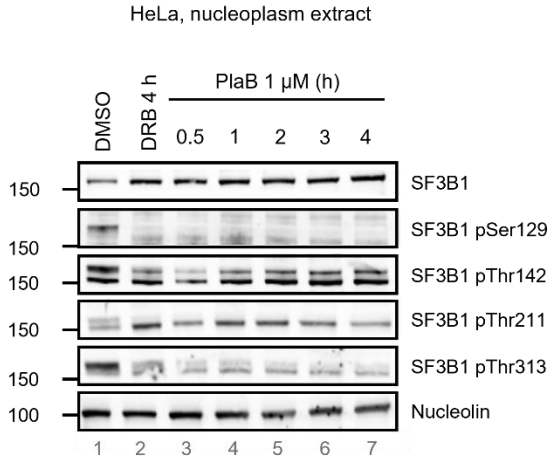
whole cell extracts of an HEK293 derived analogue-sensitive cell line of CDK9 (Tellier et al., 2022), with and without PlaB treatment for 30 minutes or the ATP analogue, 1-NA-PP1 for 30 minutes (Figure 6.3C, Figure 6.3D). The CDK9as cell line was previously characterised and shown to have the same effect on pol II elongation as small molecule CDK9 inhibitors when treated with the ATP analogue, 1-NA-PP1 (Tellier et al., 2022). The inhibition of SF3B1 on average has no effect on cellular SF3B1 level, but as previously shown (Figure 6.3A, Figure 6.3B), reduces the phosphorylation status of SF3B1 at pSer129, pThr142, pThr211, and pThr313 phospho-sites with respect to total SF3B1 level. Inhibition of CDK9 on average does not affect SF3B1 cellular levels but does induce a reduction in SF3B1 phosphorylation at pSer129, pThr142, and pThr211 phospho-sites with respect to total SF3B1 level.

These results show that there is an intimate relationship between SF3B1 function and its phosphorylation and confirms P-TEFb as a regulator of several but not all SF3B1 phosphorylation sites.

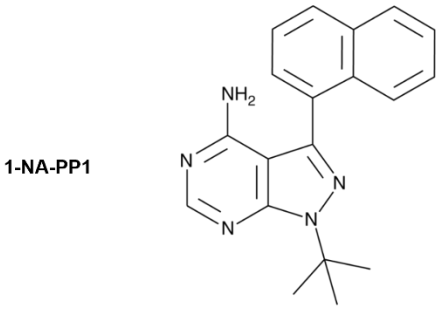
A


HeLa, chromatin extract
DMSO
DRB 4 h
PlaB 1 µM (h)
0.5 1 2 3 4
SF3B1 (heavier phospho-form)
SF3B1 (lighter phospho-form)
SF3B1 pSer129
SF3B1 pThr142
SF3B1 pThr211
SF3B1 pThr313
Histone H3
150
150
150
150
150
15
1 2 3 4 5 6 7

B


HeLa, nucleoplasm extract
DMSO
DRB 4 h
PlaB 1 µM (h)
0.5 1 2 3 4
SF3B1
SF3B1 pSer129
SF3B1 pThr142
SF3B1 pThr211
SF3B1 pThr313
Nucleolin
150
150
150
150
150
100
1 2 3 4 5 6 7

C


1-NA-PP1
NH2
N
N
N

D

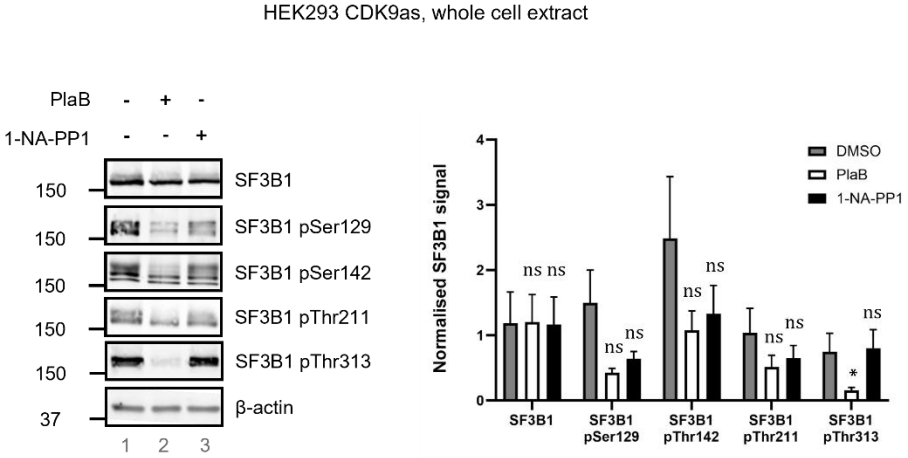

HEK293 CDK9as, whole cell extract
PlaB - + -
1-NA-PP1 - - +
SF3B1
SF3B1 pSer129
SF3B1 pSer142
SF3B1 pThr211
SF3B1 pThr313
β-actin
150
150
150
150
150
37
1 2 3
Normalised SF3B1 signal
DMSO
PlaB
1-NA-PP1
ns ns
ns
ns
ns
ns
ns
ns
ns
*
SF3B1
SF3B1 pSer129
SF3B1 pThr142
SF3B1 pThr211
SF3B1 pThr313

Figure 6.3. SF3B1 is a substrate of CDK9

(A and B) Western blot analysis of chromatin and nucleoplasm extracts of HeLa cells treated with DMSO, 100 μM DRB for 4 hours, or with 1 μM PlaB for times ranging between 30 minutes to 4 hours. Proteins were resolved by SDS-PAGE and immunoblotted with anti-SF3B1, anti-SF3B1 pSer129, anti-SF3B1 pThr142, anti-SF3B1 pThr211, anti-SF3B1 pThr313 and either anti-Histone H3 or anti-Nucleolin as a loading control. **(C)** Chemical structure of 1-NA-PP1. **(D, left)** Western blot analysis of whole cell extracts of an HEK293 derived analogue-sensitive cell line of CDK9 treated with DMSO, 1 μM PlaB, or with 15 μM 1-NA-PP1 for 30 minutes. Proteins were resolved by SDS-PAGE and immunoblotted with anti-SF3B1, anti-SF3B1 pSer129, anti-SF3B1 pThr142, anti-SF3B1 pThr211, anti-SF3B1 pThr313 and anti-β-actin as a loading control. **(D, right)** Quantification of the western blots for DMSO (grey), PlaB (white), and 1-NA-PP1 (black). Each quantification signal was normalised to the β-actin signal. Bars represent normalised antibody signal for 3 biological replicates. Error bars = standard error of the mean. Statistical test: Ordinary one-way ANOVA. P-value: ns > 0.05, * < 0.05.

6.4 SF3B1 is a substrate of other transcriptional kinases

Productive transcription elongation is associated with the progressive phosphorylation of the pol II CTD at Ser2, initially by the kinase activity of CDK9, followed by CDK12 (Laitem et al., 2015; Tellier et al., 2020b). The transcriptional kinase, CDK13, is a paralogue of CDK12 with some biological functional redundancy (Liang et al., 2015; Insco et al., 2023). To gain insight into whether other transcriptional kinases with catalytic activities directed at pol II pSer2 also target phospho-sites of SF3B1, western blotting analyses were performed with antibodies against total SF3B1 and SF3B1 phospho-marks pSer129, pThr142, pThr211, and pThr313 using whole cell extracts from HEK293 derived analogue-sensitive cell lines of CDK12 (Tellier et al., 2020b), CDK13, and the double mutant cell line CDK12+13 with and without the ATP analogue, 1-NM-PP1 for 30 minutes (Figure 6.4).

The inhibition of CDK12 on average does not affect cellular SF3B1 levels or phosphorylation of SF3B1 Ser129, Thr142, and Thr211 but decreases phosphorylation of the SF3B1 Thr313 residue when normalised to the total level of SF3B1 (Figure 6.4A).

Inhibition of CDK13 on average has no effect on cellular SF3B1 level or that of its phosphorylation status at the pThr142 or pThr313 phospho-sites but decreases phosphorylation of the SF3B1 at residues Ser129 and Thr211 when normalised to total SF3B1 level (Figure 6.4B).

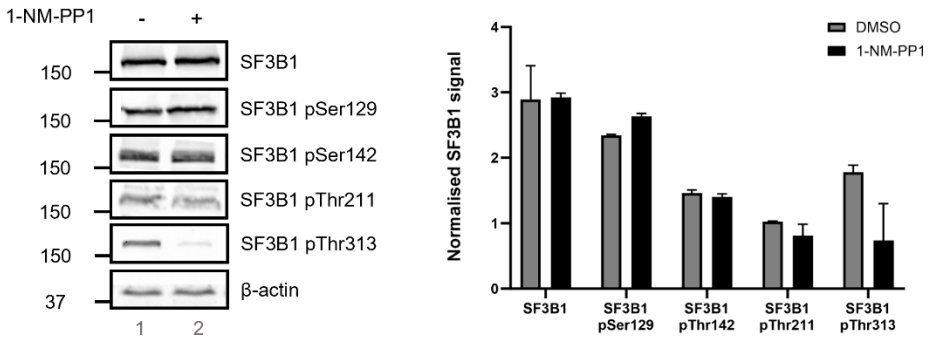
The dual inhibition of CDK12 and CDK13 on average does not have an effect on cellular SF3B1 level or phosphorylation of SF3B1 residue Thr142 but decreases phosphorylation of SF3B1 Ser129, Thr211, and Thr313 residues relative to total

SF3B1 level (Figure 6.4C). The effect on SF3B1 phosphorylation status of dual CDK12 and CDK13 inhibition reflect that of their lone inhibitions.

These results show CDK12 and CDK13 regulate SF3B1 phosphorylation, further emphasising the intimate relationship between SF3B1 and transcriptional CDKs.

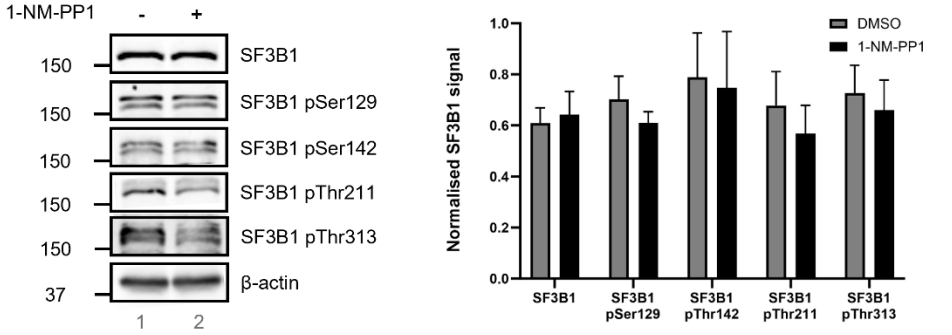
A

HEK293 CDK12as, whole cell extract



B

HEK293 CDK13as, whole cell extract



C

HEK293 CDK12/13as, whole cell extract

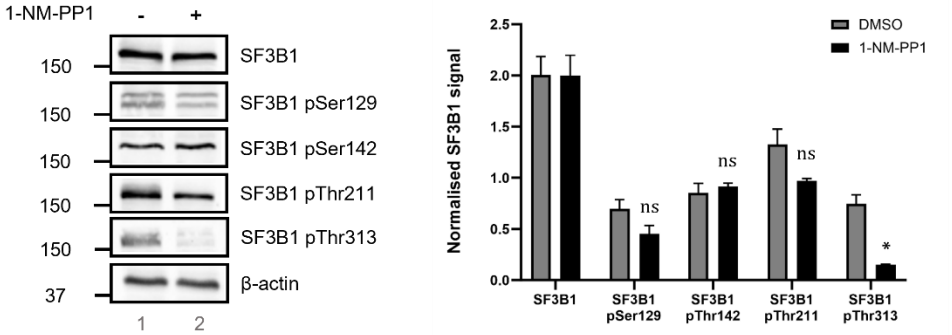


Figure 6.4. SF3B1 is a substrate of other transcriptional kinases

(A, B, C, and D, left) Western blot analysis of whole cell extracts of HEK293 derived analogue-sensitive cell lines of CDK12, CDK13, and CDK12/13 treated with DMSO or with 7.5 μM 1-NM-PP1 for 30 minutes. Proteins were resolved by SDS-PAGE and immunoblotted with anti-SF3B1, anti-SF3B1 pSer129, anti-SF3B1 pThr142, anti-SF3B1 pThr211, anti-SF3B1 pThr313 and anti-β-actin as a loading control. **(A, B, C, and D, right)** Quantification of the western blots for DMSO (grey) and 1-NM-PP1 (black). Each quantification signal was normalised to the β-actin signal. Bars represent normalised antibody signal for 3 biological replicates. Error bars = standard error of the mean. Statistical test: Ordinary one-way ANOVA. P-value: ns > 0.05, * < 0.05.

6.5 Effects of other cyclin-dependent kinases on SF3B1

To determine whether other transcriptional CDKs target phospho-sites of SF3B1, western blotting analyses were performed with antibodies against total SF3B1 and SF3B1 phospho-marks pSer129, pThr142, pThr211, and pThr313 using whole cell extracts from HEK293 derived analogue-sensitive cell lines of CDK7 and CDK8 with and without the ATP analogue, 1-NM-PP1 for 30 minutes (Figure 6.5).

Although CDK7 has previously been shown to phosphorylate SF3B1 (Rimel et al., 2020), inhibition of CDK7 here on average only slightly reduces the amount of cellular SF3B1 and its phosphorylation status at pSer129 (Figure 6.5A). On average, the magnitude of the decrease for the SF3B1 pThr142, pThr211, and pThr313 phospho-marks are equivalent to that of the decrease of cellular SF3B1, therefore indicates no change in phosphorylation status at these phospho-sites.

Inhibition of CDK8 on average does not have an effect on cellular SF3B1 level or that of the SF3B1 pSer129, pThr142, and pThr313 phospho-marks (Figure 6.5B). Although not statistically significant, CDK8 inhibition increases phosphorylation at the SF3B1 pThr211 phospho-site with respect to total SF3B1 level.

In summary, CDK7 and CDK8 were not found to directly target SF3B1 phospho-sites.

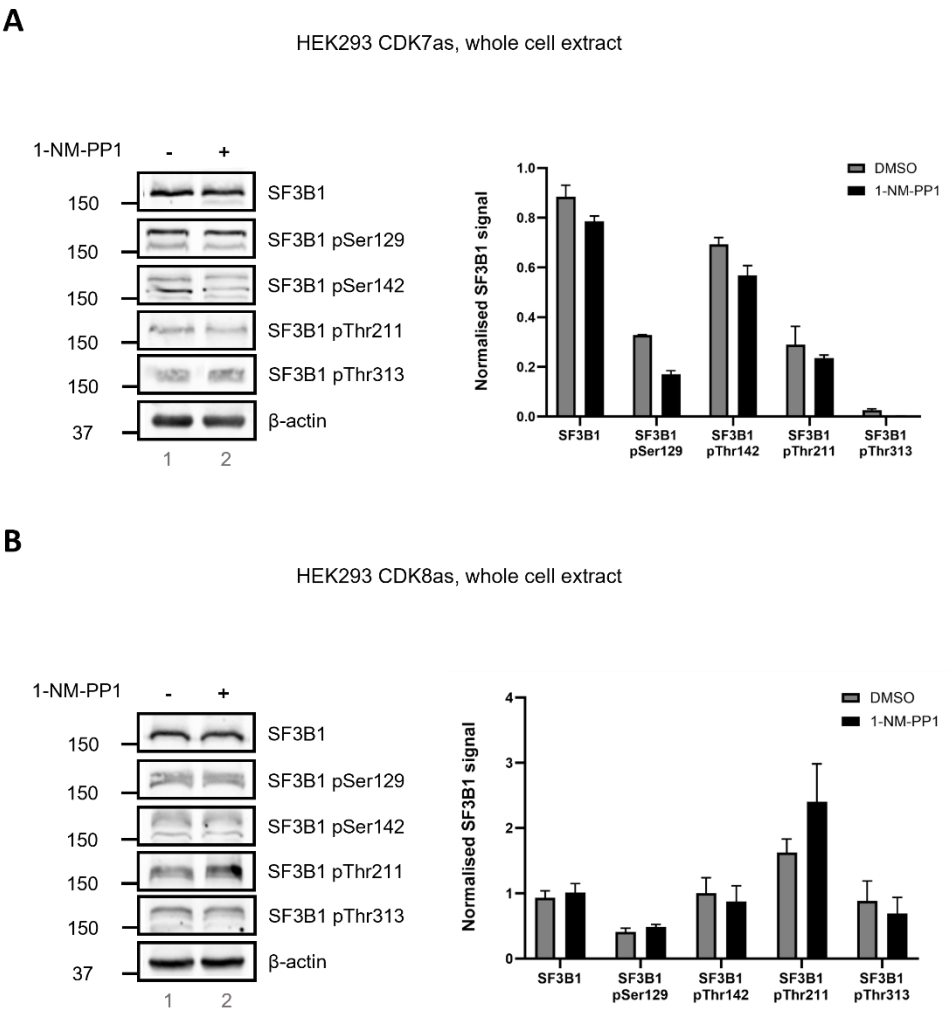


Figure 6.5. Effects of other cyclin-dependent kinases on SF3B1

(A and B, left) Western blot analysis of whole cell extracts of HEK293 derived analogue-sensitive cell lines of CDK7 and CDK8 treated with DMSO or with 7.5 μM 1-NM-PP1 for 30 minutes. Proteins were resolved by SDS-PAGE and immunoblotted with anti-SF3B1, anti-SF3B1 pSer129, anti-SF3B1 pThr142, anti-SF3B1 pThr211, anti-SF3B1 pThr313 and anti-β-actin as a loading control. **(A and B, right)** Quantification of the western blots for DMSO (grey) and 1-NM-PP1 (black). Each quantification signal was normalised to the β-actin signal. Bars represent normalised antibody signal for 3 biological replicates. Error bars = standard error of the mean. Statistical test: Ordinary one-way ANOVA.

6.6 PP1/PP2A inhibition affects SF3B1 phosphorylation

PP1 is known to activate the positive transcription elongation activity of CDK9 by dephosphorylating multiple residues on it to disrupt interactions with the 7SK/HEXIM1 complex (Chen et al., 2008; Ammosova et al., 2005). Alternatively, PP2A phosphatase activity has pleiotropic effects on CDK9 activity. On one hand, it is known to activate CDK9, facilitating the progression of transcription (Zhou et al., 2009). On the other hand, it inactivates CDK9 by dephosphorylating autophosphorylated CDK9 *in vitro* (Ammosova et al., 2005). During pre-mRNA splicing, PP1 together with PP2A activity is required for the progression of the second step of splicing catalysis by dephosphorylating phospho-residues of SF3B1 (Shi et al., 2006).

To determine whether the phosphorylation status of SF3B1 is regulated by the protein phosphatases PP1 and PP2A, western blotting analysis with antibodies against total SF3B1 and SF3B1 phospho-marks pSer129, pThr142, pThr211, and pThr313 using whole cell extracts from a HEK293 derived analogue-sensitive cell line of CDK9 with and without the ATP analogue, 1-NM-PP1, PlaB, Tautomycetin (inhibits PP1), or Calyculin A (inhibits PP2A) for 30 minutes (Figure 6.6). The inhibition of SF3B1, CDK9, PP1, PP2A or a combination does not have an effect on the cellular level of SF3B1.

Inhibition of PP1 using Tautomycetin affects the phosphorylation status of SF3B1 by reducing SF3B1 pSer129, pThr142, and pThr211 phospho-marks and increasing phosphorylation at the SF3B1 pThr313 phospho-site.

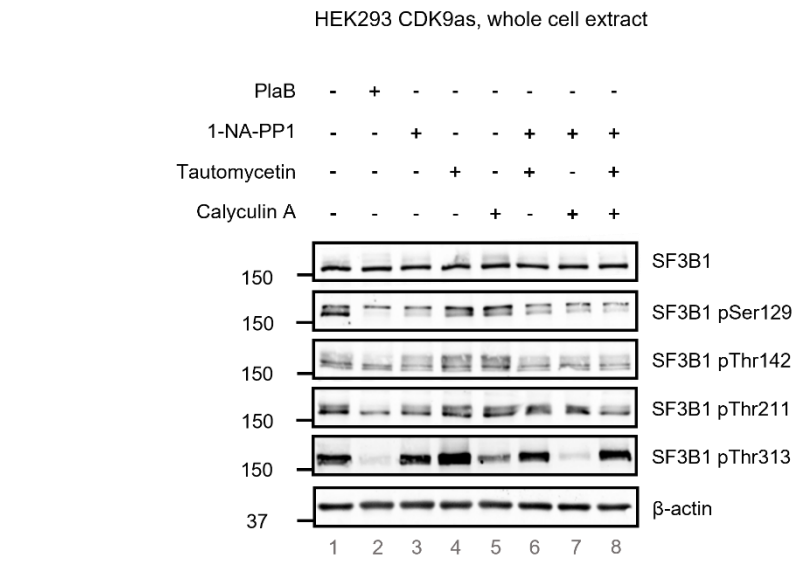
Inhibition of PP2A using Calyculin A has a different effect and reduces phosphorylation of the SF3B1 pSer129 phospho-mark but has no clear effect on the phosphorylation status of SF3B1 pThr142, pThr211, and pThr313 phospho-marks.

Dual inhibition of PP1 and CDK9 has differential effects to lone PP1 or CKD9 inhibition on the phosphorylation status of SF3B1. Although conditions of dual inhibition cause all SF3B1 phospho-sites to have reduced phosphorylation, the effect on SF3B1 pSer129 resembles more that of lone PP1 inhibition, whereas the effect seen on SF3B1 pThr142, pThr211, pThr313 are similar to that of lone CDK9 inhibition.

Dual inhibition of PP2A and CDK9 also show different effects to lone PP2A or CDK9 inhibition on SF3B1 phosphorylation. Dual inhibition resembles that of lone CDK9 inhibition, causing reduced phosphorylation of SF3B1 pSer129, pThr142, and pThr211 to the same magnitude. Dual inhibition reduces phosphorylation on SF3B1 pThr313 more profoundly than that of lone PP2A or CDK9 inhibition.

The simultaneous inhibition of PP1, PP2A, and CDK9, with exception of SF3B1 pThr313, causes reduction of all the SF3B1 phosphorylation marks, resembling that of lone CDK9 inhibition.

Taken together, it would be expected that inhibition of the phosphatases should result in an increase in phosphorylation of the sites they are regulating. Besides the effect of lone PP1 inhibition on SF3B1 pThr313, the protein phosphatases do not seem to have much direct catalytic activity against SF3B1 at the examined sites.


HEK293 CDK9as, whole cell extract
PlaB - + - - - - - -
1-NA-PP1 - - + - - + + +
Tautomycetin - - - + - + - +
Calyculin A - - - - + - + +
150
150
150
150
150
37
SF3B1
SF3B1 pSer129
SF3B1 pThr142
SF3B1 pThr211
SF3B1 pThr313
β-actin
1 2 3 4 5 6 7 8

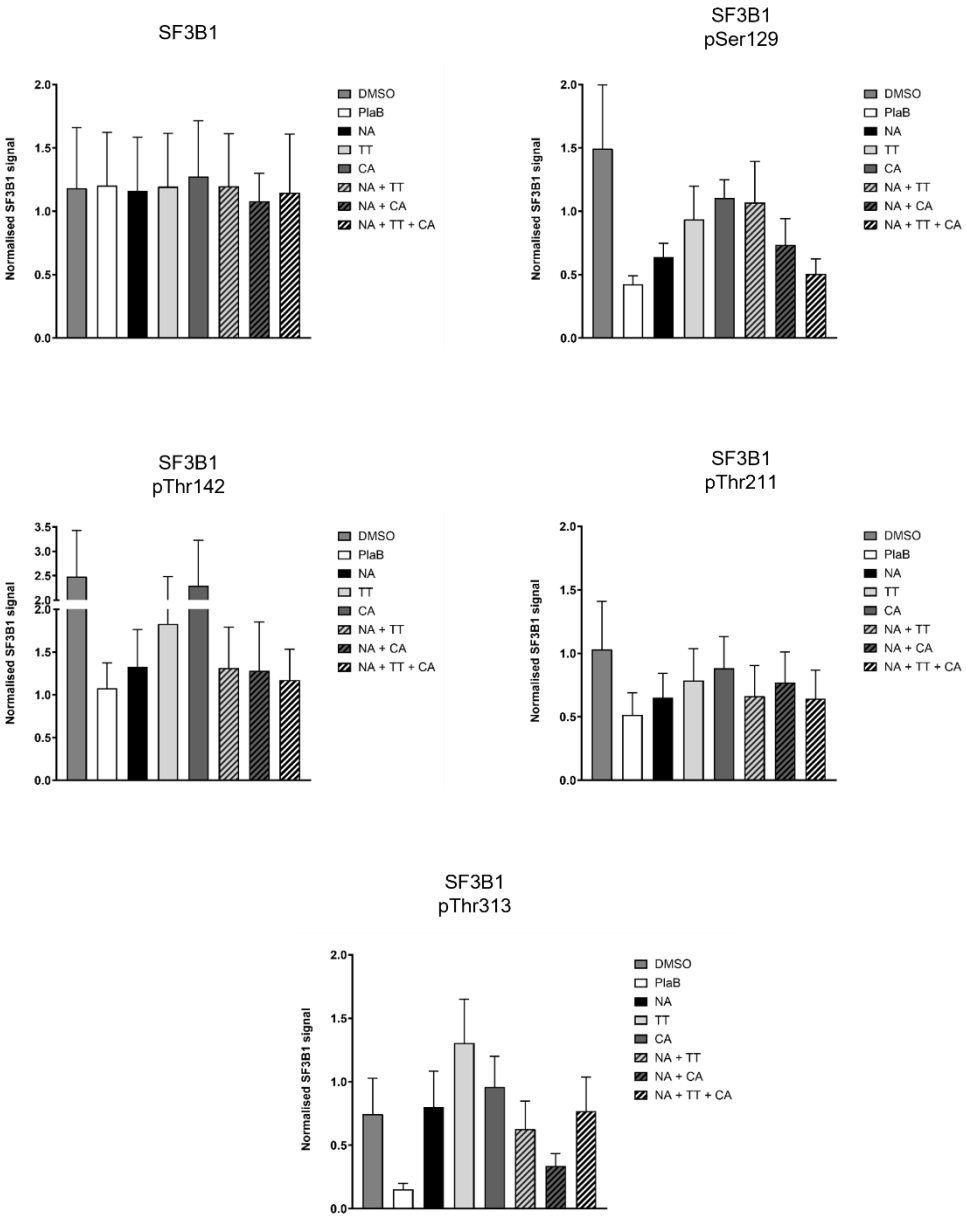

SF3B1
SF3B1 pSer129
SF3B1 pThr142
SF3B1 pThr211
SF3B1 pThr313
Normalised SF3B1 signal
DMSO
PlaB
NA
TT
CA
NA + TT
NA + CA
NA + TT + CA

Figure 6.6. PP1/PP2A inhibition affects SF3B1 phosphorylation

(Top) Western blot analysis of whole cell extracts of HEK293 derived analogue-sensitive cell lines of CDK9 treated with DMSO, 1 μM PlaB, 15 μM 1-NA-PP1, 25 nM Tautomycetin, or with 2.5 nM Calyculin A for 30 minutes. Proteins were resolved by SDS-PAGE and immunoblotted with anti-SF3B1, anti-SF3B1 pSer129, anti-SF3B1 pThr142, anti-SF3B1 pThr211, anti-SF3B1 pThr313 and anti-β-actin as a loading control. **(Bottom)** Quantification of the western blots for DMSO (grey), PlaB (white), 1-NA-PP1 (black), Tautomycetin (stone grey), Calyculin A (dark grey), 1-NA-PP1 + Tautomycetin (striped stone grey), 1-NA-PP1 + Calyculin A (striped dark grey), and 1-NA-PP1 + Tautomycetin + Calyculin A (striped light grey). Each quantification signal was normalised to the β-actin signal. Bars represent normalised antibody signal for 3 biological replicates. Error bars = standard error of the mean. Statistical test: Ordinary one-way ANOVA.

6.7 PP1/PP2A may not regulate the splicing function of SF3B1

To determine whether PP1 or PP2A inhibition affects splicing catalysis, RT-PCR was performed using Tautomycetin, Calyculin A, LB-100 or PlaB as a control for 30 minutes and 4 hours, for transcripts of the intron-containing genes, *BRD2* and *DNAJB1* (Figure 6.7A, Figure S9). The range of concentrations used for Tautomycetin primarily inhibit PP1, while Calyculin A and LB-100 mainly inhibit PP2A (Tellier et al., 2022). Inhibition of PP1 or PP2A under these conditions did not cause intron retention.

To determine whether PP1, PP2A or a combination of phosphatases coupled to SF3B1 inhibition influence splicing catalysis, RT-PCR was performed using Tautomycetin, Calyculin A, and PlaB for 4 hours, for transcripts of the intron containing genes, *BRD2* and *DNAJB1*, as well as for the transcript of the intronless gene, *RN7SK* as a control (Figure 6.7B). As expected, PP1, PP2A, SF3B1, or a combination of their inhibitions had no effect on 7SK transcript expression. In the absence or presence of SF3B1 inhibition, PP1 and or PP2A inhibition has no effect on the retention of transcript introns.

To determine the effects of combinatory PP1, PP2A, and SF3B1 inhibitions, RT-PCR was performed using Tautomycetin, Calyculin A, LB-100, and PlaB for 4 hours, for transcripts of the intron containing genes, *BRD2* and *DNAJB1* (Figure 6.7C). In the absence or presence of SF3B1 inhibition, PP1 and or PP2A inhibition has no effect on intron retention of transcripts.

Taken together, these results indicate that PP1 and or PP2A inhibitions have no clear effect on splicing.

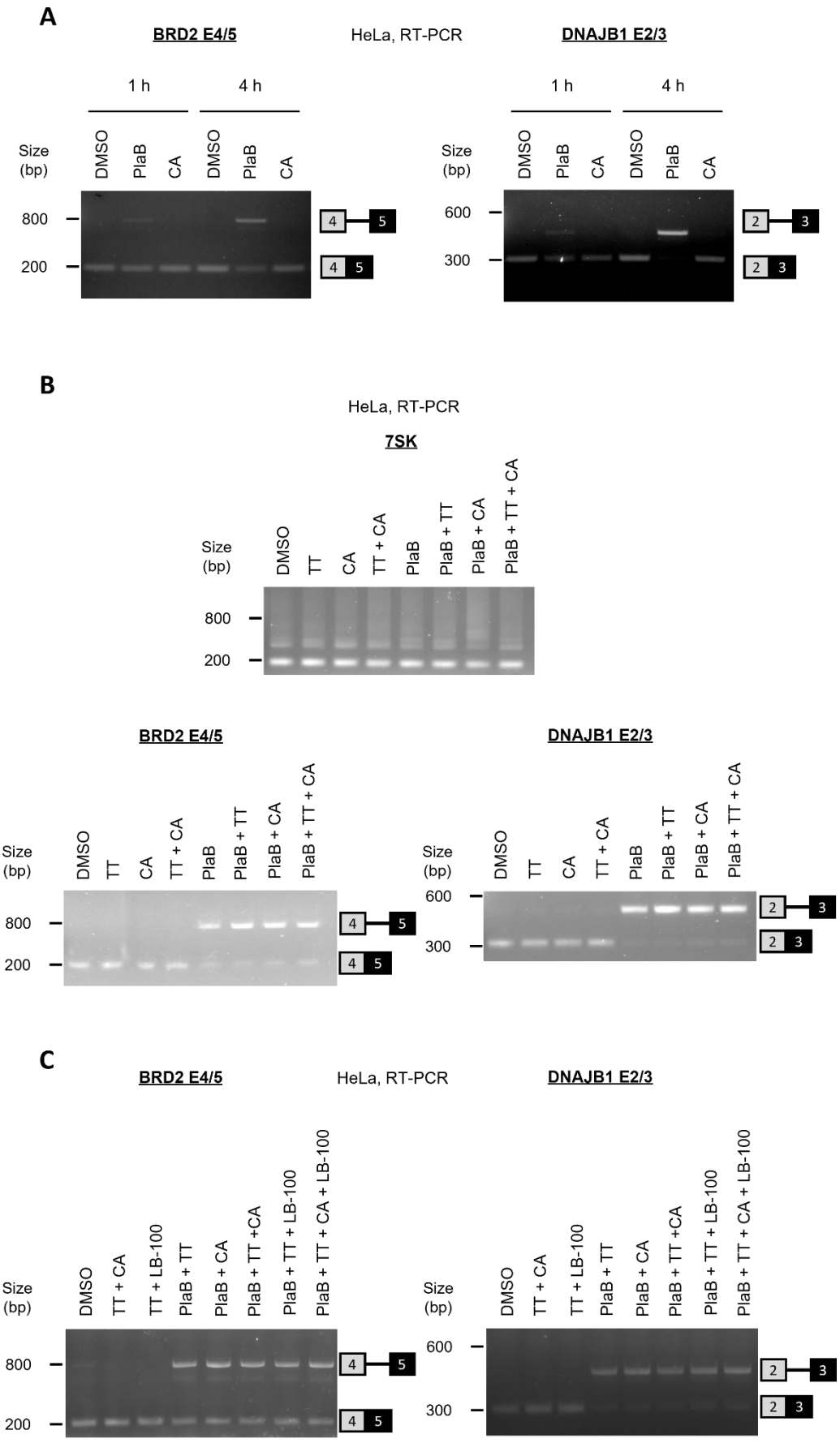

A
BRD2 E4/5
HeLa, RT-PCR
DNAJB1 E2/3
1 h
4 h
Size (bp)
DMSO
PlaB
CA
800
200
600
300
4 5
2 3
B
HeLa, RT-PCR
7SK
TT
TT + CA
PlaB + TT
PlaB + CA
PlaB + TT + CA
C
TT + LB-100
PlaB + TT +CA
PlaB + TT + LB-100
PlaB + TT + CA + LB-100

Figure 6.7. PP1/PP2A may not regulate the splicing function of SF3B1

(A) RT-PCR with primers amplifying the intron located between exons 4 and 5 of *BRD2* or the intron located between exons 2 and 3 of *DNAJB1.* HeLa cells were treated with DMSO, 1 μM PlaB, or with 2.5 nM Calyculin A for either 1 hour or 4 hours. The locations of the spliced and unspliced RNA are shown to the right of each gel image. **(B and C)** RT-PCR with primers amplifying the intron located between exons 4 and 5 of *BRD2* or the intron located between exons 2 and 3 of *DNAJB1.* Primers were also used to amplify the 7SK transcript from the intronless *RN7SK* gene as a negative control. HeLa cells were treated with DMSO, 1 μM PlaB, 25 nM Tautomycetin, 2.5 nM Calyculin or with 2.5 nM LB-100 for 4 hours. The locations of the spliced and unspliced RNA are shown to the right of each gel image.

6.8 Discussion

SF3B1 has 82 amino acid residues that can be reversibly phosphorylated (Hornbeck et al., 2015). Cellular protein kinases such as DYRK1A, CDK1, CDK2, CDK7, CDK9, CDK11, CDK12, and CDK13 have been shown to have catalytic activities for SF3B1 that regulate its canonical splicing function as well as emerging functions beyond splicing that include transcription (de Graaf et al., 2006; Boudrez et al., 2002; Tanuma et al., 2008; Rimel et al., 2020; Sansó et al. 2016; Tellier et al., 2022; Hluchý et al., 2022; Panzeri et al., 2023; Krajewska et al., 2019). However, the identity of the protein kinases that target many of the other SF3B1 phospho-sites to control SF3B1 cellular functions remain unknown. By evaluating the activity of multiple transcriptional kinases, the experiments described here reveal that different transcriptional kinases target different phospho-residues to influence the phosphorylation pattern of SF3B1.

Here, *in vivo* evidence is provided for SF3B1 as a non-CTD target of CDK9. A recent phosphoproteomics study found that the kinome of CDK9 includes SF3B1 pThr142, pThr227, and pThr436 phospho-residues (Tellier et al., 2022). In line with these previous reports, cellular protein extraction experiments using an analogue-sensitive cell line to induce the rapid and selective inhibition of CDK9 confirmed that CDK9 does have catalytic activity towards SF3B1 pThr142 (Sansó et al. 2016; Tellier et al., 2022), and additionally targets SF3B1 pSer129 and pThr211 phospho-sites (Figure 6.3D).

CDK12 and CDK13 are paralogous transcriptional kinases with catalytic activity to regulate transcription elongation and co-transcriptional processes including pre-mRNA splicing and 3’ end RNA processing (Chen et al., 2006; Liang et al., 2015;

Bartkowiak and Greenleaf, 2015). Pharmacological dual inhibition of CDK12 and CDK13 was found to mirror the effects of PlaB by selectively impairing splicing of a subset of promoter-proximal introns (Panzeri et al., 2023). The kinase activity of CDK12 and CDK13 facilitates SF3B1 recruitment to these introns, enhances the association of SF3B1 with chromatin, and promotes interactions between SF3B1 and pol II phosphorylated at Ser2. The use of isotopic labelling and SILAC-based phosphoproteomics have shown that the kinase activities of CDK12 and CDK13 directly phosphorylate SF3B1 at pThr326 *in vitro* and *in vivo* (Krajewska et al., 2019). In this study, cellular protein extraction experiments using analogue-sensitive cell lines to rapidly and selectively inhibit CDK12 and CDK13 independently or simultaneously confirm that these transcriptional kinases have catalytic activities that affect the phosphorylation of SF3B1 (Figure 6.4). The kinase activities of CDK12 and CDK13 are non-redundant, seemingly targeting different SF3B1 phospho-residues. CDK12 exclusively targets the SF3B1 pThr313 phosphor-residue, whereas CDK13 uniquely targets SF3B1 pSer129 and pThr211 phospho-sites.

The small molecule inhibitor SY-351, is a potent and highly selective covalent inhibitor of CDK7 (Hu et al., 2019; Rimel et al., 2020). SILAC phosphoproteomics of CDK7 targets revealed with high-confidence multiple SF3B1 phospho-sites including pThr211 and pThr313 to be significantly down (Rimel et al., 2020). Here, cellular protein extraction experiments using an analogue-sensitive cell line to evaluate the primary effects of rapid inactivation of CDK7 showed no clear decrease in SF3B1 pThr211 or pThr313 phosphorylation but did affect SF3B1 pSer129 (Figure 6.5A). A possible explanation for the discrepancy between data presented here and the SILAC-based phosphoproteomics could be due to the low level SY-351

inhibition on several non-target kinases including CDK12 and CDK13, which were found in this study to reduce the phosphorylation of both SF3B1 pThr211 and pThr313.

The role of the Mediator associated kinase, CDK8, in gene expression is not well understood because of its pleiotropic effects. Reports on the function of CDK8 characterise it as both a transcriptional repressor as well as a positive regulator of gene activity. For example, the addition of a sub-complex of CDK8 to *in vitro* assays induced the shutdown of transcription driven by several transactivators (Knuesel et al., 2009), and is thought to be due to CDK8 sterically blocking interactions between the Mediator complex and pol II (Elmlund et al., 2006). On the other hand, CDK8 function has also been shown not be essential for the recruitment of pol II to promoters or the initiation of transcription from gene promoters but was important for pol II elongation and phosphorylation of the pol II CTD at Ser2 and Ser5 (Donner et al., 2010). CDK8 function regulates precise steps during the assembly of a functional elongation complex by orchestrating the recruitment of CDK7, P-TEFb and its associated factor BRD4 (Yang et al., 2005; Zippo et al., 2009). In this study, cellular protein extraction experiments using an analogue-sensitive cell line to rapidly inactivate CDK8 did not show evidence of catalytic activity against SF3B1, supporting previous reports which do not find it to be involved in pre-mRNA splicing (Figure 6.5B). CDK8 inactivation did not indicate that it regulates P-TEFb recruitment as previously reported, as expected SF3B1 phosphorylation sites targeted by CDK9 remained unchanged. It is possible that the kinase activity of CDK19, a paralog of CDK8, could be sufficient as it is known to be redundant with CDK8 (Dannappel et al., 2019). Interestingly, the inactivation of CDK8 induces phosphorylation of SF3B1 Thr211, suggesting CDK8 may negatively regulate a

kinase or positively regulate a protein phosphatase with catalytic activities against pThr211 of SF3B1 (Figure 6.5B).

The cellular protein phosphatases, PP1 and PP2A, play important roles in the regulation of both transcription and pre-mRNA splicing. In transcription, both PP1 and PP2A dephosphorylate CDK9 but induce different effects (Chen et al., 2008; Ammosova et al., 2005). In pre-mRNA splicing, PP1 and PP2A are essential but redundant for the splicing reaction (Shi et al., 2006). The protein phosphatases specifically affect the splicing functions of SF3B1 (Shi et al., 2006), with the SF3B1 pThr142 phospho-residue shown to be specifically targeted by PP1 (Tellier et al., 2022). However, the extent of SF3B1 phospho-residues dephosphorylated by PP1/PP2A family phosphatases have not yet been elucidated. Here, cellular protein extraction experiments using an analogue-sensitive cell line to rapidly inactivate CDK9 coupled with specific inhibitors of PP1 and PP2A protein phosphatases indicate that these phosphatases affect SF3B1 phosphorylation (Figure 6.6). The inhibition of PP1, like that of CDK9 inhibition, causes a general reduction in the SF3B1 pSer129, pThr142 and pThr211 phospho-marks, suggesting that PP1 does not target these SF3B1 phospho-residues directly but may affect them indirectly through CDK9 regulation. Interestingly, PP1 inhibition but not CDK9 inhibition causes the phosphorylation of SF3B1 Thr313 to increase, indicating that this SF3B1 phospho-residue is directly targeted by PP1. In contrast, PP2A inhibition only causes a reduction in the phosphorylation of SF3B1 pSer129 when compared with the control, suggesting that like PP1, it does not specifically target this phospho-residue directly. Intriguingly, PP1 and PP2A inhibition coupled to CDK9 inhibition causes the same effect on SF3B1 phosphorylation as lone CDK9 inhibition. This is not seen when either PP1 or PP2A is individually inhibited with CDK9 inhibition,

demonstrating that these phosphatases likely regulate other protein kinases that also target some of these SF3B1 phospho-residues.

PP1 and PP2A are two of the four major types of Ser/Thr-specific phosphatases that block both catalytic steps of pre-mRNA splicing when inhibited (Mermoud et al., 1992). Here, the effects of PP1 and PP2A inhibitions over time were evaluated to determine the degree to which they disrupt splicing. Perhaps surprisingly, inhibition of PP1 and or PP2A does not impair the efficiency of splicing in the cells used (Figure 6.7, Figure S9). Analysing splicing defects by total RNA is sensitive to severe splicing inhibition using splicing inhibitors but more subtle changes in co-transcriptional splicing may be missed. Analysis of the effect of PP1 and PP2A inhibtions on chromatin RNA would clarify whether these protein phosatases have an effect on splicing.

Together, data presented here demonstrate the kinase activities of CDK9, CDK12, and CDK13, are important regulators of SF3B1 phosphorylation pattern with each kinase found to have little overlap with regard to phospho-sites. SF3B1 phosphorylation controls its subcellular localisation and function (Seghezzi et al., 1998; Boudrez et al., 2002). However, whether the reversable phosphorylation of each phospho-site is biologically significant is not entirely known.

Chapter 7. Concluding remarks

In the present study, pharmacological inhibition of SF3B1 coupled with systematic biochemical analyses has been effective in characterising some of the links between splicing and transcription in humans. The functions of SF3B1 in transcription are important for mediating the recruitment/stabilisation of P-TEFb to paused pol II to facilitate pol II transition into productive elongation. Further, P-TEFb recruitment/stabilisation appears to be through several key P-TEFb recruitment pathways that are dependent on SF3B1 function. This transcriptional function of SF3B1 is associated with extensive phosphorylation by multiple protein kinases that target specific residues on SF3B1.

Literature reports coupled with findings from the present study gives credence to this model for the role of SF3B1 in transcription (Figure 7.1). Several lines of evidence hint to the order of events. The U2 snRNP is recruited and stabilised to the BP sequence by interactions between SF3B1 and U2AF2 (Gozani et al., 1998). SF3B1 binds to the BP sequence in an open confirmation (Cretu et al., 2018). The U2 snRNP then helps to recruit Tat-SF1 (Fong and Zhou, 2001), which binds to SF3B1 in the open conformation (Zhang et al., 2020). The displacement of Tat-SF1 must occur to allow stable U2 snRNP to interact with the BP (Zhang et al., 2020). Tat-SF1 recruits P-TEFb to facilitate transcription elongation (Fong and Zhou, 2001). Data presented here shows Tat-SF1 equally binds to both SF3B1 and CDK9 on chromatin (Figure 3.7, Figure 4.6A). Tat-SF1 is known to bind pol II (Parada and Roeder, 1999). Tat-SF1 recruitment to the U2 snRNP *via* SF3B1 could bring SF3B1 in proximity of the pol II-associated TFIIH, where CDK7 as part of CAK, as well as other transcription protein kinases could then phosphorylate SF3B1, helping to stabilise its association with

chromatin (Figure 6.2, Figure 6.3A). Chromatin-associated SF3B1 influences, possibly through interactions, the chromatin association of AFF4, a known CDK9 recruiter (Lin et al., 2010; Zhou et al., 2022) (Figure 4.9).

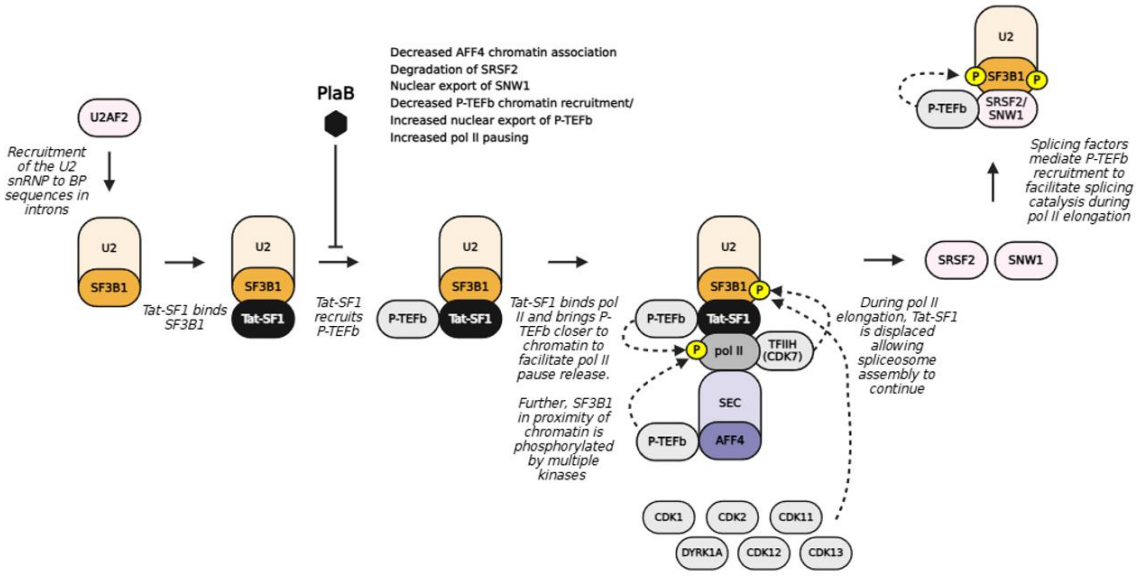


Figure 7.1. How SF3B1 links splicing and transcription

During pre-mRNA splicing, U2AF2 recruits the U2 snRNP to the branch point (BP) sequence of transcript introns. SF3B1 helps to stabilise the U2 snRNP to the BP. Tat-SF1 binds to SF3B1 positioned at the BP and recruits P-TEFb. Tat-SF1 also binds pol II and brings SF3B1 in proximity of multiple transcriptional protein kinases that phosphorylate numerous SF3B1 residues to regulate its function and stability to chromatin. The binding of Tat-SF1 to pol II also brings P-TEFb in proximity of paused pol II. Together with P-TEFb recruited by AFF4 in the super elongation complex (SEC), paused pol II is released into productive elongation by P-TEFb phosphorylating negative transcription elongation factors (not shown) that cause pol II pausing, and Ser2 of the pol II CTD. During pol II elongation, Tat-SF1 is displaced, allowing spliceosome assembly to continue with important splicing factors such as SRSF2 and SNW1 incorporated into the spliceosome. SRSF2 and SNW1 also mediate the recruitment of P-TEFb. SF3B1 inhibition by PlaB blocks Tat-SF1 binding to P-TEFb and pol II, prevents SF3B1 phosphorylation and stabilisation to chromatin, and disrupts chromatin association of P-TEFb recruiters leading to decreased P-TEFb chromatin recuitment and increased pol II pausing.

SRSF2 is another splicing factor that interacts with the U2AF2/U2AF1 heterodimer. SRSF2, unlike other SR splicing factors prefers to bind to highly degenerate RNA sequences of ESEs (Phelan et al., 2012; Daubner et al., 2012), and interact with the U1 snRNP and U2AF (Takeiwa et al., 2020). Further along the spliceosome assembly pathway, downstream of U2 snRNP recruitment is SNW1, an integral component of the spliceosome that is recruited as part of the NTC complex and interacts with the U5 snRNP (Neubauer et al, 1998; Makarova et al, 2004). SRSF2 and SNW1 are known CDK9 recruiters so they are likely to mediate the recruitment of P-TEFb (Ji et al., 2013; Verma et al., 2019).

In the presence of SF3B1 inhibition by PlaB, SF3B1 is arrested in an open confirmation (Cretu et al., 2018), which prevents the stabilisation of the association of U2 snRNP with BP sites in introns (Effenberger et al., 2016). As Tat-SF1 binds to SF3B1 in the open conformation and must be displaced to allow the U2 snRNP to stably interact with the BP, once bound it remains associated with SF3B1 and de-stabilises it from chromatin (Figure 4.6), preventing spliceosome assembly at the stage of A complex formation. The disassociation of SF3B1 from chromatin leads to subsequent release of CDK9 recruiters from chromatin. AFF4 accumulates in the nucleoplasm (Figure 4.9), SRSF2 undergoes proteolysis (Figure 4.8A) possibly through disrupted interactions with the U2AF heterodimer, and SNW1 is exported from the nucleus (Figure 4.7D). The loss of some (AFF4, SRSF2, and SNW1), but not all (BRD4 and c-MYC) CDK9 recruiters from chromatin partially impair CDK9 recruitment (Figure 3.5, Figure S3). Active CDK9 that is not recruited is likely exported from the nucleus (Figure 4.1B, Figure 4.3, Figure S4A), independent of SNW1 nuclear export (Figure 4.6), and sequestered within inactive 7SK snRNPs in

the cytoplasm (Ramanathan et al., 1999; Faust et al., 2018), as cellular levels of CDK9 do not change (Figure. 4.2).

Together, work presented here shows new insight into the complex and dynamic connections between splicing and transcription in humans. It is clear from the present work and the literature that SF3B1 function plays a key role in gene expression by modulating CDK9 recruitment to paused pol II through influencing multiple CDK9 recruitment pathways.

Several key questions remain, including: does the loss of function of other SF3B or U2 snRNP associated components induce the same effect as SF3B1 inhibition on transcription? What is the biological significance of their loss? Are the effects genome-wide? A systematic approach with and without selective inhibition of SF3B1 or U2 snRNP components complemented with genome-wide studies will provide clearer insight into the links between splicing and transcription in humans.

Chapter 8. Future directions

The work described here assessing the effects of SF3B1 on pol II and CDK9 occupancy on protein-coding genes was carried out by single-gene analysis which has obvious limitations and important insights may have been missed. Genome-wide studies would ensure that important phenomena do not go unmissed. Further, genome-wide studies using different splicing inhibitors to assess the effects on pol II and CDK9 occupancy on protein-coding genes would help to further uncover the effects of inhibiting the spliceosome at different stages of transcription.

The current model describes Tat-SF1 as an important intermediary factor mediating interaction between SF3B1 and P-TEFb. To confirm the role of Tat-SF1, rapid and selective perturbation using protein degradation systems including PROTACs, targeted protein inactivation (TPI), or dTAG, could be used to assess the primary effect loss of Tat-SF1 has on the subcellular localisation of SF3B1, CDK9, and the CDK9 recruiters AFF4, SRSF2, and SNW1. Further, measuring the effect loss of Tat-SF1 has on pol II and CDK9 occupancy on protein-coding genes would be valuable.

A key finding from the present work is the striking effect of CDK12 inhibition on SF3B1 pThr313. Further, this phospho-residue was sensitive to PP1 inhibition. SF3B1 pThr313 is associated with active splicing (Wang et al., 1998; Girard et al., 2012), therefore mutating this residue and assessing the effects it has on transcription would help to better understand the effects splicing factors have on gene expression.

Reference list

Abramczuk, M. K., Burkard, T. R., Rolland, V., Steinmann, V., Duchek, P., Jiang, Y., Wissel, S., Reichert, H. and Knoblich, J. A. (2017). The splicing co-factor Barricade/Tat-SF1 is required for cell cycle and lineage progression in Drosophila neural stem cells. *Development*, **144:** 3932–3945.

Abuhashem, A., Chivu, A. G., Zhao, Y., Rice, E. J., Siepel, A., Danko, C. G. and Hadjantonakis, A. K. (2022). RNA Pol II pausing facilitates phased pluripotency transitions by buffering transcription. *Genes & development*, **36:** 770–789.

Adelman, K. and Lis, J. T. (2012). Promoter-proximal pausing of RNA polymerase II: emerging roles in metazoans. *Nature reviews. Genetics*, **13:** 720–731.

Agafonov, D. E., Deckert, J., Wolf, E., Odenwälder, P., Bessonov, S., Will, C. L., Urlaub, H. and Lührmann, R. (2011). Semiquantitative proteomic analysis of the human spliceosome via a novel two-dimensional gel electrophoresis method. *Molecular and cellular biology*, **31:** 2667–2682.

Akhtar, M. S., Heidemann, M., Tietjen, J. R., Zhang, D. W., Chapman, R. D., Eick, D. and Ansari, A. Z. (2009). TFIIH kinase places bivalent marks on the carboxy-terminal domain of RNA polymerase II. *Molecular cell*, **34:** 387–393.

Akinyi, M. V. and Frilander, M. J. (2021). At the Intersection of Major and Minor Spliceosomes: Crosstalk Mechanisms and Their Impact on Gene Expression. *Frontiers in genetics*, **12:** 700744.

Alaimo, P. J., Shogren-Knaak, M. A. and Shokat, K. M. (2001). Chemical genetic approaches for the elucidation of signaling pathways. *Current opinion in chemical biology*, **5:** 360–367.

Albers, M., Diment, A., Muraru, M., Russell, C. S. and Beggs, J. D. (2003). Identification and characterization of Prp45p and Prp46p, essential pre-mRNA splicing factors. *RNA*, **9:** 138–150.

Amente, S., Gargano, B., Napolitano, G., Lania, L. and Majello, B. (2009). Camptothecin releases P-TEFb from the inactive 7SK snRNP complex. *Cell cycle*, **8:** 1249–1255.

Ammosova, T., Washington, K., Debebe, Z., Brady, J. and Nekhai, S. (2005). Dephosphorylation of CDK9 by protein phosphatase 2A and protein phosphatase-1 in Tat-activated HIV-1 transcription. *Retrovirology*, **2:** 47.

Anish, R., Hossain, M. B., Jacobson, R. H. and Takada, S. (2009). Characterization of transcription from TATA-less promoters: identification of a new core promoter element XCPE2 and analysis of factor requirements. *PloS one*, **4:** e5103.

Angel, M., Fleshler, E., Atrash, M. K., Kinor, N., Benichou, J. I. C. and Shav-Tal, Y. (2024). Nuclear RNA-related processes modulate the assembly of cytoplasmic RNA granules. *Nucleic acids research*, **gkae119.**

Apponi, L. H., Leung, S. W., Williams, K. R., Valentini, S. R., Corbett, A. H. and Pavlath, G. K. (2010). Loss of nuclear poly(A)-binding protein 1 causes defects in myogenesis and mRNA biogenesis. *Human molecular genetics*, **19:** 1058–1065.

Armenia, J., Wankowicz, S. A. M., Liu, D., Gao, J., Kundra, R., Reznik, E., Chatila, W. K., Chakravarty, D., Han, G. C., Coleman, I., Montgomery, B., Pritchard, C., Morrissey, C., Barbieri, C. E., Beltran, H., Sboner, A., Zafeiriou, Z., Miranda, S., Bielski, C. M., Penson, A. V., et al. (2018). The long tail of oncogenic drivers in prostate cancer. *Nature genetics*, **50:** 645–651.

Aoi, Y., Smith, E., Shah, A., Rendleman, E., Marshall, S., Woodfin, A., Chen, F., Shiekhattar, R. and Shilatifard, A. (2020). NELF Regulates a Promoter-Proximal Step Distinct from RNA Pol II Pause-Release. *Molecular cell*, **S1097-2765**.

Bai, R., Wan, R., Yan, C., Lei, J. and Shi, Y. (2018). Structures of the fully assembled Saccharomyces cerevisiae spliceosome before activation. *Science*, **360:** 1423–1429.

Banerji, S., Cibulskis, K., Rangel-Escareno, C., Brown, K. K., Carter, S. L., Frederick, A. M., Lawrence, M. S., Sivachenko, A. Y., Sougnez, C., Zou, L., Cortes, M. L., Fernandez-Lopez, J. C., Peng, S., Ardlie, K. G., Auclair, D., Bautista-Piña, V., Duke, F., Francis, J., Jung, J., Maffuz-Aziz, A., et al. (2012). Sequence analysis of mutations and translocations across breast cancer subtypes. *Nature*, **486:** 405–409.

Bangru, S., Arif, W., Seimetz, J., Bhate, A., Chen, J., Rashan, E. H., Carstens, R. P., Anakk, S. and Kalsotra, A. (2018). Alternative splicing rewires Hippo signaling pathway in hepatocytes to promote liver regeneration. *Nature structural & molecular biology*, **25:** 928–939.

Baralle, F. E. and Giudice, J. (2017). Alternative splicing as a regulator of development and tissue identity. *Nature reviews. Molecular cell biology*, **18:** 437–451.

Barbosa-Morais, N. L., Irimia, M., Pan, Q., Xiong, H. Y., Gueroussov, S., Lee, L. J., Slobodeniuc, V., Kutter, C., Watt, S., Colak, R., Kim, T., Misquitta-Ali, C. M., Wilson, M. D., Kim, P. M., Odom, D. T., Frey, B. J. and Blencowe, B. J. (2012). The evolutionary landscape of alternative splicing in vertebrate species. *Science*, **338:** 1587–1593.

Bartholomeeusen, K., Xiang, Y., Fujinaga, K. and Peterlin, B. M. (2012). Bromodomain and extra-terminal (BET) bromodomain inhibition activate transcription via transient release of positive transcription elongation factor b (P-TEFb) from 7SK small nuclear ribonucleoprotein. *The Journal of biological chemistry*, **287:** 36609–36616.

Bartkowiak, B. and Greenleaf, A. L. (2015). Expression, purification, and identification of associated proteins of the full-length hCDK12/CyclinK complex. *The Journal of biological chemistry*, **290:** 1786–1795.

Bartkowiak, B., Liu, P., Phatnani, H. P., Fuda, N. J., Cooper, J. J., Price, D. H., Adelman, K., Lis, J. T. and Greenleaf, A. L. (2010). CDK12 is a transcription elongation-associated CTD kinase, the metazoan ortholog of yeast Ctk1. *Genes & development*, **24:** 2303–2316.

Baskaran, R., Dahmus, M. E. and Wang, J. Y. (1993). Tyrosine phosphorylation of mammalian RNA polymerase II carboxyl-terminal domain. *Proceedings of the National Academy of Sciences of the United States of America*, **90:** 11167–11171.

Baskaran, R., Escobar, S. R. and Wang, J. Y. (1999). Nuclear c-Abl is a COOH-terminal repeated domain (CTD)-tyrosine (CTD)-tyrosine kinase-specific for the mammalian RNA polymerase II: possible role in transcription elongation. *Cell growth & differentiation: the molecular biology journal of the American Association for Cancer Research*, **10:** 387–396.

Bentley D. L. (2014). Coupling mRNA processing with transcription in time and space. *Nature reviews. Genetics*, **15:** 163–175.

Berglund, J. A., Abovich, N. and Rosbash, M. (1998). A cooperative interaction between U2AF65 and mBBP/SF1 facilitates branchpoint region recognition. *Genes & development*, **12:** 858–867.

Bertram, K., Agafonov, D., Dybkov, O., Haselbach, D., Leelaram, M., Will, C., Urlaub, H., Kastner, B., Lührmann, R. and Stark. H. (2017). Cryo-EM Structure of a Pre-catalytic Human Spliceosome Primed for Activation. *Cell*, **170:** 701-713.e11.

Beyer, A. L. and Osheim, Y. N. (1988). Splice site selection, rate of splicing, and alternative splicing on nascent transcripts. *Genes & development*, **2:** 754–765.

Bhate, A., Parker, D. J., Bebee, T. W., Ahn, J., Arif, W., Rashan, E. H., Chorghade, S., Chau, A., Lee, J. H., Anakk, S., Carstens, R. P., Xiao, X. and Kalsotra, A. (2015). ESRP2 controls an adult splicing programme in hepatocytes to support postnatal liver maturation. *Nature communications*, **6:** 8768.

Biankin, A. V., Waddell, N., Kassahn, K. S., Gingras, M. C., Muthuswamy, L. B., Johns, A. L., Miller, D. K., Wilson, P. J., Patch, A. M., Wu, J., Chang, D. K., Cowley, M. J., Gardiner, B. B., Song, S., Harliwong, I., Idrisoglu, S., Nourse, C., Nourbakhsh, E., Manning, S., Wani, S., et al. (2012). Pancreatic cancer genomes reveal aberrations in axon guidance pathway genes. *Nature*, **491:** 399–405.

Biglione, S., Byers, S. A., Price, J. P., Nguyen, V. T., Bensaude, O., Price, D. H. and Maury, W. (2007). Inhibition of HIV-1 replication by P-TEFb inhibitors DRB, seliciclib and flavopiridol correlates with release of free P-TEFb from the large, inactive form of the complex. *Retrovirology*, **4:** 47.

Bishop, A., Buzko, O., Heyeck-Dumas, S., Jung, I., Kraybill, B., Liu, Y., Shah, K., Ulrich, S., Witucki, L., Yang, F., Zhang, C. and Shokat, K. M. (2000). Unnatural ligands for engineered proteins: new tools for chemical genetics. *Annual review of biophysics and biomolecular structure*, **29:** 577–606.

Blazek, D., Kohoutek, J., Bartholomeeusen, K., Johansen, E., Hulinkova, P., Luo, Z., Cimermancic, P., Ule, J. and Peterlin, B. M. (2011). The Cyclin K/Cdk12 complex maintains genomic stability via regulation of expression of DNA damage response genes. *Genes & development*, **25:** 2158–2172.

Boesler, C., Rigo, N., Anokhina, M. M., Tauchert, M. J., Agafonov, D. E., Kastner, B., Urlaub, H., Ficner, R., Will, C. L. and Lührmann, R. (2016). A spliceosome intermediate with loosely associated tri-snRNP accumulates in the absence of Prp28 ATPase activity. *Nature communications*, **7:** 11997.

Bonnal, S., Vigevani, L. and Valcárcel, J. (2012). The spliceosome as a target of novel antitumour drugs. *Nature reviews. Drug discovery*, **11:** 847–859.

Boudrez, A., Beullens, M., Waelkens, E., Stalmans, W. and Bollen, M. (2002). Phosphorylation-dependent interaction between the splicing factors SAP155 and NIPP1. *The Journal of biological chemistry*, **277:** 31834–31841.

Brès, V., Gomes, N., Pickle, L. and Jones, K. A. (2005). A human splicing factor, SKIP, associates with P-TEFb and enhances transcription elongation by HIV-1 Tat. *Genes & development*, **19:** 1211–1226.

Brès, V., Yoshida, T., Pickle, L. and Jones, K. A. (2009). SKIP interacts with c-Myc and Menin to promote HIV-1 Tat transactivation. *Molecular cell*, **36:** 75–87.

Cai, M., Yang, C. and Wang, Z. (2023). N7-methylguanosine modification: from regulatory roles to therapeutic implications in cancer. *American journal of cancer research*, **13:** 1640–1655.

Caizzi, L., Monteiro-Martins, S., Schwalb, B., Lysakovskaia, K., Schmitzova, J., Sawicka, A., Chen, Y., Lidschreiber, M. and Cramer, P. (2021). Efficient RNA polymerase II pause release requires U2 snRNP function. *Molecular cell*, **81:** 1920–1934.e9.

Carrillo Oesterreich, F., Preibisch, S. and Neugebauer, K. M. (2010). Global analysis of nascent RNA reveals transcriptional pausing in terminal exons. *Molecular cell*, **40:** 571–581.

Carrocci, T. J. and Neugebauer, K. M. (2019). Pre-mRNA Splicing in the Nuclear Landscape*. Cold Spring Harbor symposia on quantitative biology*, **84:** 11–20.

Cassandri, M., Fioravanti, R., Pomella, S., Valente, S., Rotili, D., Del Baldo, G., De Angelis, B., Rota, R. and Mai, A. (2020). CDK9 as a Valuable Target in Cancer: From Natural Compounds Inhibitors to Current Treatment in Pediatric Soft Tissue Sarcomas. *Frontiers in pharmacology*, **11:** 1230.

Cazalla, D., Zhu, J., Manche, L., Huber, E., Krainer, A. R. and Cáceres, J. F. (2002). Nuclear export and retention signals in the RS domain of SR proteins*. Molecular and cellular biology*, **22:** 6871–6882.

Cazzola, M., Rossi, M., Malcovati, L. and Associazione Italiana per la Ricerca sul Cancro Gruppo Italiano Malattie Mieloproliferative. (2013). Biologic and clinical significance of somatic mutations of SF3B1 in myeloid and lymphoid neoplasms. *Blood*, **121:** 260–269.

Chanfreau, G. and Jacquier, A. (1993). Interaction of intronic boundaries is required for the second splicing step efficiency of a group II intron. *The EMBO journal*, **12:** 5173–5180.

Chanfreau, G., Legrain, P., Dujon, B. and Jacquier, A. (1994). Interaction between the first and last nucleotides of pre-mRNA introns is a determinant of 3' splice site selection in S. cerevisiae. *Nucleic acids research*, **22:** 1981–1987.

Chapman, R. D., Heidemann, M., Hintermair, C. and Eick, D. (2008). Molecular evolution of the RNA polymerase II CTD. *Trends in genetics : TIG*, **24:** 289–296.

Charenton, C. and Graille, M. (2018). mRNA decapping: finding the right structures. *Philosophical transactions of the Royal Society of London. Series B, Biological sciences*, **373:** 20180164.

Chathoth, K. T., Barrass, J. D., Webb, S. and Beggs, J. D. (2014). A splicing-dependent transcriptional checkpoint associated with prespliceosome formation. *Molecular cell*, **53:** 779–790.

Chen, H. H., Wang, Y. C. and Fann, M. J. (2006). Identification and characterization of the CDK12/cyclin L1 complex involved in alternative splicing regulation. *Molecular and cellular biology*, **26:** 2736–2745.

Chen, R., Liu, M., Li, H., Xue, Y., Ramey, W. N., He, N., Ai, N., Luo, H., Zhu, Y., Zhou, N. and Zhou, Q. (2008). PP2B and PP1alpha cooperatively disrupt 7SK snRNP to release P-TEFb for transcription in response to Ca2+ signaling. *Genes & development*, **22:** 1356–1368.

Chen, Y., Yamaguchi, Y., Tsugeno, Y., Yamamoto, J., Yamada, T., Nakamura, M., Hisatake, K. and Handa, H. (2009). DSIF, the Paf1 complex, and Tat-SF1 have nonredundant, cooperative roles in RNA polymerase II elongation. *Genes & development*, **23:** 2765–2777.

Cheng, H., Dufu, K., Lee C., Hsu, J., Dias, A. and Reed, R. (2006). Human mRNA export machinery recruited to the 5′ end of mRNA. *Cell*, **127:** 1389–1400.

Cheng, S. W., Kuzyk, M. A., Moradian, A., Ichu, T. A., Chang, V. C., Tien, J. F., Vollett, S. E., Griffith, M., Marra, M. A. and Morin, G. B. (2012). Interaction of cyclin-dependent kinase 12/CrkRS with cyclin K1 is required for the phosphorylation of the C-terminal domain of RNA polymerase II. *Molecular and cellular biology*, **32:** 4691–4704.

Cheng, X., Yoshida, H., Raoofi, D., Saleh, S., Alborzinia, H., Wenke, F., Göhring, A., Reuter, S., Mah, N., Fuchs, H., Andrade-Navarro, M. A., Adjaye, J., Gul, S., Utikal, J., Mrowka, R. and Wölfl, S. (2015). Ethyl 2-((4-Chlorophenyl)amino)thiazole-4-carboxylate and Derivatives Are Potent Inducers of Oct3/4. *Journal of medicinal chemistry*, **58:** 5742–5750.

Cho, E. J., Kobor, M. S., Kim, M., Greenblatt, J. and Buratowski, S. (2001). Opposing effects of Ctk1 kinase and Fcp1 phosphatase at Ser 2 of the RNA polymerase II C-terminal domain. *Genes & development*, **15:** 3319–3329.

Cho, S., Hoang, A., Sinha, R., Zhong, X. Y., Fu, X. D., Krainer, A. R. and Ghosh, G. (2011). Interaction between the RNA binding domains of Ser-Arg splicing factor 1 and U1-70K snRNP protein determines early spliceosome assembly. *Proceedings of the National Academy of Sciences of the United States of America*, **108:** 8233–8238.

Churchman, L. S. and Weissman, J. S. (2011). Nascent transcript sequencing visualizes transcription at nucleotide resolution. *Nature*, **469:** 368–373.

Collins, L. and Penny, D. (2005). Complex spliceosomal organization ancestral to extant eukaryotes. *Molecular biology and evolution*, **22:** 1053–1066.

Conaway, R. C. and Conaway, J. W. (1993). General initiation factors for RNA polymerase II. *Annual review of biochemistry*, **62:** 161–190.

Cordin, O. and Beggs, J. D. (2013). RNA helicases in splicing. *RNA biology*, **10:** 83–95.

Core, L. and Adelman, K. (2019). Promoter-proximal pausing of RNA polymerase II: a nexus of gene regulation. *Genes & development*, **33:** 960–982.

Core, L. J., Martins, A. L., Danko, C. G., Waters, C. T., Siepel, A. and Lis, J. T. (2014). Analysis of nascent RNA identifies a unified architecture of initiation regions at mammalian promoters and enhancers. *Nature genetics*, **46:** 1311–1320.

Core, L. J., Waterfall, J. J. and Lis, J. T. (2008). Nascent RNA sequencing reveals widespread pausing and divergent initiation at human promoters. *Science*, **322:** 1845–1848.

Corrionero, A., Miñana, B. and Valcárcel, J. (2011). Reduced fidelity of branch point recognition and alternative splicing induced by the anti-tumor drug spliceostatin A. *Genes & development*, **25:** 445–459.

Corsini, N. S., Peer, A. M., Moeseneder, P., Roiuk, M., Burkard, T. R., Theussl, H. C., Moll, I. and Knoblich, J. A. (2018). Coordinated Control of mRNA and rRNA Processing Controls Embryonic Stem Cell Pluripotency and Differentiation. *Cell stem cell*, **22:** 543–558.e12.

Cossa, G., Roeschert, I., Prinz, F., Baluapuri, A., Silveira Vidal, R., Schülein-Völk, C., Chang, Y. C., Ade, C. P., Mastrobuoni, G., Girard, C., Wortmann, L., Walz, S., Lührmann, R., Kempa, S., Kuster, B., Wolf, E., Mumberg, D. and Eilers, M. (2020). Localized Inhibition of Protein Phosphatase 1 by NUAK1 Promotes Spliceosome Activity and Reveals a MYC-Sensitive Feedback Control of Transcription. *Molecular cell*, **77:** 1322–1339.e11.

Cortazar, M. A., Sheridan, R. M., Erickson, B., Fong, N., Glover-Cutter, K., Brannan, K. and Bentley, D. L. (2019). Control of RNA Pol II Speed by PNUTS-PP1 and Spt5 Dephosphorylation Facilitates Termination by a "Sitting Duck Torpedo" Mechanism. *Molecular cell*, **76:** 896–908.e4.

Cramer, P., Pesce, C. G., Baralle, F. E. and Kornblihtt, A. R. (1997). Functional association between promoter structure and transcript alternative splicing. *Proceedings of the National Academy of Sciences of the United States of America*, **94:** 11456–11460.

Cretu, C., Agrawal, A. A., Cook, A., Will, C. L., Fekkes, P., Smith, P. G., Lührmann, R., Larsen, N., Buonamici, S. and Pena, V. (2018). Structural Basis of Splicing Modulation by Antitumor Macrolide Compounds. *Molecular cell*, **70:** 265–273.e8.

Cretu, C., Schmitzová, J., Ponce-Salvatierra, A., Dybkov, O., De Laurentiis, E. I., Sharma, K., Will, C. L., Urlaub, H., Lührmann, R. and Pena, V. (2016). Molecular Architecture of SF3b and Structural Consequences of Its Cancer-Related Mutations. *Molecular cell*, **64:** 307–319.

Cristini, A., Park, J. H., Capranico, G., Legube, G., Favre, G. and Sordet, O. (2016). DNA-PK triggers histone ubiquitination and signaling in response to DNA double-strand breaks produced during the repair of transcription-blocking topoisomerase I lesions. *Nucleic acids research*, **44:** 1161–1178.

Cristini, A., Ricci, G., Britton, S., Salimbeni, S., Huang, S. N., Marinello, J., Calsou, P., Pommier, Y., Favre, G., Capranico, G., Gromak, N. and Sordet, O. (2019). Dual Processing of R-Loops and Topoisomerase I Induces Transcription-Dependent DNA Double-Strand Breaks. *Cell reports*, **28:** 3167–3181.e6.

Danino, Y. M., Even, D., Ideses, D. and Juven-Gershon, T. (2015). The core promoter: At the heart of gene expression. *Biochimica et biophysica acta*, **1849:** 1116–1131.

Dannappel, M. V., Sooraj, D., Loh, J. J. and Firestein, R. (2019). Molecular and in vivo Functions of the CDK8 and CDK19 Kinase Modules. *Frontiers in cell and developmental biology*, **6:** 171.

Daubner, G. M., Cléry, A., Jayne, S., Stevenin, J. and Allain, F. H. (2012). A syn-anti conformational difference allows SRSF2 to recognize guanines and cytosines equally well. *The EMBO journal*, **31:** 162–174.

de Graaf, K., Czajkowska, H., Rottmann, S., Packman, L. C., Lilischkis, R., Lüscher, B. and Becker, W. (2006). The protein kinase DYRK1A phosphorylates the splicing factor SF3b1/SAP155 at Thr434, a novel in vivo phosphorylation site. *BMC biochemistry*, **7:** 7.

Debéthune, L., Kohlhagen, G., Grandas, A. and Pommier, Y. (2002). Processing of nucleopeptides mimicking the topoisomerase I-DNA covalent complex by tyrosyl-DNA phosphodiesterase. *Nucleic acids research*, **30:** 1198–1204.

Decker, T. M., Forné, I., Straub, T., Elsaman, H., Ma, G., Shah, N., Imhof, A. and Eick, D. (2019). Analog-sensitive cell line identifies cellular substrates of CDK9. *Oncotarget*, **10:** 6934–6943.

Deckert, J., Hartmuth, K., Boehringer, D., Behzadnia, N., Will, C. L., Kastner, B., Stark, H., Urlaub, H. and Lührmann, R. (2006). Protein composition and electron microscopy structure of affinity-purified human spliceosomal B complexes isolated under physiological conditions. *Molecular and cellular biology*, **26:** 5528–5543.

Deng, W. and Roberts, S. G. (2007). TFIIB and the regulation of transcription by RNA polymerase II. *Chromosoma*, **116:** 417–429.

Descostes, N., Heidemann, M., Spinelli, L., Schüller, R., Maqbool, M. A., Fenouil, R., Koch, F., Innocenti, C., Gut, M., Gut, I., Eick, D. and Andrau, J. C. (2014). Tyrosine phosphorylation of RNA polymerase II CTD is associated with antisense promoter transcription and active enhancers in mammalian cells. *eLife*, **3:** e02105.

Dienemann, C., Schwalb, B., Schilbach, S. and Cramer, P. (2019). Promoter Distortion and Opening in the RNA Polymerase II Cleft. *Molecular cell*, **73:** 97–106.e4.

Donczew, R. and Hahn, S. (2017). Mechanistic Differences in Transcription Initiation at TATA-Less and TATA-Containing Promoters. *Molecular and cellular biology*, **38:** e00448-17.

Donner, A. J., Ebmeier, C. C., Taatjes, D. J. and Espinosa, J. M. (2010). CDK8 is a positive regulator of transcriptional elongation within the serum response network. *Nature structural & molecular biology*, **17:** 194–201.

Eaton, J. D. and West, S. (2020). Termination of Transcription by RNA Polymerase II: BOOM!. *Trends in genetics : TIG*, **36:** 664–675.

Effenberger, K. A., Anderson, D. D., Bray, W. M., Prichard, B. E., Ma, N., Adams, M. S., Ghosh, A. K. and Jurica, M. S. (2014). Coherence between cellular responses and in vitro splicing inhibition for the anti-tumor drug pladienolide B and its analogs. *The Journal of biological chemistry*, **289:** 1938–1947.

Effenberger, K. A., Urabe, V. K. and Jurica, M. S. (2017). Modulating splicing with small molecular inhibitors of the spliceosome. *Wiley interdisciplinary reviews. RNA*, **8:** 10.1002/wrna.1381.

Effenberger, K. A., Urabe, V. K., Prichard, B. E., Ghosh, A. K. and Jurica, M. S. (2016). Interchangeable SF3B1 inhibitors interfere with pre-mRNA splicing at multiple stages. *RNA*, **22:** 350–359.

Egloff, S., Dienstbier, M. and Murphy, S. (2012). Updating the RNA polymerase CTD code: adding gene-specific layers. *Trends in genetics : TIG*, **28:** 333–341.

Egloff, S., O'Reilly, D., Chapman, R. D., Taylor, A., Tanzhaus, K., Pitts, L., Eick, D. and Murphy, S. (2007). Serine-7 of the RNA polymerase II CTD is specifically required for snRNA gene expression. *Science*, **318:** 1777–1779.

Eick, D. and Geyer, M. (2013). The RNA polymerase II carboxy-terminal domain (CTD) code. *Chemical reviews*, **113:** 8456–8490.

El Marabti, E., Malek, J. and Younis, I. (2021). Minor Intron Splicing from Basic Science to Disease. *International journal of molecular sciences*, **22:** 6062.

Ellis, M. J., Ding, L., Shen, D., Luo, J., Suman, V. J., Wallis, J. W., Van Tine, B. A., Hoog, J., Goiffon, R. J., Goldstein, T. C., Ng, S., Lin, L., Crowder, R., Snider, J., Ballman, K., Weber, J., Chen, K., Koboldt, D. C., Kandoth, C., Schierding, W. S., et al. (2012). Whole-genome analysis informs breast cancer response to aromatase inhibition. *Nature*, **486:** 353–360.

Elmlund, H., Baraznenok, V., Lindahl, M., Samuelsen, C. O., Koeck, P. J., Holmberg, S., Hebert, H. and Gustafsson, C. M. (2006). The cyclin-dependent kinase 8 module sterically blocks Mediator interactions with RNA polymerase II. *Proceedings of the National Academy of Sciences of the United States of America*, **103:** 15788–15793.

Fabrizio, P., Dannenberg, J., Dube, P., Kastner, B., Stark, H., Urlaub, H. and Lührmann, R. (2009). The evolutionarily conserved core design of the catalytic activation step of the yeast spliceosome. *Molecular cell*, **36:** 593–608.

Faust, T. B., Li, Y., Bacon, C. W., Jang, G. M., Weiss, A., Jayaraman, B., Newton, B. W., Krogan, N. J., D'Orso, I. and Frankel, A. D. (2018). The HIV-1 Tat protein recruits a ubiquitin ligase to reorganize the 7SK snRNP for transcriptional activation. *eLife*, **7:** e31879.

Fishburn, J., Galburt, E. and Hahn, S. (2016). Transcription Start Site Scanning and the Requirement for ATP during Transcription Initiation by RNA Polymerase II. *The Journal of biological chemistry*, **291:** 13040–13047.

Fiszbein, A., Krick, K. S., Begg, B. E. and Burge, C. B. (2019). Exon-Mediated Activation of Transcription Starts. *Cell*, **179:** 1551–1565.e17.

Fleckner, J., Zhang, M., Valcárcel, J. and Green, M. R. (1997). U2AF65 recruits a novel human DEAD box protein required for the U2 snRNP-branchpoint interaction. *Genes & development*, **11:** 1864–1872.

Flynn, R. A., Do, B. T., Rubin, A. J., Calo, E., Lee, B., Kuchelmeister, H., Rale, M., Chu, C., Kool, E. T., Wysocka, J., Khavari, P. A. and Chang, H. Y. (2016). 7SK-BAF axis controls pervasive transcription at enhancers. *Nature structural & molecular biology*, **23:** 231–238.

Fong, N., Brannan, K., Erickson, B., Kim, H., Cortazar, M. A., Sheridan, R. M., Nguyen, T., Karp, S. and Bentley, D. L. (2015). Effects of Transcription Elongation Rate and Xrn2 Exonuclease Activity on RNA Polymerase II Termination Suggest Widespread Kinetic Competition. *Molecular cell*, **60:** 256–267.

Fong, Y. W. and Zhou, Q. (2001). Stimulatory effect of splicing factors on transcriptional elongation. *Nature*, **414:** 929–933.

Fornerod, M., Ohno, M., Yoshida, M. and Mattaj, I. W. (1997). CRM1 is an export receptor for leucine-rich nuclear export signals. *Cell*, **90:** 1051–1060.

Friend, K., Lovejoy, A. F. and Steitz, J. A. (2007). U2 snRNP binds intronless histone pre-mRNAs to facilitate U7-snRNP-dependent 3' end formation. *Molecular cell*, **28:** 240–252.

Fujinaga, K., Irwin, D., Huang, Y., Taube, R., Kurosu, T. and Peterlin, B. M. (2004). Dynamics of human immunodeficiency virus transcription: P-TEFb phosphorylates RD and dissociates negative effectors from the transactivation response element. *Molecular and cellular biology*, **24:** 787–795.

Fukuda, M., Asano, S., Nakamura, T., Adachi, M., Yoshida, M., Yanagida, M. and Nishida, E. (1997). CRM1 is responsible for intracellular transport mediated by the nuclear export signal. *Nature*, **390:** 308–311.

Gama-Brambila, R. A., Chen, J., Zhou, J., Tascher, G., Münch, C. and Cheng, X. (2021). A PROTAC targets splicing factor 3B1. *Cell chemical biology*, **S2451-9456** 00211-7.

Gallie D. R. (1991). The cap and poly(A) tail function synergistically to regulate mRNA translational efficiency. *Genes & development*, **5:** 2108–2116.

Gao, K., Masuda, A., Matsuura, T. and Ohno, K. (2008). Human branch point consensus sequence is yUnAy. *Nucleic acids research*, **36:** 2257–2267.

Ghosh, A., Shuman, S. and Lima, C. D. (2008). The structure of Fcp1, an essential RNA polymerase II CTD phosphatase. *Molecular cell*, **32:** 478–490.

Gilmour, D. S. and Lis, J. T. (1986). RNA polymerase II interacts with the promoter region of the noninduced hsp70 gene in Drosophila melanogaster cells. *Molecular and cellular biology*, **6:** 3984–3989.

Girard, C., Will, C. L., Peng, J., Makarov, E. M., Kastner, B., Lemm, I., Urlaub, H., Hartmuth, K. and Lührmann, R. (2012). Post-transcriptional spliceosomes are retained in nuclear speckles until splicing completion. *Nature communications*, **3:** 994.

Gozani, O., Potashkin, J. and Reed, R. (1998). A potential role for U2AF-SAP 155 interactions in recruiting U2 snRNP to the branch site. *Molecular and cellular biology*, **18:** 4752–4760.

Gregersen, L. H., Mitter, R., Ugalde, A. P., Nojima, T., Proudfoot, N. J., Agami, R., Stewart, A. and Svejstrup, J. Q. (2019). SCAF4 and SCAF8, mRNA Anti-Terminator Proteins. *Cell*, **177:** 1797–1813.e18.

Gressel, S., Schwalb, B., Decker, T. M., Qin, W., Leonhardt, H., Eick, D. and Cramer, P. (2017). CDK9-dependent RNA polymerase II pausing controls transcription initiation. *eLife*, **6:** e29736.

Grünberg, S. and Hahn, S. (2013). Structural insights into transcription initiation by RNA polymerase II. *Trends in biochemical sciences*, **38:** 603–611.

Guiro, J. and Murphy, S. (2017). Regulation of expression of human RNA polymerase II-transcribed snRNA genes. *Open biology*, **7:** 170073.

Häcker, I., Sander, B., Golas, M. M., Wolf, E., Karagöz, E., Kastner, B., Stark, H., Fabrizio, P. and Lührmann, R. (2008). Localization of Prp8, Brr2, Snu114 and U4/U6 proteins in the yeast tri-snRNP by electron microscopy. *Nature structural & molecular biology*, **15:** 1206–1212.

Haimov, O., Sinvani, H. and Dikstein, R. (2015). Cap-dependent, scanning-free translation initiation mechanisms. *Biochimica et biophysica acta*, **1849:** 1313–1318.

Harlen, K. M. and Churchman, L. S. (2017). The code and beyond: transcription regulation by the RNA polymerase II carboxy-terminal domain. *Nature Reviews Molecular Cell Biology,* **18:** 263–273.

Harlen, K. M., Trotta, K. L., Smith, E. E., Mosaheb, M. M., Fuchs, S. M. and Churchman, L. S. (2016). Comprehensive RNA Polymerase II Interactomes Reveal Distinct and Varied Roles for Each Phospho-CTD Residue. *Cell reports*, **15:** 2147–2158.

Hasegawa, M., Miura, T., Kuzuya, K., Inoue, A., Won Ki, S., Horinouchi, S., Yoshida, T., Kunoh, T., Koseki, K., Mino, K., Sasaki, R., Yoshida, M. and Mizukami, T. (2011). Identification of SAP155 as the target of GEX1A (Herboxidiene), an antitumor natural product. *ACS chemical biology*, **6:** 229–233.

Herrmann, C. H. and Mancini, M. A. (2001). The Cdk9 and cyclin T subunits of TAK/P-TEFb localize to splicing factor-rich nuclear speckle regions. *Journal of cell science*, **114:** 1491–1503.

Herzel, L., Ottoz, D. S. M., Alpert, T. and Neugebauer, K. M. (2017). Splicing and transcription touch base: co-transcriptional spliceosome assembly and function. *Nature reviews. Molecular cell biology*, **18:** 637–650.

Hintermair, C., Heidemann, M., Koch, F., Descostes, N., Gut, M., Gut, I., Fenouil, R., Ferrier, P., Flatley, A., Kremmer, E., Chapman, R. D., Andrau, J. C. and Eick, D. (2012). Threonine-4 of mammalian RNA polymerase II CTD is targeted by Polo-like kinase 3 and required for transcriptional elongation. *The EMBO journal*, **31:** 2784–2797.

Hintermair, C., Voß, K., Forné, I., Heidemann, M., Flatley, A., Kremmer, E., Imhof, A. and Eick, D. (2016). Specific threonine-4 phosphorylation and function of RNA polymerase II CTD during M phase progression. *Scientific reports*, **6:** 27401.

Hornbeck, P. V., Zhang, B., Murray, B., Kornhauser, J. M., Latham, V. and Skrzypek, E. (2015). PhosphoSitePlus, 2014: mutations, PTMs and recalibrations. *Nucleic acids research*, **43:** D512–D520.

Horowitz D. S. (2012). The mechanism of the second step of pre-mRNA splicing. *Wiley interdisciplinary reviews*. *RNA*, **3:** 331–350.

Hluchý, M., Gajdušková, P., Ruiz de Los Mozos, I., Rájecký, M., Kluge, M., Berger, B. T., Slabá, Z., Potěšil, D., Weiß, E., Ule, J., Zdráhal, Z., Knapp, S., Paruch, K., Friedel, C. C. and Blazek, D. (2022). CDK11 regulates pre-mRNA splicing by phosphorylation of SF3B1. *Nature*, **609:** 829–834.

Hsin, J. P., Sheth, A. and Manley, J. L. (2011). RNAP II CTD phosphorylated on threonine-4 is required for histone mRNA 3' end processing. *Science*, **334:** 683–686.

Hsin, J. P., Xiang, K. and Manley, J. L. (2014). Function and control of RNA polymerase II C-terminal domain phosphorylation in vertebrate transcription and RNA processing. *Molecular and cellular biology*, **34:** 2488–2498.

Hu, S., Marineau, J. J., Rajagopal, N., Hamman, K. B., Choi, Y. J., Schmidt, D. R., Ke, N., Johannessen, L., Bradley, M. J., Orlando, D. A., Alnemy, S. R., Ren, Y., Ciblat, S., Winter, D. K., Kabro, A., Sprott, K. T., Hodgson, J. G., Fritz, C. C., Carulli, J. P., di Tomaso, E., et al. (2019). Discovery and Characterization of SY-1365, a Selective, Covalent Inhibitor of CDK7. *Cancer research*, **79:** 3479–3491.

Huang, K. L., Jee, D., Stein, C. B., Elrod, N. D., Henriques, T., Mascibroda, L. G., Baillat, D., Russell, W. K., Adelman, K. and Wagner, E. J. (2020). Integrator Recruits Protein Phosphatase 2A to Prevent Pause Release and Facilitate Transcription Termination. *Molecular cell*, **80:** 345–358.e9.

Insco, M. L., Abraham, B. J., Dubbury, S. J., Kaltheuner, I. H., Dust, S., Wu, C., Chen, K. Y., Liu, D., Bellaousov, S., Cox, A. M., Martin, B. J. E., Zhang, T., Ludwig, C. G., Fabo, T., Modhurima, R., Esgdaille, D. E., Henriques, T., Brown, K. M., Chanock, S. J., Geyer, M., et al. (2023). Oncogenic CDK13 mutations impede nuclear RNA surveillance. *Science*, **380:** eabn7625.

Interthal, H., Chen, H. J. and Champoux, J. J. (2005). Human Tdp1 cleaves a broad spectrum of substrates, including phosphoamide linkages. *The Journal of biological chemistry*, **280:** 36518–36528.

Isaac, B. G., Ayer, S. W., Elliott, R. C. and Stonard, R. J. (1992). Herboxidiene: A Potent Phytotoxic Polyketide from *Streptomyces* sp. A7847. *The Journal of biological chemistry*, **57:** 7220–6.

Jang, M. K., Mochizuki, K., Zhou, M., Jeong, H. S., Brady, J. N. and Ozato, K. (2005). The bromodomain protein Brd4 is a positive regulatory component of P-TEFb and stimulates RNA polymerase II-dependent transcription. *Molecular cell*, **19:** 523–534.

Je, E. M., Yoo, N. J., Kim, Y. J., Kim, M. S. and Lee, S. H. (2013). Mutational analysis of splicing machinery genes SF3B1, U2AF1 and SRSF2 in myelodysplasia and other common tumors. *International journal of cancer*, **133:** 260–265.

Jeronimo, C., Collin, P. and Robert, F. (2016). The RNA Polymerase II CTD: The Increasing Complexity of a Low-Complexity Protein Domain. *Journal of molecular biology*, **428:** 2607–2622.

Ji, X., Zhou, Y., Pandit, S., Huang, J., Li, H., Lin, C. Y., Xiao, R., Burge, C. B. and Fu, X. D. (2013). SR proteins collaborate with 7SK and promoter-associated nascent RNA to release paused polymerase. *Cell*, **153:** 855–868.

Jurica, M. S. and Moore, M. J. (2003). Pre-mRNA splicing: awash in a sea of proteins. *Molecular cell*, **12:** 5–14.

Juven-Gershon, T., Hsu, J. Y., Theisen, J. W. and Kadonaga, J. T. (2008). The RNA polymerase II core promoter - the gateway to transcription. *Current opinion in cell biology*, **20:** 253–259.

Kachaev, Z. M., Lebedeva, L. A., Kozlov, E. N. and Shidlovskii, Y. V. (2020). Interplay of mRNA capping and transcription machineries. *Bioscience reports*, **40:** BSR20192825.

Kaida, D., Motoyoshi, H., Tashiro, E., Nojima, T., Hagiwara, M., Ishigami, K., Watanabe, H., Kitahara, T., Yoshida, T., Nakajima, H., Tani, T., Horinouchi, S. and Yoshida, M. (2007). Spliceostatin A targets SF3b and inhibits both splicing and nuclear retention of pre-mRNA. *Nature chemical biology*, **3:** 576–583.

Kanazawa, S., Soucek, L., Evan, G., Okamoto, T. and Peterlin, B. M. (2003). c-Myc recruits P-TEFb for transcription, cellular proliferation and apoptosis. *Oncogene*, **22:** 5707–5711.

Kastner, B., Will, C. L., Stark, H. and Lührmann, R. (2019). Structural Insights into Nuclear pre-mRNA Splicing in Higher Eukaryotes. *Cold Spring Harbor perspectives in biology*, **11:** a032417.

Kedersha, N., Panas, M. D., Achorn, C. A., Lyons, S., Tisdale, S., Hickman, T., Thomas, M., Lieberman, J., McInerney, G. M., Ivanov, P. and Anderson, P. (2016). G3BP-Caprin1-USP10 complexes mediate stress granule condensation and associate with 40S subunits. *The Journal of cell biology*, **212:** 845–860.

Keller, E. B. and Noon, W. A. (1985). Intron splicing: a conserved internal signal in introns of Drosophila pre-mRNAs. *Nucleic acids research*, **13:** 4971–4981.

Kfir, N., Lev-Maor, G., Glaich, O., Alajem, A., Datta, A., Sze, S. K., Meshorer, E. and Ast, G. (2015). SF3B1 association with chromatin determines splicing outcomes. *Cell reports*, **11:** 618–629.

Kielkopf, C. L., Lücke, S. and Green, M. R. (2004). U2AF homology motifs: protein recognition in the RRM world. *Genes & development*, **18:** 1513–1526.

Kim, J. B. and Sharp, P. A. (2001). Positive transcription elongation factor B phosphorylates hSPT5 and RNA polymerase II carboxyl-terminal domain independently of cyclin-dependent kinase-activating kinase. *The Journal of biological chemistry*, **276:** 12317–12323.

Knuesel, M. T., Meyer, K. D., Bernecky, C. and Taatjes, D. J. (2009). The human CDK8 subcomplex is a molecular switch that controls Mediator coactivator function. *Genes & development*, **23:** 439–451.

Koga, M., Hayashi, M. and Kaida, D. (2015). Splicing inhibition decreases phosphorylation level of Ser2 in Pol II CTD. *Nucleic acids research*, **43:** 8258–8267.

Kornblihtt, A. R., de la Mata, M., Fededa, J. P., Munoz, M. J. and Nogues, G. (2004). Multiple links between transcription and splicing. *RNA*, **10:** 1489–1498.

Kotake, Y., Sagane, K., Owa, T., Mimori-Kiyosue, Y., Shimizu, H., Uesugi, M., Ishihama, Y., Iwata, M. and Mizui, Y. (2007). Splicing factor SF3b as a target of the antitumor natural product pladienolide. *Nature chemical biology*, **3:** 570–575.

Krajewska, M., Dries, R., Grassetti, A. V., Dust, S., Gao, Y., Huang, H., Sharma, B., Day, D. S., Kwiatkowski, N., Pomaville, M., Dodd, O., Chipumuro, E., Zhang, T., Greenleaf, A. L., Yuan, G. C., Gray, N. S., Young, R. A., Geyer, M., Gerber, S. A. and George, R. E. (2019). CDK12 loss in cancer cells affects DNA damage response genes through premature cleavage and polyadenylation. *Nature communications*, **10:** 1757.

Krogan, N. J., Cagney, G., Yu, H., Zhong, G., Guo, X., Ignatchenko, A., Li, J., Pu, S., Datta, N., Tikuisis, A. P., Punna, T., Peregrín-Alvarez, J. M., Shales, M., Zhang, X., Davey, M., Robinson, M. D., Paccanaro, A., Bray, J. E., Sheung, A., Beattie, B., et al. (2006). Global landscape of protein complexes in the yeast Saccharomyces cerevisiae. *Nature*, **440:** 637–643.

Kudo, N., Wolff, B., Sekimoto, T., Schreiner, E. P., Yoneda, Y., Yanagida, M., Horinouchi, S. and Yoshida, M. (1998). Leptomycin B inhibition of signal-mediated nuclear export by direct binding to CRM1. *Experimental cell research*, **242:** 540–547.

Kong, Y., Krauthammer, M. and Halaban, R. (2014). Rare SF3B1 R625 mutations in cutaneous melanoma. *Melanoma research*, **24:** 332–334.

Küsters-Vandevelde, H. V., Creytens, D., van Engen-van Grunsven, A. C., Jeunink, M., Winnepenninckx, V., Groenen, P. J., Küsters, B., Wesseling, P., Blokx, W. A. and Prinsen, C. F. (2016). SF3B1 and EIF1AX mutations occur in primary leptomeningeal melanocytic neoplasms; yet another similarity to uveal melanomas. *Acta neuropathologica communications*, **4:** 5.

Kyburz, A., Friedlein, A., Langen, H. and Keller, W. (2006). Direct interactions between subunits of CPSF and the U2 snRNP contribute to the coupling of pre-mRNA 3' end processing and splicing. *Molecular cell*, **23:** 195–205.

Laetsch, T. W., Liu, X., Vu, A., Sliozberg, M., Vido, M., Elci, O. U., Goldsmith, K. C. and Hogarty, M. D. (2014). Multiple components of the spliceosome regulate Mcl1 activity in neuroblastoma. *Cell death & disease*, **5:** e1072.

Lainé, J. P. and Egly, J. M. (2006). When transcription and repair meet: a complex system. *Trends in genetics : TIG*, **22:** 430–436.

Laitem, C., Zaborowska, J., Isa, N. F., Kufs, J., Dienstbier, M. and Murphy, S. (2015). CDK9 inhibitors define elongation checkpoints at both ends of RNA polymerase II-transcribed genes. *Nature structural & molecular biology*, **22:** 396–403.

Langford, C. J., Klinz, F. J., Donath, C. and Gallwitz, D. (1984). Point mutations identify the conserved, intron-contained TACTAAC box as an essential splicing signal sequence in yeast. *Cell*, **36:** 645–653.

Lee, S., Liu, H., Hill, R., Chen, C., Hong, X., Crawford, F., Kingsley, M., Zhang, Q., Liu, X., Chen, Z., Lengeling, A., Bernt, K. M., Marrack, P., Kappler, J., Zhou, Q., Li, C. Y., Xue, Y., Hansen, K. and Zhang, G. (2020). JMJD6 cleaves MePCE to release positive transcription elongation factor b (P-TEFb) in higher eukaryotes. *eLife*, **9:** e53930.

Li, C., Xie, W., Rosenblum, J. S., Zhou, J., Guo, J., Miao, Y., Shen, Y., Wang, H., Gong, L., Li, M., Zhao, S., Cheng, S., Zhu, H., Jiang, T., Ling, S., Wang, F., Zhang, H., Zhang, M., Qu, Y., Zhang, Q., et al. (2020). Somatic SF3B1 hotspot mutation in prolactinomas. *Nature communications*, **11:** 2506.

Liang, K., Gao, X., Gilmore, J. M., Florens, L., Washburn, M. P., Smith, E. and Shilatifard, A. (2015). Characterization of human cyclin-dependent kinase 12 (CDK12) and CDK13 complexes in C-terminal domain phosphorylation, gene transcription, and RNA processing. *Molecular and cellular biology*, **35:** 928–938.

Lin, C., Smith, E. R., Takahashi, H., Lai, K. C., Martin-Brown, S., Florens, L., Washburn, M. P., Conaway, J. W., Conaway, R. C. and Shilatifard, A. (2010). AFF4, a component of the ELL/P-TEFb elongation complex and a shared subunit of MLL chimeras, can link transcription elongation to leukemia. *Molecular cell*, **37:** 429–437.

Lin, S., Coutinho-Mansfield, G., Wang, D., Pandit, S. and Fu, X. D. (2008). The splicing factor SC35 has an active role in transcriptional elongation. *Nature structural & molecular biology*, **15:** 819–826.

Liu, C. X. and Chen, L. L. (2022). Circular RNAs: Characterization, cellular roles, and applications. *Cell*, **185:** 2016–2034.

Liu, W., Ma, Q., Wong, K., Li, W., Ohgi, K., Zhang, J., Aggarwal, A. and Rosenfeld, M. G. (2013). Brd4 and JMJD6-associated anti-pause enhancers in regulation of transcriptional pause release. *Cell*, **155:** 1581–1595.

Loerch, S., Leach, J. R., Horner, S. W., Maji, D., Jenkins, J. L., Pulvino, M. J. and Kielkopf, C. L. (2019). The pre-mRNA splicing and transcription factor Tat-SF1 is a functional partner of the spliceosome SF3b1 subunit via a U2AF homology motif interface. *The Journal of biological chemistry*, **294:** 2892–2902.

Luse D. S. (2014). The RNA polymerase II preinitiation complex. Through what pathway is the complex assembled?. *Transcription*, **5:** e27050.

Makarova, O. V., Makarov, E. M., Urlaub, H., Will, C. L., Gentzel, M., Wilm, M. and Lührmann, R. (2004). A subset of human 35S U5 proteins, including Prp19, function prior to catalytic step 1 of splicing. *The EMBO journal*, **23:** 2381–2391.

Malbec, L., Zhang, T., Chen, Y. S., Zhang, Y., Sun, B. F., Shi, B. Y., Zhao, Y. L., Yang, Y. and Yang, Y. G. (2019). Dynamic methylome of internal mRNA N7-methylguanosine and its regulatory role in translation. *Cell research*, **29:** 927–941.

Malik, S. and Roeder, R. G. (2023). Regulation of the RNA polymerase II pre-initiation complex by its associated coactivators. *Nature reviews. Genetics*, **24:** 767–782.

Marasco, L. E. and Kornblihtt, A. R. (2023). The physiology of alternative splicing. *Nature reviews. Molecular cell biology*, **24:** 242–254.

Massiello, A., Roesser, J. R. and Chalfant, C. E. (2006). SAP155 Binds to ceramide-responsive RNA cis-element 1 and regulates the alternative 5' splice site selection of Bcl-x pre-mRNA. *FASEB journal : official publication of the Federation of American Societies for Experimental Biology*, **20:** 1680–1682.

Matera, A. G. and Wang, Z. (2014). A day in the life of the spliceosome. *Nature reviews. Molecular cell biology*, **15:** 108–121.

Mathis, D. J. and Chambon, P. (1981). The SV40 early region TATA box is required for accurate in vitro initiation of transcription. *Nature*, **290:** 310–315.

Mayer, A., di Iulio, J., Maleri, S., Eser, U., Vierstra, J., Reynolds, A., Sandstrom, R., Stamatoyannopoulos, J. A. and Churchman, L. S. (2015). Native elongating transcript sequencing reveals human transcriptional activity at nucleotide resolution. *Cell*, **16:** 541–554.

Mayer, A., Heidemann, M., Lidschreiber, M., Schreieck, A., Sun, M., Hintermair, C., Kremmer, E., Eick, D. and Cramer, P. (2012). CTD tyrosine phosphorylation impairs termination factor recruitment to RNA polymerase II. *Science*, **336:** 1723–1725.

McGlincy, N. J., Valomon, A., Chesham, J. E., Maywood, E. S., Hastings, M. H. and Ule, J. (2012). Regulation of alternative splicing by the circadian clock and food related cues. *Genome biology*, **13:** R54.

McNamara, R. P., Reeder, J. E., McMillan, E. A., Bacon, C. W., McCann, J. L. and D'Orso, I. (2016). KAP1 Recruitment of the 7SK snRNP Complex to Promoters Enables Transcription Elongation by RNA Polymerase II. *Molecular cell*, **61:** 39–53.

Merkhofer, E. C., Hu, P. and Johnson, T. L. (2014). Introduction to cotranscriptional RNA splicing. *Methods in molecular biology*, **1126:** 83–96.

Merkin, J., Russell, C., Chen, P. and Burge, C. B. (2012). Evolutionary dynamics of gene and isoform regulation in Mammalian tissues. *Science*, **338:** 1593–1599.

Mermoud, J. E., Cohen, P. and Lamond, A. I. (1992). Ser/Thr-specific protein phosphatases are required for both catalytic steps of pre-mRNA splicing. *Nucleic acids research*, **20:** 5263–5269.

Michaud, S. and Reed, R. (1993). A functional association between the 5' and 3' splice site is established in the earliest prespliceosome complex (E) in mammals. *Genes & development*, **7:** 1008–1020.

Miller-Wideman, M., Makkar, N., Tran, M., Isaac, B., Biest, N. and Stonard, R. (1992). Herboxidiene, a new herbicidal substance from *Streptomyces chromofuscus* A7847. Taxonomy, fermentation, isolation, physico-chemical and biological properties. *The Journal of antibiotics*, **45:** 914–921.

Mischo, H. E. and Proudfoot, N. J. (2013). Disengaging polymerase: terminating RNA polymerase II transcription in budding yeast. *Biochimica et biophysica acta*, **1829:** 174–185.

Missra, A. and Gilmour, D. S. (2010). Interactions between DSIF (DRB sensitivity inducing factor), NELF (negative elongation factor), and the Drosophila RNA polymerase II transcription elongation complex. *Proceedings of the National Academy of Sciences of the United States of America*, **107:** 11301–11306.

Mizui, Y., Sakai, T., Iwata, M., Uenaka, T., Okamoto, K., Shimizu, H., Yamori, T., Yoshimatsu, K. and Asada, M. (2004). Pladienolides, new substances from culture of Streptomyces platensis Mer-11107. III. In vitro and in vivo antitumor activities. *The Journal of antibiotics*, **57:** 188–196.

Molenaar, J. J., Koster, J., Zwijnenburg, D. A., van Sluis, P., Valentijn, L. J., van der Ploeg, I., Hamdi, M., van Nes, J., Westerman, B. A., van Arkel, J., Ebus, M. E., Haneveld, F., Lakeman, A., Schild, L., Molenaar, P., Stroeken, P., van Noesel, M. M., Ora, I., Santo, E. E., Caron, H. N., et al. (2012). Sequencing of neuroblastoma identifies chromothripsis and defects in neuritogenesis genes. *Nature*, **483:** 589–593.

Moorhead, G. B., Trinkle-Mulcahy, L. and Ulke-Lemée, A. (2007). Emerging roles of nuclear protein phosphatases. *Nature reviews. Molecular cell biology*, **8:** 234–244.

Morales, F. and Giordano, A. (2016). Overview of CDK9 as a target in cancer research. *Cell cycle*, **15:** 519–527.

Mosley, A. L., Pattenden, S. G., Carey, M., Venkatesh, S., Gilmore, J. M., Florens, L., Workman, J. L. and Washburn, M. P. (2009). Rtr1 is a CTD phosphatase that regulates RNA polymerase II during the transition from serine 5 to serine 2 phosphorylation. *Molecular cell*, **34:** 168–178.

Mougel, M., Akkawi, C., Chamontin, C., Feuillard, J., Pessel-Vivares, L., Socol, M. and Laine, S. (2020). NXF1 and CRM1 nuclear export pathways orchestrate nuclear export, translation and packaging of murine leukaemia retrovirus unspliced RNA. *RNA biology*, **17:** 528–538.

Murthy, T., Bluemn, T., Gupta, A. K., Reimer, M., Jr, Rao, S., Pillai, M. M. and Minella, A. C. (2018). Cyclin-dependent kinase 1 (CDK1) and CDK2 have opposing roles in regulating interactions of splicing factor 3B1 with chromatin. *The Journal of biological chemistry*, **293:** 10220–10234.

Nakajima, H., Hori, Y., Terano, H., Okuhara, M., Manda, T., Matsumoto, S. and Shimomura, K. (1996). New antitumor substances, FR901463, FR901464 and FR901465. II. Activities against experimental tumors in mice and mechanism of action. *The Journal of antibiotics*, **49:** 1204–1211.

Napolitano, G., Licciardo, P., Carbone, R., Majello, B. and Lania, L. (2002). CDK9 has the intrinsic property to shuttle between nucleus and cytoplasm, and enhanced expression of cyclin T1 promotes its nuclear localization. *Journal of cellular physiology*, **192:** 209–215.

Neubauer, G., King, A., Rappsilber, J., Calvio, C., Watson, M., Ajuh, P., Sleeman, J., Lamond, A. and Mann, M. (1998). Mass spectrometry and EST-database searching allows characterization of the multi-protein spliceosome complex. *Nature genetics*, **20:** 46–50.

Nguyen, V. T., Kiss, T., Michels, A. A. and Bensaude, O. (2001). 7SK small nuclear RNA binds to and inhibits the activity of CDK9/cyclin T complexes. *Nature*, **414:** 322–325.

Ni, Z., Xu, C., Guo, X., Hunter, G. O., Kuznetsova, O. V., Tempel, W., Marcon, E., Zhong, G., Guo, H., Kuo, W. W., Li, J., Young, P., Olsen, J. B., Wan, C., Loppnau, P., El Bakkouri, M., Senisterra, G. A., He, H., Huang, H., Sidhu, S. S., Emili, A., Murphy, S., Mosley, A. L., Arrowsmith, C. H., Min, J. and Greenblatt, J. F. (2014). RPRD1A and RPRD1B are human RNA polymerase II C-terminal domain scaffolds for Ser5 dephosphorylation. *Nature structural & molecular biology*, **21:** 686–695.

Nojima, T., Gomes, T., Grosso, A. R. F., Kimura, H., Dye, M. J., Dhir, S., Carmo-Fonseca, M. and Proudfoot, N. J. (2015). Mammalian NET-Seq Reveals Genome-wide Nascent Transcription Coupled to RNA Processing. *Cell*, **161:** 526–540.

Ossareh-Nazari, B., Bachelerie, F. and Dargemont, C. (1997). Evidence for a role of CRM1 in signal-mediated nuclear protein export. *Science*, **278:** 141–144.

O'Brien, K., Matlin, A. J., Lowell, A. M. and Moore, M. J. (2008). The biflavonoid isoginkgetin is a general inhibitor of Pre-mRNA splicing. *The Journal of biological chemistry*, **283:** 33147–33154.

Pabis, M., Neufeld, N., Steiner, M. C., Bojic, T., Shav-Tal, Y. and Neugebauer, K. M. (2013). The nuclear cap-binding complex interacts with the U4/U6·U5 tri-snRNP and promotes spliceosome assembly in mammalian cells. *RNA*, **19:** 1054–1063.

Padgett R. A. (2012). New connections between splicing and human disease. *Trends in genetics : TIG,* **28:** 147–154.

Pan, Q., Shai, O., Lee, L. J., Frey, B. J. and Blencowe, B. J. (2008). Deep surveying of alternative splicing complexity in the human transcriptome by high-throughput sequencing. *Nature genetics*, **40:** 1413–1415.

Panzeri, V., Pieraccioli, M., Cesari, E., de la Grange, P. and Sette, C. (2023). CDK12/13 promote splicing of proximal introns by enhancing the interaction between RNA polymerase II and the splicing factor SF3B1. *Nucleic acids research*, **51:** 5512–5526.

Papasaikas, P., Tejedor, J. R., Vigevani, L. and Valcárcel, J. (2015). Functional splicing network reveals extensive regulatory potential of the core spliceosomal machinery. *Molecular cell*, **57:** 7–22.

Parada, C. A. and Roeder, R. G. (1999). A novel RNA polymerase II-containing complex potentiates Tat-enhanced HIV-1 transcription. *The EMBO journal*, **18:** 3688–3701.

Parua, P. K., Booth, G. T., Sansó, M., Benjamin, B., Tanny, J. C., Lis, J. T. and Fisher, R. P. (2018). A Cdk9-PP1 switch regulates the elongation-termination transition of RNA polymerase II. *Nature*, **558:** 460–464.

Parua, P. K., Kalan, S., Benjamin, B., Sansó, M. and Fisher, R. P. (2020). Distinct Cdk9-phosphatase switches act at the beginning and end of elongation by RNA polymerase II. *Nature communications*, **11:** 4338.

Passmore, L. A. and Coller, J. (2022). Roles of mRNA poly(A) tails in regulation of eukaryotic gene expression. *Nature reviews. Molecular cell biology*, **23:** 93–106.

Pawellek, A., McElroy, S., Samatov, T., Mitchell, L., Woodland, A., Ryder, U., Gray, D., Lührmann, R. and Lamond, A. I. (2014). Identification of small molecule inhibitors of pre-mRNA splicing. *The Journal of biological chemistry*, **289:** 34683–34698.

Pecori, R., Di Giorgio, S., Paulo Lorenzo, J. and Nina Papavasiliou, F. (2022). Functions and consequences of AID/APOBEC-mediated DNA and RNA deamination. *Nature reviews. Genetics*, **23:** 505–518.

Peterlin, B. M. and Price, D. H. (2006). Controlling the elongation phase of transcription with P-TEFb. *Molecular cell*, **23:** 297–305.

Phelan, M. M., Goult, B. T., Clayton, J. C., Hautbergue, G. M., Wilson, S. A. and Lian, L. Y. (2012). The structure and selectivity of the SR protein SRSF2 RRM domain with RNA. *Nucleic acids research*, **40:** 3232–3244.

Plaschka, C., Lin, P. C., Charenton, C. and Nagai, K. (2018). Prespliceosome structure provides insights into spliceosome assembly and regulation. *Nature*, **559:** 419–422.

Pommier Y. (2006). Topoisomerase I inhibitors: camptothecins and beyond. *Nature reviews. Cancer*, **6:** 789–802.

Porrua, O., Boudvillain, M. and Libri, D. (2016). Transcription Termination: Variations on Common Themes. *Trends in genetics : TIG*, **32:** 508–522.

Preußner, M., Goldammer, G., Neumann, A., Haltenhof, T., Rautenstrauch, P., Müller-McNicoll, M. and Heyd, F. (2017). Body Temperature Cycles Control Rhythmic Alternative Splicing in Mammals. *Molecular cell*, **67:** 433–446.e4.

Rahl, P. B., Lin, C. Y., Seila, A. C., Flynn, R. A., McCuine, S., Burge, C. B., Sharp, P. A. and Young, R. A. (2010). c-Myc regulates transcriptional pause release. Cell, **141:** 432–445.

Rahmani, K. and Dean, D. A. (2017). Leptomycin B alters the subcellular distribution of CRM1 (Exportin 1). Biochemical and biophysical research communications, **488:** 253–258.

Ramanathan, Y., Reza, S. M., Young, T. M., Mathews, M. B. and Pe'ery, T. (1999). Human and rodent transcription elongation factor P-TEFb: interactions with human immunodeficiency virus type 1 tat and carboxy-terminal domain substrate. *Journal of virology*, **73:** 5448–5458.

Rebelo, S., Santos, M., Martins, F., da Cruz e Silva, E. F. and da Cruz e Silva, O. A. (2015). Protein phosphatase 1 is a key player in nuclear events. *Cellular signalling*, **27:** 2589–2598.

Rimel, J. K., Poss, Z. C., Erickson, B., Maas, Z. L., Ebmeier, C. C., Johnson, J. L., Decker, T. M., Yaron, T. M., Bradley, M. J., Hamman, K. B., Hu, S., Malojcic, G., Marineau, J. J., White, P. W., Brault, M., Tao, L., DeRoy, P., Clavette, C., Nayak, S., Damon, L. J., et al. (2020). Selective inhibition of CDK7 reveals high-confidence targets and new models for TFIIH function in transcription. *Genes & development*, **34:** 1452–1473.

Roeder R. G. (1996). The role of general initiation factors in transcription by RNA polymerase II. *Trends in biochemical sciences*, **21:** 327–335.

Rose, A. M., Luo, R., Radia, U. K., Kalirai, H., Thornton, S., Luthert, P. J., Jayasena, C. N., Verity, D. H., Coupland, S. E. and Rose, G. E. (2018). Detection of mutations in SF3B1, EIF1AX and GNAQ in primary orbital melanoma by candidate gene analysis. *BMC cancer*, **18:** 1262.

Rosonina, E., Yurko, N., Li, W., Hoque, M., Tian, B. and Manley, J. L. (2014). Threonine-4 of the budding yeast RNAP II CTD couples transcription with Htz1-mediated chromatin remodeling. *Proceedings of the National Academy of Sciences of the United States of America*, **111:** 11924–11931.

Rougvie, A. E. and Lis, J. T. (1988). The RNA polymerase II molecule at the 5' end of the uninduced hsp70 gene of D. melanogaster is transcriptionally engaged. *Cell*, **54:** 795–804.

Sakai, T., Sameshima, T., Matsufuji, M., Kawamura, N., Dobashi, K. and Mizui, Y. (2004a). Pladienolides, new substances from culture of Streptomyces platensis Mer-11107. I. Taxonomy, fermentation, isolation and screening. *The Journal of antibiotics*, **57:** 173–179.

Sakai, Y., Tsujita, T., Akiyama, T., Yoshida, T., Mizukami, T., Akinaga, S., Horinouchi, S., Yoshida, M. and Yoshida, T. (2002b). GEX1 compounds, novel antitumor antibiotics related to herboxidiene, produced by Streptomyces sp. II. The effects on cell cycle progression and gene expression. *The Journal of antibiotics*, **55:** 863–872.

Sakai, Y., Yoshida, T., Ochiai, K., Uosaki, Y., Saitoh, Y., Tanaka, F., Akiyama, T., Akinaga, S. and Mizukami, T. (2002). GEX1 compounds, novel antitumor antibiotics related to herboxidiene, produced by Streptomyces sp. I. Taxonomy, production, isolation, physicochemical properties and biological activities. *The Journal of antibiotics*, **55:** 855–862.

Saldi, T., Cortazar, M. A., Sheridan, R. M. and Bentley, D. L. (2016). Coupling of RNA Polymerase II Transcription Elongation with Pre-mRNA Splicing. *Journal of molecular biology*, **428:** 2623–2635.

Sansó, M., Levin, R. S., Lipp, J. J., Wang, V. Y., Greifenberg, A. K., Quezada, E. M., Ali, A., Ghosh, A., Larochelle, S., Rana, T. M., Geyer, M., Tong, L., Shokat, K. M. and Fisher, R. P. (2016). P-TEFb regulation of transcription termination factor Xrn2 revealed by a chemical genetic screen for Cdk9 substrates. *Genes & development*, **30:** 117–131.

Schilbach, S., Hantsche, M., Tegunov, D., Dienemann, C., Wigge, C., Urlaub, H. and Cramer, P. (2017). Structures of transcription pre-initiation complex with TFIIH and Mediator. *Nature*, **551:** 204–209.

Schlackow, M., Nojima, T., Gomes, T., Dhir, A., Carmo-Fonseca, M. and Proudfoot, N. J. (2017). Distinctive Patterns of Transcription and RNA Processing for Human lincRNAs. *Molecular cell*, **65:** 25–38.

Schreieck, A., Easter, A. D., Etzold, S., Wiederhold, K., Lidschreiber, M., Cramer, P. and Passmore, L. A. (2014). RNA polymerase II termination involves C-terminal-domain tyrosine dephosphorylation by CPF subunit Glc7. *Nature structural & molecular biology*, **21:** 175–179.

Schröder, S., Cho, S., Zeng, L., Zhang, Q., Kaehlcke, K., Mak, L., Lau, J., Bisgrove, D., Schnölzer, M., Verdin, E., Zhou, M. M. and Ott, M. (2012). Two-pronged binding with bromodomain-containing protein 4 liberates positive transcription elongation factor b from inactive ribonucleoprotein complexes. *The Journal of biological chemistry*, **287:** 1090–1099.

Scott, L. M. and Rebel, V. I. (2013). Acquired mutations that affect pre-mRNA splicing in hematologic malignancies and solid tumors. *Journal of the National Cancer Institute*, **105:** 1540–1549.

Scotti, M. M. and Swanson, M. S. (2016). RNA mis-splicing in disease. *Nature reviews. Genetics*, **17:** 19–32.

Seghezzi, W., Chua, K., Shanahan, F., Gozani, O., Reed, R. and Lees, E. (1998). Cyclin E associates with components of the pre-mRNA splicing machinery in mammalian cells. *Molecular and cellular biology*, **18:** 4526–4536.

Shandilya, J. and Roberts, S. G. (2012). The transcription cycle in eukaryotes: from productive initiation to RNA polymerase II recycling. *Biochimica et biophysica acta*, **1819:** 391–400.

Sheth, N., Roca, X., Hastings, M. L., Roeder, T., Krainer, A. R. and Sachidanandam, R. (2006). Comprehensive splice-site analysis using comparative genomics. *Nucleic acids research*, **34:** 3955–3967.

Shi Y. (2009). Serine/threonine phosphatases: mechanism through structure. *Cell*, **139:** 468–484.

Shi Y. (2017). Mechanistic insights into precursor messenger RNA splicing by the spliceosome. *Nature reviews. Molecular cell biology*, **18:** 655–670.

Shi, Y., Reddy, B. and Manley, J. L. (2006). PP1/PP2A phosphatases are required for the second step of Pre-mRNA splicing and target specific snRNP proteins. *Molecular cell*, **23:** 819–829.

Simonti, C. N., Pollard, K. S., Schröder, S., He, D., Bruneau, B. G., Ott, M. and Capra, J. A. (2015). Evolution of lysine acetylation in the RNA polymerase II C-terminal domain. *BMC evolutionary biology*, **15**, 35.

Singh, R. K. and Cooper, T. A. (2012). Pre-mRNA splicing in disease and therapeutics. *Trends in molecular medicine*, **18:** 472–482.

Soemedi, R., Cygan, K. J., Rhine, C. L., Wang, J., Bulacan, C., Yang, J., Bayrak-Toydemir, P., McDonald, J. and Fairbrother, W. G. (2017). Pathogenic variants that alter protein code often disrupt splicing. *Nature genetics*, **49:** 848–855.

St Amour, C. V., Sansó, M., Bösken, C. A., Lee, K. M., Larochelle, S., Zhang, C., Shokat, K. M., Geyer, M. and Fisher, R. P. (2012). Separate domains of fission yeast Cdk9 (P-TEFb) are required for capping enzyme recruitment and primed (Ser7-phosphorylated) Rpb1 carboxyl-terminal domain substrate recognition. *Molecular and cellular biology*, **32:** 2372–2383.

Starr, D. B., Hoopes, B. C. and Hawley, D. K. (1995). DNA bending is an important component of site-specific recognition by the TATA binding protein. *Journal of molecular biology*, **250:** 434–446.

Sun C. (2020). The SF3b complex: splicing and beyond. *Cellular and molecular life sciences : CMLS*, **77:** 3583–3595.

Szklarczyk, D., Kirsch, R., Koutrouli, M., Nastou, K., Mehryary, F., Hachilif, R., Gable, A. L., Fang, T., Doncheva, N. T., Pyysalo, S., Bork, P., Jensen, L. J. and von Mering, C. (2023). The STRING database in 2023: protein-protein association networks and functional enrichment analyses for any sequenced genome of interest. *Nucleic acids research*, **51:** D638–D646.

Takeiwa, T., Mitobe, Y., Ikeda, K., Horie-Inoue, K. and Inoue, S. (2020). Roles of Splicing Factors in Hormone-Related Cancer Progression. *International journal of molecular sciences*, **21:** 1551.

Talkish, J., Igel, H., Hunter, O., Horner, S. W., Jeffery, N. N., Leach, J. R., Jenkins, J. L., Kielkopf, C. L. and Ares, M. (2019). Cus2 enforces the first ATP-dependent step of splicing by binding to yeast SF3b1 through a UHM-ULM interaction. *RNA*, **25:** 1020–1037.

Tanuma, N., Kim, S. E., Beullens, M., Tsubaki, Y., Mitsuhashi, S., Nomura, M., Kawamura, T., Isono, K., Koseki, H., Sato, M., Bollen, M., Kikuchi, K. and Shima, H. (2008). Nuclear inhibitor of protein phosphatase-1 (NIPP1) directs protein phosphatase-1 (PP1) to dephosphorylate the U2 small nuclear ribonucleoprotein particle (snRNP) component, spliceosome-associated protein 155 (Sap155). *The Journal of biological chemistry*, **283:** 35805–35814.

Tardiff, D. F., Lacadie, S. A. and Rosbash, M. (2006). A genome-wide analysis indicates that yeast pre-mRNA splicing is predominantly posttranscriptional. *Molecular cell*, **24:** 917–929.

Tavakolian, S., Goudarzi, H. and Faghihloo, E. (2020). Cyclin-dependent kinases and CDK inhibitors in virus-associated cancers. *Infectious agents and cancer*, **15:** 27.

Tellier, M., Maudlin, I. and Murphy, S. (2020a). Transcription and splicing: A two-way street. *Wiley interdisciplinary reviews. RNA*, **11:** e1593.

Tellier, M., Zaborowska, J., Caizzi, L., Mohammad, E., Velychko, T., Schwalb, B., Ferrer-Vicens, I., Blears, D., Nojima, T., Cramer, P. and Murphy, S. (2020b). CDK12 globally stimulates RNA polymerase II transcription elongation and carboxyl-terminal domain phosphorylation. *Nucleic acids research*, **48:** 7712–7727.

Tellier, M., Zaborowska, J., Neve, J., Nojima, T., Hester, S., Fournier, M., Furger, A. and Murphy, S. (2022). CDK9 and PP2A regulate RNA polymerase II transcription termination and coupled RNA maturation. *EMBO reports*, **23:** e54520.

Thickman, K. R., Swenson, M. C., Kabogo, J. M., Gryczynski, Z. and Kielkopf, C. L. (2006). Multiple U2AF65 binding sites within SF3b155: thermodynamic and spectroscopic characterization of protein-protein interactions among pre-mRNA splicing factors. *Journal of molecular biology*, **356:** 664–683.

Tholen, J., Razew, M., Weis, F. and Galej, W. P. (2022). Structural basis of branch site recognition by the human spliceosome. *Science*, **375:** 50–57.

Tomiyama, A., Kobayashi, T., Mori, K. and Ichimura, K. (2019). Protein Phosphatases-A Touchy Enemy in the Battle Against Glioblastomas: A Review. *Cancers*, **11:** 241.

Tripathi, V., Song, D. Y., Zong, X., Shevtsov, S. P., Hearn, S., Fu, X. D., Dundr, M. and Prasanth, K. V. (2012). SRSF1 regulates the assembly of pre-mRNA processing factors in nuclear speckles. *Molecular biology of the cell*, **23:** 3694–3706.

Turunen, J. J., Niemelä, E. H., Verma, B. and Frilander, M. J. (2013). The significant other: splicing by the minor spliceosome. *Wiley interdisciplinary reviews. RNA*, **4:** 61–76.

Ujvári, A. and Luse, D. S. (2004). Newly Initiated RNA encounters a factor involved in splicing immediately upon emerging from within RNA polymerase II. *The Journal of biological chemistry*, **279:** 49773–49779.

Vasiljeva, L., Kim, M., Mutschler, H., Buratowski, S. and Meinhart, A. (2008). The Nrd1-Nab3-Sen1 termination complex interacts with the Ser5-phosphorylated RNA polymerase II C-terminal domain. *Nature structural & molecular biology*, **15:** 795–804.

Verma, S., De Jesus, P., Chanda, S. K. and Verma, I. M. (2019). SNW1, a Novel Transcriptional Regulator of the NF-κB Pathway. *Molecular and cellular biology*, **39:** e00415-18.

Vos, S., Farnung, L., Urlaub, H. and Cramer, P. (2018). Structure of paused transcription complex Pol II-DSIFNELF. *Nature*, **560:** 601-606.

Wahl, M. C., Will, C. L. and Lührmann, R. (2009). The spliceosome: design principles of a dynamic RNP machine. *Cell*, **136:** 701–718.

Wallace, E. W. J. and Beggs, J. D. (2017). Extremely fast and incredibly close: cotranscriptional splicing in budding yeast. *RNA*, **23:** 601–610.

Wang, C., Chua, K., Seghezzi, W., Lees, E., Gozani, O. and Reed, R. (1998). Phosphorylation of spliceosomal protein SAP 155 coupled with splicing catalysis. *Genes & development*, **12:** 1409–1414.

Wang, G. S. and Cooper, T. A. (2007). Splicing in disease: disruption of the splicing code and the decoding machinery. *Nature reviews. Genetics*, **8:** 749–761.

Wang, K., Yin, C., Du, X., Chen, S., Wang, J., Zhang, L., Wang, L., Yu, Y., Chi, B., Shi, M., Wang, C., Reed, R., Zhou, Y., Huang, J. and Cheng, H. (2019). A U2-snRNP-independent role of SF3b in promoting mRNA export. *Proceedings of the National Academy of Sciences of the United States of America*, **116:** 7837–7846.

Wang, Y., Liu, J., Huang, B. O., Xu, Y. M., Li, J., Huang, L. F., Lin, J., Zhang, J., Min, Q. H., Yang, W. M. and Wang, X. Z. (2015). Mechanism of alternative splicing and its regulation. *Biomedical reports*, **3:** 152–158.

Wani, S., Yuda, M., Fujiwara, Y., Yamamoto, M., Harada, F., Ohkuma, Y. and Hirose, Y. (2014). Vertebrate Ssu72 regulates and coordinates 3'-end formation of RNAs transcribed by RNA polymerase II. *PloS one*, **9:** e106040.

Welsh, S. A. and Gardini, A. (2023). Genomic regulation of transcription and RNA processing by the multitasking Integrator complex. *Nature reviews. Molecular cell biology*, **24:** 204–220.

West, S., Gromak, N. and Proudfoot, N. J. (2004). Human 5' --> 3' exonuclease Xrn2 promotes transcription termination at co-transcriptional cleavage sites. *Nature*, **432:** 522–525.

Will, C. L. and Lührmann, R. (2011). Spliceosome structure and function. *Cold Spring Harbor perspectives in biology*, **3:** a003707.

Wilkinson, M. E., Charenton, C. and Nagai, K. (2020). RNA Splicing by the Spliceosome. *Annual review of biochemistry*, **89:** 359–388.

Wolin, S. L. and Maquat, L. E. (2019). Cellular RNA surveillance in health and disease. *Science*, **366:** 822–827.

Wright, C. J., Smith, C. W. J. and Jiggins, C. D. (2022). Alternative splicing as a source of phenotypic diversity. *Nature reviews. Genetics*, **23:** 697–710.

Yamamoto, M., Onogi, H., Kii, I., Yoshida, S., Iida, K., Sakai, H., Abe, M., Tsubota, T., Ito, N., Hosoya, T. and Hagiwara, M. (2014). CDK9 inhibitor FIT-039 prevents replication of multiple DNA viruses. *The Journal of clinical investigation*, **124:** 3479–3488.

Yan, D., Perriman, R., Igel, H., Howe, K. J., Neville, M. and Ares, M., Jr (1998). CUS2, a yeast homolog of human Tat-SF1, rescues function of misfolded U2 through an unusual RNA recognition motif. *Molecular and cellular biology*, **18:** 5000–5009.

Yang, F., Bian, T., Zhan, X., Chen, Z., Xing, Z., Larsen, N. A., Zhang, X. and Shi, Y. (2023). Mechanisms of the RNA helicases DDX42 and DDX46 in human U2 snRNP assembly. *Nature communications*, **14:** 897.

Yang, Z., Yik, J. H., Chen, R., He, N., Jang, M. K., Ozato, K. and Zhou, Q. (2005). Recruitment of P-TEFb for stimulation of transcriptional elongation by the bromodomain protein Brd4. *Molecular cell*, **19:** 535–545.

Yella, V. R. and Bansal, M. (2017). DNA structural features of eukaryotic TATA-containing and TATA-less promoters. *FEBS open bio*, **7:** 324–334.

Yeo, M., Lin, P. S., Dahmus, M. E. and Gill, G. N. (2003). A novel RNA polymerase II C-terminal domain phosphatase that preferentially dephosphorylates serine 5. *The Journal of biological chemistry*, **278:** 26078–26085.

Yokoi, A., Kotake, Y., Takahashi, K., Kadowaki, T., Matsumoto, Y., Minoshima, Y., Sugi, N. H., Sagane, K., Hamaguchi, M., Iwata, M. and Mizui, Y. (2011). Biological validation that SF3b is a target of the antitumor macrolide pladienolide. *The FEBS journal*, **278:** 4870–4880.

Yoon, S. O., Shin, S., Lee, H. J., Chun, H. K. and Chung, A. S. (2006). Isoginkgetin inhibits tumor cell invasion by regulating phosphatidylinositol 3-kinase/Akt-dependent matrix metalloproteinase-9 expression. *Molecular cancer therapeutics*, **5:** 2666–2675.

Yu, J., Li, Y., Zhang, D., Wan, D. and Jiang, Z. (2020). Clinical implications of recurrent gene mutations in acute myeloid leukemia. *Experimental hematology & oncology*, **9**: 4.

Yurko, N., Liu, X., Yamazaki, T., Hoque, M., Tian, B. and Manley, J. L. (2017). MPK1/SLT2 Links Multiple Stress Responses with Gene Expression in Budding Yeast by Phosphorylating Tyr1 of the RNAP II CTD. *Molecular cell*, **68:** 913–925.e3.

Yurko, N. M. and Manley, J. L. (2018). The RNA polymerase II CTD "orphan" residues: Emerging insights into the functions of Tyr-1, Thr-4, and Ser-7. *Transcription*, **9:** 30–40.

Zaborowska, J., Egloff, S. and Murphy, S. (2016). The pol II CTD: new twists in the tail. *Nature structural & molecular biology*, **23:** 771–777.

Zhang, D. W., Mosley, A. L., Ramisetty, S. R., Rodríguez-Molina, J. B., Washburn, M. P. and Ansari, A. Z. (2012). Ssu72 phosphatase-dependent erasure of phospho-Ser7 marks on the RNA polymerase II C-terminal domain is essential for viability and transcription termination. *The Journal of biological chemistry*, **287:** 8541–8551.

Zhang, M. and Green, M. R. (2001). Identification and characterization of yUAP/Sub2p, a yeast homolog of the essential human pre-mRNA splicing factor hUAP56. *Genes & development*, **15:** 30–35.

Zhang, X., Yan, C., Zhan, X., Li, L., Lei, J. and Shi, Y. (2018). Structure of the human activated spliceosome in three conformational states. *Cell research*, **28:** 307–322.

Zhang, Z., Will, C. L., Bertram, K., Dybkov, O., Hartmuth, K., Agafonov, D. E., Hofele, R., Urlaub, H., Kastner, B., Lührmann, R. and Stark, H. (2020). Molecular architecture of the human 17S U2 snRNP. *Nature*, **583:** 310–313.

Zhou, K., Zhuang, S., Liu, F., Chen, Y., Li, Y., Wang, S., Li, Y., Wen, H., Lin, X., Wang, J., Huang, Y., He, C., Xu, N., Li, Z., Xu, L., Zhang, Z., Chen, L. F., Chen, R. and Liu, M. (2022). Disrupting the Cdk9/Cyclin T1 heterodimer of 7SK snRNP for the Brd4 and AFF1/4 guided reconstitution of active P-TEFb. *Nucleic acids research*, **50:** 750–762.

Zhou, M., Huang, K., Jung, K. J., Cho, W. K., Klase, Z., Kashanchi, F., Pise-Masison, C. A. and Brady, J. N. (2009). Bromodomain protein Brd4 regulates human immunodeficiency virus transcription through phosphorylation of CDK9 at threonine 29. *Journal of virology*, **83:** 1036–1044.

Zhou, Q., Chen, D., Pierstorff, E. and Luo, K. (1998). Transcription elongation factor P-TEFb mediates Tat activation of HIV-1 transcription at multiple stages. *The EMBO journal*, **17:** 3681–3691.

Zimmerman, W. C. and Erikson, R. L. (2007). Finding Plk3. *Cell cycle*, **6:** 1314–1318.

Zippo, A., Serafini, R., Rocchigiani, M., Pennacchini, S., Krepelova, A. and Oliviero, S. (2009). Histone crosstalk between H3S10ph and H4K16ac generates a histone code that mediates transcription elongation. *Cell*, **138:** 1122–1136.

Supplementary Material

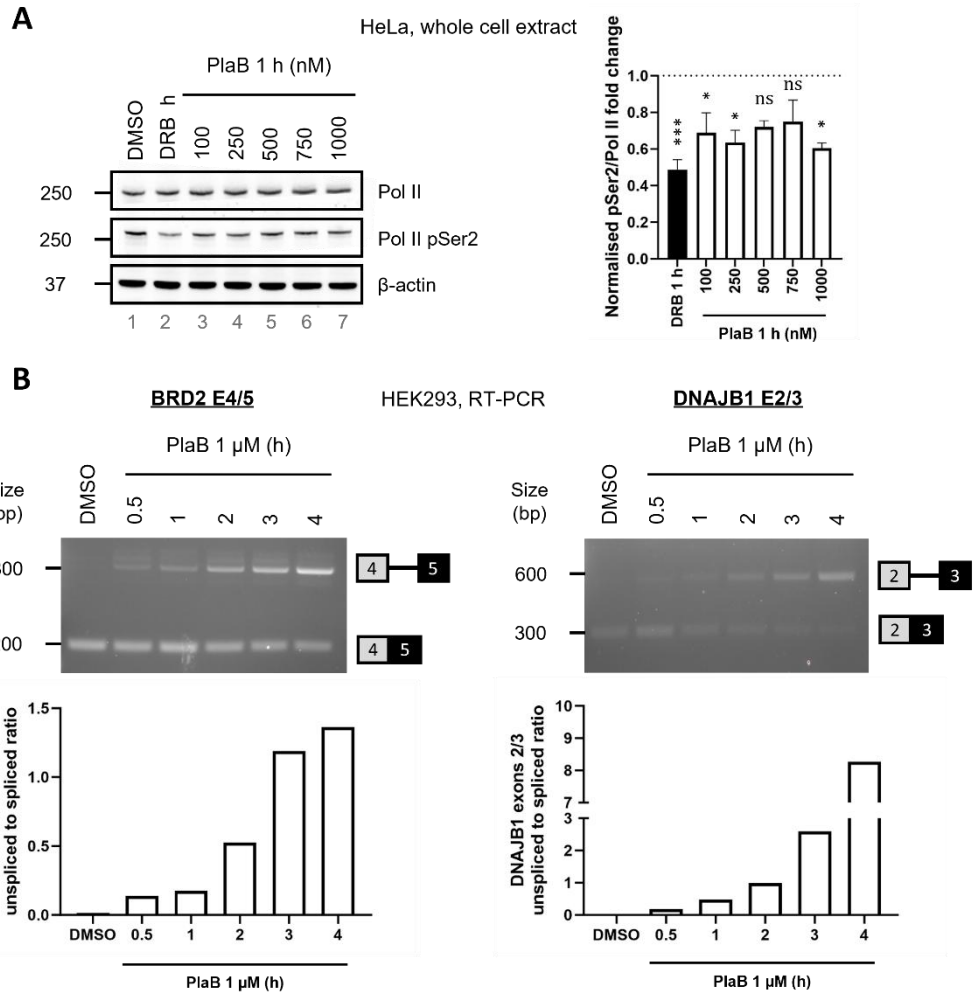

A
HeLa, whole cell extract
PlaB 1 h (nM)
DMSO
DRB 1 h
100
250
500
750
1000
250
Pol II
250
Pol II pSer2
37
β-actin
1 2 3 4 5 6 7
Normalised pSer2/Pol II fold change
DRB 1 h
PlaB 1 h (nM)
B
BRD2 E4/5
HEK293, RT-PCR
DNAJB1 E2/3
PlaB 1 μM (h)
Size (bp)
DMSO
0.5
1
2
3
4
800
200
600
300
BRD2 exons 4/5 unspliced to spliced ratio
DNAJB1 exons 2/3 unspliced to spliced ratio
PlaB 1 μM (h)
C
HEK293, whole cell extract
PlaB 1 h (nM)
Pol II
Pol II pSer2
β-actin
Normalised pSer2/Pol II fold change
D
HEK293, whole cell extract
PlaB 1 μM (h)
DRB 4 h
Pol II
Pol II pSer2
β-actin
Normalised pSer2/Pol II fold change
DRB 4 h
PlaB 1 μM (h)

Figure S1. Short SF3B1 inhibition causes rapid defects in pre-mRNA splicing and inhibits nascent transcription in human cells

(A and C, left) Western blot analysis of whole cell extracts of HeLa or HEK293 cells treated with DMSO, 100 μM DRB for 1 hour, or with 1 μM PlaB for concentrations ranging between 100 nM to 1 μM for 1 hour. Proteins were resolved by SDS-PAGE and immunoblotted with anti-pol II, anti-pol II pSer2, and anti-β-actin as a loading control. **(A and C, right)** Quantification of the western blots for DMSO (black horizonal line), DRB (black bar) and PlaB (white bar). Each pol II or pol II pSer2 quantification signal was normalised to the β-actin signal, pol II pSer2 to total pol II ratio determined, then compared to the ratio for the DMSO condition. Bars represent the normalised pol II pSer2 to total pol II fold change relative to DMSO of 3 biological replicates. Error bars = standard error of the mean. Statistical test: ordinary one-way ANOVA test. P-value: * < 0.05, *** < 0.001. **(B, top)** RT-PCR with primers amplifying the intron located between exons 4 and 5 of *BRD2* or the intron located between exons 2 and 3 of *DNAJB1.* HEK293 cells were treated with DMSO or 1 μM PlaB for times ranging between 30 minutes to 4 hours. The locations of the spliced and unspliced RNA are shown to the right of each gel image. **(B, bottom)** Quantification of relative band intensity as a ratio of unspliced to spliced RNA for DMSO (grey) and Pla B (white). **(D, left)** Western blot analysis of whole cell extracts of HEK293 cells treated with DMSO, 100 μM DRB for 4 hours, or with 1 μM PlaB for times ranging between 30 minutes to 4 hours. Proteins were resolved by SDS-PAGE and immunoblotted with anti-pol II, anti-pol II pSer2, and anti-β-actin as a loading control. **(D, right)** Quantification of the western blots for DMSO (black horizonal line), DRB (black bar) and PlaB (white bar). Each pol II or pol II pSer2 quantification signal was normalised to the β-actin signal, pol II pSer2 to total pol II ratio determined, then compared to the ratio for the DMSO condition. Bars represent the normalised pol II pSer2 to total pol II fold change relative to DMSO of 3 biological replicates. Error bars = standard error of the mean. Statistical test: ordinary one-way ANOVA test.

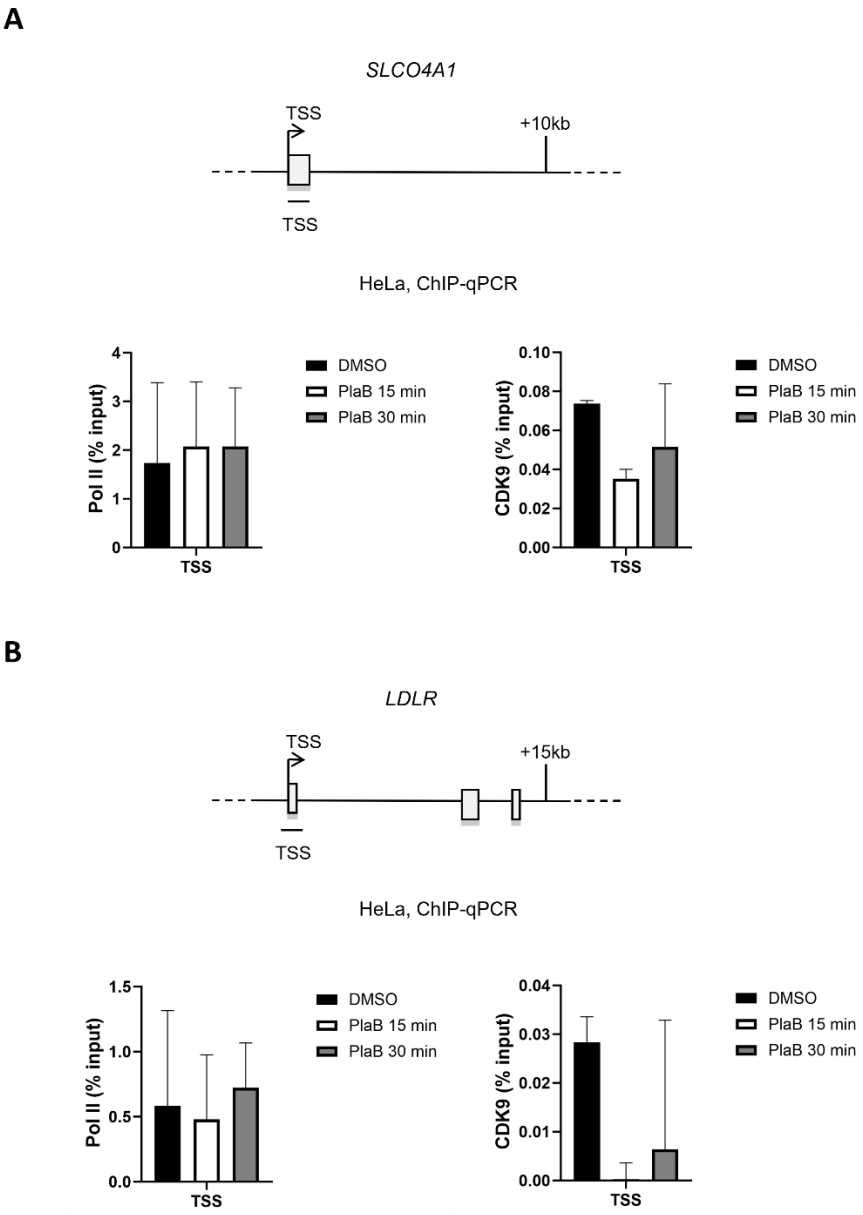


Figure S2. Inhibition of SF3B1 function impairs early transcription elongation

(A, top) Schematic of genic region around the promoter of SLCO4A1. **(A, bottom)** ChIP-qPCR of total pol II and CDK9 at the promoter region of the SLCO4A1 intron-containing gene in HeLa cells treated with DMSO (black) or 1 μM PlaB for 15 minutes (white) or 30 minutes (grey). Mean of 3 biological repeats. Error bars = standard error of the mean. Statistical test: Dunnett's multiple comparison test. **(B, top)** Schematic of genic region around the promoter of LDLR. **(B, bottom)** ChIP-qPCR of total pol II and CDK9 at the promoter region of the LDLR intron-containing gene in HeLa cells treated with DMSO (black) or 1 μM PlaB for 15 minutes (white) or 30 minutes (grey). Mean of 3 biological repeats. Error bars = standard error of the mean. Statistical test: Dunnett's multiple comparison test.

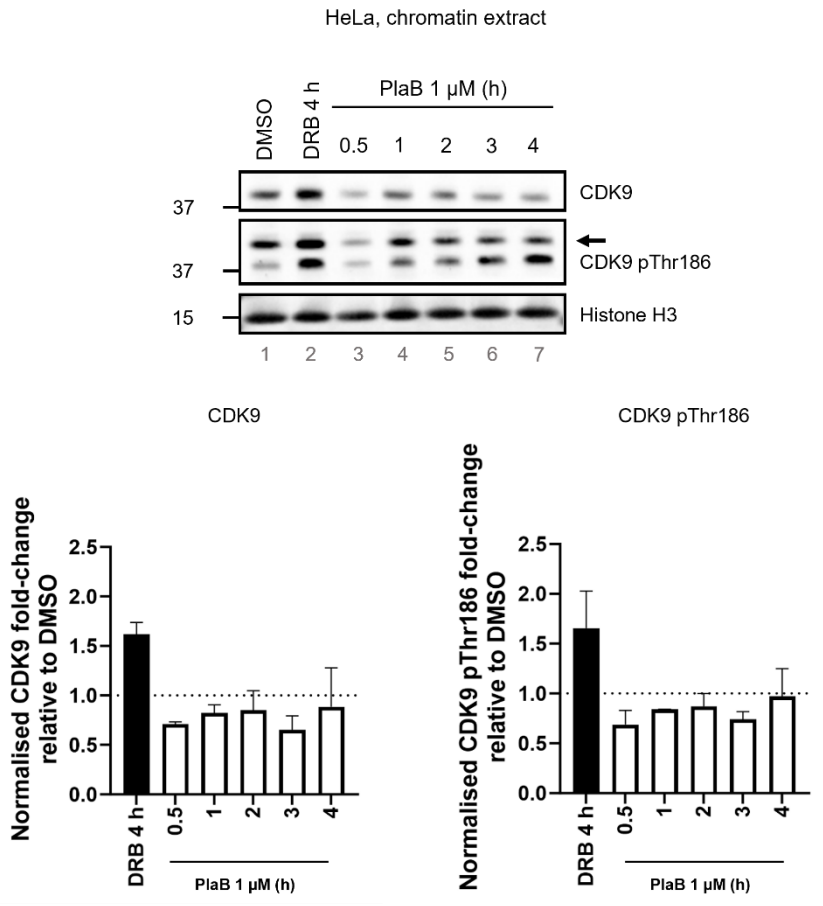
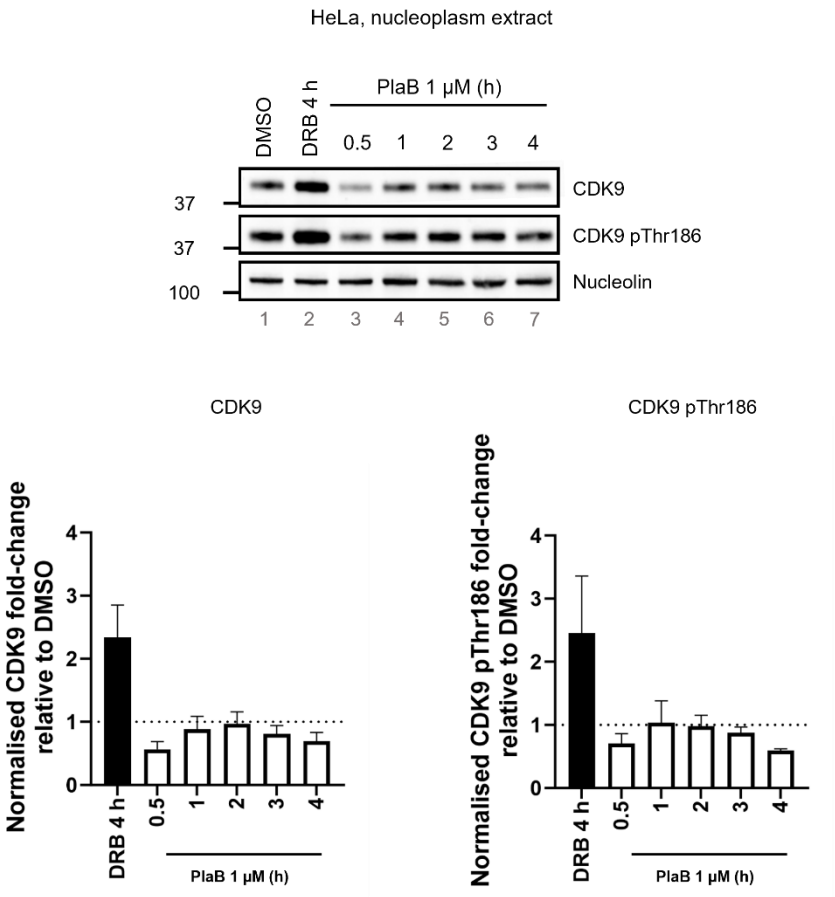


Figure S3. SF3B1 inhibition causes a global loss of SF3B1 and CDK9 from chromatin

(Top) Western blot analysis of chromatin extracts of HeLa cells treated with DMSO, 100 µM DRB for 4 hours, or with 1 µM PlaB for times ranging between 30 minutes to 4 hours. Proteins were resolved by SDS-PAGE and immunoblotted with anti-CDK9, anti-CDK9 pThr186, and anti-Histone H3 as a loading control. **(Bottom)** Quantification of the western blots for DMSO (black horizonal line), DRB (black bar), and PlaB (white bar). Each quantification signal was normalised to the Histone H3 signal, then to the DMSO condition. Bars represent normalised antibody fold-change relative to the DMSO condition for 2 biological replicates. Error bars = standard error of the mean.

A


HeLa, nucleoplasm extract
DMSO
DRB 4 h
PlaB 1 µM (h)
0.5
1
2
3
4
37
37
100
CDK9
CDK9 pThr186
Nucleolin
1 2 3 4 5 6 7
CDK9
CDK9 pThr186
Normalised CDK9 fold-change relative to DMSO
Normalised CDK9 pThr186 fold-change relative to DMSO
DRB 4 h
PlaB 1 µM (h)

B

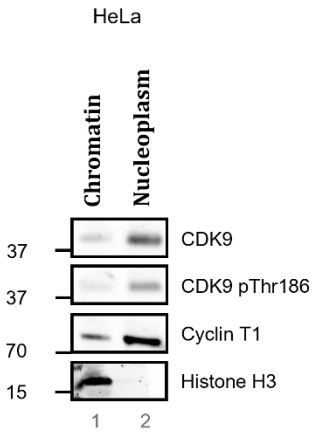

HeLa
Chromatin
Nucleoplasm
37
37
70
15
CDK9
CDK9 pThr186
Cyclin T1
Histone H3
1 2

Figure S4. SF3B1 inhibition changes the nuclear localisation of SF3B1 and CDK9

(A, top) Western blot analysis of nucleoplasm extracts of HeLa cells treated with DMSO, 100 μM DRB for 4 hours, or with 1 μM PlaB for times ranging between 30 minutes to 4 hours. Proteins were resolved by SDS-PAGE and immunoblotted with anti-CDK9, anti-CDK9 pThr186, and anti-Nucleolin as a loading control. **(A, bottom)** Quantification of the western blots for DMSO (black horizonal line), DRB (black bar), and PlaB (white bar). Each quantification signal was normalised to the nucleolin signal, then to the DMSO condition. Bars represent normalised antibody fold-change relative to the DMSO condition for 2 biological replicates. Error bars = standard error of the mean. **(B)** Western blot analysis of chromatin and nucleoplasm extracts of HeLa cells without any treatment. Cell nuclei equivalents were used for each blot. Proteins were resolved by SDS-PAGE and immunoblotted with anti-CDK9, anti-CDK9 pThr186, anti-Cyclin T1 and anti-Histone H3 as a loading control.

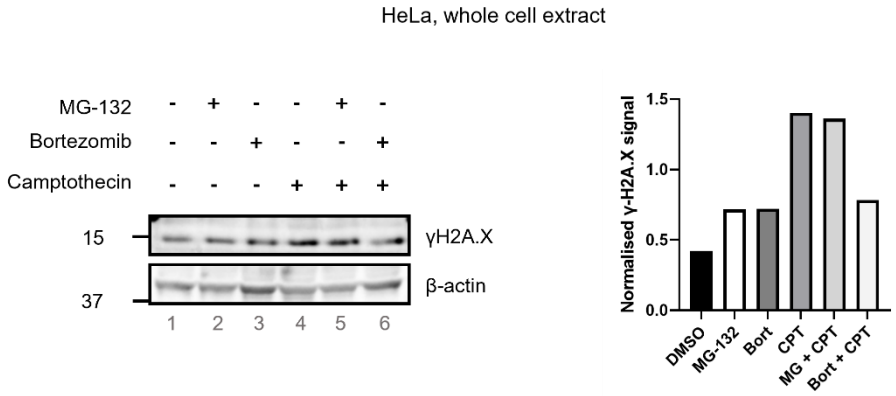


Figure S5. SF3B1 inhibition does not affect the protein stability of SF3B1 and CDK9

(Left) Western blot analysis of whole cell extracts of HeLa cells treated with DMSO, 5 μM MG-132, 1 μM Bortezomib, or with 25 μM Camptothecin for 1 hour. Proteins were resolved by SDS-PAGE and immunoblotted with anti-γH2A.X and anti-β-actin as a loading control. **(Right)** Quantification of the western blots for DMSO (black), MG-132 (white), Bortezomib (dark grey), Camptothecin (grey), and dual treatments (lighter tones of grey). Each quantification signal was normalised to the anti-γH2A.X signal., Bars represent normalised antibody signal for 1 biological replicate.

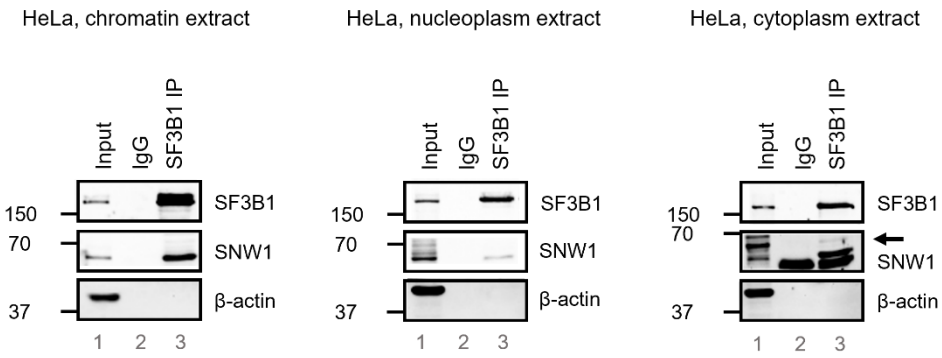


Figure S6. Tat-SF1 interacts with SF3B1 and CDK9 only on chromatin

(A) Western blot analysis from co-immunoprecipitation experiments on chromatin, nucleoplasm, and cytoplasm extracts of HeLa cells. SF3B1 was immunoprecipitated using an antibody against the endogenous protein. Rabbit IgG was used as a negative control for non-specific binding. Proteins were resolved by SDS-PAGE and immunoblotted with anti-SF3B1, anti-SNW1, and anti-β-actin as a control.

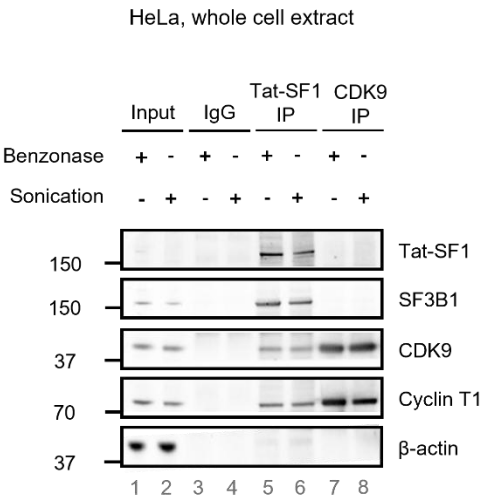


Figure S7. Chromatin is a binding platform mediating SF3B1 and CDK9 protein interactions

(Top) Western blot analysis from co-immunoprecipitation experiments on whole cell extracts of HeLa cells exposed to 1 µl/U Benzonase treatment or 40% amplitude 15 cycles 30s ON/ 30s OFF sonication (Sonica Thermocube Q800R). Tat-SF1 and CDK9 were immunoprecipitated using antibodies against the endogenous proteins. Rabbit IgG were used as negative controls for non-specific binding. Proteins were resolved by SDS-PAGE and immunoblotted with anti-Tat-SF1, anti-SF3B1, anti-CDK9, anti-Cyclin T1, and anti-β-actin as a control.

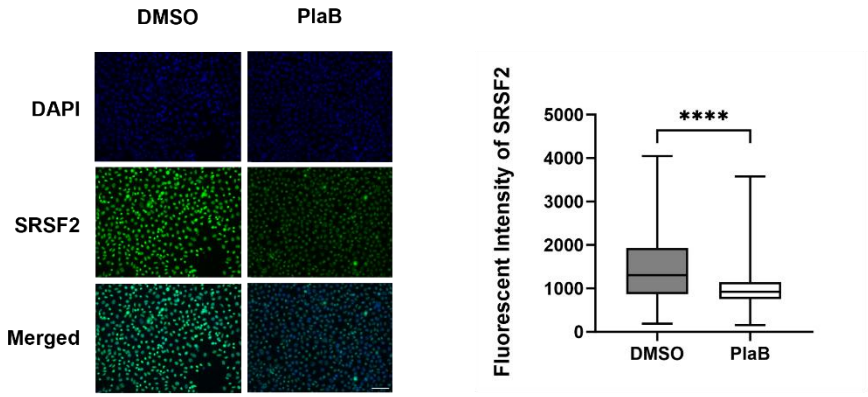


Figure S8. Other interactors of SF3B1 and CDK9

(Left) Representative images of immunofluorescence analysis in HeLa cells treated with DMSO or with 1 µM PlaB for 30 minutes. DAPI (blue), G3BP1 (green), scale bar: 100 µm. **(A, right)**. Quantification of fluorescent intensity per nucleus for DMSO (grey) and PlaB (white). Box plot settings are: min to max values with the median and 25-75 percentile range. >10,000 nuclei were quantified per condition. Statistical test: Kruskal-Wallis test. P-value: **** < 0.0001.

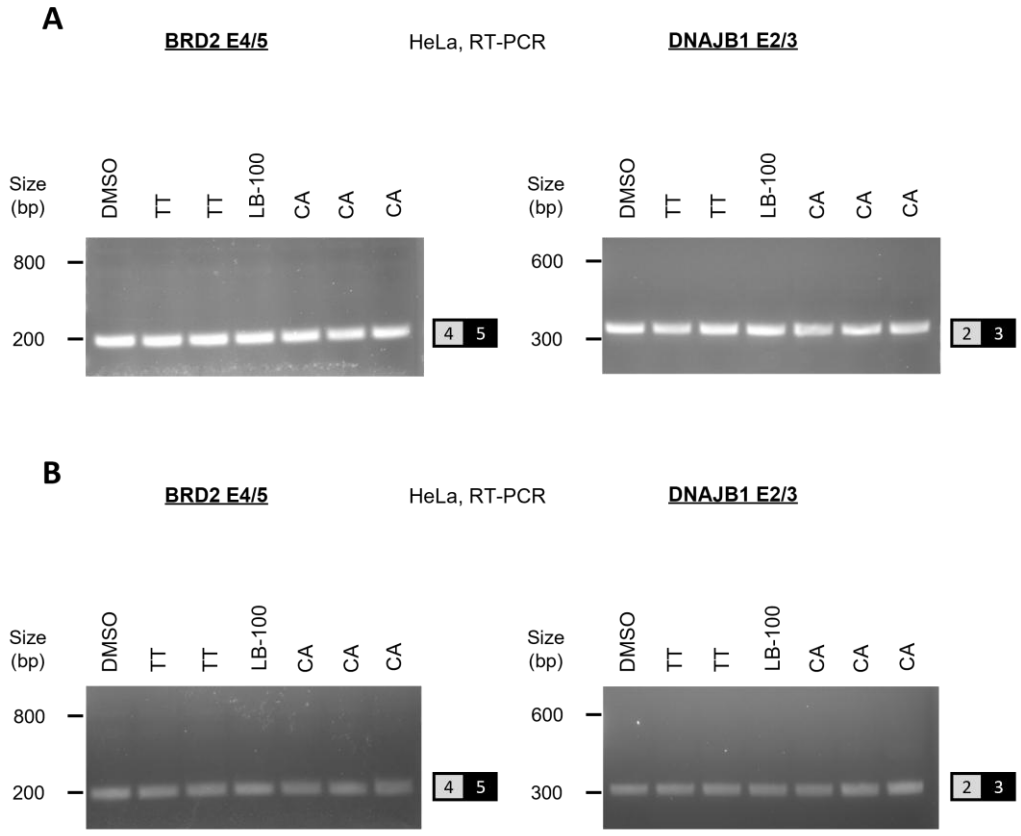


Figure S9. PP1/PP2A may not regulate the splicing function of SF3B1

(A and B) RT-PCR with primers amplifying the intron located between exons 4 and 5 of *BRD2* or the intron located between exons 2 and 3 of *DNAJB1.* HeLa cells were treated with DMSO, 25 nM or 100 nM Tautomycetin, 2.5 nM LB-100, or with 0.5 nM, 1 nM, or 2.5 nM Calyculin A for either 1 hour (panel A) or 4 hours (panel B). The locations of the spliced and unspliced RNA are shown to the right of each gel image.